EXPERIMENTAL AND ANALYTICAL STUDY OF A HIGH-TEMPERATURE BIOMASS GASIFICATION SYSTEM

By

AKIKO HIRAMATSU

A DISSERTATION PRESENTED TO THE GRADUATE SCHOOL
OF THE UNIVERSITY OF FLORIDA IN PARTIAL FULFILLMENT
OF THE REQUIREMENTS FOR THE DEGREE OF
DOCTOR OF PHILOSOPHY

UNIVERSITY OF FLORIDA

2011

To my parents

ACKNOWLEDGMENTS

I would like to sincerely thank Dr. Herbert. A. Ingley, my supervisory committee chair, for his guidance, patience, and very warm support through my graduate studies at the University of Florida. Without his support, understanding and encouragement, I would never be able to achieve my research work. I would also thank to Dr. Jacob Chung, co-chair of my committee, for his understanding and support for my studies. I thank members of my supervisory committees.

TABLE OF CONTENTS

page

LIST OF TABLES

LIST OF FIGURES

LIST OF ABBREVIATIONS

T_0	Temperature (273.15 K)
P_0	Pressure (1atm or 1bar)
T	Temperature
P	Pressure
m	Mass (kg)
g	Gravitational acceleration, 9.81 m/s^2
$\bar{R}$	Gas constant (8.31451 kJ/kmol-K)
Cp	Specific Heat (kJ/kg-K)
H	Total enthalpy (kJ)
U	Total internal energy (kJ)
$\dot{Q}$	Time rate of total heat (kJ/s)
$\dot{W}$	Time rate of total work (kJ/s)
h	Enthalpy on a unit mass bases (kJ/kg)
s	Entropy on a unit mass bases (kJ/kg-K)
$\overline{h_f^0}$	Enthalpy of formation (kJ/kmol) at 273.15 K, 1 bar
$\bar{s}^0$	Absolute entropy (kJ/kmol-K) at 273.15 K, 1bar
V	Velocity (m/s)
z	Position or the height from the environmental state (m)
U_0	Total internal energy at the restricted dead state (kJ)
V_0	Volume at the restricted dead state (m^3)
S	Total entropy (kJ/K)
S_0	Total entropy at the restricted dead state (kJ/K)
E, Ex	Total energy (kJ) or Total exergy (kJ)

E^{PH}	Total physical exergy (kJ)
E^{CH}	Total chemical exergy (kJ)
E^{PE}	Total potential exergy (kJ)
E^{KE}	Total kinetic exergy (kJ)
e	exergy on a unit mass bases (kJ/kg)
e^{PH}	Physical exergy on a unit mass bases (kJ/kg)
e^{CH}	Chemical exergy on a unit mass bases (kJ/kg)
e^{PE}	Potential exergy on a unit mass bases (kJ/kg)
e^{KE}	Kinetic exergy on a unit mass bases (kJ/kg)
$\dot{I}$	Time rate of irriversibility (kJ/sec)
$\bar{e}_k^{CH}$	Chemical exergy per mole of gas k (kJ/kmol)
x_k, y_k	Mole fraction of a gaseous species k in a gas mixture
n_A	Number of moles of species A
G	Gibbs function
ΔG^0	Standard-state change in Gibbs function
K	Equilibrium constant
z_i	Mass fraction of species, i
MCE	Mass conversion efficiency
TECE	Thermal energy conversion efficiency
CGE	Cold gas efficiency
GEC	Global energy content
SB, SBT	Steam to Biomass Ratio
HTBGS	High-Temperature Biomass Gasification System
SG	Specific gravity
V_{H2O}	Volume of water (ml)

Greek Symbols:

ν_A	Number of mole of species, A (kmol)
ξ	Degree of reaction
ψ	Exergetic efficiency
β	The ratio of chemical exergy to the LHV of dry organic substance
η	Efficiency

Subscripts:

C.M.	Control mass
C.V.	Control volume
i	Inlet
e	Exit
o	Output
T	Value at temperature T
P	Value at pressure P
P^0	Value at pressure P^0
org	Organic fraction
i,b	Input, biomass
i,stm	Input, steam
o,g	Output, gas
o,c	Output, char
BM	Biomass
Th	Thermal
Ex	Exergetic

Abstract of Dissertation Presented to the Graduate School
of the University of Florida in Partial Fulfillment of the
Requirements for the Degree of Doctor of Philosophy

EXPERIMENTAL AND ANALYTICAL STUDY OF A HIGH-TEMPERATURE BIOMASS GASIFICATION SYSTEM

By

Akiko Hiramatsu

August 2011

Chair: Herbert A. Ingley, III
Major: Mechanical Engineering

Biomass gasification is one of the most environmentally friendly alternative energy conversion methods to produce transportation fuel. An extended review is first provided to discuss the general overview of the biomass gasification process starting with the definition of biomass, chemical reactions involved in the process, type of reactors used, operation parameters, contaminants and their treatments, syngas composition, applications of syngas and the final products. In the present work, a study of high-temperature biomass gasification using steam was conducted. Some of the required conditions included fixed-bed gasification, high operation temperatures, steam gasification and a target product of liquid transportation fuel. There are three main objectives in the present study. The first objective is the demonstration of the biomass steam gasification at very high temperature at up to 1500^{o}C. The second objective is the production of synthesis gas which serves as a feedstock for FTS for biodiesel production. The last objective is the investigation of the biomass gasification process as well as the system level thermal efficiency. The system level energy and exergy analyses were also conducted to determine the efficiency in quantity and quality of energy.

The thermodynamic fundamentals were reviewed first to discuss the chemistry associated with gasification and the first and second laws analyses of thermodynamics are also included. A literature review of analytical mass, energy and exergy studies for biomass gasification system follows. Lastly, the analytical treatment and methods used in the high-temperature biomass gasification process are presented. These methods include the basic gasification conditions and the methods for computing gasification product composition, overall gasification mass balance, energy balance and exergy balance. The calculation methods for several parameters including steam to biomass ratio, carbon conversion ratio, thermal efficiency and exergetic efficiency are also presented.

The design and construction of the High-Temperature Biomass Gasification System (HTBGS), the control/data acquisition (DAQ) system, the experimental method including detailed explanations for the experimental set up, biomass analysis results and experimental conditions are presented.

The results and discussion of both theoretical analysis and experimental works are included in this work. In a conclusion, a bench-scale high-temperature steam biomass gasification system was designed and constructed. High-temperature steam gasification was demonstrated at temperatures as high as 1650^{o}C. Using the bench-scale gasification system, synthesis gas was produced using woody biomass as a feedstock. It was determined that the syngas produced during the experiments resulted in a hydrogen to carbon dioxide mole ratio of approximately 2:1, which is one of the main requirements for the gas to be used in FTS for biodiesel production. However, there were several uncertainties involved in the data acquisition process as well as data treatment process, thus a further investigation and verification of the results are necessary. The energy and exergy analysis were conducted to evaluate the system

level thermal efficiency. It was found the thermal and exergetic efficiencies of the system were very low in all experimental cases. It is recommended to conduct an overall investigation of the experimental system before proceeding with further experiments. It is also recommended to develop a transient gasification model to better compare the syngas production with the current experimental results. Once these conditions are met, it is recommended to conduct gasification experiments using other feedstocks such as municipal solid waste.

CHAPTER 1
INTRODUCTION AND BACKGROUND

1.1 Introduction

At the writing of this dissertation the world energy consumption keeps continues to increase. The Energy Information Administration (EIA) reports that the world energy consumption in 1980 was 283.48 Quadrillion BTU and this increased to 482.80 Quadrillion BTU in 2005, a 2.4% annual increase in energy demand on average [1]. The majority of the energy consumed comes from fossil based fuel [1]. Contrary to the increasing demand for energy, fossil fuel is a limited resource; thus, it is critical to look for alternative fuel sources in order to support the continuous high rate of energy demand in developed countries as well as an accelerated increase of energy needs in developing countries for population growth and industrial development.

There are increasing economical issues as well as social interest in environmental protection. The major environmental issues in today's worlds include air, water and soil pollution, global warming, deforestation, decline in biodiversity and degradation of soil and water resources. A large part of these issues connect directly to the energy consumption by human kind. It is very likely that our environment will be further damaged by human activities if the current style of energy selection and consumption continues. To avoid this scenario and to aim for a future with a cleaner environment, it is essential to seek a wise energy source, which is clean, sustainable and produces the least impact to the environment.

Considering both energy demand and environmental points of view, the importance of clean, renewable energy becomes a point of focus. Renewable energy sources such as wind, solar, hydro, and biomass are receiving increased attention in both developed and developing countries. In the United States in year 2007, 7.206 EJ (6.83 Quadrillion BTU) of the energy

consumed came from renewable sources, which make up 7% of the country's total energy consumption [1]. The breakdown of the renewable energy use: biomass (biofuel, waste and wood derived fuel) was 3.814 EJ (3.615 Quadrillion BTU) (53% of the renewable total), geothermal energy was 0.372 EJ (0.353 Quadrillion BTU) (5%), hydroelectric power was 2.598 EJ (2.463 Quadrillion BTU) (36%), solar energy was 0.084 EJ (0.080 Quadrillion Btu) (1%) and wind energy was 0.337 EJ (0.319 Quadrillion BTU) (5%). Thus biomass is by far the largest renewable energy source utilized in the United States, followed by hydroelectric power. Renewable energy creates energy independence at the national and local levels, promotes the economic and social security, and supports a long term sustainable development.

Woody biomass gasification for synthesis gas production is the thermochemical conversion of biomass to a gaseous product, which could provide environmentally friendly renewable energy. There are several advantages to select woody biomass as an energy crop in Florida. First of all, woody biomass is an abundant renewable energy source. The energy in biomass, the energy stored in its chemical bonds, was originally obtained from the solar energy that plants received and converted via photosynthesis. This means that utilizing biomass energy is to release the solar energy which the plants captured. Since this cycle of release and capture of solar energy occurs within the time scale of human kind, unlike fossil fuels, biomass is generally considered renewable. Second of all, biomass is considered as a carbon neutral energy source, meaning there is no net carbon dioxide emission when biomass is burned or gasified. Theoretically, the carbon dioxide released when biomass is utilized as energy is that carbon dioxide the plants absorbed from the atmosphere when they grew. In reality, there are some induced amounts of carbon dioxide discharge regarding a plant's growth, harvesting and transportation of biomass and so on. Thus how close it can reach the theoretical condition of carbon neutrality depends on the

efficiency of biomass utilization. Finally, woody biomass is a locally available abundant source in Florida, and the sustainable commercial production of wood has already been established.

Among several methods of utilizing biomass to produce energy or alternative fuels, the gasification process to produce synthesis gas or syngas is an option. The gasification technology itself is not new and has been practiced for many years with wood and coal. Starting from the observation of gas from coal by a Belgian chemist, Jan van Helmont in 1609, and the first commercial gasification of coal pioneered by Scottish engineer, William Murdock in 1792, coal has been the dominant energy source in industrialized regions in the world for the several centuries [2], [3]. By the mid 1920s, coal supplied about 20% of the gas in the U.S. About 20,000 gasifiers were in operation prior to World War II [2], [3], and about 60% of U.S. energy needs were supplied by coal by the end of World War II [2].

The biomass gasification is a particularly interesting energy conversion process, because the gasification product, namely syngas, has the flexibility to be processed to various forms of fuels required in today's world, which are mostly gaseous or liquid. Conversion to gaseous fuels is also advantageous in terms of transportation, because gases (or liquids) can be handled easily with a system of pipes, tanks, pumps, and valves, while solid fuels needs to be loaded to and from rail cars or trucks, can be eroded during moving and storage, and needs to be crushed or pulverized to use in conventional combustion processes [2]. Another advantage is that the gasification process provides opportunities to clean impurities contained in the biomass during the process in which the biomass is converted to the gas. If biomass is simply burned for heat, these opportunities would be lost and the contaminants could escape into the atmosphere. Once the biomass is converted to a gaseous form, the syngas can be further processed to make it suitable for the specific end use. Final forms of syngas processing include hydrogen, liquid

hydrocarbon fuels, electricity and some useful chemicals such as aldehydes and alcohols. Hydrogen production is a principal use of syngas, and this hydrogen is used in the synthesis of ammonia [4]. Hydrogen can also be used in fuel cells if a high purity is achieved. Environmental concerns have also been a driving force for increasing hydrogen use as a clean fuel [4]. The manufacture of methanol for the synthesis of methyl t-butyl ether (MTBE) is another use of syngas. Chemicals and liquid fuel processing through Fischer-Tropsch synthesis (FTS) is the third largest use of syngas. Syngas is also available for a chemical feedstock. As an example, the hydroformylation of olefins to aldehydes and alcohols is the fourth largest use of syngas [4]. Furthermore, syngas is a moderately high heating value fuel, which can be combusted in turbines to generate electricity.

The Fischer-Tropsch synthesis of liquid fuels is a particularly interesting use of syngas, because biomass gasification to FTS diesel and gasoline production is the only method to produce renewable, carbon neutral liquid transportation fuels [5]. Transportation fuel demand has increased constantly in the United States (Figure 1-2) as well as other parts of the world. The EIA reported that the transportation sector consumed about 30.595 EJ (29 Quadrillion BTU) of energy in year 2007 in the United States [1]. This ranks transportation as the second largest energy consumption sector comprising 29% of the total end-use energy consumption.

The fuel demand is expected to keep increasing in the future, and the EIA forecasts that the transportation fuel consumption will increase to 34.815 EJ (33 Quadrillion BTU) by the year 2030 [1]. Thus, it is particularly important to develop a secure method of clean and renewable liquid transportation products, and biodiesel production from syngas via FTS may serve a primary roll. Meanwhile, the equipment efficiency improvement, namely fleet mileage increase over the years, is also an important factor when the history and forecast of transportation fuel

demand is considered. The fleet mileage performance has been increased constantly over the past decades. According to the U.S. Department of Transportation, it was reported that a passenger car average mileage increased from 19.9 MPG in 1978 to 28.8 MPG in 1988, while that of light trucks changed from 18.2 MPG in 1979 to 21.3 MPG in 1988 [6]. In the year 2006, the overall average fleet mileage was 29.0 mpg [6]. The change of the average fleet mileage in U.S. from 1980 to 2006 is provided in Figure 1-3.

Because of the factors discussed above, it can be said that biomass gasification for syngas production is a very attractive and promising technology to support the future energy demand as well as the transition the energy use from a petroleum base to a more renewable base. Therefore, it is very important to analyze and understand the gasification system and establish an optimum operation procedure for better utilizing existing renewable energy sources such as woody biomass. This study was initiated for the purpose of investigating the use of Florida woody biomass to make a gaseous fuel called syngas. This dissertation has been organized to cover several topics including the Florida woody biomass (pine tree) availability, general methods of gasification and the use of an innovative high temperature gasification process to produce syngas using Florida pine as a feedstock. Parallel studies conducted during this dissertation focused on using the syngas from the gasification of woody biomass to liquid fuels using catalytic reactors.

1.2 Ecology and Commercial Use of Florida Pine Trees

This section discusses the ecology of several pine trees in Florida and their commercial use. The purpose of this section is to discuss the availability of Florida's pine trees as renewable energy crops for the biomass gasification process.

The pine flatwoods are the most extensive type of ecosystem in Florida and occupy about 50% of the natural land area in the state [7]. Besides forming a floral ecosystem, these flatwoods also serve as very important habitat for various animals including many populations of birds,

small and large mammals, 20 to 30 species of amphibians and reptiles and small birds [7]. There are about 10 kinds of pine trees commonly found in Florida; among them Slash Pine (*Pinus elliottii* Engelm.), Longleaf Pine (*Pinus plaustris* Mill.) and Loblolly Pine (*Pinus taeda* L.) are the dominant types today. Historically, Longleaf Pine is the dominant type of tree in the Florida flatwood ecosystem, however the majority of the original longleaf are now replaced by faster-growing Slash Pine. The dominance of Slash Pine is expected to grow as the state government recommends the commercial growth of this kind for timber plantation.

1.2.1 Slash Pine

Slash Pines (*Pinus elliottii*) are hard yellow pines distributed over the southeastern United States (Figure 1-4). Because of its rapid growth, it is very valuable in reforestation projects and timber plantations and one of the most frequently planted species [8]. Slash Pine is found in the range over 8^{o} latitude and 10^{o} longitude [8] and favors flatwoods, wet lowlands such as swamps and ponds. It takes about 30 years to become saw timber size which diameter of about 0.23 m (9 inches). Slash Pine is a medium to large size tree and can reach a height of 73 to 105 m (240 to 345 ft).

1.2.2 Longleaf Pine

Longleaf Pine (*Pinus palustris*) is also found in the southeastern United States (Figure 1-5). It once occupied about 60 million acres in this area, though the coverage reduced to only 4 million acres in 1985 as it was replaced by Slash Pines [8]. Several modern reforestation projects try to restore the longleaf pines. Longleaf pine inhabits a wide range of sites from wet and poorly drained flatwoods to dry, rocky mountain terrain [8]. Longleaf pine is a medium to large size tree, which reaches the height of 73 to 91 m (240 to 300 ft), but it takes 100 to 150 years to grow to full size.

1.2.3 Loblolly Pine

Loblolly pine (*Pinus taeda*) is the most important commercial timber in the southeastern United States and constitutes more than 50% of the pines in the area (Figure 1-6) [8]. It is a fast-growing type tree and widely grown in plantation and commercial timber plantations. It grows in the coastal plain, Piedmont regions, favors acid soils, but can adapt to variety of sites. Because of its high biomass productivity, various studies have been done on loblolly trees as an alternative energy source. Commercially, it is used for pulp and paper, lumber and plywood. The height of loblolly threes could reach around 82 to 100 m (270 to 330 ft).

1.2.4 Sand Pine

Sand Pine (*Pinus clausa* Vasey) is one of the minor southern pines with its natural habitat almost limited to Florida (Figure 1-7) [8]. The largest concentration of sand pine stands occupies 250,000 acres in the Ocala National Forest. The tree favors acidic soils for its habitat. It generally takes approximately 8 to 10 years for sand pine to reach a height of 5 to 10 m (16.4 to 32.8 ft), and 15 to 18 years to reach 20 m (65.6 ft). Due to its relatively small height, the commercial value is limited to some pulpwood or fuel uses.

1.2.5 Utilization of Florida Pine Trees

There are various commercial products made from timber resources in Florida ranging from a large variety of pulp and paper products to other miscellaneous products such as soap, cosmetics perfume, shampoo and chewing gum. Although Florida pine trees are used to make various commercial products, the interest to utilize pine trees as the energy production feedstock is increasing as well. Miles Andrews, a member of Timberland harvesters, the largest wood dealers in the southeastern United States, says that “for the past several years the timber industry all over the U.S. seems to have gotten worse with each passing year and many forest land owners

are not re-planting their lands". However, he has "chosen to grow timber on (his) land for a profit" and he has a strong desire to keep his timber land, since he knows his timber land "produce(s) clean air, clean water, wildlife habitat and recreational opportunities" and "has supported the communities and small towns and the way of life that makes (the) part of the state unique". Therefore, rather than reducing his practice in a period of economic down time in the timber industry, he seeks a possibility of utilizing his timber resources as energy production feedstock.

1.3 Overview of Biomass Gasification

This section discusses the general overview of biomass gasification process starting from the definition of biomass, chemical reactions involved in the process, type of reactors used, operation parameters, contaminants and their treatments, syngas composition, applications of syngas and the final products. The purpose of this section is to provide the gasification process fundamentals which are necessary to understand the analytical and experimental studies for the high-temperature biomass gasification system in the following chapters.

1.3.1 Biomass

Biomass is any organic materials from recently living plants and animals. Biomass is available in various forms such as residues from agricultural products, forestry, municipal solid waste or sewage. Biomass is originally formed from plant photosynthesis, a mechanism involving sunlight, atmospheric carbon dioxide and water according to the following reaction:

$$6H_2O + 6CO_2 \rightarrow C_6H_{12}O_6 + 6O_2 \qquad 1\text{-}1$$

Photosynthesis is a conversion process of sunlight to chemical energy. This converted energy is stored in chemical bonds of plants. When the bonds between adjacent carbon, hydrogen and oxygen molecules in plants are broken, the stored chemical energy is released [9] as some

forms of energy. (Therefore, biomass conversion such as gasification is really an energy extraction from chemical bonds in plants by thermally breaking the bonds.) Biomass contains cellulose, hemi-cellulose, and lignin with an average composition of $C_6H_{10}O_5$ [10]. The cellulose and lignin content is one of the important characteristics in the biomass to affect the pyrolysis rate. A study shows that the pyrolysis rate is fast with high cellulose content and is slow with high lignin content. Biomass is generally considered as carbon neutral fuel source, since carbon dioxide emitted during biomass processing such as gasification is simply what is originally absorbed from atmosphere during photosynthesis when plants grow. Coal and petroleum share the same carbon cycle characteristics as biomass. However, in case of coal and petroleum, it takes millions of years to convert plants and animals into fossil fuels unlike biomass growth and utilization cycle, which occurs in much shorter time period. Thus, burning fossil fuels use old carbon dioxide captured by ancient plants and converts it to new carbon dioxide, which would otherwise not contribute to the amount of carbon dioxide in the atmosphere. For the same reason, fossilized fuels are not renewable within a time-scale of mankind [9].

Biomass is the oldest energy source and has been the primary source of energy to mankind, but its contribution to the primary energy consumption in developed countries is small in today's world [11]. In nineteenth century, coal began to be exploited in quantity and in twentieth century, petroleum fuels dominated the energy consumption, and biomass was gradually substituted to cheap coal, petroleum and natural gas. On top of these cost economics, solid biomass had a huge disadvantage when various technological applications required liquid and gaseous form of fuels for transportation and domestic and industrial use.

However, there are growing social, environmental and economic concern regarding energy issues including carbon dioxide emissions resulting from fossil fuel consumption, forecast of depletion of fossil based fuel in near future and resulting price increase in oil, interest to renewable energy for sustainability, independence from insecure foreign oil and so on. Especially, concerns grow for global warming and the resulting climate change by carbon dioxide emission from consumption of fossil fuels. To reduce the carbon dioxide emissions, it is required to increase the share of renewable energy in the primary energy consumption, and biomass is considered to be one of the most important renewable energy sources [11]. Water vapor is another greenhouse gas, and is actually the most abundant type of greenhouse gas. Although it is generally accepted that human activities do not affect the concentration of water vapor in the atmosphere [12], [1], it is also true that the measurements of global water vapor has been poor compare with carbon dioxide and methane measurements [13]. Thus it is advisable to be cautious about water consumptions and water vapor emissions involved in biomass growth, when the biomass selection is made.

Because of these factors, renewable biomass as an alternative energy is regaining its popularity today. Biomass is carbon neutral, renewable, and is indigenous energy source available in most countries [9]. Especially if an efficient conversion process of biomass to gaseous and liquid form of fuel is established, biomass could become an important energy resource again [14].

For the high-temperature biomass gasification study, woody biomass (pine trees local to Florida) was selected as fuel. The detailed description about biomass properties is provided in Chapters 2 and 3.

1.3.2 Gasification Reaction

Gasification is a thermochemical conversion of solid carbonaceous fuel such as biomass and coal by partial oxidation to a gaseous product called synthesis gas or syngas. The main objective of gasification is to convert the solid biomass to gaseous form, which can be more easily handled for various applications requiring gaseous and liquid form of energy, not a solid form. For biomass gasification, this conversion occurs when biomass feedstock reacts with oxidant. Oxidant includes air, pure oxygen, steam or mixture of them. There is also catalytic steam gasification of which the presence of catalyst influences the overall performance and efficiency [15]. The product gas can be categorized to three groups depending on its heating value content. Low heating value gas ranging from 4-6 MJ/Nm^3 is produced when air and steam/air is used for oxidant. This low heating value is due to the nitrogen in air, which dilute the product gas. Air is the typical gasification oxidant in small scale operations of up to about 50 MW [15]. Medium heating value gas contains 12-18 MJ/Nm^3 and is produced when oxygen and steam are used for oxidant. Finally high heating value gas with 40 MJ/Nm^3 is produced when hydrogen and hydrogenation are used [15]. The reaction generally occurs at temperature ranging from 500 to 1400^oC. The product gas, syngas is composed primarily by hydrogen (H_2) and carbon monoxide (CO) together with smaller amounts of carbon dioxide (CO_2), water (H_2O), methane (CH_4), higher hydrocarbons and nitrogen (N_2) if air is used for oxidant. Unlike combustion, which is complete oxidation reaction, gasification reaction involves partial oxidation, therefore, gasification products could be thought as intermediate products of combustion. There are also various contaminants exist in product gas such as small char particles, ash and tars. The syngas can be either used directly in gaseous form or further react to other gaseous or liquid fuels, or chemicals. Syngas can be 1) burned externally in a boiler for

producing hot water 2) used in a gas turbine for electricity production 3) used as a fuel in an internal combustion engine and 4) used to upgrade methanol through synthesis [14], [3].

1.3.3 Pyrolysis

Pyrolysis is a thermal decomposition of solid fuel into simple molecules in the absence of an oxidizing agent. Pyrolysis is an endothermic process requiring an external heat source, and the reaction typically occurs at temperature range of 200 to 500^{o}C [16][9,15]. Prior to pyrolysis reaction, original biomass feedstock needs to be dried. Once moisture is removed, dry feedstock can go through this devolatization reaction. The pyrolysis produces mixture of liquid and gaseous volatile matter, oil and tars, and solid carbonaceous char [17], [18]. The actual pyrolysis reaction is very complicated as it involves the formation of more than a hundred intermediates [18]. Mathieu et al [19] obtained the experimental compositions of pyrolysis products from beech wood with a residence time of one second at 1088K as 0.057 kg char, 0.758 kg dry gas, 0.06 kg tar and 0.125kg water per 1 kg of biomass. The dry gas contains 21.2 vol% hydrogen, 50.5 vol% carbon monoxide, 13.2 vol% methane, 11.4 vol% carbon dioxide and 3.7 vol% C_{2+} hydrocarbons [19]. The gaseous part of volatiles can be used as a fuel to produce heat for power generation or synthesized to produce methanol, while the liquid portion can be processed to hydrocarbon liquids fuels for combustion engines. Char forms the residual solids having a higher concentration of carbon than the dry feedstock. This concentrated carbon in char is used for the following gasification reactions. In general, the most important parameters to affect the pyrolysis process are temperature, concentration, time and heating condition [18].

1.3.4 In a Gasification Reactor

In general biomass gasification, typical flow of reaction process is the combustion of part of biomass followed by pyrolysis of dry biomass and finally gasification of carbon produced in pyrolysis. These reactions occur in complex and competing manner, and in a varying degree.

Depending on the gasification configuration, typical major reactions taken place in a gasifier are the followings [15], [10]:

$$C + O_2 \rightarrow CO_2 \qquad \Delta h_{298} = -394\,kJ/mol \tag{1-2}$$

$$C + \frac{1}{2}O_2 \rightarrow CO \qquad \Delta h_{298} = -268\,kJ/mol \tag{1-3}$$

$$H_2 + \frac{1}{2}O_2 \rightarrow H_2O \qquad \Delta h_{298} = -241.8\,kJ/mol \tag{1-4}$$

$$C + H_2O \rightleftharpoons CO + H_2 \qquad \Delta h_{298} = 131.3\,kJ/mol \tag{1-5}$$

$$C + 2H_2O \rightleftharpoons CO_2 + 2H_2 \qquad \Delta h_{298} = 89.7\,kJ/mol \tag{1-6}$$

$$C + CO_2 \rightleftharpoons 2CO \qquad \Delta h_{298} = 172.1\,kJ/mol \tag{1-7}$$

$$C + 2H_2 \rightleftharpoons CH_4 \qquad \Delta h_{298} = 52.47\,kJ/mol \tag{1-8}$$

$$CO + H_2O \rightleftharpoons H_2 + CO_2 \qquad \Delta h_{298} = -41.2\,kJ/mol \tag{1-9}$$

$$CO + 3H_2 \rightleftharpoons CH_4 + H_2O \qquad \Delta h_{298} = -88\,kJ/mol \tag{1-10}$$

$$C + H_2O \rightleftharpoons \frac{1}{2}CH_4 + \frac{1}{2}CO_2 \qquad \Delta h_{298} = 7.7\,kJ/mol \tag{1-11}$$

Equations 1-2 to 1-4 are exothermic combustion reactions. Most of oxygen injected to the gasification reactor is consumed in these reactions. The purpose of these reactions is to provide the heat required to dry the biomass and to conduct the following endothermic reactions. The gasifiers self-sufficient in heat are called auto-thermal and the ones require external heat input are called allothermal, while most common gasifiers are auto-thermal [15]. The high-temperature biomass gasification study discussed in the following chapters uses allothermal gasification. It is considered to be allothermal because all the heat required for both pyrolysis and gasification is provided by high-temperature steam created by the combustion of hydrogen and oxygen, and none of the biomass is combusted for the heat supply.

Once sufficient moisture is removed from the original feedstock and enough heat is supplied, dry biomass goes through the pyrolysis reaction. During pyrolysis, dry biomass is decomposed to char, volatiles and also form some tars. Then carbons in char are used for the following gasification reactions.

Equations 1-5 to 1-11 represent the major gasification reactions. Equations 1-5 and 1-6 are known as water-gas reactions, where Equation 1-5 is the primary and Equation 1-6 is the secondary reaction. These are the principal reactions in the gasification process, and require heat input. They prefer high temperatures and low pressures to proceed.

Equation 1-7 is called the Boudouard reaction, and is the equilibrium reaction between carbon (graphite) plus carbon dioxide and carbon monoxide. Without catalyst, the reaction rate is much slower than the combustion reaction (Equation 1-2). According to Le Chatelier's Principle, the equilibrium is on the exothermic carbon dioxide side at low temperature condition, and is on the endothermic carbon monoxide side at high temperature. In temperature range of typical biomass gasification or above 1000^{o}C [19], Boudouard reaction is endothermic and produce carbon monoxide.

Equation 1-8 is called hydro-gasification. Without high pressure condition, this reaction is very slow.

Equation 1-9 is water-gas shift reaction. This is an equilibrium reaction of carbon monoxide and water to form hydrogen and carbon dioxide, and is important when hydrogen production is preferred. With a presence of catalyst such as magnetite (Fe_3O_4), it may reach equilibrium at temperature about around 250^{o}C [20]. At higher temperature, the direction of the reaction shifts towards the reactants. Pressure does not have any effect on this reaction in terms of hydrogen production.

Equation 1-10 is known as methanation, and the main purpose of this reaction is either to remove carbon monoxide from the gas or to produce methane. Without catalyst, this reaction is very slow at low temperatures.

Equation 1-11 is another methanation reaction. It is seen from the enthalpy of combustion at standard state that this reaction is fairly thermal neutral. This reaction could produce more methane with small amount of heat input, but the reaction rate is compare with water-gas reactions without catalyst.

Due to heat and mass transfer limitation, gas to gas phase reactions are much more rapid than solid to gas phase reactions. Thus, among all reactions starting from combustion, pyrolysis to gasification, the slowest are the gasification reactions of solid carbon in char to gas phase reactions (Equations 1-5 to 1-8 and 1-11). However, reaction rate of Equation 1-8, hydro-gasification reaction, can be increased under high pressure and that of Equation 1-11 can also be increased with catalytic use. Therefore, the remaining water-gas reactions and Boudouard reaction are the overall rate limiting reactions in gasification process [10]. A study suggests that water-gas reactions and Boudouard reaction could particularly be prevailing for gasification temperatures above 830^{o}C [21].

1.3.5 Gasification Reactor Types

Gasification processes are classified based on how fuel (biomass) comes to contact with the gasifying medium or oxidant. The three principal types of gasifiers are fixed bed, fluidized bed and entrained bed gasifiers, where fixed bed gasifiers are further classified to updraft and downdraft gasifiers.

1.3.5.1 Updraft fixed-bed reactor

Updraft fixed-bed gasifiers have the simplest structure among four types of gasifiers mentioned above, and were the first type of gasifier developed. Fixed bed gasifiers are generally

used in the small-scale application while fluidized bed gasifiers are more suitable for larger scale [22]. In updraft fixed-bed gasifier fuel (biomass) is introduced from the top and oxidant is supplied from the bottom of the gasifier (Figure 1-8). The reacting bed is supported by a grate at the bottom of the reactor and oxidants supplied from the bottom diffuse up through it. When oxidants meet the biomass at the bottom of the bed, combustion reaction takes place to produce high temperature heat and carbon dioxide and water as products. These hot carbon dioxide and water reduce char to hydrogen and carbon monoxide and cooled to around 750^{o}C. This remaining gas of hydrogen and carbon monoxide continues moving up the reactor to pyrolyse, heat and dry the descending biomass. The tars are produced mainly during the pyrolysis process. Since there is no high temperature zone after pyrolysis zone to thermally destroy the tars, large amount of tars are produced in updraft fixed bed gasification [22]. After all these processes, the gas and tars leave from the top of the reactor at the temperature around 500^{o}C [22], [14]. Some of the advantages of updraft fixed bed gasifier include simple structure, low cost, ability to handle feedstock with high moisture and inorganic contents and well proven system. The main disadvantage is the high tar content in syngas. These tars are required to be cleaned before the syngas is used for engine, turbine and synthesis applications. Updraft fixed-bed reactor was chosen for the high-temperature biomass gasification study which was discussed in more details in the following chapters.

1.3.5.2 Downdraft fixed-bed reactor

Downdraft fixed-bed gasifiers have the similar mechanism as updraft fixed bed gasifiers. The difference is in downdraft gaifiers, both fuel (biomass) and oxidant are introduced from the top of the reactors and move down concurrently (Figure 1-9). The purpose of this different structure is to reduce the tar content in syngas, which was the main issue in updraft fixed bed gasifiers. The reaction zone order from the top are drying, pyrolysis, oxidation and reduction and

finally syngas with low tar content appear at the bottom [22]. Downdraft fixed bed gasifiers share the similar advantages as updraft gasifiers such as simple structure, low cost, but the largest advantage is the small amount of tar content in syngas. Some disadvantages include slagging and sintering of ash, requirement of feed drying and low carbon conversion rate [22]. Various studies have been done on modified fixed bed gasifiers aiming to improve the efficiency of gasification process. For instance, a twin-fired fixed bed, which combines the advantages of both updraft and down draft gaifiers and avoid the disadvantages of both. More specifically, this gasifier has two air feeding openings at upper portion and lower portion. Unlike a typical downdraft fixed bed gasifier, there is another high temperature zone above the grate to oxidize pyrolysis char, which contributes to lower amount of tar formation [22]. Another modification of gasification process is two-stage gasification, which implements pyrolysis and gasification process separately. Contrast to a typical gasification where pyrolysis and gasification occur in one chamber, the two-stage gasifier provides a better opportunity of controlling the process temperatures resulting in less amount of tar production [23].

1.3.5.3 Fluidized bed reactor

In a fluidized bed gasifier, there exists a vertical upward gas stream through inert particulate materials [14]. The rapid turbulent mixing and heat transfer bring uniform composition and temperature throughout the reactor, therefore, there is no distinct zone of combustion, pyrolysis and tar cracking exist [3], [14]. Advantages of fluidized bed are uniform product gas, uniform temperature distribution throughout the reactor, acceptance of a wide range of fuel particle sizes and moisture content, whereas disadvantages include high exit gas temperature and high particulate burdens in gas [14]. There are several studies on modified fluidized bed gasification processes. A process called supercritical water fluidized bed gasification is a gasification process which uses water temperature higher than its critical

temperature (647K) and the critical pressure (22.1 MPa) [24]. Under this condition, biomass is rapidly decomposed to smaller molecules and can achieve the carbon gasification efficiency of close to unity [24].

1.3.5.4 Entrained bed reactor

In an entrained flow gasifier, feed is finely pulverized and enter the reactor together with oxidants. This type of gasifier has high operation temperatures at around 1100 to 1400^{o}C. Entrained flow gasifiers are originally developed for steam-oxygen gasification of coal, and contain various advantages including ability to gasify all type of coals, uniform temperature in reactor and very short fuel residence times. However, there are also other requirements such as very finely sized homogeneous solid fuel range of 1 to 3 mm [25] and large amount of sensible heat [3]. These requirements prohibits the economical application of this type of gasifiers to biomass gasification because it is very expensive to reduce the size of biomass to meet the criteria and difficult of meet the high temperature with biomass due to its low energy density [14].

1.3.5.5 Plasma gasification

The plasma arc biomass gasification process is an application of plasma use to syngas production. However, the main recognition of plasma arc gasification in the recent decades has been as a waste treatment technology rather than a syngas production system. The type of waste treated includes municipal solid waste (MSW), industrial hazardous waste, medical waste and incinerator ash. In the plasma arc gasifier, the plasma, hot ionized gas from an electrical discharge, created by an electrical energy input [26] heats gases such as oxygen or nitrogen to 3000^{o}C or above. This extremely hot gas can then serve as a heat source for other applications. In the case of waste treatment, the main objective is to decompose waste materials to harmless simple chemical structures by the extremely high temperature gas. A controlled amount of

oxygen is fed to gasify waste materials to insure that the gasification, not the combustion reaction occurs. This process melts or vitrifies the inorganic fraction of the wastes and gasifies the organic fraction of the wastes [26]. Depending on the waste composition and the heating value, it is possible to obtain syngas as a product. This syngas can be used for electricity generation by going through a combustion turbine combined cycle (CTCC), and the product electricity can be used to support the plasma and other applications if excess electricity is left. However, due to economic cost, combining plasma arc gasification and CTCC is not justifiable unless a large scale waste treatment facility is considered. For example, one MSW treatment facility in Yoshii, Japan (25 TPD) is not combined with CTCC system, while another plant, the EcoValley Plant in Utashinai, Japan (166 TPD) is large enough to be combined with a power generation system.

Advantages of plasma arc gasifiers include a very low level of tar production due to the extremely high temperature gasification [26], [27] and decomposition of dioxins and furans when treating hazardous wastes. The disadvantage is its high cost to create high temperature plasma. There are also issues with a short equipment life and frequent maintenance requirement due to high thermal burden from the high temperature operation [28]. In spite of the high electrical power consumption and unnecessary high plasma temperature for the pyrolysis process, studies of plasma arc gasification of biomass for syngas production are carried on aiming to improve the process performance by better design of the system [28], [29], [26], [27]. For example, Tang et al. conducted capacitively coupled radio frequency (RF) plasma pyrolysis of wood to study the effect of RF power, operation pressure and an electrode structure on the conversion performance [28]. It was found that the solid conversion increased from 38.8 to 76.4%, and the hydrogen yield increased from 0.65 to 1.14cm^3/s, when the RF power was

increased from 1600 to 2000 W. It was also found that both solid conversion and hydrogen yield increased as the operation pressure increased from 3 to 8 kPa. It was found that an increase in electrode distance leads to decreases in concentration of product gas components and the solid conversion.

1.3.6 Pyrolysis/Gasification Operation Parameters

There are various feedstock properties and operation parameters to affect the pyrolytic and gasification product components. The major parameters to be considers are feedstock composition, feedstock pretreatment, heating rate and residence time in the gasification reactor the reactor temperature, and air and steam ratio.

1.3.6.1 Feedstock composition

Biomass feedstock properties can be expressed in some chemical analyses: ultimate analysis, proximate analysis and biochemical analysis. Ultimate analysis is a type of chemical analysis to tell the elemental composition of the biomass such as carbon, hydrogen, oxygen, nitrogen, sulfur, and chlorine along with moisture and ash. This information is critical to compute the mass balance on biomass conversion during gasification process. Proximate analysis reports moisture, volatile matter, fixed carbon and ash content in biomass. This information is important in developing thermochemical conversion processes. Biochemical analysis reports plant chemicals including proteins, oils, sugars, starches and lignocellulose (fiber) [14]. Hanaoka et al [30] studied the effects of woody biomass biochemical composition such as cellulose, xylan and lignin on air-steam gasification and found the conversions on a carbon basis were 97.9%, 92.2%, and 52.8%, respectively. It was also found that the fundamental information of cellulose and lignin components in biomass affect char reactivity considerably, and can be used to predict the product gas composition [21], [30].

Heating value is another important parameter to evaluate biomass property. The heating value defines the energy content of a biomass fuel and is one of the most important characteristics parameters for designing thermal systems [31]. The heating value of a biomass can be determined experimentally using a bomb calorimeter, while many attempts have been made to estimate the heating value based on the results of ultimate [32], proximate [33] and bio-chemical analysis for thermal system modeling and calculations.

1.3.6.2 Feedstock pretreatment

Feed pretreatment involves size and shape selection and moisture content control of biomass. Feedstock preparation is very important in planning the overall gasification process because the particle shape and the particle size of biomass could largely influence the gasification operation.

Size of the feedstock is one of the important parameters to consider in feed pretreatment. As biomass particle size increases, heat flux and heating rate decrease. This results in slow pyrolysis rate thus requires longer time for devolatization reaction. However, the optimum particle size range depends on the type of gaisfier. Fixed bed gasifiers require chunks of material of several centimeters in diameter, while fluidized bed gasifiers require much finer particles [34], and woody biomass size range used are 0.3 mm to 40 mm [35], [19], [36], [37]. It is important to have uniform size particles for efficient operation, regardless the size required for the certain gasification process. Chipping is one of the size reduction methods to be used. The energy required for chipping woody biomass to 1 to 1.5 cm size is about 1% of heating value of the wood itself. However, considering some heat loss and mechanical inefficiency in gasification operation, the actual energy required could become about 5% of gross heating value [34]. Conventional fixed bed gasifiers utilizing wood based biomass as feedstock use woodchips with size ranging from 8 cm x 4 cm x 4 cm to 1 cm x 0.5 cm x 0.5 cm [38]. Saravanakumar et al. [38]

have operated an air-blown updraft fixed bed gasifier using long wood stick of 68 cm x 6 cm in aim of minimizing the issues relating to size reduction of woods including consumption of electricity, high manpower requirement, dust collection, noise production. (They obtained the product gas with calorific value of about 4200 kJ/m^3.)

Shape of feedstock could also influence the gasification performance. Kramreiter et al. [22] have demonstrated a pilot plant gasification twin-fire fixed bed gasification, which combines the structure and advantages of updraft and downdraft fixed bed gasifiers. In this demonstration, they used and compared the woody biomass chips of particle size between 11.2 mm and 31.5 mm and proved that wood chips with spherical particles are superior in operational behavior to those with long and sharp, because spherical particles prompt smooth flow behavior and avoid the formation of bridges in the gasifier.

Moisture content control of biomass feedstock is an important aspect. High moisture content in feedstock reduces the reaction temperature due to its evaporation in gasification process, which may increase the methane (CH_4) content and decrease the hydrogen (H_2) content in product gas. Therefore, gasification of biomass with high moisture content requires higher system energy input. The biomass is generally air dry first to about 20% of moisture content, then is further dried with driers to the moisture below 10-15% prior to gasification process [15].

1.3.6.3 Heating rate

It is difficult to clearly mention the effect of heating rate on pyrolysis since several other parameters also need to be changed to control the heating rate. However the general understanding is that rapid heating and high temperature in pyrolysis results in liquids, higher volatile components, and highly reactive char [39], [40]. With slow heating rate, the condition gives enough time for char and volatiles to react further to produce more amounts of char. Thus higher char yield is expected with slow heating rate.

1.3.6.4 Residence time

In general, longer residence time of the volatile phase results in a larger amount of product gas, because a long residence time offers a better chance for tars to be cracked. However, the optimum residence time still varies depending on the process conditions. For example, the optimum residence time could be longer when the pyrolysis temperature is low [39].

1.3.6.5 Reactor temperature

Temperature significantly affects the pyrolysis product composition. High temperature promotes higher amount of gas production and low temperature results in higher proportion of solid fraction like char and tars [39]. In general, as reactor temperature increases the gas and hydrogen yields increases while higher heating value (HHV) in the product remains fairly constant. Keeping the other parameters identical, the use of different oxidation agent affects the reactor temperature. When steam is used for oxidation agent, while the content of hydrogen in the product gas increases, the process temperature decreases sharply [41].

1.3.6.6 Air and steam ratios

The air to fuel ratio, steam to fuel (biomass) ratio are also factors to affect the gasification product composition. Van der Drift et al. [37] studied the relationship between air to fuel ratio in an atmospheric air-blown circulating fluidized-bed gasifier of the size of 500 kWth, and found that the higher heating value of the product gas HHV decreases linearly with increasing air to fuel ratio ranging from 0.3 to 0.65. This result is also supported by Prins et al. [42] who compared the energy content in the product gas of air gasification and steam gasification, and obtained air to fuel ratio of 0.25 as the point of producing the maximum heating value gas. At low air to fuel ratio, small amount of oxygen supply limits the production of hydrocarbons. Since hydrocarbons have high heating values, higher concentration of hydrocarbons in the product gas

at low air to fuel ratio contributes to high overall heating value of the gas and a low concentration of hydrocarbons at high air to fuel ratio results in low heating value gas.

When steam, in lieu of air is used as an oxidation media, steam to biomass ratio becomes an important factor. Franco et al. [21] studied some effects of steam to biomass ratio in a bench scale fluidized bed reactor with the operation temperature ranging from 730 to 850^{o}C. It was observed that the production of gaseous product favoring in hydrogen production was the maximum at steam to biomass ratio of 0.6 to 0.7 w/w. The gas yield, energy and carbon conversion were also maximum at this range of ratio. Contrary, heating value was observed to be the minimum at this range of ratio. The resulting low heating value is caused by the same reason as air to fuel ratio case where low concentration of carbon monoxide and other hydrocarbons resulted in an overall low heating value gas.

1.3.7 Contaminants

The product gas from gasification generally contains several contaminants including particulates, alkali compounds, tars, BTX, nitrogen-containing compound, sulfur and low-molecular weight hydrocarbons such as methane and ethane [43], [10]. It is important to eliminate these contaminants from the syngas because the following fuel processing and energy conversions such as Fischer-Tropsch synthesis and gas turbines are very sensitive to some of these contaminants. It is also important to eliminate the contaminants for environmental and public health point of view.

1.3.7.1 Particulates

Particulates are solid-phase materials such as inorganic ash from mineral matter in biomass, unconverted char, and some materials from gasifier bed. Particulates need to be removed from the product gas because they could damage the downstream equipments. Particulates from char are formed when the biomass is not completely gasified. Since large-scale gasifiers can convert

the carbon from the biomass in 98 to 99% efficiency, remaining 1 to 2% of carbon would be left as solid particulates at the end. The re-injection of this unconverted carbon can not only reduce the particulates formation but also increase conversion efficiency, and subsequently overall gasification efficiencies.

1.3.7.2 Alkali compounds

Alkali compounds are another type of contaminants found in gasification product gas and formed particularly from potassium in biomass. Alkali compounds can vaporize at about 700^{o}C and start to condensate at about 650^{o}C. Alkali compounds deposit on cool surface such as heat exchanger and turbine blade and harm the equipment performance. Alkali salts are also corrosive to metal surface and poisonous to some catalysts in tar cracking and syngas applications [10].

1.3.7.3 Tar treatment

Tar is generally considered to be one of the most unpleasant constituents in the gasification product gas. Tar is defined as "all organic contaminants with a molecular weight larger than benzene" [44] and has boiling points between 80 to 350^{o}C [11]. Tar is formed mostly during pyrolysis process and is one of the main issues in biomass gasification. If syngas is used for the further applications without properly cleaned, tars can deposit on surfaces of equipment including internal combustion engine, fuel cell, methanol synthesis reactions and cause detrimental effects on their performance and thus increase maintenance requirement [45], [46], [47]. Tars also lower cold gas efficiency of system and lower heating value of the fuel gas produced [46]. It is also important to properly clean tars because tars have carcinogenic characteristics [48] and could be harmful to human health. Therefore, it is required to efficiently process and eliminate the tars from the syngas before it is further processed. When syngas is used for Fischer-Tropsch synthesis, the concentration of tar must be below condensation point at FTS pressure [43]. On the other hand, tars have significant amount of energy that can be

converted to useful form of fuel gases including hydrogen, carbon monoxide and methane [43], [49], thus it is important to crack tars into smaller hydrocarbons to increase the carbon monoxide and hydrogen amount in the gas. There are mainly two types of tar treatment categories, and classification depends on the location of the tar removed. One method is called primary method and tar is removed inside the gasifier. The other method is called secondary method and tar is removed from the syngas after the gas leaving the gasifier [47].

Secondary methods are the tar treatment methods conducted after the syngas leaving the gasifier. Secondary methods consist of two types of treatment: chemical and physical treatment. Chemical treatment is either thermal or catalytic tar cracking downstream the gasifier. Physical treatment is a tar removal from the gas using mechanical equipment such as filtering and wet scrubbing.

Primary method is a way of tar treatment conducted during the gasification process by either preventing the tar formation or by converting tar formed during the pyrolysis [47]. Cao et al. [46] suggest that the there are various operating parameters to control the tar formation such as temperature, gasifying agent, equivalence ratio, residence time and catalytic additives. Several studies were conducted to show that the formation of tars strongly depends on the gasification temperature. For example, Pan et al. [35] conducted experimental study on fluidized bed and showed that injecting secondary air during the gasification process at temperatures over 830 to 850^{o}C would decrease the tar contents of syngas by a factor of 3 to 9 depending on the type of feedstock. Cao et al. [46] studied a novel two-region (secondary air injection) combined fluidized bed gasifier with air as oxidant and showed that the tar formation could be controlled about 10 mg/Nm^{3} at optimal conditions. In this study, it was concluded that the optimum temperatures at the upper and bottom regions of gasifier were 860^{o}C and 750^{o}C, respectively.

Physical treatment is generally conducted at temperature at 150^{o}C or less [49]. Physical processes such as filtering and wet scrubbing are effective in removing the tar from syngas and require a simple maintenance. However, these methods do not truly alleviate the problem, since with these treatments, tar is not destroyed and could cause environmental issue during disposal of it [49].

Thermal processes require the producer gas to have the temperature at about 1000^{o}C in order to crack the heavy aromatic tars to species such as hydrogen, carbon monoxide and lighter hydrocarbons [49]. This high temperature process requires additional heat input to the system, which increases the operation cost. In the gasification experiment in this study, the high temperature gasification (1500^{o}C) with steam could help cracking tar to reduce the overall tar production.

Catalytic processes are generally operated at temperature range from 600^{o}C to 800^{o}C [49]. This temperature range is considered advantageous because the gas neither need to be cooled nor heated extensively. Catalytic tar conversion is also interesting because this process has a potential to eliminate tars at the same time increasing the conversion efficiencies of fuel to desirable products like hydrogen and carbon monoxide [48]. Furthermore, the presence of additive could influence the heating value of the product gas [50]. Catalysts used for catalytic conversion of tars or hot gas cleaning can also divided to two groups depending on where in gasification process the catalysts are used. A group called primary catalyst is added directly to the biomass prior to gasification [51]. Primary catalysts go through the gasification process together with biomass feedstock, thus share the same operation condition with them. With this method, tar is removed in the gasifier itself [48]. The second group of catalysts are used downstream of the gasifier in a secondary reactor [48], [51]. The typical catalysts used in the tar

removal include nickel-based catalysts, calcined dolomites and magnesites, zeolite, iron catalysts and olivine [50], [52], [53]. Among them, dolomite and nickel-based steam reforming catalysts are well proven catalysts for tar reduction.

1.3.7.4 BTX

BTX (benzene, toluene, and xylenes) are organic impurities and account for about 0.5 vol% of the syngas [43]. Like a tar cracking, a thermal tar cracker operated at above 1300^{o}C can crack all BTX [11]. Boerrigter [11] indicates that the removal of BTX from the syngas is more critical than tar removal since tars can be removed under conditions for BTX removal. The concentration of organic compounds like tars and BTX in syngas should be the level at which no condensation occurs when the gas is compressed to FTS pressure (25 to 60 bars), and the corresponding BTX concentration is 2500 ppmV (for 40 bar at 20^{o}C) [11]. Except for carbon monoxide and hydrogen, BTX is the third largest energy containing compounds (10.5 vol% LHV) in the syngas following to methane (24.1%) and ethylene (12.4%), while BTX is not a form to contribute to FTS [54]. Thus, in order to maximize the use of energy content in syngas, ideally BTX should be converted to carbon monoxide and hydrogen prior to FTS.

1.3.7.5 Nitrogen-containing compounds

Nitrogen oxide or NO_X is a type of contaminants formed as a result of gasification. Although the gasification product gas itself may contain a low level of NO_X, it is produced when the product gas is burned as fuel in later applications. NO_X is formed when nitrogen or nitrogen-containing molecules react with oxygen at elevated temperature. NO_X is considered to be detrimental pollutant because it could cause various health and environmental issues including respiratory problems, formation of acid rain, atmospheric visibility impairment, global warming, nutrient overloading in water ecology, further reactions to form toxic chemicals and so forth. Thus, it becomes very important to remove the nitrogen-containing compounds from the product

gas. One advantage of gasification, in terms of using gaseous biomass fuel rather than using solid biomass is that it provides an opportunity of better control the combustion process, which results in lowering the NO_X emissions.

1.3.7.6 Sulfur

Sulfur dioxide or SO_X is another type of contaminant in concern in gasification product gas. Generally, sulfur content of biomass is very low at less than 0.1% by weight in typical wood, thus SO_X level in product gas is below the requirement of cleanup. However, together with NO_X, SO_X is a major precursor of several health and environmental issues such as acid rain and respiratory illness. Furthermore, in terms of fuel processing and applications, even a small amount of sulfur could have negative effect on catalytic works in tar cracking and fuel cell systems. Therefore, careful removal of sulfur contaminants from the product gas is required.

1.3.7.7 Low-molecular weight hydrocarbons

Low-molecular weight hydrocarbons such as methane and ethane are generally beneficial for fuel gas as they add heating value to the gas. However, in syngas, they tend to be unreactive and reduce conversion efficiencies in syngas applications. Excess amount of lower number hydrocarbons could also be detrimental to catalysts in some systems.

1.3.8 Syngas Cleanup Methods

Particulate removal requirement level depends on the gas application: below 50 mg/Nm^3 for gas engines, below 15 mg/Nm^3 for turbines, and approximately 0.02 mg/Nm^3 for synthesis gas systems [10]. Primary types of physical particulate removal systems include cyclones, barrier filters, electrostatic filters, and wet scrubbers.

Cyclone is a primary system of bulk particulates removal using centrifugal force to separate solid from the gas. Cyclone is typically used as the first stage clean up system followed by a barrier filter as the second. In a fluidized bed reactor, a cyclone is already an integrated part of

the reactor. Cyclone can operates over a wide range of temperature, and remove more than 90% of particulates of about 5 μm with pressure drop of 0.01 atm [10]. Condensed tars and alkali materials can also be removed by a cyclone, but no vapor form of them is removed. Cyclones are readily available as many commercial systems are out by venders.

Barrier filter remove particulates by blocking the penetration of particulates with porous materials, and can remove particulates of 0.5 to 100 μm in size [10]. A barrier filter can be design to filter any small size of particulates, but with expense of increasing pressure drop. Once tars cling onto the filter surface, they could foul and plug the filter and it is difficult to remove them. When a cyclone and a barrier filter are used, product gas needs to be cooled prior to going through these cleaning systems.

Electrostatic filter works in such that high-voltage electrodes charge the particulates as the gas flowing through, then collector plates of opposite polarity collect the charged particulates. After particulate deposit on the collector place surface, they are removed from the plates by either wet or dry scrubber methods. Dry scrubber method can operate at temperature of 500^{o}C or above, but the wet method requires 65^{o}C [10]. Because of its physical size and high cost, electrostatic filters are cleanup system being best suited for large-scale operation.

Wet scrubbers remove particulates in the gas by spraying liquid water. Liquid droplets holding particulates descend from the gas to a demister [10]. Most wet scrubber use ventri design to create pressure drop to promote spraying, and particulate removal efficiency increases as pressure drop decreases [10]. Since this system uses liquid water, there is a restriction that the gas temperature needs to be below 100^{o}C [10].

1.3.9 Syngas Composition Adjustment

The syngas mainly consists of hydrogen, carbon monoxide, carbon dioxide and methane. This syngas composition can be adjusted either during the gasification in the same reactor or

after the gasification in a separate compartment, and the degree of adjustment depends on the need of the following processing and applications. Types of adjustment are steam methane reforming, water gas shift reaction and carbon dioxide removal.

The purpose of steam methane reforming is a conversion of methane with steam to carbon monoxide and hydrogen. While methane can add heating value to the gas, certain process such as Fischer-Tropsch synthesis prefers maximum amount of hydrogen and carbon monoxide in a certain ratio. Thus the methane reforming becomes important when high hydrogen and carbon monoxide contents are desired.

The water gas shift reaction is important when higher amount of hydrogen is desired in terms of adjusting the hydrogen to carbon monoxide ratio. This shift reaction converts carbon monoxide and steam to hydrogen and carbon dioxide. This is one of the three typical steps required in hydrogen production: steam gasification, water-gas shift reaction, and carbon dioxide removal process [55]. Typical aim to use this reaction is to eliminate carbon monoxide from the gasification product gas in order to obtain as pure hydrogen as possible for applications requiring high purity in hydrogen such as fuel cell systems. To achieve this purpose, several catalysts are used to decrease the reaction temperature and ceria-supported precious metals are the widely studied kind [56], [57], [58]. The ratio of hydrogen to carbon monoxide increases with residence time, but there exists a maximum value of hydrogen to carbon monoxide ratio for the different temperatures [59][5].

The carbon dioxide removal is also important process to reduce the amount of inert gases for FTS [5]. Again for hydrogen production from gasification, carbon dioxide removal is the final process commonly required. In case of hydrogen production from biomass gasification, Hanaoka et al. [60] studied steam gasification of woody biomass using calcium oxide (CaO) as

carbon dioxide absorption sorbent by combining typical gasification, water gas shift reaction and carbon dioxide absorption processes in one reactor, and demonstrated that calcium oxide to carbon dioxide ratio ([Ca]/[C]) of higher than unity would bring no carbon dioxide in the product gas. It was also shown that the hydrogen yield increased with increasing reaction temperature from 873 to 973 K, and the maximum hydrogen yield at [Ca]/[C] = 2, and 973 K was around 900 ml H_2/g-wood [60]. Furthermore, it was also proved that calcium oxide worked not only a sorbent of carbon dioxide, but also a catalyst to enhance the hydrogen production. In this case however, since the main objective was hydrogen production, there was no carbon monoxide contained in the product gas as required in some processes such as Fischer-Tropsch synthesis of liquid fuel.

1.3.10 Syngas Applications

The syngas can be further processed to produce different forms of fuels and chemicals. These processing include manufacturing of hydrogen to use in the synthesis of ammonia, manufacturing of methanol for the synthesis of methyl *t*-butyl ether (MTBE), Fischer-Tropsch synthesis to form liquid fuels and chemicals, they hydroformylation of olefins to aldehydes and alcohols, and direct use of syngas in integrated gasification combined cycle (IGCC) units for the electricity generation and so on.

In this high-temperature biomass gasification study, the objective is the production of the liquid transportation fuel (biodiesel) from a renewable local biomass. Thus Fischer-Tropsch synthesis was selected as syngas processing method. Accompanying research for Fischer-Tropsch synthesis focusing on development of a new catalyst was conducted by a group headed by Dr. Helena Hagelin-Weaver and Dr. Jason Weaver in the Chemical Engineering Department and Dr. Jacob Chung and Dr. Herbert Ingley in the Mechanical and Aerospace Engineering

Department at the University of Florida. A fundamental review for FTS is provided in Appendix A.

1.3.11 Biodiesel

Biodiesel is any diesel fuel derived from renewable biomass. American Society for Testing and Materials (ASTM) defines biodiesel as the monoalkyl esters of long-chain fatty acids derived from renewable lipid feedstocks [61]. Biodiesel is free of sulfur and aromatics, and can be viewed as alternative fuel for diesel engine. In Europe, biodiesel is widely available in both neat form (100% biodiesel or B100) and blends with petroleum diesel. There are several advantages of biodiesel over petroleum based diesel; domestic energy security or independence from foreign petroleum, being renewable fuel, associated reduction of greenhouse gas emission [62], [63] such as carbon dioxide, methane, hydrocarbons (CHs), reduction of air pollutants such as particulate matter (PM), carbon monoxide, hydrocarbons (HCs) and sulfur oxides (SO_X), and support of domestic economy. On the other hands, there are disadvantages of biodiesel such as higher NO_X emissions and high production cost unless produced in a large scale. Biodiesel is considered to be very attractive alternative of petroleum diesel because an existing diesel engine can be used with biodiesel without modification [62], [63]. There are several paths of biodiesel production. Among them, one of the major pathways is esterification of oil seeds and animal fats, another is gasification plus FTS of wood and other types of biomass.

There exists a numerous research of the biomass gasification to syngas production. Majority of them focused on the gasifier study of the effect of process parameters such as temperature, pressure, air to biomass ratio, steam to biomass ratio, and type of biomass. There are also many research efforts focused on developing new catalysts or improving existing catalysts to promote the gasification reactions and eliminating contaminants in the syngas.

However, research on a system level thermodynamic analysis and an optimization of the biomass gasification to the syngas production has been relatively limited.

1.4 Objectives of the Present Work

In the present work, a study for high-temperature biomass gasification using steam was conducted. This gasification system is based on an existing gasification facility in Live Oak, Florida, thus various system settings and operation parameters were adopted from it. Some of the required conditions include fixed-bed gasification, high operation temperature, steam gasification and target product of liquid transportation fuel. Furthermore, woody biomass was selected as gasification feedstock because of its local availability and other reasons suggested earlier.

There are three main objectives in the present study. First objective is the demonstration of the biomass steam gasification at very high temperature at up to 1500^{o}C. Second objective is the production of synthesis gas which serves as a feedstock for FTS for biodiesel production. A bench-scale gasification reactor was designed and constructed to satisfy the first objective as well as to investigate the gasification reactions at various operational conditions to achieve the second objective. An analytical modeling of gasification reaction was also conducted to first predict the behavior of gasification reaction and second to compare the results with the experimental study to assist to achieve the second objective. The last objective is the investigation of the biomass gasification process as well as the system level thermal efficiency. The system level energy and exergy analyses were conducted to determine the efficiency in quantity and quality of energy.

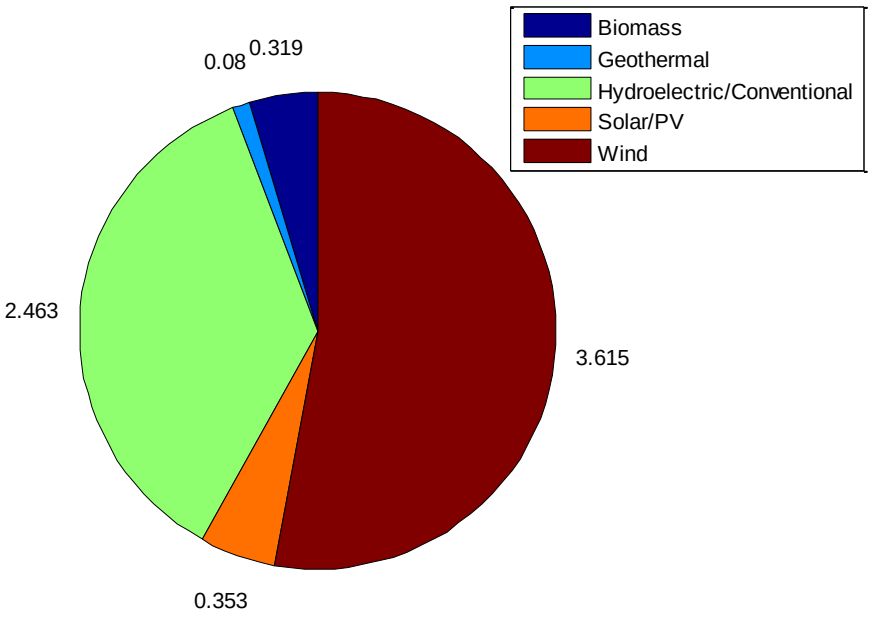

Figure 1-1. U.S. Renewable energy consumption (Quadrillion BTU) in 2007 [1].

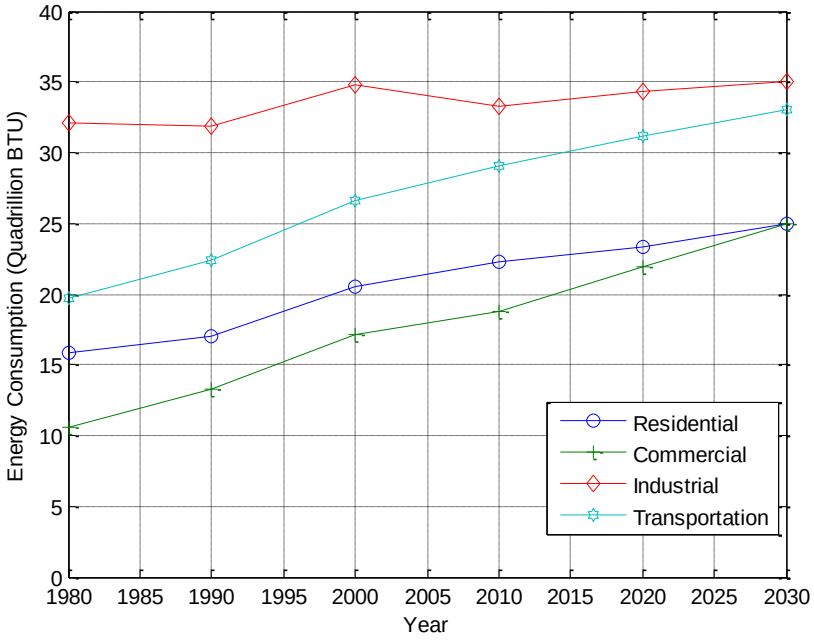

Figure 1-2. Energy consumption by sector in the United States. [1].

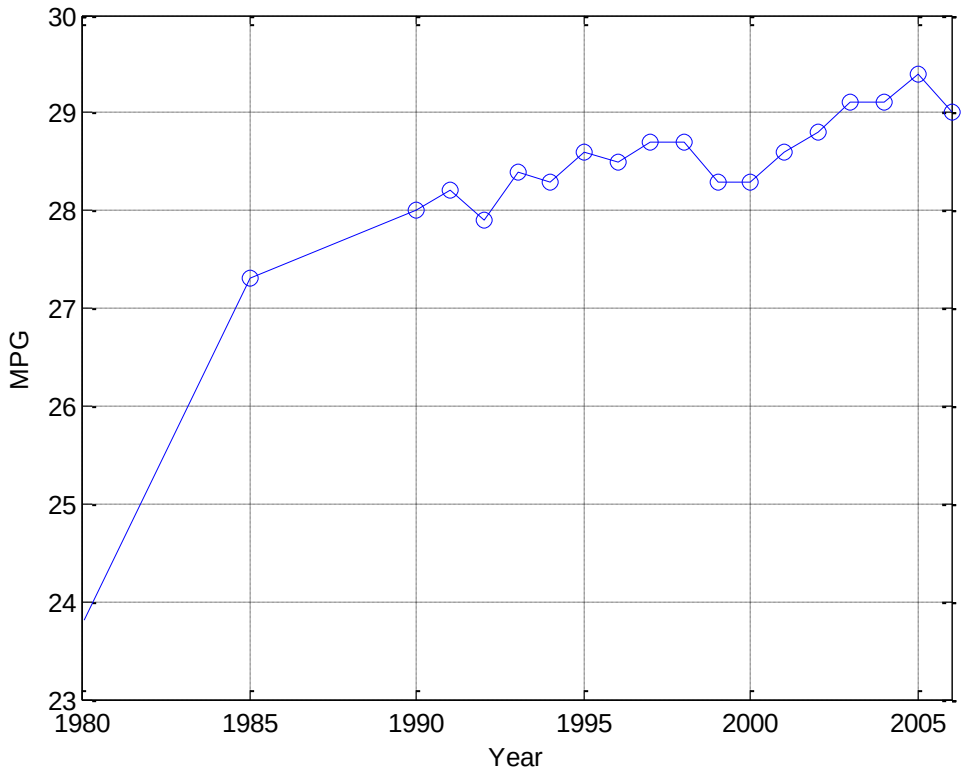

Figure 1-3. The history of the average fleet mileage in U.S. [6].

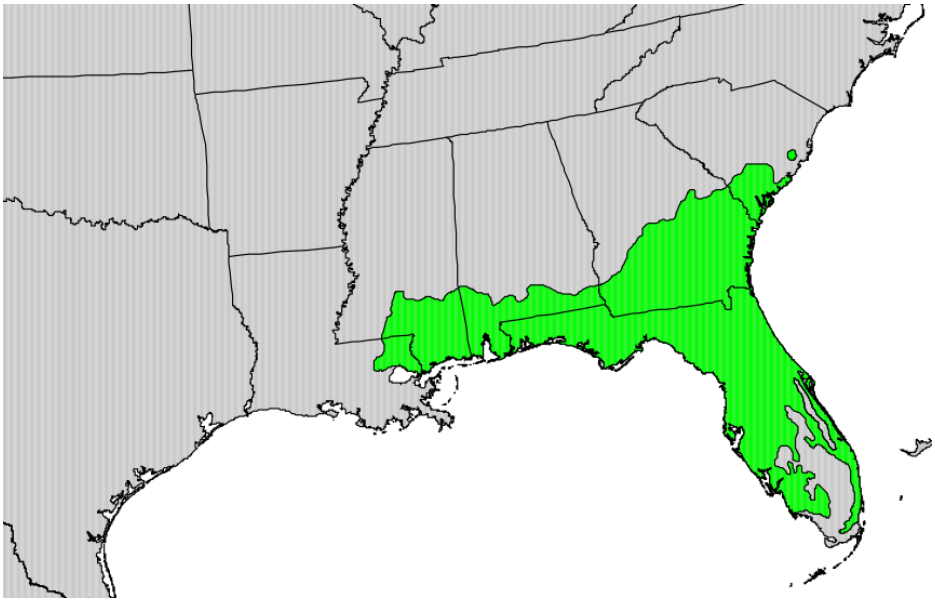

Figure 1-4. Distribution of Slash Pine in the United States. Courtesy of the U.S. Geological Survey [64].

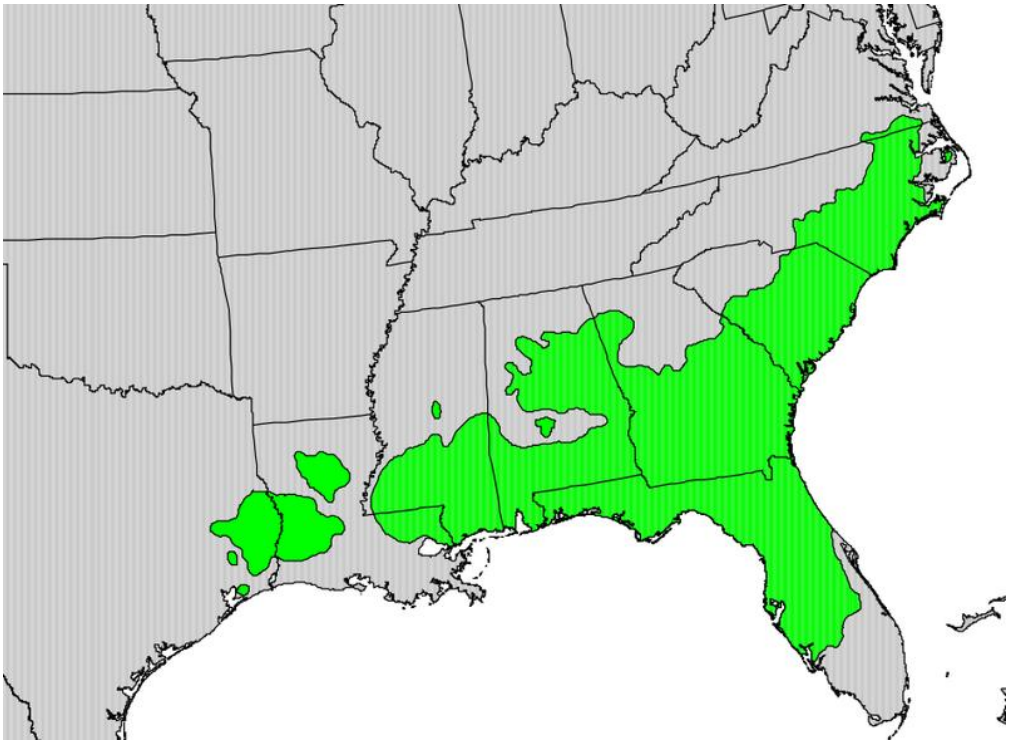

Figure 1-5. Longleaf Pine distribution in the United States. Courtesy of the U.S. Geological Survey [64].

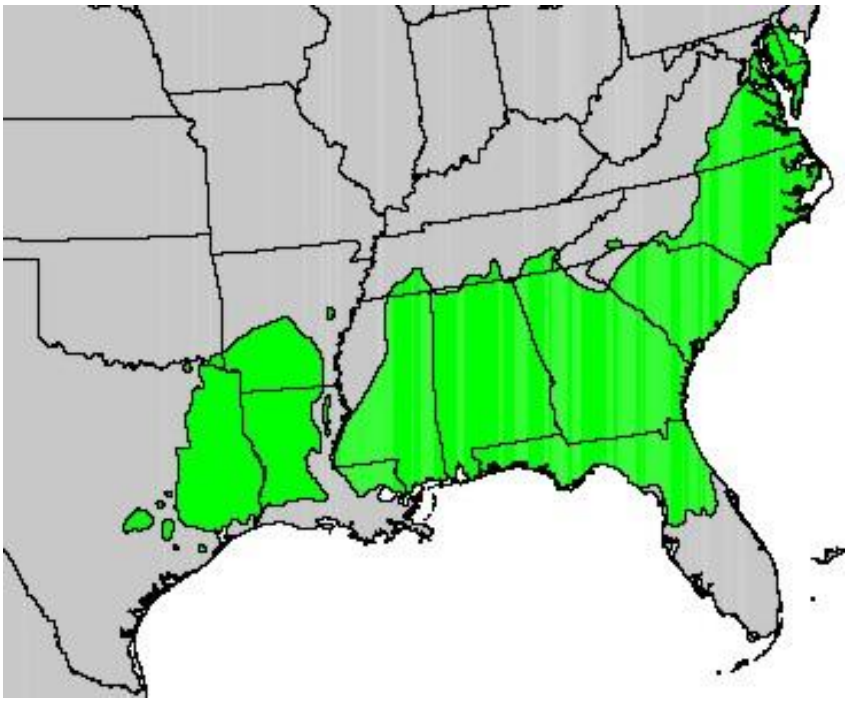

Figure 1-6. Distribution of loblolly pine in the United States. Courtesy of the U.S. Geological Survey [64].

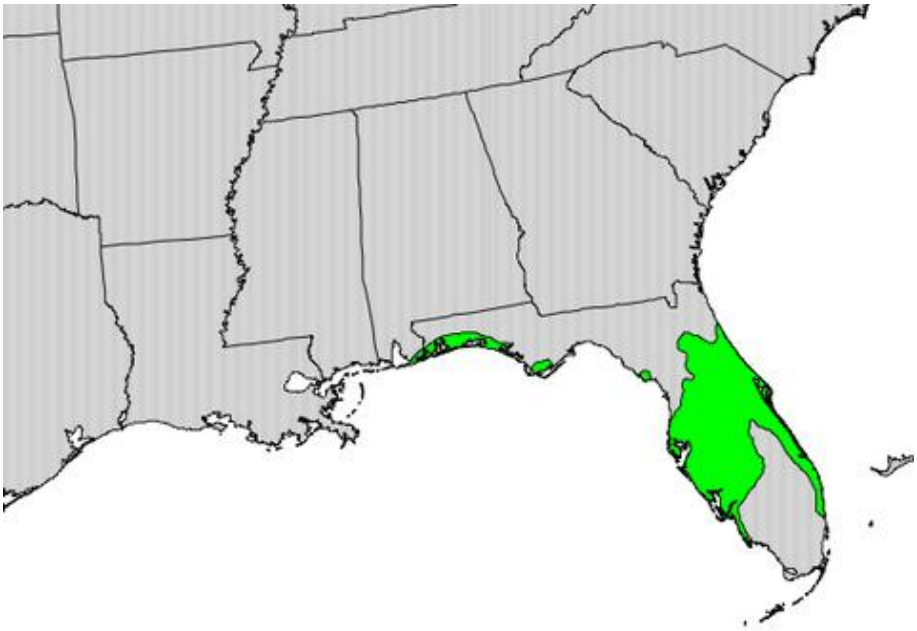

Figure 1-7. Distribution of sand pine in the United States. Courtesy of the U.S. Geological Survey [64].

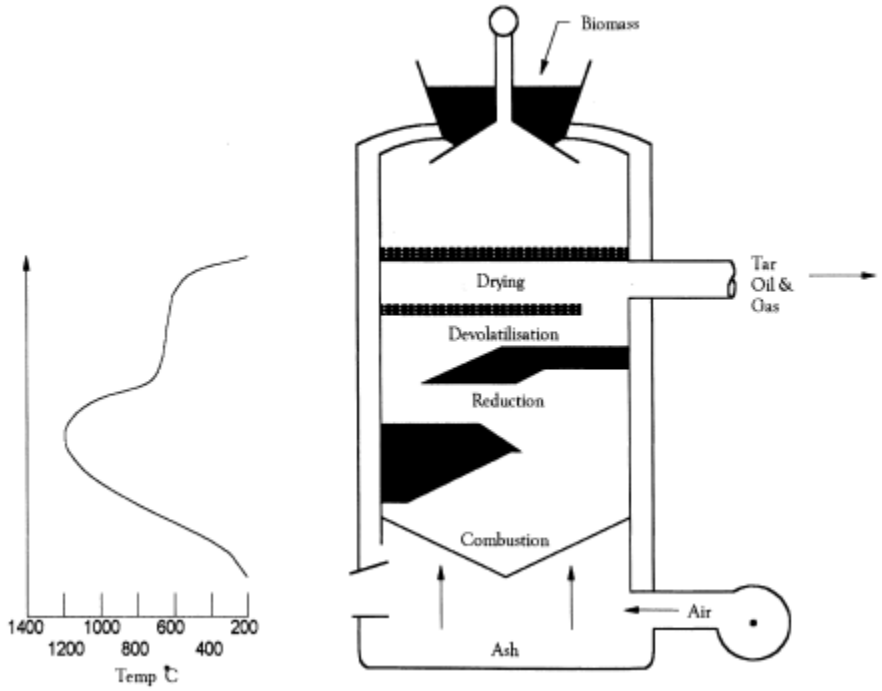

Figure 1-8. A view of an updraft gasifier [15].

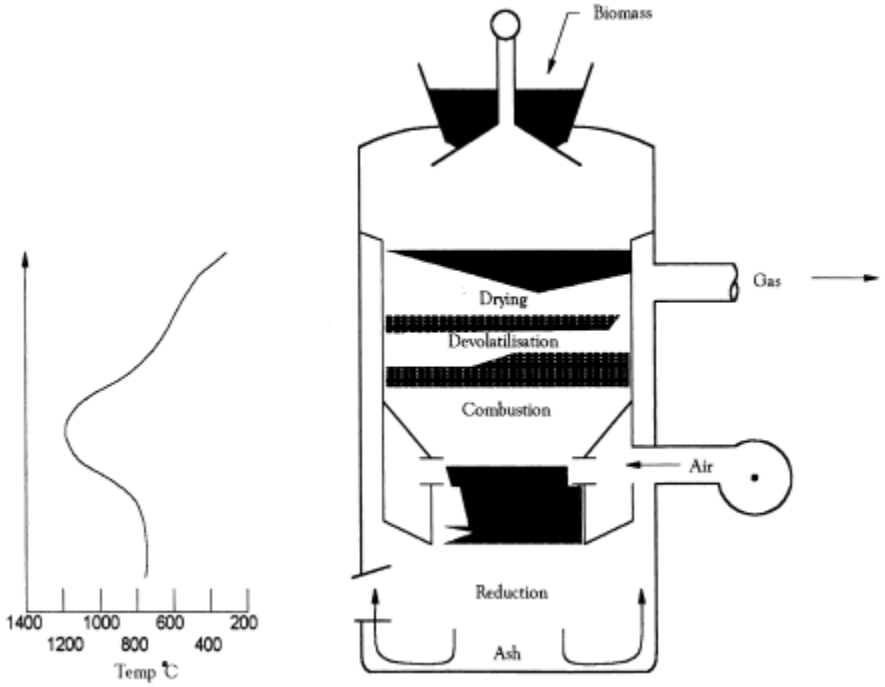

Figure 1-9. A view of a downdraft gasifier [15].

CHAPTER 2
ANALYTICAL TREATMENT OF THE GASIFICATION PROCESS

This chapter discusses the theoretical background necessary for understanding the high-temperature biomass gasification system. The thermodynamic fundamentals are presented first to discuss the chemistry associated with gasification and the first and second laws of thermodynamics are also included. Literature review of analytical mass, energy and exergy studies for biomass gasification system follows. The purpose of this section is to review the type of study and methods used for analyzing biomass gasification. Lastly, the analytical method used in this work is presented.

2.1 Thermodynamic Fundamentals

This section discusses some thermodynamic fundamentals required to understand the gasification process including mass, energy and exergy balances. This section also includes the derivation of equations which are used in the thermal analysis of a gasification system.

2.1.1 H_2-O_2 Combustion

The High-Temperature Biomass Gasification System (HTBGS) uses gaseous hydrogen and gaseous oxygen for the heat source, the oxidation agent and the water-gas shift reaction for the gasification reaction. These gases are injected separately into the ignition torch. In the combustion chamber, these gases are mixed and ignited as it comes out of the torch. The high-temperature steam produced from the combustion of hydrogen is used as the gasification agent to react with woody biomass to forward the gasification reactions. Using the hydrogen combustion chemistry as well as biomass gasification chemistry allows control of the HTBGS operational conditions.

The chemical equation for the stoichiometric reaction between hydrogen and oxygen can be written as shown in Equation 2-1.

$$H_2 + \frac{1}{2}O_2 \leftrightarrow H_2O \qquad \Delta H_{298} = 141.89\,kJ/mol \tag{2-1}$$

In the HTBGS, high-temperature steam possesses dual purposes in terms of heat and mass. First, unlike typical biomass gasification with partial oxidation using air or pure oxygen, the high-temperature combustion products of the hydrogen and oxygen (steam) provide the force of heat for the system. This heat is used for the pyrolysis of biomass to decompose the wood to elemental forms as well as for the following endothermic gasification reactions. Second, high-temperature steam serves as a reactant for the water gas reactions and the water gas shift reaction, which are three main gasification reactions. Therefore, it is important to consider both a heat and mass balance when one determines the optimum hydrogen and oxygen supply.

2.1.2 Energy Analysis

The first law of thermodynamics or conservation of energy states that the total amount of energy in an isolated system is neither constructed nor destroyed, and it is expressed as:

$$\frac{dE_{C.M.}}{dt} = \dot{Q} - \dot{W} \tag{2-2}$$

$$\delta Q = dU + \delta W \tag{2-3}$$

For the general control volume, the first law of thermodynamics can be written as

$$\frac{dE_{C.V.}}{dt} = \dot{Q}_{C.V.} - \dot{W}_{C.V.} + \sum \dot{m}_i \left(h_i + \frac{1}{2}V_i^2 + gz_i \right) - \sum \dot{m}_e \left(h_e + \frac{1}{2}V_e^2 + gz_e \right) \tag{2-4}$$

For steady state problem with negligible kinetic energy and potential energy system, the Equation 2-4 can be reduced to:

$$\dot{Q}_{C.V.} + \sum_i \dot{m}_i h_i = \sum_e \dot{m}_e h_e + \dot{W}_{C.V.} \tag{2-5}$$

The first law equation for a steady-state process involving chemical reactions, neglecting changes in kinetic and potential energy, can be expressed as:

$$\dot{Q}_{C.V.} + \sum_i \dot{n}_i \left(\bar{h}_f^0 + \Delta \bar{h} \right)_i = \dot{W}_{C.V.} + \sum_e \dot{n}_e \left(\bar{h}_f^0 + \Delta \bar{h} \right)_e \quad \text{2-6}$$

2.1.3 Exergy Analysis

Exergy is an important tool for the design and analysis of thermal systems. Exergy analysis, unlike energy analysis, includes the concept of both the first law and the second law together, and accounts for not only the quantity of energy but also the quality of energy. Thus exergy analysis could present a better indication for the use and management of energy resources and the system optimization. Szagut defined exergy as "the amount of work obtainable when some matter is brought to a state of thermodynamic equilibrium with the common components of the natural surroundings by means of reversible processes, involving interaction only with the abovementioned components of nature" [65]. Bejan also defined exergy as: "When one of the two systems is a suitably idealized system called an *environment* and the other is some system of interest, *exergy* is the maximum theoretical useful work, (shaft work or electrical work) obtainable as the systems interact to equilibrium, heat transfer occurring with the environment only" [66].

Before proceeding, some terms are defined to help the further discussion, including environment, dead state and restricted dead state. Environment is "some portion of the surrounding, the intensive properties of each phase of which are uniform and do not change significantly as a result of any process under consideration". The environment is also "free of irreversibilities" [66]. The environment is modeled as a simple compressible system with uniform temperature T_0 and pressure P_0. When the system and the environment are in perfect equilibrium in terms of the pressure, temperature, composition, velocity, elevation or any other potential to do work, the state of the system is called the *dead state*. On the other hand, when

only the conditions of mechanical and thermal equilibrium are satisfied, this state of the system is called the *restricted dead state* [66].

$$E = E^{PH} + E^{KE} + E^{PE} + E^{CH} \tag{2-7}$$

where E^{PH} represents the physical exergy, E^{CH} is the chemical exergy, E^{PE} is the potential exergy and E^{KE} is the kinetic exergy. On a unit mass or molar bases [66]:

$$e = e^{PH} + e^{KE} + e^{PE} + e^{CH} \tag{2-8}$$

$$e^{KE} = \frac{1}{2}V^2 \tag{2-9}$$

$$e^{PE} = gz \tag{2-10}$$

$$e = e^{PE} + \frac{1}{2}V^2 + gz + e^{CH} \tag{2-11}$$

2.1.3.1 Physical exergy

The physical exergy is the maximum work extractable when the system is at the initial state where the temperature T and the pressure P comes to equilibrium with the environmental state (T_0 = 298.15K, P_0 = 1 atm) through thermal and mechanical energy exchange.

$$E^{PH} = (U - U_0) + P_0(V - V_0) - T_0(S - S_0) \tag{2-12}$$

On a unit-of-mass or molar basis:

$$e^{PH} = (u - u_0) + P_0(v - v_0) - T_0(s - s_0) \tag{2-13}$$

Exergy balance equation:

$$\frac{dE_{C.V.}}{dt} = \sum_j \left(1 - \frac{T_0}{T_j}\right)\dot{Q}_j - \left(\dot{W}_{C.V.} - P_0\frac{dV_{C.V.}}{dt}\right) + \sum_i \dot{m}_i e_i - \sum_e \dot{m}_e e_e - \dot{I} \tag{2-14}$$

The total exergy transfer associated with a stream of matter is

$$e = (h - h_0) - T_0(s - s_0) + \frac{1}{2}V^2 + gz + e^{CH} \tag{2-15}$$

$$e^{PH} = (h - T_0 s) - (h_0 - T_0 s_0) \quad \text{2-16}$$

2.1.3.2 Chemical exergy

When the substance comes to an equilibrium with its surroundings not only in temperature, pressure, velocity and elevation but also in chemical concentration of the reference substance, this state of the system is called the dead state, where reference substances are gaseous components in the atmosphere, ionic and nonionic substances from the oceans and solid substances from the lithosphere [66]. The chemical exergy is the maximum work obtainable when the substance is brought from the environmental state to the dead state.

The chemical exergy per mole of gas k is

$$\bar{e}_k^{CH} = -\bar{R}T_0 \ln \frac{x_k^e p_0}{P_0} \quad \text{2-17}$$

The chemical exergy per mole of mixture is

$$\bar{e}^{CH} = -\bar{R}T_0 \sum x_k \ln \frac{x_k^e}{x_k} \quad \text{2-18}$$

Substituting Equations 2-17 and 2-18, the chemical exergy of mixture is given in the following form:

$$\bar{e}^{CH} = \sum x_k \bar{e}_k^{CH} + \bar{R}T_0 \sum x_k \ln x_k \quad \text{2-19}$$

where the first term in the right hand side is the summation of exergy of the pure element at its molar fraction and the second term in the right hand side is the mixture of elements, which is actually a source of irreversibility thus always a negative quantity.

2.1.4 Chemical Equilibrium

For species A, B, C and D, which are in chemical equilibrium at a given temperature and pressure, the chemical reaction takes place between these species can be written as

$$\nu_A A + \nu_B B \rightleftharpoons \nu_C C + \nu_D D \tag{2-20}$$

where ν_A, ν_B, ν_C and ν_D are the number of moles of each species. At equilibrium, the reaction progresses an infinitesimal amount in forward direction resulting in a decrease in the moles of reactants and increase in the moles of products. Degree (extent) of reaction is the progress in chemical reaction defined by the number of chemical transformations divided by the amount of chemical transformations (Avogadro constant) [67]. Change in the number of moles of each species, by using degree of reaction, ξ, can be expressed as follows:

$$dn_A = -\nu_A d\xi \tag{2-21}$$

$$dn_B = -\nu_B d\xi \tag{2-22}$$

$$dn_C = +\nu_C d\xi \tag{2-23}$$

$$dn_D = +\nu_D d\xi \tag{2-24}$$

The change in Gibbs function associated with this reaction is

$$dG_{T,P} = \bar{G}_A dn_A + \bar{G}_B dn_B + \bar{G}_C dn_C + \bar{G}_D dn_D \tag{2-25}$$

Substituting the set of change in amount of chemical transformations dn_i (Equations 2-21 to 2-24), the change in Gibbs function can be re-written as

$$dG_{T,P} = \left(\nu_C \bar{G}_C + \nu_D \bar{G}_D - \nu_A \bar{G}_A - \nu_B \bar{G}_B\right) d\xi \tag{2-26}$$

From the definition of Gibbs function,

$$G = H - TS \tag{2-27}$$

For a mixture of i components, Equation 2-27 was differentiated with respect to n_A at constant T, P and n_i as follows:

$$\left(\frac{\partial G}{\partial n_A}\right)_{T,P,n_i} = \left(\frac{\partial H}{\partial n_A}\right)_{T,P,n_i} - T\left(\frac{\partial S}{\partial n_A}\right)_{T,P,n_i} \qquad 2\text{-}28$$

Since all G, H and S are extensive properties, Equation 2-27 at constant temperature and pressure can be written for species A using partial molal properties $\bar{G}$, $\bar{H}$ and $\bar{S}$:

$$\bar{G}_A = \bar{H}_A - T\bar{S}_A \qquad 2\text{-}29$$

Since enthalpy is a function of temperature only for ideal-gas mixture,

$$\bar{H}_A = \bar{h}_{ATP} = \bar{h}^0_{ATP^0} \qquad 2\text{-}30$$

while entropy is a function of both temperature and pressure,

$$\bar{S}_A = \bar{s}^0_{ATP^0} - \bar{R}\ln\left(\frac{y_A P}{P^0}\right) \qquad 2\text{-}31$$

where

$$\bar{G}_A = \bar{h}^0_{ATP^0} - T\bar{s}^0_{ATP^0} + \bar{R}T\ln\left(\frac{y_A P}{P^0}\right) = \bar{g}^0_{ATP^0} + \bar{R}T\ln\left(\frac{y_A P}{P^0}\right) \qquad 2\text{-}32$$

$$dG_{T,P} = \left\{\nu_C\left[\bar{g}^0_C + \bar{R}T\ln\left(\frac{y_C P}{P^0}\right)\right] + \nu_D\left[\bar{g}^0_D + \bar{R}T\ln\left(\frac{y_D P}{P^0}\right)\right] - \nu_A\left[\bar{g}^0_A + \bar{R}T\ln\left(\frac{y_A P}{P^0}\right)\right] - \nu_B\left[\bar{g}^0_B + \bar{R}T\ln\left(\frac{y_B P}{P^0}\right)\right]\right\} d\xi \qquad 2\text{-}33$$

or

$$dG_{T,P} = \left\{\Delta G^0 + \bar{R}T\ln\left[\frac{y_C^{\nu_C} y_D^{\nu_D}}{y_A^{\nu_A} y_B^{\nu_B}}\left(\frac{P}{P^0}\right)^{\nu_C+\nu_D-\nu_A-\nu_B}\right]\right\} d\xi \qquad 2\text{-}34$$

where ΔG^0 is the standard-state change in Gibbs function defined as the following:

$$\Delta G^0 = \nu_C\bar{g}^0_C + \nu_D\bar{g}^0_D - \nu_A\bar{g}^0_A - \nu_B\bar{g}^0_B \qquad 2\text{-}35$$

At the equilibrium where $dG_{T,P} = 0$, inside the parenthesis of the right-hand side of Equation 2-34 is also zero. Thus, Equation 2-34 can be written as:

$$\ln\left[\frac{y_C^{\nu_C} y_D^{\nu_D}}{y_A^{\nu_A} y_B^{\nu_B}}\left(\frac{P}{P^0}\right)^{\nu_C+\nu_D-\nu_A-\nu_B}\right] = -\frac{\Delta G^0}{\bar{R}T} \qquad 2\text{-}36$$

Defining the equilibrium constant K as the expression inside of the parenthesis in Equation 2-36

$$\ln K = -\frac{\Delta G^0}{\bar{R}T} \qquad 2\text{-}37$$

Substitute the above expressions, Equation 2-36 can be written as:

$$K = \frac{y_C^{\nu_C} y_D^{\nu_D}}{y_A^{\nu_A} y_B^{\nu_B}}\left(\frac{P}{P^0}\right)^{\nu_C+\nu_D-\nu_A-\nu_B} \qquad 2\text{-}38$$

This is the chemical equilibrium equation corresponding to the chemical reaction, Equation 2-20.

2.2 Literature Review for Analytical Works

In this section, analytical studies for biomass gasification are reviewed including the method to analyze the gasification path. Various studies were performed to obtain the gasification product composition, and to compute the energy and the system efficiencies.

Prins et al. [42]conducted an analytical study of energy and exergy for the gasification of biomass using air and steam. The C-H-O ternary diagram was introduced in this study. This diagram is an equilateral triangle showing the compositional balance between carbon, hydrogen and oxygen (Figure 2-1). In this diagram, all three species are dependent on each other and the sum of carbon, hydrogen and oxygen anywhere in the triangle is constant (100%). In the C-H-O ternary diagram, several lines called carbon deposition boundaries could be drawn. Above the solid carbon boundary, solid carbon exists in heterogeneous equilibrium with gaseous components, while below the carbon boundary, all compositions exist in gaseous form and no solid carbon exists. Since the general goal of biomass gasification is to convert all the solid

carbon in the biomass to a gaseous form, this ternary diagram can help to depict which area in the triangle, thus which composition of carbon, hydrogen and oxygen, the product gas needs to be located.

Prins et al. [42] used a Gibbs free energy minimization method to calculate the equilibrium composition of gas and solid carbon (graphite). Using this result, the effect of equivalence ratio on energy and exergy for air gasification of biomass and the effect of steam to biomass ratio on steam gasification of biomass were simulated. The gasification process was assumed to be adiabatic and isobaric at 1 atm. The initial feedstock temperature and air temperature were set to 25^{o}C, while steam temperature was set to 500 K. The authors found that for the air gasification the total energy of the product gas remained constant for different equivalence ratios, while total exergy decreased with increasing equivalence ratio. For steam gasification, it was shown that both energy and exergy of the product gas reached the maximum at the carbon boundary point where the conversion of solid carbon to gaseous carbon was just completed. There was a continuous increase in energy and exergy after carbon boundary point. This increase was attributed to the thermal energy and exergy from high-temperature steam input. Prins et al. [42] also studied exergetic efficiency for air and steam gasification using three different formulas. The first formula is defined as the ratio of the sum of exergy of gaseous products to the total process inputs; biomass and air or steam depending on the gasification cases:

$$\psi_1 = \frac{E_{gas}}{E_{biomass} + E_{steam} + E_{air}} \qquad 2\text{-}39$$

The second case considered the unconverted carbon as a potentially useful product since this could be recovered as a product and/or recycled back to the gasifier. The second exergetic efficiency formula is defined as the exergy of the gaseous product plus the exergy of the char divided by the exergy of the input including biomass and air or steam.

$$\psi_2 = \frac{E_{gas} + E_{char}}{E_{biomass} + E_{steam} + E_{air}} \quad 2\text{-}40$$

The third definition, also known as the rational or intrinsic efficiency, considers that energy is transferred from a solid fuel to a gaseous product. The rational efficiency is defined as:

$$\psi_3 = \frac{E_{gas} + E_{char,ph}}{(E_{biomass} - E_{char,ph}) + E_{steam} + E_{air}} \quad 2\text{-}41$$

From the efficiency study using these three formula, Prins et al. showed that the exergetic efficiency reaches a maximum at the carbon boundary point for both air and steam gasification. For the air gasification case, the carbon boundary point corresponds to the equivalence ratio at 0.255 and for steam gasification, the carbon boundary point occurred at a steam to biomass ratio of 1.30. It was also observed that exergetic efficiency is sensitive to equivalence ratio for air gasification, while efficiency is relatively independent of steam to biomass ratio for steam gasification especially after reaching the carbon boundary point. Thus it is expected that change in the steam to biomass ratio would not affect the exergetic efficiency in the HTBGF, where only a steam would be used as the gasification agent and the operation temperature is high enough so that all solid carbon would be converted to a gaseous form.

Krzysztof J. Ptasinski et al. [68] studied the gasification efficiency of various biomass feed stocks such as wood, vegetable oil, sludge and manure and compared them with coal. Again, the composition of fuels was specified based on a molar ternary C-H-O diagram at the carbon boundary point. For the gasification products, it was assumed that chemical equilibrium was reached, and the equilibrium composition at a given temperature and pressure was computed using Aspen Plus based on minimization of the Gibbs free energy. It was assumed for the analysis that the gaseous products leave the gasifier at the same temperature as the reactor temperature (set to be above 600^{o}C), the gasifier operates under adiabatic condition, and the

reactor is at atmospheric pressure. The energetic efficiency of a gasification process, cold-gas efficiency was determined as

$$\psi_4 = \frac{LHV_{gas}}{LHV_{biomass}} \quad 2\text{-}42$$

The exergetic efficiency shows the ratio between the exergy of useful gasification products and the feedstock exergy. The exergetic efficiency was defined as

$$\psi_5 = \frac{\varepsilon_{ch,gas} + \varepsilon_{ph,gas}}{\varepsilon_{ch,biomass}} \quad 2\text{-}43$$

Chemical exergy of the biomass was calculated using the statistical correlation proposed by Szargut et al. [65] as following:

$$\varepsilon_{ch,total} = z_{org}\left(\beta \cdot LHV_{org}\right) + z_s\left(\varepsilon_{ch,s} - C_s\right) + z_{water}\varepsilon_{ch,water} + z_{ash}\varepsilon_{ch,ash} \quad 2\text{-}44$$

Where z is the mass fraction, β is the ratio of the chemical exergy to the LHV of dry organic substances and org indicates organic fraction.

Krzysztof J. Ptasinski et al. [68] also showed that there exists the optimum point for the gasification operation when the chemical equilibrium is attained for the gasification product. This optimum point corresponds to the carbon boundary point in the C-H-O ternary diagram, since at this point, exactly enough oxygen (or other gasification agent) is added to achieve complete gasification. Further addition of oxygen after this point results in decreasing heating value until eventual complete combustion would have taken place. Using the Gibbs free energy minimization method with the gasification conditions presented in Table 2-1, the equilibrium chemical composition was computed. Based on these compositions, the energy and exergy efficiencies were calculated as 83% and 78%, respectively. Based on this study, it was shown that there existed the optimum operation point when an equilibrium condition was assumed.

Rao et al. [69] conducted the mass energy and exergy balance study for input and output stream of a countercurrent fixed-bed gasifier with three different fuels: municipal residue, wood chips and agricultural residue with operating temperatures in range of 600 to 1200^{o}C. For analytical modeling, it was considered that the process input stream is comprised of dry feedstock material, dry air and water while the output stream is comprised of dry gas, char, tar and water. The gasification output composition necessary for analytical studies for each fuel were obtained from experimental results. For an energy balance, they assumed the sensible heat of graphite for char, sensible heat of crude oil for tar and sensible heat of silicone dioxide for ash. Rao el al. [69] also introduced a mass performance parameter and three energy performance parameters. The correlations to compute specific chemical enthalpy and specific chemical exergy for biomass were also introduced. The mass performance parameter is the mass conversion efficiency (MCE) was expressed as:

$$MCE = \frac{\left\{Mass\ of\ the\ dry\ gas\ output\ rate\left(kg\ h^{-1}\right)\right\}}{\left\{Wet\ \ feed\ input\ rate\left(kg\ h^{-1}\right) + Wet\ air\ input\ rate\left(kg\ h^{-1}\right)\right\}} \times 100 \qquad 2\text{-}45$$

The first energy performance parameter is thermal energy conversion efficiency (TECE) of gasifier expressed as:

$$TECE = \frac{Thermal\ energy\ content\left(HHV\right) of\ \ gas\ MJ\ kg^{-1}}{Chemical\ energy\ content\left(HHV\right) of\ \ \ feedstock\ MJ\ kg^{-1}} \times 100 \qquad 2\text{-}46$$

The second energy performance parameter is cold gas efficiency (CGE)

$$CGE = \frac{\left\{Gas\ yield\left(Nm^{3}\ kg^{-1}\ \ fuel\right) \times HHV\ of\ \ gas\ MJ\ \ Nm^{-3}\right\}}{\left\{HHV\ of\ \ \ fuel\ MJ\ kg^{-1}\right\}} \times 100 \qquad 2\text{-}47$$

where HHV is the higher heating value of solid feedstock or gas. The third parameter is global energy content (GEC) of the gas defined as:

$$GEC = \left\{ Gas\ yield\ (Nm^3\ KG^{-1}\ fuel) \times LHV\ of\ gas\ MJ\ Nm^{-3} \right\} \quad \text{2-48}$$

where LHV is the lower heating value of the gas produced. The specific chemical enthalpy for biomass is expressed as:

$$H_{biomass} = 4.1868\left\{ (1+0.15[O])(7837.667[C]+33888.889[H]-\frac{[O]}{8}) \right\} \quad \text{2-49}$$

The specific chemical exergy:

$$E_{biomass} = 4.1868\begin{Bmatrix} 8177.79[C]+5.25[N]+27892.63[H]-3173.66[O]+0.15[O]+ \\ \left(7837.667[C]+33888.889[H]-4236.1[O]\right) \end{Bmatrix} \quad \text{2-50}$$

Baratieri et al. [70] have conducted an analytical study for the gasification of biomass using air and steam. In their study, first entire compositional possibility of 61 species using 6 atoms, C, H, O, N and S was modeled, and then the species present in the syngas in a significant fraction were selected for the analytical modeling. These syngas species include hydrogen (H_2), steam (H_2O), methane (CH_4), carbon monoxide (CO), carbon dioxide (CO_2), and nitrogen (N_2). It was assumed that solid carbon is perfectly converted to a gaseous form, thus solid carbon was not included in the product. Based on the selected product species, the Gibbs free energy minimization method was applied to estimate the product composition at equilibrium. The simulation result, at a temperature of 800^{o}C and a process pressure of 1 bar is summarized in the Table 2-2. Baratieri et al. [70] also simulated the syngas equilibrium composition as a function of process temperature (1 bar). It was found that methane and carbon dioxide formation were favored at lower temperatures, while carbon monoxide and hydrogen production dominated at higher temperatures. The simulation results showed that hydrogen and carbon monoxide were the only existing species above 900^{o}C. The simulation for syngas equilibrium composition as a function of pressure (800^{o}C) showed that increasing pressure tends to decrease the equilibrium concentrations of hydrogen and carbon monoxide and increase the methane and carbon dioxide

concentrations. Therefore, it is not favorable to increase the operation pressure if the formation of hydrogen and carbon monoxide are desired for the further processing such as Fischer-Tropsh synthesis for biodiesel production. It was also simulated that for the same thermodynamic conditions (800^{o}C, 1 bar) the optimum equivalence ratio is 0.14 to maximize the formation of hydrogen and oxygen. The equivalence ratios above this point showed the tendency of decreasing hydrogen and oxygen formation and increasing water and carbon dioxide. It was presented that steam to carbon (biomass) ratios of 0.25 to 0.5 are the optimum values for hydrogen and oxygen formations. Any steam to carbon ratios above this value results in a decrease of hydrogen and carbon monoxide formation and significant increase in water.

Prins et al. [71] performed an exergy analysis of the Fischer Tropsch (FT) fuel production through biomass gasification. The study was conducted by first dividing the entire process into a sequence of smaller processes. A block diagram of the system and thermal interactions among smaller processes were established. Mass and energy balances were obtained from Aspen Plus simulations. Exergy analysis was applied on each process to identify the specific units within the system with the largest process irreversibilities. A parametric study was also conducted to maximize efficiency of producing FT liquid fuels.

Prins and Ptasinski [72]performed an exergy loss analysis of gasification considering two cases; an isothermal case and an adiabatic case. The operation process was divided into hypothetical sub-processes including 1) reactant diffusion, 2) fuel oxidation 3) heat transfer between product molecules, and reactant molecules and 4) product mixing, and exergy loss of each sub-process was quantified to investigate sources of inefficiency. In the first half of the study, the above mentioned analysis was done to compare the process between combustion and

gasification. In the second half of the study, the efficiency difference was compared by changing the oxidation media to air, oxygen and oxygen/steam mixture.

Pellegrini and Oliveira Jr. [73] introduced a model for a gasification process to predict the energy and exergy behavior. Their approach was to establish energy balances and exergy balances of inlet and outlet streams of gasifier and solve these equations based on the minimization of Gibbs free energy of the product gas using Microsoft engineering equation solver. They also conducted the parametric study of variables including biomass moisture content, air temperature, biomass temperature, volume of steam added and thermal losses. Results were also compared with experimental data and presented in tables.

Mahishi and Goswami [74] conducted a study of a biomass gasifier to maximize hydrogen production. Stanjan software (v 3.93L) was used to obtain the molar composition of the product gas at an equilibrium state based on the minimization of Gibbs free energy. The gasifier was modeled as an equilibrium reactor and the first law analysis was applied to determine the maximum thermal efficiency at this state. Gasification parameters such as temperature, pressure, steam to biomass ratio, equivalence ratio were controlled to achieve the optimum hydrogen yield. Finally the product composition was compared with experimental yields.

2.3 The High-Temperature Biomass Gasification Model

This section discusses methods for the analytical modeling of the high-temperature biomass gasification process. The discussions include the basic gasification conditions and the methods for computing gasification product composition, overall gasification mass balance, energy balance and exergy balance. This section also discusses the calculation methods for several parameters including steam to biomass ratio, carbon conversion ratio, thermal efficiency and exergetic efficiency. The purpose of the analytical model is to predict the optimum amount and conditions for input biomass and high-temperature steam before experimental work was

conducted. These calculations are also important to compare with the experimental results as well as to analyze and optimize the overall system efficiency.

2.3.1 Basic Conditions

This analytical model was established to predict and compare the performance with the experimental results from the high-temperature biomass gasification system, thus some operational conditions were based on the capabilities of the experimental system. Based on this requirement, the following conditions and assumptions were used for modeling:

- The feedstock is Slash Pine local to Florida.
- The feedstock will be assumed to be dry and ash free (DAF), and is approximated as CH_aO_b, where a is 1.5 and b is 0.66 based on the ultimate analysis conducted on biomass.
- The feedstock is at the temperature of 25^oC and the pressure of 1 atm.
- High-temperature steam is the only gasification (water-gas shift) agent.
- The gasification process is assumed to be allothermal: heat of combustion from the reaction between pure oxygen and pure hydrogen is the sole heat source for the gasification process.
- The operation temperature goal is 1500^oC.
- The operation pressure is expected to be around 1 atmosphere.
- It is assumed that equilibrium is attained at the gasification output state.
- The gasification product consists of either solid carbon and gas mixture or gas mixture only depending on the operation conditions for the gasification process.

The relationship between input and output for the biomass gasification model is presented in Figure 2-2.

2.3.2 Equilibrium Mass Composition

The gasification product composition is required to conduct any of the mass, energy and exergy balance analyses. To obtain the equilibrium composition for the gasification product, the Gibbs free energy minimization method was used. The set of chemical reactions used in this

analysis were heterogeneous Boudouard reaction (Equation 2-51), homogeneous steam methane reforming (SMR) (Equation 2-52) and homogeneous water gas shift reaction (Equation 2-53) as follows:

$$C(s) + CO_2 \leftrightarrow 2CO \quad \text{2-51}$$

$$CO + 3H_2 \leftrightarrow CH_4 + H_2O \quad \text{2-52}$$

$$CO + H_2O \leftrightarrow H_2 + CO_2 \quad \text{2-53}$$

By selecting these three reactions, it was assumed that solid carbon (C), hydrogen (H_2), carbon monoxide (CO), carbon dioxide (CO_2), water (H_2O) and methane (CH_4) were the only species existing in the gasification product. For chemical reactions above, coefficient for each species, i, was set to ν_i. Degree of reaction, ξ_k, was assigned for each chemical reaction, k. Using ν_i and ξ_k, the change in number of moles for each species involving k chemical reactions can be expressed as

$$dn_i = \sum_k \nu_{k,i} d\xi_k \quad \text{2-54}$$

The mole fraction of each species, i, at the equilibrium can be expressed as the ratio of the number of mole of species i to the total number of mole of the all gaseous species:

$$y_i = \frac{n_i}{n_{gas}} \quad \text{2-55}$$

where n_i is the number of moles for each species and n_{gas} is the total number of moles for the gaseous species. It is worth noting that the mole fraction, y_i, can also be expressed in terms of ν_i and ξ_k. Using the expressions for the mole fraction, a set of chemical equilibrium equations corresponding to the set of chemical reactions can be constructed as follow:

$$K_k = \prod_i (y_i)^{\nu_{k,i}} \left(\frac{P}{P^0} \right)^{-\nu_{k,i}} \quad 2\text{-}56$$

where K_k is the equilibrium constant for reaction k, P is the operation pressure and P^0 is the standard pressure (1 atm). The equilibrium constant K_i can be computed if the standard-state change in Gibbs function was determined. The expressions of standard-state change in Gibbs function and the Gibbs function were as presented in Equations 2-34 and 2-28. Thus, the equilibrium constant K_i can be computed if the enthalpy and the entropy of species i at the given state were known. To evaluate the enthalpy and entropy for the gases and solid carbon, the following assumptions were made:

- Pressure variations through the gasifier were insignificant.
- Product gas behavior is similar to that of an ideal gas.

Using the above assumptions, enthalpy and absolute entropy for the gaseous species were as following:

$$\bar{h} = \bar{h}_f^0 + \left(\bar{h}^0 - \bar{h}_{298.15}^0 \right) \quad 2\text{-}57$$

where $\bar{h}^0 - \bar{h}_{298.15}^0$ is computed using the Shomate equations [75] given as:

$$\bar{h}^0 - \bar{h}_{298.15}^0 = At + \frac{B}{2}t^2 + \frac{C}{3}t^3 + \frac{D}{4}t^4 - \frac{E}{t} + F - H \quad 2\text{-}58$$

$$\bar{S}^o = A\ln(t) + Bt + \frac{C}{2}t^2 + \frac{D}{3}t^3 - \frac{E}{2t^2} + G \quad 2\text{-}59$$

$$t = \frac{T}{1000} \quad 2\text{-}60$$

where A, B, C, D, E, F, G and H are coefficients for each species at different temperature ranges (Appendix B) and T is the temperature in Kelvin. For solid carbon, which was assumed to be graphite, enthalpy and entropy were calculated as:

$$\bar{h} = \bar{h}_f^0 + \int_{T_0}^{T} C_p dT \qquad 2\text{-}61$$

$$\bar{s} = \bar{s}_f^0 + \int_{T_0}^{T} \frac{C_p}{T} dT \qquad 2\text{-}62$$

where C_p is [75]

$$C_p = A + BT + \frac{C}{T} + \frac{D}{T^2} + \frac{E}{T^3} + \frac{F}{T^4} \quad [200 \sim 3500K] \qquad 2\text{-}63$$

where A, B, C, D, E and F are coefficients (Appendix B). By solving a set of k chemical equilibrium equations for k unknowns, ξ_k, the number of moles, n_i as well as the mole fraction, y_i, of species i at the equilibrium can be determined accordingly. Applying the computed results (equilibrium product composition), the overall gasification reaction on a basis of 1 kmol of biomass can be determined as following:

$$CH_aO_b + n_{stm}H_2O \longrightarrow n_C C_{(S)} + n_{CO}CO + n_{H_2}H_2 + n_{H_2O}H_2O + n_{CO_2}CO_2 + n_{CH_4}CH_4 \qquad 2\text{-}64$$

where a = 1.5 and b = 0.66 based on the ultimate analysis conducted on the biomass (slash pine). A more detailed computation description is provided in Appendix B.

2.3.3 Mass Balance

Mass balance analysis can be conducted to examine the quantitative mass balance closure of chemical elements involved in the overall gasification reaction. Conservation of mass was applied to the gasification process:

$$\sum M_i = \sum M_o \qquad 2\text{-}65$$

where

$$\sum M_i = M_{i,b} + M_{i,stm} \qquad 2\text{-}66$$

$$\sum M_o = M_{o,g} + M_{o,c} \qquad 2\text{-}67$$

and i stands for the process input and o stands for the process output.

2.3.4 Energy Balance

Applying the conservation of energy, the energy balance of the gasification system was evaluated. The first law equation for a steady-state process, neglecting changes in kinetic and potential energy and shaft work, becomes:

$$\dot{Q}_{C.V.} + \sum_i \dot{m}_i h_i = \sum_e \dot{m}_e h_e \qquad 2\text{-}68$$

where

$$\sum_i \dot{m}_i h_i = \dot{m}_{BM} h_{BM} + \dot{m}_{stm} h_{stm} \qquad 2\text{-}69$$

$$\sum_e \dot{m}_e h_e = \dot{m}_c h_c + \dot{m}_{H_2} h_{H_2} + \dot{m}_{CO} h_{CO} + \dot{m}_{CO_2} h_{CO_2} + \dot{m}_{H_2O} h_{H_2O} + \dot{m}_{CH_4} h_{CH_4} \qquad 2\text{-}70$$

On a basis of 1 kmol of biomass (n_{BM} =1)

$$\sum_i n_i h_i = n_{BM} h_{BM} + n_{stm} h_{stm} \qquad 2\text{-}71$$

$$\sum_e n_e h_e = n_c h_c + n_{H_2} h_{H_2} + n_{CO} h_{CO} + n_{CO_2} h_{CO_2} + n_{H_2O} h_{H_2O} + n_{CH_4} h_{CH_4} \qquad 2\text{-}72$$

The enthalpy of biomass at standard temperature and pressure is equal to the enthalpy of formation of the biomass. The enthalpy of formation of the biomass is calculated using the combustion of biomass with oxygen and the HHV of biomass (19738.45 kJ/kg).

$$CH_{1.5}O_{0.66} + n_{O_2} O_2 \leftrightarrow n_{CO_2} CO_2 + n_{H_2O} H_2O(l) \qquad 2\text{-}73$$

$$\bar{h}^0_{f,BM} = HHV_{BM} + n_{O_2} h_{O_2} + n_{CO_2} h_{CO_2} + n_{H_2O} h_{H_2O(l)} \qquad 2\text{-}74$$

2.3.5 Exergy Balance

An exergy analysis was also conducted on the gasification system to evaluate the balance of the quality of energy. The overall exergy balance, neglecting exergy for potential energy and kinetic energy can be expressed as

$$\sum_i \dot{m}_i e_i = \sum_e \dot{m}_e e_e - \dot{I} \tag{2-75}$$

where

$$\sum_i \dot{m}_i e_i = \dot{m}_{BM} e_{BM} + \dot{m}_{stm} e_{stm} \tag{2-76}$$

$$\sum_e \dot{m}_e e_e = \dot{m}_C e_C + \dot{m}_{H_2} e_{H_2} + \dot{m}_{CO} e_{CO} + \dot{m}_{CO_2} e_{CO_2} + \dot{m}_{H_2O} e_{H_2O} + \dot{m}_{CH_4} e_{CH_4} \tag{2-77}$$

The chemical exergy for biomass was calculated using the statistical correlation of Szargut and Styrylska [65]

$$e_{BM}^{CH} = \beta \cdot LHV_{BM} \tag{2-78}$$

where

$$\beta = \frac{1.0412 + 0.2160\frac{z_{H_2}}{z_C} - 0.2499\frac{z_{O_2}}{z_C}\left[1 + 0.7884\frac{z_{H_2}}{z_C}\right] + 0.0450\frac{z_{N_2}}{z_C}}{1 - 0.3035\frac{z_{O2}}{z_C}} \tag{2-79}$$

valid for $\frac{z_{O2}}{z_C} \le 2.67$ and z_C, z_{H_2}, z_{O_2} and z_{N_2} are the mass fractions of oxygen, carbon, hydrogen and nitrogen, respectively in the biomass.

2.3.6 Steam to Biomass Ratio

The steam to biomass ratio represents the ratio between the supplied steam and the biomass. The steam to biomass ratio is defined as the number of moles of steam input to the number of moles of the biomass:

$$SB = \frac{n_{steam}}{n_{Biomass}} \quad \text{2-80}$$

2.3.7 Carbon Conversion Efficiency

The carbon conversion efficiency is defined as the ratio of the number of moles of the solid carbon reacted during the process to the number of moles of the solid carbon in the biomass:

$$\eta_C = \frac{\left(n_{C(S),Biomass} - n_{C(S),in the product}\right)}{n_{C(S),Biomass}} \times 100 \quad \text{2-81}$$

Carbon conversion efficiency indicates the effectiveness in converting the solid biomass into gaseous form during the gasification process.

2.3.8 Thermal Efficiency

Thermal efficiency for the biomass gasification system was computed as the ratio of enthalpy of syngas mixture divided by the enthalpy of biomass (enthalpy of formation of biomass) and the enthalpy of steam. The expression is given as follows:

$$\eta_{th} = \frac{H_{gas}}{H_{biomass} + H_{steam}} \times 100 \quad \text{2-82}$$

2.3.9 Exergetic Efficiency

Exergetic efficiency for the biomass gasification system was determined as the ratio of exergy of syngas divided by the exergy of biomass and the exergy of steam. The expression is given as follows:

$$\eta_{Ex} = \frac{Ex_{gas}}{Ex_{biomass} + Ex_{steam}} \times 100 \quad \text{2-83}$$

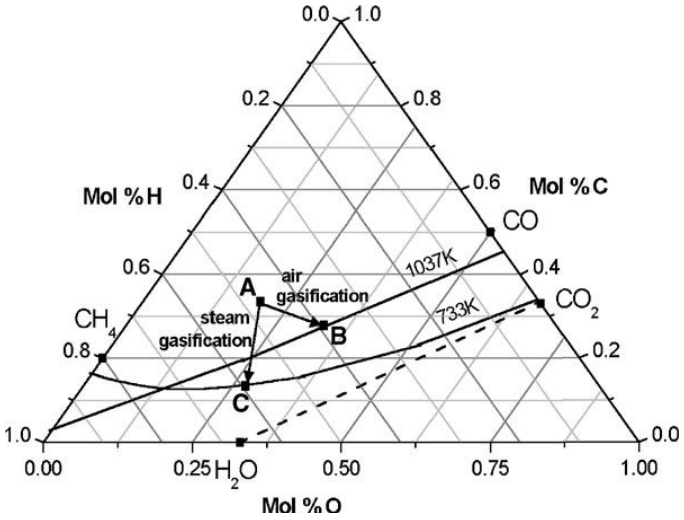

Figure 2-1. The C-H-O ternary diagram presented by Prins et al [42].

Table 2-1. Summary of Gasification Condition used by Krzysztof J. Ptasinski et al. [68].

		Air flow (kg/kg	Product gas composition (mole fraction)						
Fuel	T (^{o}C)	biomass)	H_2O	N_2	H_2	CO	CO_2	CH_4	H_2S
Treated wood	655	1.628	0.062	0.409	0.213	0.194	0.112	0.01	0

Table 2-2. Syngas molar composition (%) (800^{o}C, 1 bar) [70].

		Product gas composition (mole fraction)					
Fuel	T (^{o}C)	H_2	CO	CO_2	CH_4	N_2	O_2
Pine sawdust	800	50.9	43.38	4.09	1.56	0.07	0

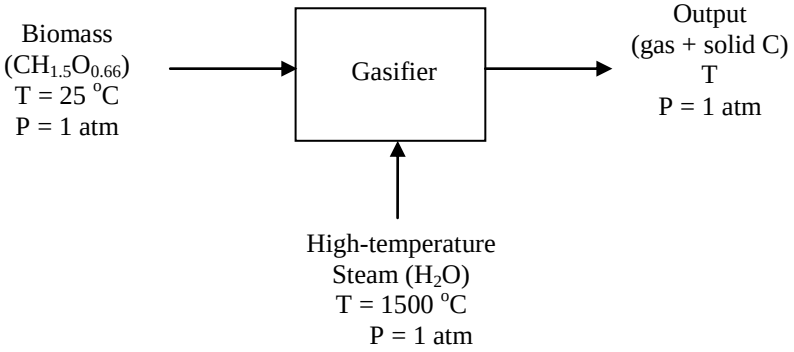

Figure 2-2. Flow diagram of the theoretical model of biomass gasification process.

CHAPTER 3
EXPERIMENTAL TREATMENT OF THE GASIFICATION PROCESS

This chapter discusses in detail the design and construction of the High-Temperature Biomass Gasification System (HTBGS). This discussion incorporates every aspect of the biomass gasification system and the control/data acquisition (DAQ) system. Each system is further divided into components in the following sections for design/discussion purposes. This chapter also discusses the experimental method including detailed explanations for the experimental set up, biomass analysis results and experimental conditions.

3.1 Biomass Gasification System

The biomass gasification system includes three main components, a gasification reactor, a gas injection and ignition system and a cooling and cleaning system. Other parts of the system including a gas exhaust system and gas sampling port are also discussed. The gasification reactor and the gas injection and ignition system are further broken down into multiple components which are all discussed in the following sections. The gasification system employs each of these components together for proper functionality.

3.1.1 Gasification Reactor

The gasification reactor is the main component in the overall gasification system where the selected biomass is transformed from solid to gas by a partial oxidation process. There are several criteria which affect the reactor design. The first requirement is a tolerance to operate the gasification reaction at extremely high temperatures (at around 1500^{o}C). This thermal criterion places a large number of restrictions on material selection and geometry. The main characteristic of the reactor was the modularity of the gasification chambers, which played a large role in determining the geometry of the entire reactor. The overall configuration of the gasification reactor resulted in a tower constructed of concentric cylindrical modules (Figure 3-1). As

mentioned previously, the gasification reactor is composed of a number of subcomponents. The components to be discussed here include the combustion chamber, the gasification chamber, the grate, the lid and the biomass feeding system, the gasket and insulation blanket.

3.1.1.1 Combustion chamber

The main design goal of the combustion chamber was to house the extremely high temperature combustion products of oxygen and hydrogen. This objective played directly into selecting both the chamber material and chamber geometry.

The combustion chamber was constructed with several layers of materials to provide an insulated shell for the combustion process. The main thermal criterion of the inner chamber layer was to provide the thermal tolerance to temperatures up to 1500^{o}C. This extremely high temperature prohibited the use of common metals such as stainless steel since the melting temperatures of many metals are lower than 1500^{o}C. Furthermore, the use of a refractory metal, such as tungsten, was not an option, because many of the refractory metals are very susceptible to the oxidizing environment created in the chamber. Some ceramics, on the other hand, provide both tolerance to high temperatures and oxidizing environments. Zirconium Oxide (ZrO_2) or zirconia is a refractory ceramic with high temperature properties, having a very high strength and fracture toughness when combined with compounds of Yttria. Zirconia can be used in high temperature environments as high as 2400^{o}C, which would provide an ample thermal safety zone when the reactor is operated at around 1500^{o}C. Moreover, this material has a porosity of 0% and a density of 6.60 gm/cm^3 (0.238 lb/ft^3), which is excellent for the prevention of gas leakage. Zirconia possesses a low thermal conductivity of 2.20 W/m-K (15.3 BTU/ft^2-hr-^{o}F/in. at room temperature), which works favorably for insulation purposes [76]. Thus based on these mechanical and thermal properties, zirconia ceramic appeared to be a good candidate for the combustion chamber material. However, there are some critical downsides with Zirconia.

Zirconia is a very expensive material thus from the economic point of view it is preferable to use an alternative material as long as it possesses similar mechanical and thermal properties. The other and the more critical issue was its long lead-time for parts availability. Zirconia is not a readily available material especially when particular sizes and shapes are required for construction. Therefore, it was preferred to find a replacement material in terms of the constraints placed on the project time. High-density machinable alumina (AL_2O_3) is another type of high-temperature ceramic, which can work at temperatures as high as 1800^oC depending on the purity of alumina. High-density machinable alumina is a dense, zero porosity, high-strength alumina. High-density machinable alumina also possesses extreme wear and abrasion resistance, high strength and chemical corrosion resistance under high temperature. High-density machinable alumina is reported as being machinable with conventional tooling on standard shop equipment and does not require heat treatment. High-density alumina, unlike zirconia, is relatively a low cost material. For these reasons, 96% purity high-density machinable alumina was selected for the combustion chamber inner layer material.

The main purpose of the middle layer of the combustion chamber was to provide thermal insulation. This is to protect the outer metallic shell from thermal degradation. Low-density alumina is a type of ceramic commonly used as a high-temperature insulation material and serves perfectly for this application. Low-density alumina has a melting point of 1870^oC (3392^oF) and a maximum operation temperature of 1700^oC (3092^oF) [77]. Unlike high-density alumina, which has a density of 3 g/cm^3 and high thermal conductivity of 4.62 W/m-K [78], low-density alumina has a high porosity of 84%, density of 0.48 g/cm^3 and thermal conductivity of 0.39 W/m-K (at 1400^oC) [77], which is less than one tenth of that in high-density alumina. The cost and availability of low-density alumina is comparative to high-density alumina with a typical

delivery time of 3 to 6 weeks. For these reasons, low-density alumina was chosen for the middle layer insulation material.

The purpose of the outer layer of the combustion chamber was to provide the physical strength as a shell for the reactor. Stainless steel has a melting temperature of 1400^{o}C (2550^{o}F) and thermal conductivity of 16.2 W/m-K (112 BTU-in/hr-ft^{2}-^{o}F) [79]. Stainless steel is a very commonly used metal, thus there is no issue regarding availability. For these reasons, stainless steel (SAE304) was selected as the outer layer of the combustion chamber. The property summary of high-density alumina, low-density alumina and stainless steel is provided in Table 3-1.

The cylindrical chamber geometry was chosen for minimizing the surface area for heat loss and ease of construction. Furthermore, a cylindrical geometry is preferred in gasification chambers to facilitate a smooth fluidization of gas. The wall thickness of the chamber is a very important design element. It is important to select the thickness of the layer walls so that the temperature at each point of the wall is lower than the operation maximum temperature of the material at that location. While enough thickness is required for insulation, it is also important to design the thickness to be as thin as possible from economic point of view. To confirm the temperature drop through three layers, ProEngineer/ProMechanica was used to perform thermal modeling on the designed reactor assuming a constant chamber inner wall temperature of 1500^{o}C and typical convective heat transfer coefficient of 0.011 kW/m^{2}-K (2 BTU/h-ft^{2}-^{o}F) for air, convection and radiation effects included. A thermal model for the gasification reactor and a front view of the combustion chamber are shown in Figures 3-2 and 3-3, respectively.

3.1.1.2 Gasification chamber

The main function of the gasification chamber is to host the high temperature gasification of woody biomass. The gasification chamber provides the place for the biomass gasification

reaction, and occupies the largest section of the entire reactor followed by the combustion chamber. In the gasification chamber, woody biomass first receives the heat and steam from the oxygen and hydrogen combusted in the combustion chamber, and goes through a number of chemical reactions to be converted to the product gas and solid. As previously discussed, the gasification chamber is constructed by connecting several cylindrical modules. Each module is bolted together at the flange for frame support as well as for the purpose of sealing the gas inside the chamber. The main purpose of the modular reactor chamber is to add flexibility in changing the size of the reactor by adding or removing modules and rotating each module to move the temperature measurement locations (more detail is described in the following section).

The conditions that the gasification chamber materials need to withstand include the high temperature and the oxidation environment. The thermal criterion remains the same: keeping the gasification chamber temperature at 1500^{o}C. The pressure inside the reactor is difficult to predict because the pressure will be affected by several unknown factors including the number and the type of chemical reactions, the volume expansion due to those chemical reactions and the actual temperature rise in the reactor. However, the operation goal in terms of the gasification pressure is to keep the reactor pressure within a few psig.

The gasification chamber materials need to provide the tolerance to the conditions described above. Since the thermal condition inside of the gasification chamber is similar to that in the combustion chamber, high-density machinable alumina with 96% purity is selected for the gasification chamber inner layer material. Again the purpose of the middle-layer is to provide insulation as in the combustion chamber case, thus low-temperature alumina (Al_2O_3 80, SiO_2 20) was chosen. The purpose of the outer layer of the gasification chamber was to provide the strength for support, to serve as available surface for welding and threading as needed and to

provide a flange section to fit each module together. These requirements are the same as those for the combustion chamber outer layer, thus stainless steel (SAE304) was chosen as the material for the gasification chamber outer layer.

As previously discussed, the geometry of the gasification chamber is developed by stacking the cylindrical modules. Each module has an inner diameter of 100 mm and an outer diameter of 220 mm, where high-density alumina inner-layer wall thickness is 25 mm, low-density alumina middle-layer wall thickness is 25 mm and stainless steel outer-layer wall thickness is 10 mm. There are 10 mm thick flanges attached at the top and the bottom of the stainless steel outer-layer, which can also serve as the top and the bottom of the module. The flange has a diameter of 340 mm. On each flange, there are 6 holes (13 mm diameter) which are used to bolt the flanges of the modules together. On the side of the module, there are three holes of 7 mm in diameter drilled through the wall. These holes are located at the center of the module: 50 mm from both the top and the bottom. These holes serve a multiple of purposes, including thermocouple insertion openings for temperature measurement, pressure transducer connections for pressure measurement and additional steam injection openings. It was also considered to build one module with all the shape and dimensions identical to what has been described but having six side holes instead of three. The purpose of this module is to replace one of the modules in the gasification reactor so that the temperatures of more inner locations are to be measured. In HTBGS, the number of modules of four was selected as the standard size based on the expected amount of biomass of 0.5 to 1 kg. It was later determined that only 56 and 28 g of wood sawdust was used in each experiment.

3.1.1.3 Grate

The grate is located between the combustion chamber and the bottom gasification chamber. The functions of the grate are to support the woody biomass above the combustion

chamber. The grate experiences the same property restrictions as the combustion chamber and the oxidizing environment. Considering these thermal and chemical conditions, high-density machinable alumina with 96% purity and low-density alumina were selected for the biomass grate material. Figure 3-5 presents the top view of the grade. A few extra grates with a different design feature were also prepared including a grate with low-density alumina, a grate with different thickness and grates with different hole sizes.

3.1.1.4 Lid and biomass feeding system

The lid is located over the gas flange to seal the content of gasification reactants. The flange of this lid lays on top of the flange of the top module (separated by a graphite gasket) in the gasification chamber, and these two flanges are bolted together. Due to the low temperature expected for the lid and required machining flexibility, stainless steel (SAE304) was selected for the lid material. The dimension of the top lid was chosen to be compatible with the gasification chamber module. The diameter of the lid is 340 mm and the thickness of the lid is 15 mm. The gasification product gas exits from the reactor through the transition pipe which is welded on the lid (Figure 3-6). The pipe outer diameter is 70 mm, the pipe inner diameter is 50mm, and pipe height is 85 mm.

A biomass feeding system is attached to the top of the gasification lid. The main purpose of this feeding system is to provide a gas tight storage and biomass feeding system. The important criterion of this system was to prevent gas leakage from the reactor body through this system while introducing the biomass. In order to satisfy both the main purpose and the criterion, the biomass feeding system was constructed of a series of pipes and valves as shown in Figure 3-7. The system is composed of a curved stainless steel coupling welded on the lid, two 2 inch brass ball valves, two 2 to 4 inch schedule 40 pipe reducers, a 4 x 6 inch schedule 40 pipe nipple and two 2 inch schedule 40 short nipples. In the experiment, prior to the ignition of the torch, the

biomass was placed in a pipe space between the two ball valves. The top valve serves to separate the biomass from the environment. The bottom valve is closed to hold the biomass during the heating period. Once the reactor is heated and ready for the gasification, the bottom valve is opened to release the biomass into the system. The feeding system was purged with carbon dioxide prior to loading it with biomass.

3.1.1.5 Gaskets

The main purpose of the gaskets was to seal the space between each module to prevent gas leakage. The gasket material has to have certain thermal and chemical characteristics such as tolerance to high temperature and oxidizing environments. Typical high-temperature gasket materials available include mica, ceramic and graphite. Mica however can only take temperatures up to 1000^{o}C, thus this is not an option. Ceramic gaskets could be used at temperatures up to 1320^{o}C, while the combustion and gasification temperature goal in the HTBGF is 1500^{o}C. Graphite gaskets, on the other hand, can be used at significantly higher temperature (up to 3000^{o}C) in inert or reducing environments. However the operation temperature range reduces to 650^{o}C in steam environments and 500^{o}C in air due to its susceptibility to an oxidizing atmosphere. Oxidation of the gasket depends on several variables such as exposed surface area of the gasket, temperature, time of exposure, and purity of carbon. Any oxidation is dependent on the exposed surface area of the gasket thus a thicker gasket is subject to higher oxidation for a larger exposed edge. Oxidation effects also become more severe at higher temperatures and longer exposures at these temperatures. The purity of graphite or the ash content also affects oxidation in a way that the higher the purity of graphite, the smaller the oxidation effect. Based on these facts, no gasket material possesses both tolerances to the operation temperature of 1500^{o}C and an oxidizing environment simultaneously. However, since mica and ceramic cannot be used in this temperature range at all, a graphite gasket was

considered as the best possibility to handle the condition. The thickness of 3 mm was chosen for the gaskets. The gaskets were recessed in slots to reduce exposure to the steam environment while still providing a gas tight seal.

3.1.1.6 Insulation blanket

An insulation blanket was applied around the gasification reactor to prevent heat loss through the reactor wall to the ambient. The insulation material was carefully selected in order to contain the heat as much as possible in the reactor and at the same time keep the temperature of the stainless steel below its maximum operational temperature. A ceramic flexible blanket was selected to serve this purpose. The summary of the property of this insulation blanket is provided in Table 3-2.

3.1.2 Gas Injection and Ignition System

In the HTBGS system, high-temperature steam is used to provide the heat necessary for the gasification reaction as well as to serve as the gasification agent to react with the biomass. This high-temperature steam is produced by injecting hydrogen and oxygen through a torch mounted on the combustion chamber and subsequently igniting these gases as they come out the torch.

3.1.2.1 Process gases used

The types of process gas used in the HTBGS system are hydrogen, oxygen and carbon dioxide. This hydrogen is ultra high purity gas and has 99.999% purity. This oxygen gas and the carbon dioxide gases are both industrial grade and have 99.9% purity. Hydrogen was used to combust with oxygen to produce high-temperature steam. There were two main purposes of using carbon dioxide. The first purpose was to dilute the oxygen with carbon dioxide before the combustion with hydrogen occurs so as to control the combustion temperature. The second purpose was to use the carbon dioxide to purge the system before and after the operation as well as during any operational emergency.

3.1.2.2 Torch

The main function of the torch was to introduce the hydrogen and oxygen gas to the gasification reactor and to combust the gas mixtures to produce high-temperature steam. The material selection for the torch followed the same requirement as that for the combustion chamber, the tolerance for high temperature and an oxidizing environment. For the same reasons that the chamber was made of alumina, the main torch body was made of high-density machinable alumina with 96% purity. On the other hand, stainless steel was used to construct the back portion of the torch. The stainless steel provided the structural strength required at this section because of the stresses involved in connecting the torch to the combustion chamber and connecting the gas tubes to the torch. The structure of the torch was comprised of a ceramic rod with one concentric hole in the center and two smaller holes running parallel to this hole. A stainless steel tube of a smaller diameter was inserted through the center hole (Figure 3-8). The hydrogen gas was introduced to the reactor though this stainless steel tube, while oxygen and/or carbon dioxide gas was introduced through the annular space of this tube in the concentric hole. This way, the hydrogen and the oxygen met only at the moment when they were ignited; the flame attaching itself to the end of the stainless steel tube. A CAD image of hydrogen/oxygen torch mounted on the combustion chamber is shown in Figure 3-9, and the side, front and the back views of the torch are presented in Figure 3-10.

For the electrodes used under these high temperature conditions, platinum was considered due to its high melting point (1772^{o}C) and its high conductivity of heat (71.6 W/m-K) and electricity (9.66 x 10^{6}/m-Ω) as well as its ability to resist chemical corrosion [80]. However, because of its high cost, an alternative metal was considered. Another very commonly used material for this application is iridium, which has higher melting point and conductivity, and is significantly more economical. Iridium is a transition metal of the platinum family possessing a

high melting point (2793 K or 2466^{o}C) and a high thermal conductivity (147 W/m-K at 300K) as well as electrical conductivity (19.7 x 10^{6}/m-Ω) [80]. Iridium is known as the most corrosion resistant metal, and used extensively as spark plug material. For these reasons, iridium was selected for the electrodes. It was later discovered during the experiment that iridium became extremely brittle after several test runs possibly due to the sudden cooling of the torch following the high temperature runs. The iridium wires were later replaced with heavy gage copper wires with expendable small gage copper wires soldered to the end for producing the arc for ignition.

The diameter of the torch was 32 mm and it is 200 mm in length. The concentric hole at the center of the torch was 4.8 mm in diameter, the hydrogen injection stainless steel tube was 1/8 inch outer diameter and the iridium rods were 1mm in diameter. At the torch tip, iridium rods extend out and are bent toward each other to form a spark gap. On the other side of the igniter, the extended iridium rods are protected by plastic tubes to insulate them from the stainless steel section so that a short would not occur between the ignition wires and the surrounding metals.

3.1.2.3 Ignition system

A piezoelectric gas grille igniter was connected to the ignition wire passing through the torch (Figure 3-11). A spark is generated at the front of the torch as the igniter is struck.

3.1.3 Cooling and Cleaning System

The gasification product gas is cooled and cleaned by going through the cooling and cleaning system. This cooling and cleaning system was designed to handle approximately 0.034 m^{3}/s of gas based on the gasification model using 1.5 kg of woody biomass at the operation temperature of 1500^{o}C, a pressure of 1.5 bar, a steam to biomass ratio of 1.1 and reactor exit temperature of 1100^{o}C. Each container body is in cylindrical shape with 15 cm (6 inches) in inner diameter and 24 cm (9.5 inches) in height. The gas enters the container through a ¾ inches pipe welded on the lid. This pipe extends all the way down to the bottom of the container and is

shaped to create a cyclonic effect as the gas stream leaves the pipe. The gas in the container exits through another ¾ inches pipe welded on the lid and moves to the next container. A 304 stainless steel was selected for the container material considering the temperature expected for the gases leaving the reactor. A photo of the cooling and cleaning container is presented in Figure 3-12.

This system is composed of three identical size containers connected in series where the first container is empty, the second container is filled with glass marbles and the third container is filled with a stainless steel mesh (Figure 3-13). All these containers are emerged in an ice bath during the experiment. As the gasification product gas goes through the first container, the steam is cooled and condenses. In the second and the third containers, the marbles and the mesh provide further contact area for cooling of the gas as well as mechanical filtration of any particulates from the gas. Figure 3-14 presents the overall view of the three containers connected in series and placed in coolers to cool the exit gases from the gasification reactor. The steam condensing in the containers during the reactor warm up period provides a scrubbing agent when the actual gasification process begins.

3.1.4 Gas Exhaust and Gas Sampling Port

In HTBGS, the gas produced inside of the gasification reactor goes through the cooling and cleaning system, sampling port, a flow meter and then is sent through a hose to finally be exhausted to the ambient. The gas can be exhausted either naturally or by being evacuated by the vacuum created by an air compressor and an ejector. Figure 3-15 presents a view of the exhaust system; a flow meter, the hose and the ejector.

Product gas is sampled at the sampling port located after the cooling and cleaning system (Figure 3-16). At this location, the gas is sufficiently cooled and cleaned to send to the gas chromatograph for composition analysis. 0.5 litter gas tight bags were used in the experiments to

collect sample gases. After the gas analysis, any gas left in the sampling bags was removed using a vacuum pump so that the bags can be recycled.

3.2 Control/DAQ System

The control/DAQ system manages the power supply to all components of the HTBGF and provides a variety of data acquisition capabilities for the gasification tests including temperature and pressure measurements. A schematic flowchart of the control/DAQ system is shown in Figure 3-17. The control/DAQ hardware is responsible for managing the input/output signals and feedback signals. The hardware consists of the DAQ hardware, DAQ sensors and a gas chromatograph. The DAQ hardware includes DAQ boards, a PC card controller and a power supply cable. The DAQ sensors include thermocouples, pressure transducers, pressure gauges and rotameters.

3.2.1 DAQ hardware

The DAQ hardware consists of an Omega instruNet100 A/D box (Figure 3-18), the Omega instruNet230 PC-card controller (Figure 3-19) and an Omega instruNet-312-8 power supply cable. The instruNet100 A/D box is used for reading all temperature sensors. This box provides 16 single-ended/8 differential analog inputs, 8 analog outputs and 8 digital I/O lines, and contains signal conditioning amplifiers for each channel, which can directly attach to sensors. The instruNet230 PC-card controller is the communication device required to connect the instruNet100 to the computer. The instruNet-312-8 is an external power supply to transform the voltage down from 110 V to 5 V.

3.2.2 DAQ Sensors

The DAQ sensors are used to obtain various combustion/gasification test data as well as to provide in-situ feedback to the computer for operational control and safety purposes. The DAQ sensors include thermocouples to measure the gas temperature at various points of the system,

pressure transducers to measure the pressure inside of the gasification reactor and at the reactor exit, pressure gauges to measure the pressure of hydrogen, oxygen and carbon dioxide entering the reactor, rotameters to measure and control the volume flow rate of hydrogen, oxygen and carbon dioxide entering the reactor as well as the gas flow rate exiting the system and the pressure gauges to observe the inlet gas pressures of hydrogen, oxygen and carbon dioxide. The discussions of design, details of features and placement of these sensors are provided in the following sections.

A number of thermocouples are employed in the HTBGS that continuously take temperature measurements for combustion and gasification test characterization in the gasification reactor as well as for monitoring the outer piping system after the gasification products are exhausted from the reactor. There are three kinds of thermocouples for a total of 16 employed in the HTBGS. The selection of the type of thermocouple is based on the temperature range requirement at each measurement point. The Omega B-type thermocouples (Figure 3-20) consisting of platinum wires with a 0.25 mm (0.0100 in.) thickness and alumina protection tubes with a diameter of 6.0 mm (0.25 in.) are used at each gasification chamber module. Eight B-type thermocouples are required for these modules. One of two thermocouples is set up to read the temperature on the inner gasification chamber wall, and the other is set up to read the temperature at the center of the reactor as shown in Figure 3-21. There is another Omega B-type thermocouple set up at the combustion chamber. This thermocouple consists of the same material and structure as the other B-type thermocouple, but has the thicker platinum wire with 0.8 mm (0.032 in.) and an alumina protection tube with a diameter of 9.5 mm (0.375 in.). This thermocouple is selected to measure the combustion flame temperature. These thermocouples provide valuable information on the radial and axial temperature gradients inside the reactor

during the gasification process. This set of temperature readings were extremely important data sets collected during the experiment since they indicated whether or not the desired high-temperature gasification was achieved in the reactor.

Omega K-type thermocouples (Figure 3-22) with a Super OMEGACLAD XL sheath with a 3.175 mm (0.125 in.) sheath diameter and ungrounded junction are used in the HTBGS. One is located at the exit of the gasification reactor to measure the temperature of the gasification product gas and the other is located between the first and the second cooling and cleaning containers to measure the temperature decrease of the product gas as it goes through the first container (Figure 3-23).

The third type thermocouple is an Omega T-type thermocouple with a sheath diameter of 3.175 mm (0.125 in.). The sheath material type and junction type are not known. Three T-type thermocouples are used to measure the inlet gas temperatures of hydrogen, oxygen and carbon dioxide (Figure 3-24), and two T-type thermocouples are set up at between the second and the third cooling and cleaning containers and after the third cooling and cleaning container, respectively (Figure 3-23).

There are two of the OMEGA PX309-001GV pressure transducers in the HTBGS. These pressure transducers read 0 to 0.07 bar (0 to 1 psig) and output 0 to 20 mV signal. One pressure transducer is set up at the gasification reactor to measure the gas pressure inside of the reactor. The other is set at the exit of the gasification reactor to measure the product gas pressure. These information are required to compute the energy and exergy values of the gas and are very important to evaluate the gas quality and the reactor performance. The Omega PST-10 power supply is used together to provide the necessary power to the pressure transducers (Figure 3-25). This power supply has regulated 10 V output.

There are four rotameters employed in the HTBGS. Three rotameters are located between gas cylinders and the gasification reactor to measure and control the volume flow rate of inlet hydrogen, oxygen and carbon dioxide gases (Figure 3-26). One Omega FL-2040, which rages 1 to 10 LPM of air is used to control the hydrogen flow, an Omega FL-2042, which ranges 3 to 30 LPM of air is used to control the oxygen flow, and an Omega FL-2044, which measures the gas flow of 10 to 100 LPM of air is used to control the carbon dioxide flow. These rotameters have an accuracy of ± 3% of full scale panel mount. The fourth rotameter is located at after the third cooling container to measure the volume flow rate of exit gas from the system (Figure 3-27). A glass flowmeter ranging 1 to 36 LPM of air was selected to measure the exit gas flow. This rotameter has an accuracy of ± 5% of the flow or 2 mm, whichever is grater.

Three Swagelok Bourdon pressure gauges with 1 to 30 psig reading are set to measure the pressure of hydrogen, oxygen and carbon dioxide inlet gases (Figure 3-24). These gauges are important to confirm that the controlled amounts of gases are introduced to the gasification reactor. A 1 to 30 psig pressure gauge and a 1 to 3 psig pressure gauge was added to measure the pressure of the gasification reactor. The readings from these gauges were used to support or to replace the pressure readings from the pressure transducer where the pressure transducer ceased to function properly. Another set of 1 to 30 and 1 to 3 psig pressure gauges were installed after the third cooling container to obtain the pressure information for the exit gas (Figure 3-28).

3.2.3 Gas Chromatography

The SRI gas chromatograph model 8610-C (Figure 3-29) was used to analyze the gasification product gas composition together using the software called PeakSimple which is also provided by SRI. In this GC, both flame ionization detector (FID) and thermal conductivity detector (TCD) were used.

In order to analyze the product gas composition with the GC, a calibration gas was first prepared. The calibration gas needs to represent the composition of the actual sample gas. Therefore, the composition of the calibration gas was selected to represent the ideal syngas composition for steam gasification of biomass. There were two calibration gas cylinders prepared because hydrogen cannot mix with other types of gas representing syngas. Both cylinders were balanced with Nitrogen. The summary of the calibration gas composition is provided in Table 3-3. Argon gas was selected as the carrier gas in this test instead of Helium or Nitrogen. Helium gas is not suitable when Hydrogen needs to be detected because both gases have the same molecular weight which makes the distinction of one element from the other difficult. Similarly, nitrogen has the same molecular weight as carbon monoxide thus nitrogen was not selected.

3.3 Gasification Experimental Methods

The overall goal of the experimental portion of this study was to demonstrate, characterize and analyze the high temperature biomass steam gasification system. To achieve this goal, more specific sub-objectives were (1) to experimentally determine the product gas composition focusing on the production of hydrogen and carbon monoxide for various experimental conditions (temperature, pressure, steam to biomass ratio, steam flow rate and resident time), (2) to determine possible increase in hydrogen yield and decrease in liquid and solid residues, (3) to determine the carbon conversion efficiency and (4) to determine the thermal and exergetic efficiencies of the gasification system.

3.3.1 Experimental Setup

A flow diagram of the test set-up for the biomass gasification system is provided in Figure 3-30. It consists of the following components:

1. Injection gases

2. Gasification reactor
3. Cooling and cleaning system
4. Gas exhaust system

3.3.2 Ultimate and Proximate Analysis on Wood Chips

Ultimate and proximate analyses were conducted on six samples of wood chips obtained from Miles Andrews' Timber. Samples included four types of soft wood pines (Sand pine, Longleaf pine, Loblolly pine and Slash pine) and two types of hard wood mix; one is the mix with only hard woods, the other is the mix with hard woods and soft woods. The results for the ultimate and proximate analysis were summarized in Tables 3-4 and 3-5, respectively.

The results for wood chip samples were comparable to those of similar woody biomass sample referred to in the literature (Tables 3-6 and 3-7). Furthermore, it was observed that there was no wide variation in each composition among four soft wood samples, thus it is estimated that the gasification result be very similar regardless which type of pine wood would be available to us.

Since slash pine among six samples is the type of tree encouraged by Department of Forestry in state of Florida for commercial timber growth and is most available for experimental use, slash pine was selected for our gasification study. The ultimate and proximate analysis results for our slash pine and other woody biomass from literatures are compared (Figures 3-31 and 3-32). It is seen that there is very little variation in the components among four type of woody biomass being compared. The form of the woody biomass used in this experiment is presented in Figure 3-33.

3.3.3 Experimental Procedures

Following is the basic experimental procedure conducted in the experiment. The more detail procedure is provided in Appendix C.

1. Fill the ice bath with 70 lb of ice.
2. Set the regulator pressure at 40 psig for the carbon dioxide, hydrogen and oxygen gases.
3. Purge the biomass feeding system with carbon dioxide.
4. Place the biomass (sawdust) in the feeding system.
5. Purge the entire system for 3 minutes.
6. Turn on the air compressor.
7. Start introducing the oxygen gas to the system.
8. Start introducing the hydrogen gas to the system. At the same time, strike the piezoelectric igniter and start recording data at iNET100.
9. Continue the process once the ignition is confirmed by the temperature increase in the combustion chamber. Otherwise, stop introducing the hydrogen and the oxygen and repeat from the step 5.
10. Once the temperatures of the combustion chamber and the gasification module 1 increased to a desired level, introduce the biomass to the system.
11. Sample the gas.
12. Turn off the hydrogen and the oxygen flows.
13. Purge the system with the carbon dioxide for 3 minutes.
14. Once the system is cooled, disassemble the cooling/cleaning containers and measure the water condensed in the containers.
15. Analyze the gas composition with the GC.

3.4 Data Processing Methodology

Each gasification test collects data from 16 thermocouples and 2 pressure transducers. A data processing methodology was necessary to handle this large amount of data. The data processing package employed Matlab to perform the majority of the processing and analysis.

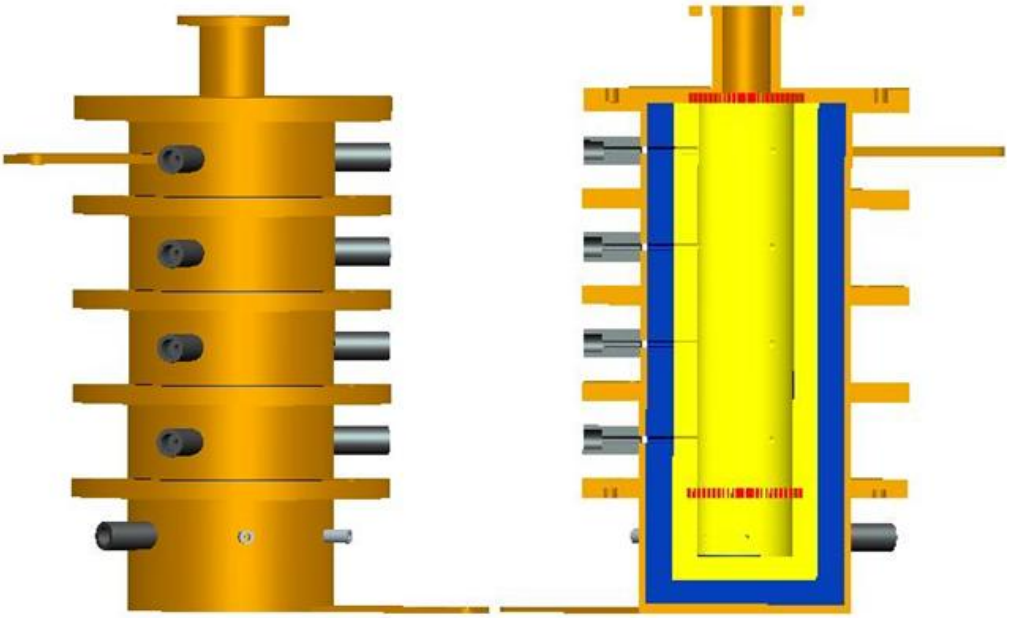

Figure 3-1. A CAD image of an overall configuration of the gasification reactor.

Table 3-1. Summary of the HTBGS reactor material properties.

	High-Density Alumina*	Low-Density Alumina	Stainless Steel (304)*
Composition		Al_2O_3 / 80 SiO_2 / 20	
Density, g/cm^3 (lbs/ft^3)	3.0 (168)	0.48 (30)	8.00 (499)
Open Porosity, %		84	
Maximum Use Temperature, ^{o}C (^{o}F)	1650 (3000)	1700 (3092)	
Melting Temperature, ^{o}C (^{o}F)	1870 (3400)	1870 (3392)	1400 (2550)
Flexural Strength, MPa (psi)	-38,000	2.07 (300)	
Compressibe Strength, MPa (psi)	-60,000	1.31 (190)	
Thermal Conductivity, W/m-K (BTU-in/hr-ft^2-^{o}F)	4.62 (32)	0.39 (2.9)**	21.5 (149)
Specific Heat, J/kg-K (BTU/lb-^{o}F)		1047 (0.25)	500 (0.120)
CTE, x10^{-6}/^{o}C (10^{-6}/^{o}F)	7.74 (4.3)	8.0 (4.5)[a]	18.7 (10.4)

* Property values at room temperature

** Temperature at 1400^{o}C (2252^{o}F)

[a] Room temperature to 1100^{o}C (1832^{o}F)

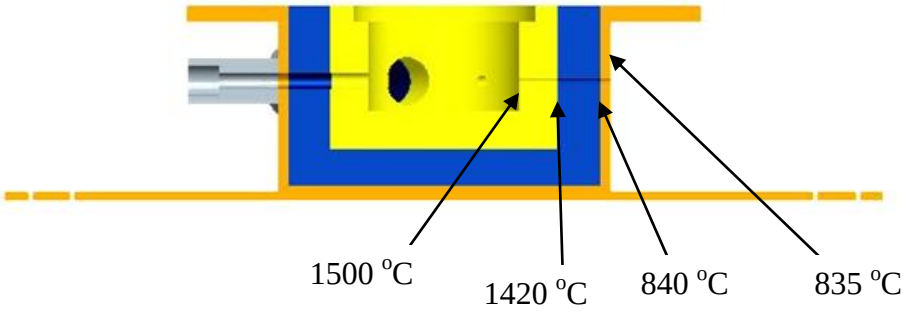

Figure 3-2. A thermal analysis for the reactor wall.

Figure 3-3. A front view of the combustion chamber where the torch is mounted in front and the other tubes extruding from the side are the openings for thermocouples.

Figure 3-4. A stack of three gasification chamber modules.

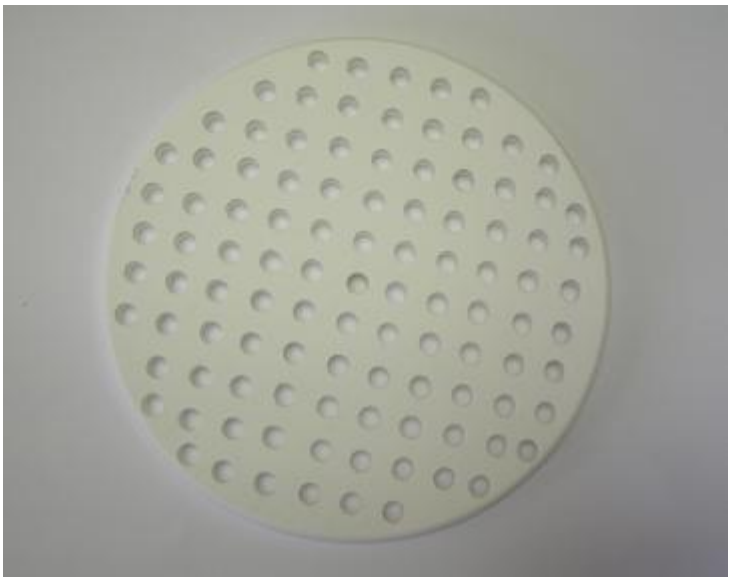

Figure 3-5. A top view of a grate.

Figure 3-6. A view of the gas exit pipe welded on the gasification reactor lid.

Figure 3-7. A view of the biomass feeding system attached to the top of the gasification reactor lid.

Table 3-2. Summary of the insulation blanket material properties.

Properties	
Melting Point, ^{o}C (^{o}F)	1760 (3200)
Service Temperautre, ^{o}C (^{o}F)	1260 (2300)
Density, #/m^3 (#/ft^3)	212-424 (6-12)
Dielectric Constant, @10^8 cps	1.61
Dielectric Strength, volts/mil.	100
Loss Factor	0.017
Specific Heat, J/#-K (BTU/#-^{o}F)	146.5(0.25)
Thermal Conductivity, (BTU-in/hr-ft^2-^{o}F)	
500^{o}F	0.38
1000^{o}F	0.6
1500^{o}F	0.9
2000^{o}F	1.33

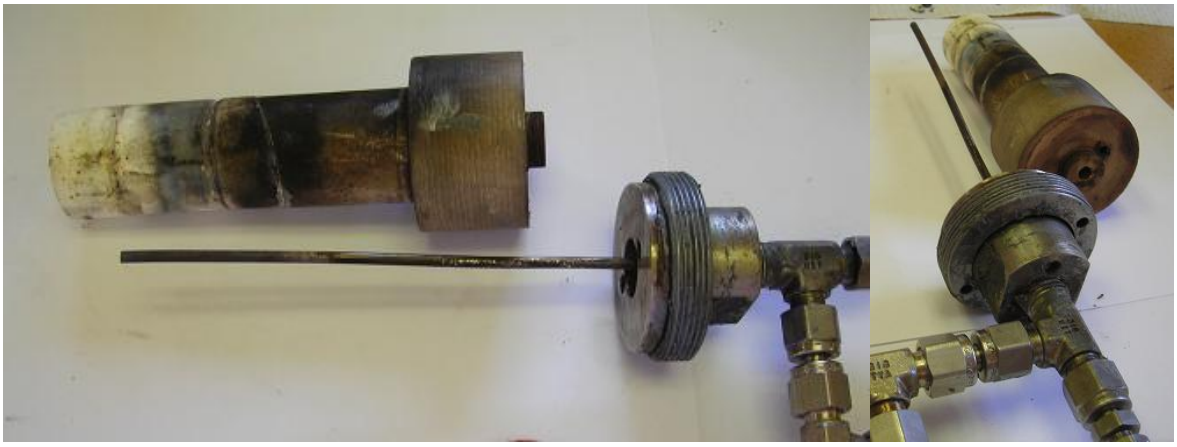

Figure 3-8. A view of the ignition torch illustrating that the stainless steel tube is structured and connected to the torch body.

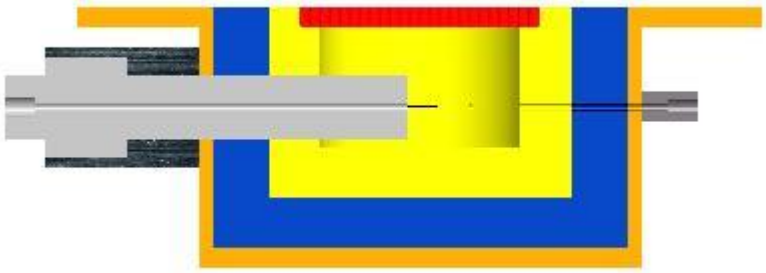

Figure 3-9. A CAD image showing the cross section of the hydrogen/oxygen torch mounted on the combustion chamber.

(a)

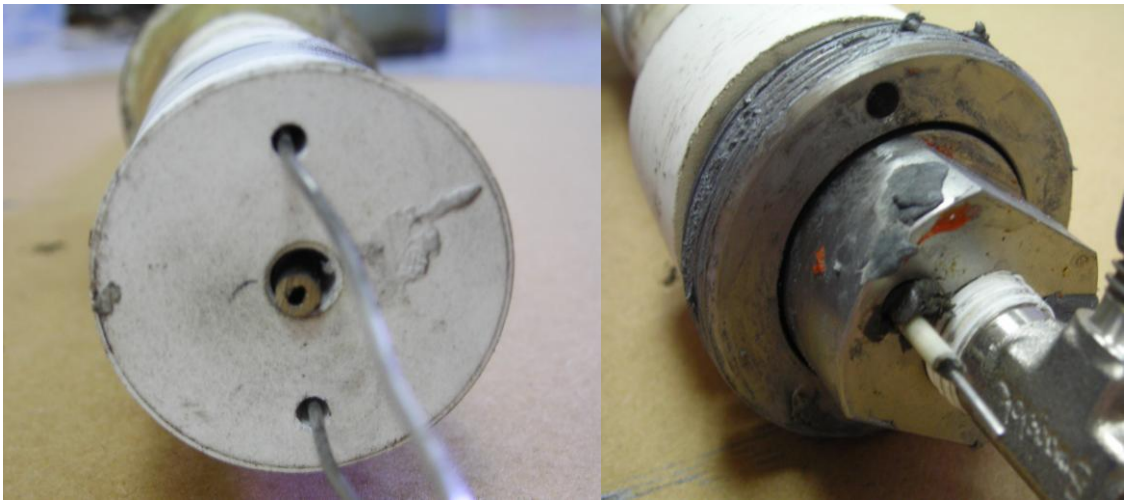

(b) (c)

Figure 3-10. Three views of the ignition torch. (a) A torch view from the side. The main body of the torch is made with high-density alumina while the back portion of the torch is made with stainless steel. (b) A torch view from the front where the hydrogen and oxygen gas exit the torch and meet to start combustion. The concentric tube at the center is where the hydrogen comes out, the annular area of that tube is where the oxygen comes out. The ignition wires are protruding out from the torch. (c) A back view of the ignition torch. The stainless steel ring is to connect the torch to the combustion chamber. A wire protruding out is one of the ignition wires.

Figure 3-11. A view showing the connection between the ignition wires passing through the torch (shown as white lines in the figure) are connected to the igniter wires (shown as a red and a black lines in the figure).

Figure 3-12. A view of a single cooling and cleaning container.

(a)

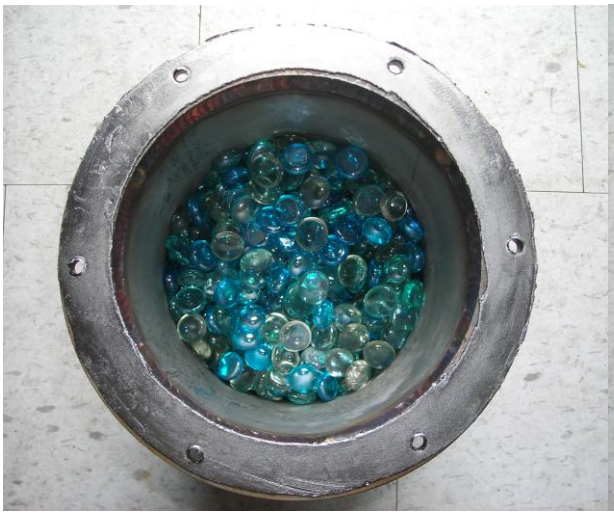

(b)

(c)

Figure 3-13. The views showing the cooling and cleaning containers. (a) The first cooling/cleaning container which is empty inside. (b) The second cooling/cleaning container with marbles. (c) The third cooling/cleaning container with mesh.

(a)

(b)

Figure 3-14. A view showing the three cooling/cleaning containers connected and placed in coolers. (a) A front view of the cooling/cleaning containers. (b) A view of cooling/cleaning containers also showing the connection to the gasification reactor.

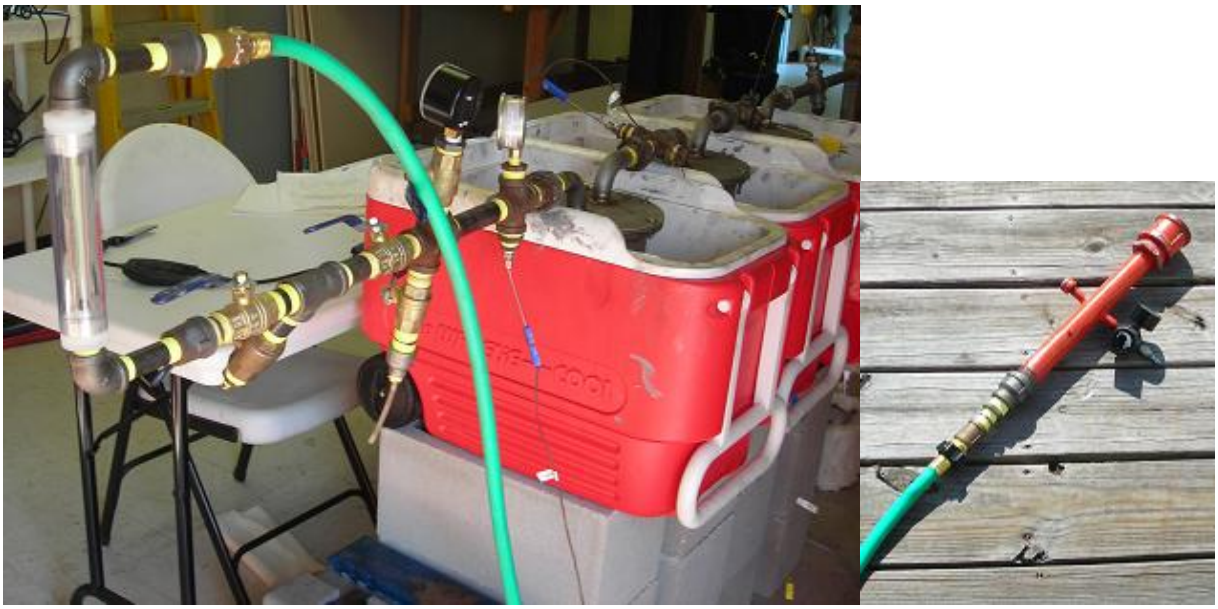

(a) (b)

Figure 3-15. A view of gas exhaust system. (a) The gas passes through the flow meter is sent to the hose and is exhausted outside. (b) The ejector is connected at the end of the hose. The ejector was connected to an air compressor to provide the motive fluid to effect ejection.

(a) (b)

Figure 3-16. A view of gas sampling port (a) The sampling port with a gas sampling bag connected. (b) The location of the gas sampling port.

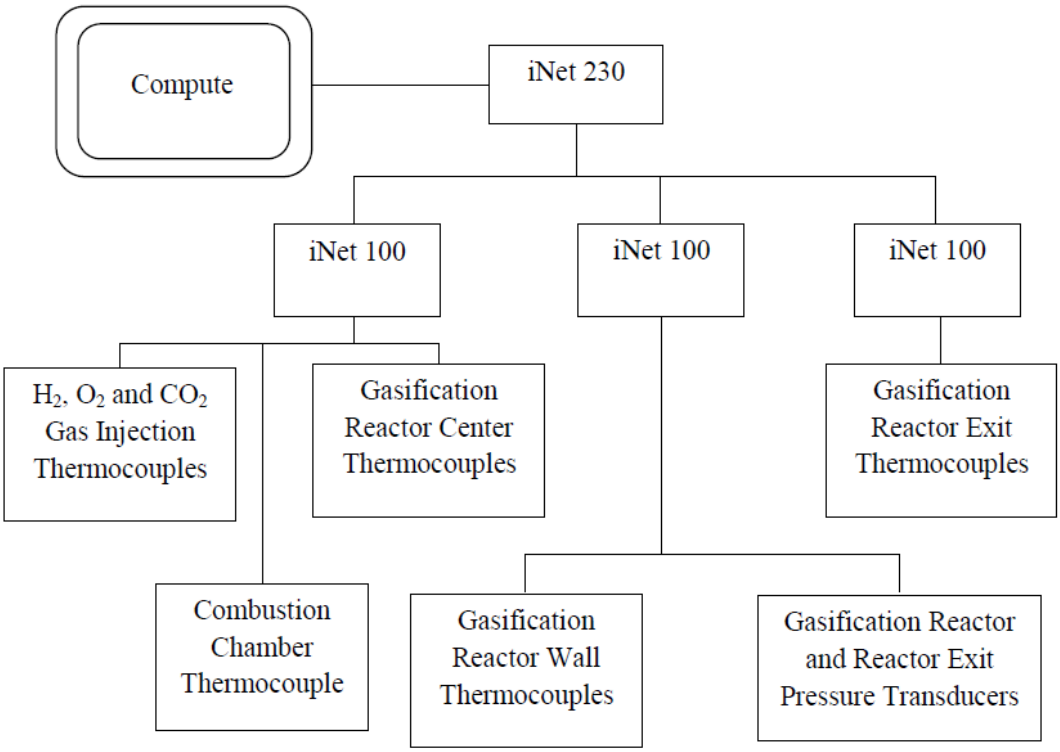

Figure 3-17. Flowchart of the control/DAQ system.

Figure 3-18. Omega instruNet100 DAQ board.

Figure 3-19. Omega instruNet230 PC-card controller.

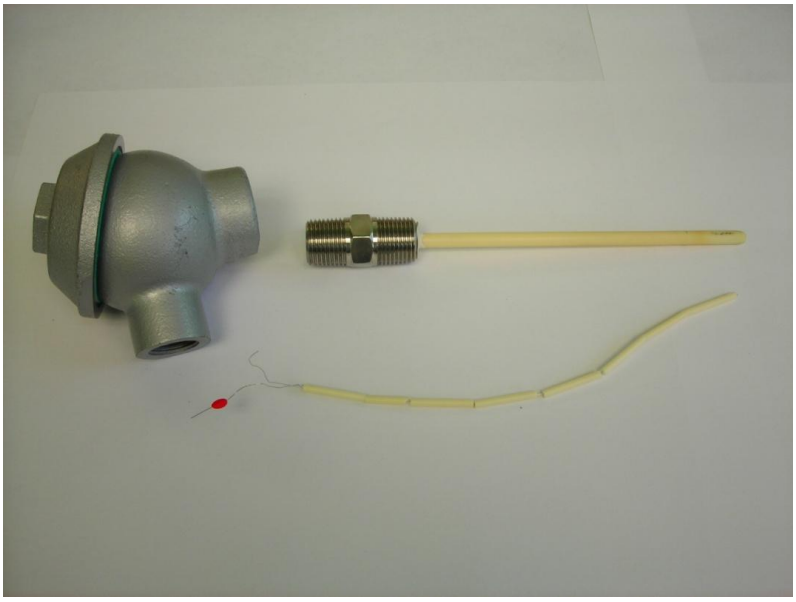
Figure 3-20. Omega B-type thermocouple.

(a) (b)

Figure 3-21. B-type thermocouples on the gasification reactor. (a) An external view of B-type thermocouples mounted on the gasification reactor wall. (b) A top view of the gasification reactor showing B-type thermocouples mounted on the reactor to read the temperatures at the center of the reactor.

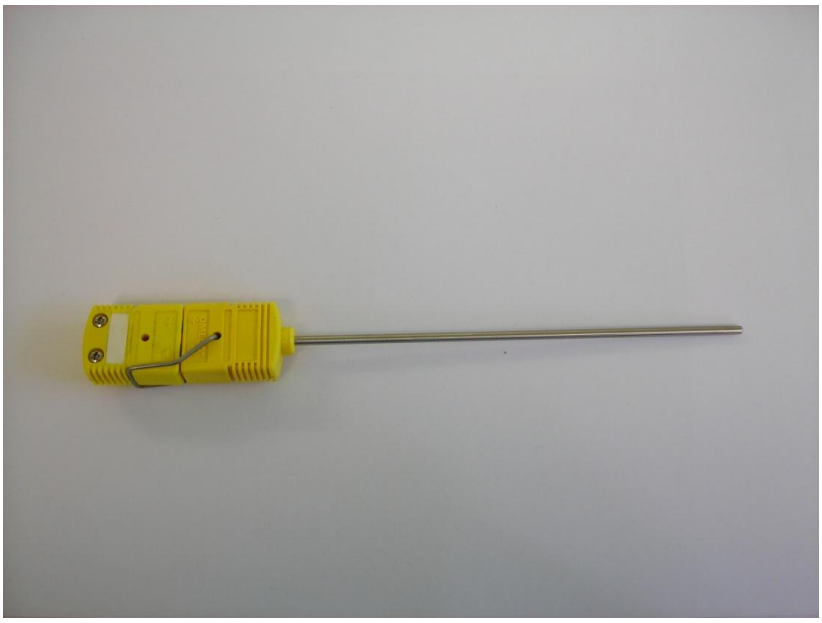

Figure 3-22. Omega K-type thermocouple.

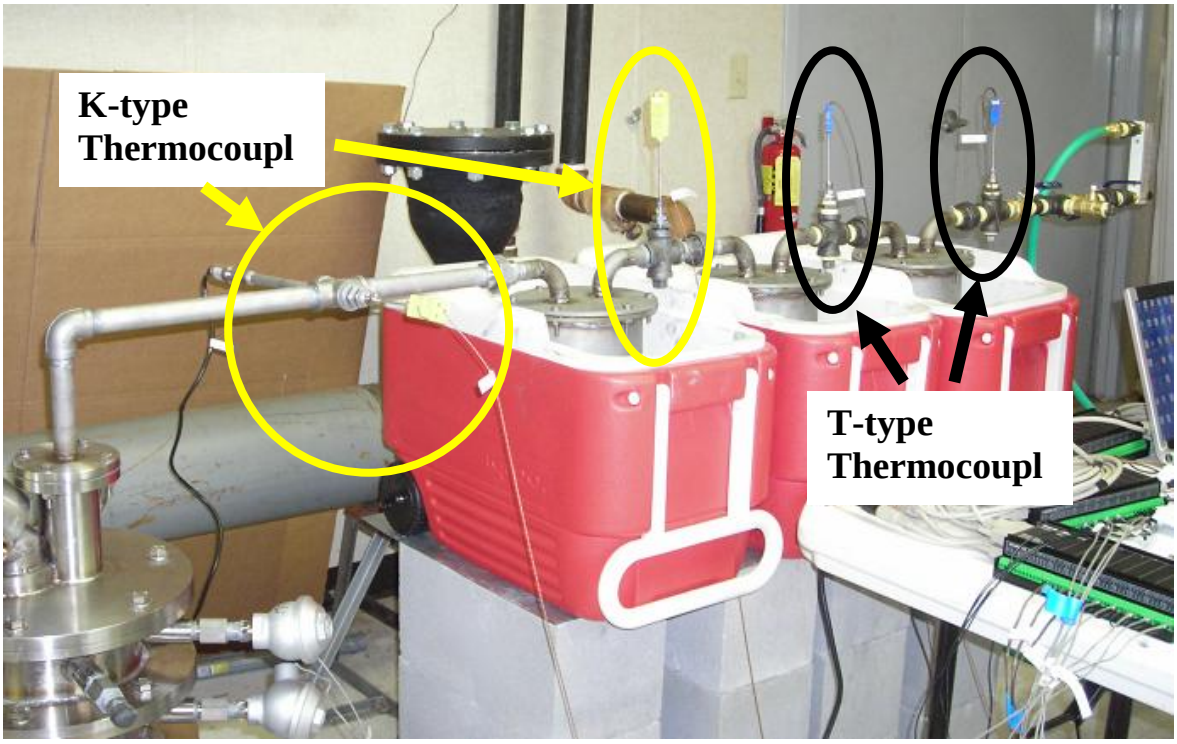

Figure 3-23. A view of the gasification reactor exit and the cooling and cleaning containers showing the locations of K-type thermocouples and T-type thermocouples.

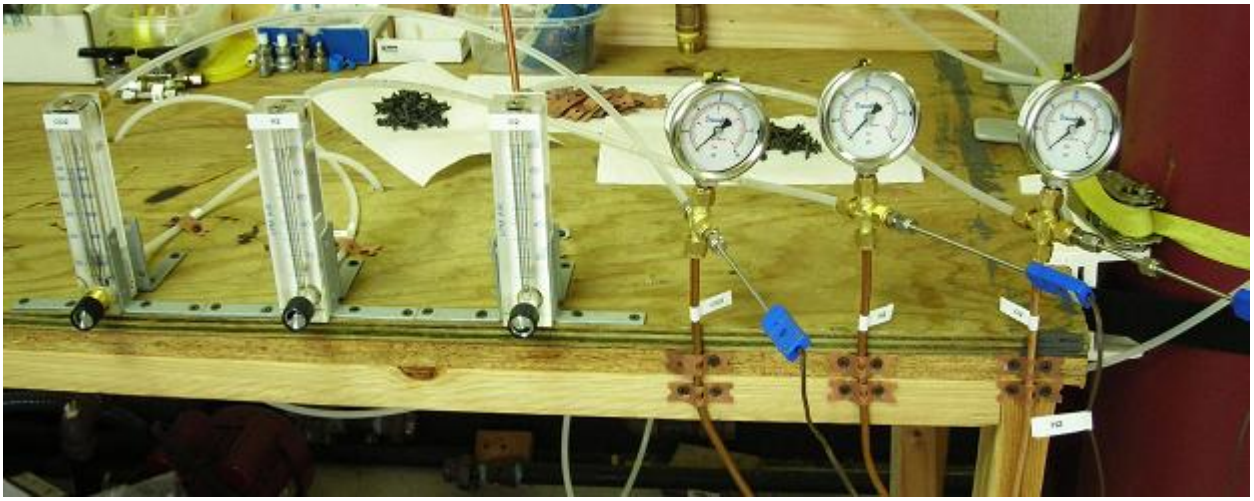
Figure 3-24. A view showing the rotameters, pressure gauges and thermocouples to control and measure the inlet gas flows of hydrogen, oxygen and carbon dioxide.

Figure 3-25. The pressure transducer and the power supply.

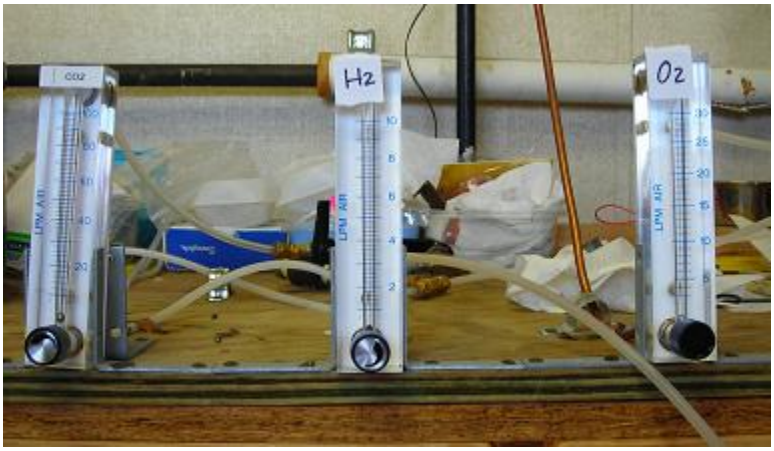

Figure 3-26. A view showing the rotameters which measure and control the volume flow rates of the hydrogen, oxygen and carbon dioxide inlet gases.

Figure 3-27. A view of the flowmeter which measures the volume flow rate (LPM) of exit gas from the system.

Figure 3-28. A view of pressure gages showing 1 to 3 psig gauge and 1 to 30 psig gauge to read the pressure of the gas exiting the system.

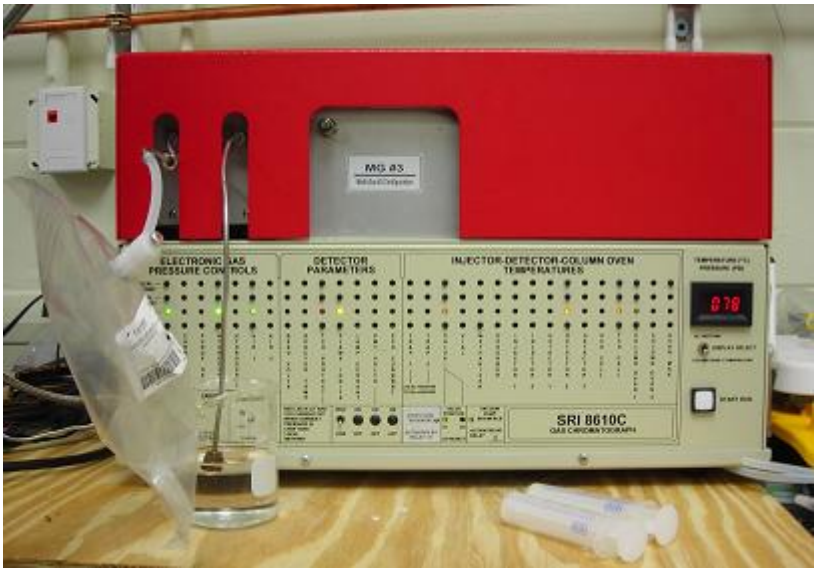

Figure 3-29. A view of the SRI Gas Chromatograph 8610-C.

Table 3-3. Summary of the calibration gas compositions.

Calibration Gas 1	Vol.%	Calibration Gas 2	Vol.%
Hydrogen	60	Methane	2.01
Nitrogen	40	Carbon Dioxide	9.93
		Carbon Monoxide	50.3
		Nitrogen	37.76

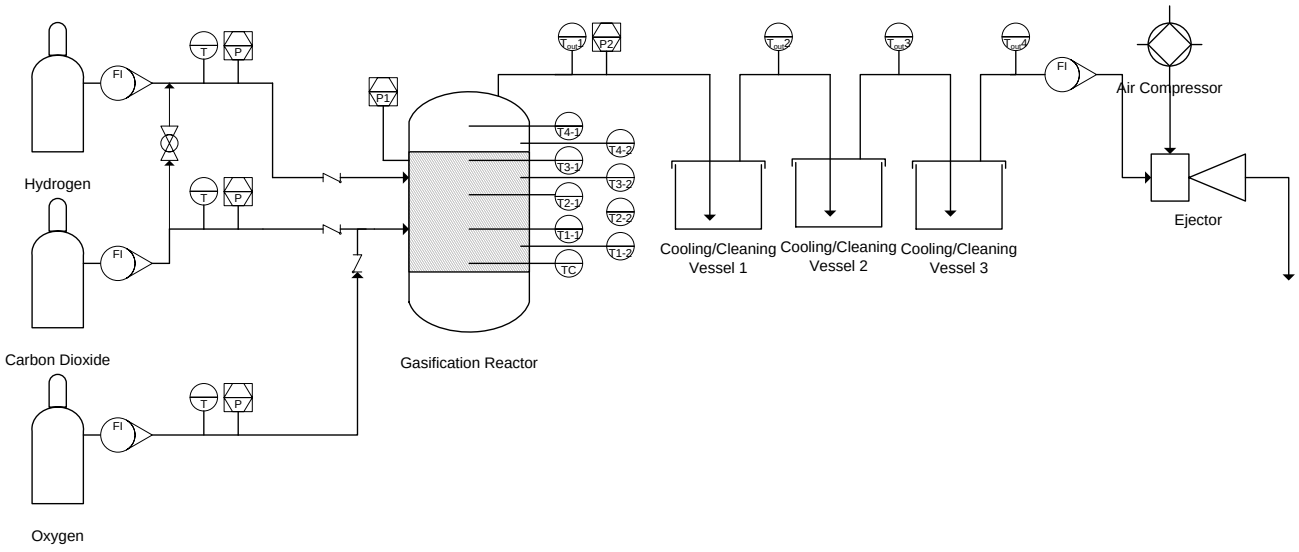

Figure 3-30. Flow diagram of the overall gasification system.

Table 3-4. Summary of ultimate analysis results of six types of wood.

	Softwood				Hardwood	
mass basis	Sand Pine	Longleaf Pine	Loblolly Pine	Slash Pine	Hardwood mix (hard)	Hardwood mix (soft)
Drying Loss	42.46	43.62	42.32	40.46	34.1	40.75
Carbon	49.36	49.97	49.74	49.76	48.49	48.43
Hydrogen	6.17	6.21	6.16	6.27	6.02	6.1
Nitrogen	0.05	0.06	0.06	0.05	0.13	0.09
Oxygen	44.26	43.78	44.5	43.8	44.77	44.86
Sulfur	<0.05	<0.05	<0.05	<0.05	<0.05	<0.05

Table 3-5. Summary of proximate analysis results of six types of wood.

	Softwood				Hardwood	
mass basis	Sand Pine	Longleaf Pine	Loblolly Pine	Slash Pine	Hardwood mix (hard)	Hardwood mix (soft)
Volatile Matter	80.79	79.98	80.62	80.99	79.61	80.51
Fixed Carbon	23.54	23.88	23.19	21.73	14.58	21.88
HHV [kJ/kg]	19410.48	19740.77	19666.34	19738.44	18891.78	19296.5

Table 3-6. Summary of ultimate analysis of woody biomass from literatures.

(wt%)	Pine residues [81]	Sawdust [82]	*Pinus pinaster* [21]
Carbon	51.57	50.91	51.6
Hydrogen	4.94	6.13	4.9
Nitrogen	0.9	0.23	0.9
Oxygen	42.58	42.14	42.6
Sulfur	0	0	0

Table 3-7. Summary of proximate analysis of woody biomass from literatures.

(wt%)	Pine residues [81]	Sawdust [82]	*Pinus pinaster* [21]
Volatile Matter	81.3	82.54	71.5
Fixed Carbon	18.1	17.13	16
HHV (kJ/kg)	22750	21001	20189

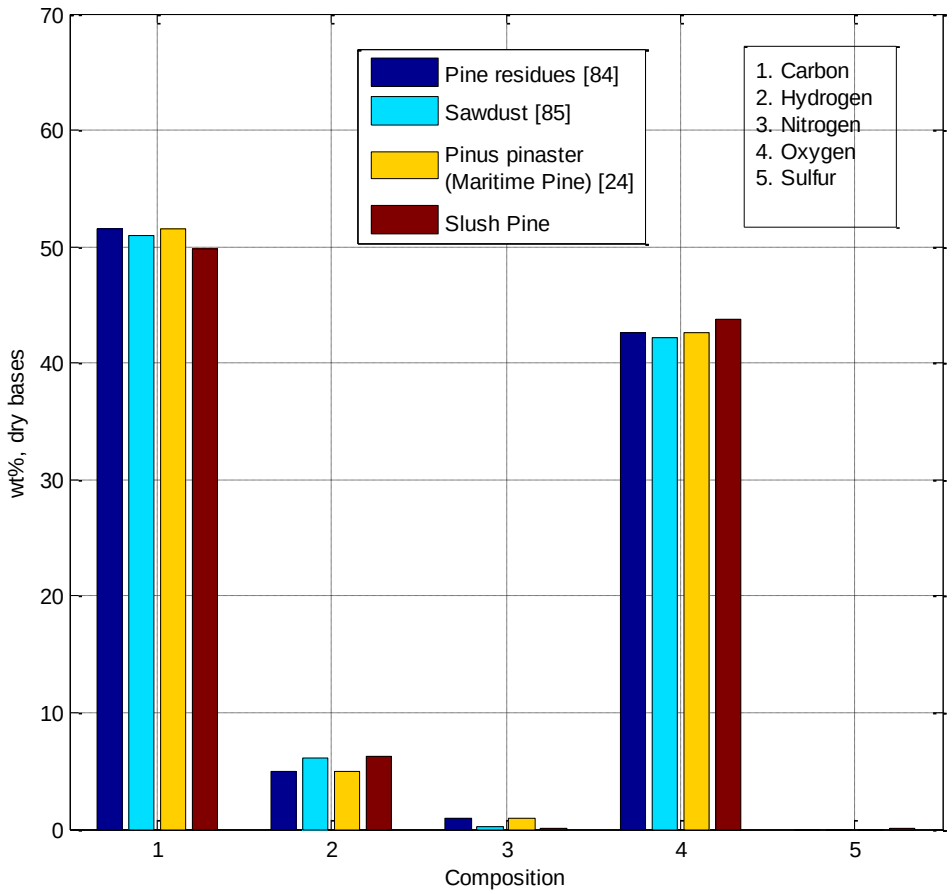

Figure 3-31. Ultimate Analysis Comparison of Woody Biomass (wt% dry bases). [81], [82] and [21].

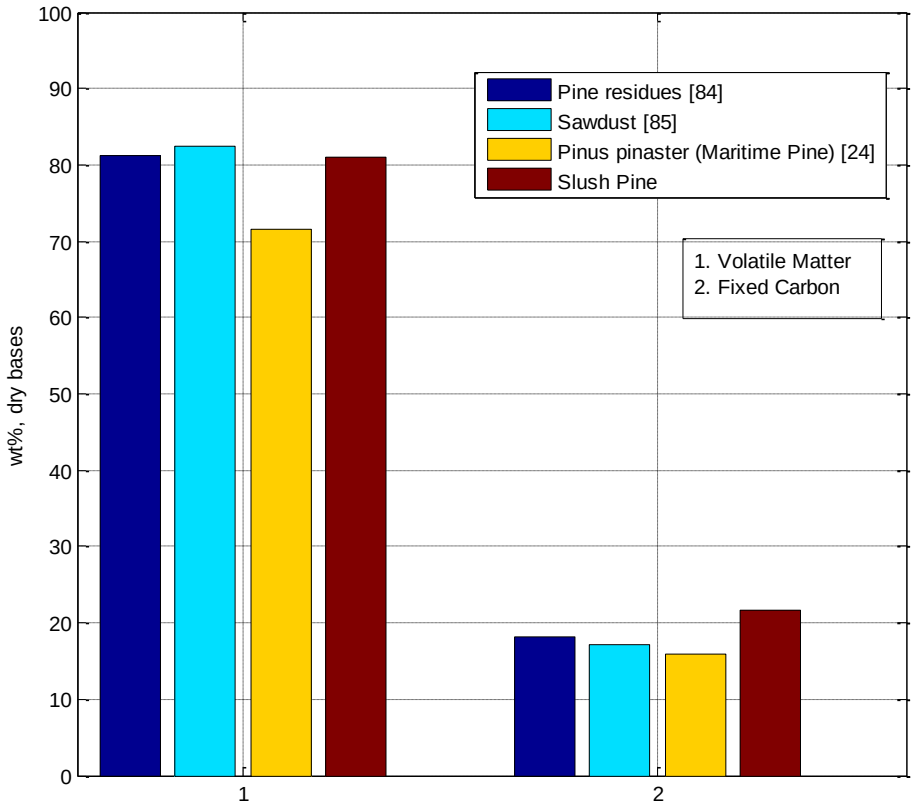

Figure 3-32. Proximate Analysis Comparison of Woody Biomass (wt% dry bases). [81], [82] and [21].

Figure 3-33. A view of wood sawdust used in experiments.

CHAPTER 4
RESULTS AND DISCUSSION

4.1 Theoretical Analysis Results

This section discusses theoretical analysis results including equilibrium composition for the gasification output products, mass, energy and exergy balances, and other parameters to evaluate the gasification process efficiency.

The equilibrium composition for biomass gasification products calculated using the procedures in section 2.4 were tabulated at various temperatures (Table 4-1).

The equilibrium composition of gasification products was also simulated for temperatures ranging from 300^{o}C to 1500^{o}C for the pressure at 2 bar and a steam to biomass ratio of 0.5 (Figure 4-1). It was observed from this plot that there would be no solid carbon left at above 700^{o}C. The fractions of the rest of the gaseous components were stabilized at above 900^{o}C except a slight decrease in hydrogen and carbon dioxide. According to this analysis, the syngas composition from the gasification reaction at 1500^{o}C after condensing the steam is expected to be approximately 52 mol% of hydrogen, 46 mol% of carbon monoxide and 2 mol% of carbon dioxide.

Figure 4-2 presents the syngas composition (kmol/kmol of biomass) as a function of steam to biomass ratio at 500^{o}C and 2 bar. In the range of steam to biomass ratio (mol/mol) from 0.1 to 1.5, the number of mol of all syngas compositions except the solid carbon increase as the steam to biomass ratio increase. A sharp increase in water (steam) production as the increase in steam to biomass ratio was simply reflected by the increase in input steam amount. It is observed that the production of hydrogen and carbon dioxide increased as the steam to biomass ratio increased due to the water-gas shift reaction of steam and carbon monoxide to hydrogen and carbon dioxide. The production of carbon monoxide stayed almost constant with the increase in the

steam to biomass ratio. Figure 4-3 presents the syngas composition (kmol/kmol of biomass) as a function of steam to biomass ratio at 1000^{o}C and 2 bar. A sharp increase in steam production with increase in steam to biomass ratio remains the same at this temperature. The hydrogen production, however, is approximately three to four times higher than the production at 500^{o}C case through the entire range of steam to biomass ratio plotted. It is noticeable that the increase in hydrogen and carbon dioxide production correspond to the decrease in carbon monoxide indicating that water-gas shift reaction occurred. It is observed that the production of solid carbon and methane are negligible and independent of the steam to biomass ratio at 1000^{o}C. The gasification product composition (kmol/kmol of biomass) as a function of steam to biomass ratio at 1500^{o}C and 2 bar is presented in Figure 4-4. At this temperature, the overall trend of the production of each species is almost identical to the case at 1000^{o}C; a sharp increase in steam production with increase in steam to biomass ratio, increase in hydrogen and carbon dioxide production corresponding to decrease in carbon monoxide and negligible production of solid carbon and methane. The differences between 1500^{o}C case and 1000^{o}C case include the higher kmol production of steam, lower kmol production of hydrogen and carbon dioxide and higher kmol production of carbon monoxide at steam to biomass ratio of 1.5. It is observed through Figures 4-2 through 4-4 that the syngas composition production trend is different between the low temperature gasification (500^{o}C) and high temperature gasification (above 1000^{o}C). In gasification with the reaction temperature above 1000^{o}C, the trend of the influence of steam to biomass ratio on the syngas composition production is very similar. The general result is the increase in steam production, hydrogen production and carbon dioxide production while the decrease in carbon monoxide production with increase in steam to biomass ratio.

The product composition production (kmol/kmol of biomass) as a function of gasification pressure at 500^{o}C and 0.5 steam to biomass ratio is presented in Figure 4-5. In the range of the gasification pressures from 1 bar to 3 bar, all the product compositions are constant and stable except a slight decreasing tendency in hydrogen production with the increasing pressure. Figure 4-6 also presents the product composition production (kmol/kmol of biomass) as a function of gasification pressure but at 700^{o}C. At this condition, there is not solid carbon production. The production of carbon dioxide, methane and steam increases gradually with the increase in pressure, while the production of hydrogen and carbon monoxide decrease with the increase in gasification pressure. Figures 4-7 and 4-8 present the production composition as a function of gasification pressure at 1100^{o}C and 1500^{o}C, respectively, with 0.5 steam to biomass ratio. In both cases, all product compositions are constant and stable through the range of pressures. The mole production of the hydrogen is the largest and the mole production of carbon monoxide is the second largest while the production of the rest of species is almost negligible. It can be said that the product compositions are independent of the gasification pressure at the elevated (above 1100^{o}C) gasification temperature.

As a summary, the following would be expected in the biomass gasification at 1500^{o}C: 1) In range of steam to biomass ratio of 1 to 1.5, the higher steam to biomass ratio would promote increasing numbers of moles of hydrogen production and decreasing numbers of moles of carbon monoxide production. The production of carbon dioxide would also increase with the increase in steam to biomass ratio. 2) At the gasification temperature of 1500^{o}C, the product compositions would be relatively constant with changes in pressure in the pressure range of 1 to 3 bar.

4.2 Experimental Results

This section provides results and a discussion of experimental tests. Torch tests and several dry runs were conducted as preliminary tests to examine the operational conditions of the system

as well as to calibrate the optimum experimental conditions for the gasification tests. Following these initial test, further tests were conducted using a woody biomass feedstock.

4.2.1 Torch Evaluation

4.2.1.1 Objectives

Torch tests were conducted as the first step of the series of bench scale gasification examinations. In the torch test, hydrogen, oxygen and carbon dioxide inlet gas tubes were connected to the torch, which was mounted on the gasification chamber. All the modules were removed from the combustion chamber thus the combustion chamber was open to the air (Figures 4-9 and 4-10). The flow rates of inlet gases were controlled at the rotameters located between the gas cylinders and the torch. The combustion chamber temperature was recorded through the torch performance evaluation.

The general purpose of the torch test was to examine the thermodynamic conditions of inlet gases, the torch and the combustion chamber so that to determine the optimum operational conditions for the gasification test. In order to satisfy this purpose, three specific objectives were suggested. The first objective was to test the operational procedures for the torch. The second objective was to examine the relationship between the flow rates of hydrogen and oxygen and the temperature in the combustion chamber. The last objective was to examine an deleterious effects of the torch operation on the combustion chamber and grate materials.

4.2.1.2 Results and discussions

It was found that the ignition timing needed to be very precise. Too early ignition attempts did not give the gases time to reach the chamber and ignite. Too slow ignition attempts caused an explosion which would crack the grate. Once the timing was addressed properly, the rest of the torch test process was conducted successfully and smoothly.

The following tables and figures (Tables 4-2 through 4-4 and Figures 4-11 through 4-13) show the results from three sets of torch tests. Table 4-2 provides the inlet hydrogen and oxygen flow rates, the chamber temperature reached with that set of hydrogen and oxygen rates and the time required to reach that temperature. Figure 4-11 shows the change in the chamber temperature as a function of the various sets of hydrogen and oxygen flow rates tested. The system was purged with carbon dioxide prior to introducing the hydrogen and oxygen gases. If ignition failed, the system was purged again with carbon dioxide. Note: Tables 4-3, 4-5 and 4-8 present the hydrogen and oxygen flow rates at STP (298.15 K and 25^{o}C), after correcting the air-standard rotameter readings to the actual hydrogen and oxygen flow rates. Since the pressure for hydrogen and oxygen flows were not available, 4 psig (an average flow pressure recorded during the complete gasification tests), was assumed. These corrections were later verified but were not available at the stage of torch tests.

Torch test 2 was conducted to observe the change in the chamber temperature and the change in heating rate as functions of inlet gas flow rate/ratios. All of the gas pressures were set to 40 psig at the gas regulators. In this test, 6 different sets of hydrogen and oxygen flow rates/ratios were tested and these are summarized in Table 4-4.

Table 4-8 shows an overall summary of the torch tests including the volume flow rates of input gases, heating rate of the torch and the stabilization temperature of the chamber. Prior to conduct an experiment, it was considered that diluting oxygen with carbon dioxide would be necessary to control the chamber temperature in terms of cooling the combustion gas which was expected to be significantly higher than 1500^{o}C. However, from some torch tests, it was discovered that it was not necessary to concern overheating the reactor as long as keeping a certain range of hydrogen to oxygen ratios. As a matter of fact, an introduction of carbon dioxide

significantly cools the system thus it is expected that the use of carbon dioxide would overcool the system if it is used in a heating period. On top of it, introduction of any species other than hydrogen, oxygen or steam to the gasification reactor is not preferred because it could interferre the gasification reactions and disturb the proper analysis of syngas composition. Therefore, it was decided to use carbon dioxide only for purging or cooling of the system. It is seen in Table 4-8 that three sets of flow rates namely H_2:O_2 = 8:16, 10:10 and 12:22 meet or exceed the target temperature of the gasification reactor, 1500^{o}C. Hydrogen to oxygen flow rates of 12 to 22 was expected to reach the temperature much higher than 1500^{o}C. The hydrogen to oxygen flow rates of 8 to 16, while there may not have an issue with the stabilization temperature at the chamber, was reversed in hydrogen to oxygen ratio from the stoichiometric ratio of 2:1. Thus, hydrogen to oxygen flow rates of 10 to 10 was selected as the target flow rates to use during the dry runs and gasification tests. This rate would be refined as further examination was conducted about the relationship between inlet gas flow rates and heating condition in the gasification reactor.

After examining the effects of the torch operation on the combustion chamber and grate materials, several observations were made. When a small popping sound was heard as the first ignition was attempted, it was considered that the ignition timing was too early so that the ignition was attempted before the hydrogen reached the torch outlet. The ignition was made successfully at the second attempt. The timing associated with igniting the hydrogen oxygen mixture is critical. If the ignition is attempted too early there will be no ignition, while too late ignition attempt causes an explosive mixture which will damage the grate.

Because the grate was made from Alumina and was brittle, the grate was broken to small pieces when a detonation occurred from the ignition failure. In some torch tests, the grate had been repaired with the broken pieces glued together to make a disk shape using a high

temperature adhesive. It was observed that the grate started failing along the glued section as the chamber temperature increased during the torch test. Figure 4-14 shows the view of the broken grate during the cooling period after the system was shut down. After the torch tests, several cracks were found both on the torch and the combustion chamber wall (Figures 4-15 through 4-17). It was noticeable that where the combustion flame directly impacted the wall of the chamber, that there was significant damage in both cracking and melting of the material. It is considered that the damage to the chamber was attributed to thermal effects caused by the combustion of hydrogen. During several test the chamber temperature exceeded 1600^{o}C, reaching highs of approximately 1650^{o}C. The maximum operation temperature of high-density alumina is 1650^{o}C. Thus, it is obvious that when the temperature exceeded the operation maximum it resulted in thermal stress on the material and regional thermal expansion which may have caused cracks on the material surface. It was also observed some areas of the chamber wall actually melted. Since the melting temperature of the high-density alumina is 1870^{o}C, It can be concluded that some sections of the chamber reached 1870^{o}C or above. Due to the size of the flame, it was possible that the flame front reached the chamber wall and the hottest point of the flame directly hit the wall to cause melting.

4.2.2 Reactor Dry Run

4.2.2.1 Objectives

Dry runs comprised the second step of the gasification experiments. In dry runs, all parts of the gasification system were connected together and the tests were conducted as the real gasification tests might be conducted except biomass was not introduced into the system. Since dry runs are the final step before the real tests, the general purposes of the dry runs were to examine the overall system and its behavior, and to determine the optimum operational conditions to be used in the real tests. There were four specific objectives to satisfy this purpose.

The first objective was to test the complete gasifier, cooling/cleaning system configuration without the introduction of feedstock. The second objective was to determine the relationship between time and gasification reactor temperatures to evaluate heat losses from the gasifier. The third objective was to evaluate the performance of the cleaning system in condensing the steam produced in the gasifier. The last objective was to evaluate the operation of sensors and DAQ system. The naming and the locations of the combustion chamber and the gasification modules used in the following discussions are presented in Figure 4-18.

4.2.2.2 Results and discussion

Three sets of dry runs were conducted and the results are presented here. The operation of the system was tested and procedures for start-up, steady state operation and shut-down were established.

Tables 4-9, 4-11 and 4-13 present the summary of the change in inlet gas flow rates and the corresponding chamber temperature. Hydrogen gas flow rates of approximately 10 LPM were met through this test since this was the target volume flow rate established from the series of torch tests. While the hydrogen flow rate was fixed, the oxygen flow rate was varied to examine the effect on gasification reactor temperatures. It was important to determine the effects of excess oxygen or hydrogen on the gasification temperature.

Figures 4-19 through 4-21 presents the gasification reactor temperatures as a function of time based on different inlet gas flow rates being applied as reported in Tables 4-9, 4-11 and 4-13. It is first observed that the combustion chamber temperature in all test cases reached 1600^{o}C or above. It is also observed that the combustion chamber temperature initially increased very rapidly and reach at 1200^{o}C or above within first 5 minutes. The increase in temperature continue until it reached at 1650^{o}C when the increase was forced to stop at this point, but the speed of increase is much slower than the initial 5 minutes. Because the same trend in

temperature increase was repeated in all three dry runs while almost the same inlet gas conditions were used in all runs, it can be said that this is the temperature condition to expect when using 10 to 16 LPM hydrogen to oxygen inlet gas flows. The next observation is the temperature distribution at different height of the reactor during the runs. It is noticed between the first dry run and the second dry run that there was a large difference between the combustion chamber temperature and the rest of the temperatures at modules. Three reasons could be used to explain this phenomenon. The first reason is the direction of the combustion flame. Due to the structural issue of the reactor, the ignition torch is horizontally mounted on the chamber. This positioning may be effective to heat the combustion chamber but may not be as effective to heat the upper sections of the reactor because there is no direct vertical force to promote the upward forced convection. The second reason is a radiation effect. Since the combustion chamber is enclosed by alumina all direction, there could be more radiation reflecting back from the surroundings toward the center of the chamber where the thermocouple is located and increase the temperature there. On the other hand, gasification module thermocouples are surrounded by wall, but the floor and the ceiling are not sealed for each thermocouple to receive as much radiation effect as the chamber thermocouple does. The last and the main reason to explain the temperature gradient in the reactor is effect of the grate. Several interesting observations and comparisons can be made between the dry run 2 and dry run 3. It is seen that the flow rates and pressures of hydrogen and oxygen gases were at very similar condition between the dry run 2 and the dry run 3 (Tables 4-11 and 4-13), though the temperature of gases were approximately 5^{o}C on average higher in the dry run 2 than the dry run 3. Based on these inlet gas conditions, it is expected in the dry run 2 and 3 that thermal behaviors in the reactor would be very similar. However, it is observed that it took approximately 21 minutes for the combustion chamber

temperature to reach to 1650^{o}C in the dry run 2 while it took approximately 63 minutes in the dry run 3 for the chamber temperature to increase at the same level. Furthermore, the temperature of the gasification module 1 (the temperature of the bottom module) reached to only 880^{o}C when the chamber temperature reached at its maximum in the dry run 2, while the module 1 temperature in the run 3 reached as high as 1350^{o}C at the corresponding time. It is also noticeable that the rest of the gasification module temperatures in dry run 2 were also significantly lower than the chamber temperature while in the dry run 3 the module temperatures were lower than the chamber temperature but evenly lower as its distance from the chamber increases. There was one difference between the dry run 2 and dry run 3. In the dry run 3, a popping sound was heard following to the ignition of the torch. It is very likely that this popping was associated with breaking of the grate since broken pieces of the grate were discovered after the test was completed and the reactor was disassembled. If the main difference was the existence of the grate, this could explain the discrepancy observed between the dry run 2 and the dry run 3. In the test 3, because there was the grade to separate the combustion chamber and the gasification modules, the heat generated in the chamber could not be transferred upward efficiently thus the heat was mostly used to heat up the chamber inside. As a result, the chamber temperature increase rapidly to 1650^{o}C while the rest of the reactor was not heated as efficiently as the chamber was. In the dry run 3, on the other hand, because the grate was broken and thus not preventing the path from the chamber to the modules, the heat generated in the combustion chamber was transferred upward more efficiently comparing with the case in the dry run 2. As a result, since the heat was not retained in the camber, it took three times as long for the chamber temperature as that in test 2 to reach the same temperature. Meanwhile, because the heat was transferred to the modules more smoothly in the test 3, the module temperatures in test 3 reached

much higher than those in test 2. Note: Tables 4-10, 4-13 and 4-14 present the hydrogen and oxygen flow rates at STP (298.15 K and 25^{o}C), after correcting the air-standard rotameter readings to the actual hydrogen and oxygen flow rates. A pressure of 4 psig was assumed for both hydrogen and oxygen flows unless the gas pressures are provided in the table. These corrections were not available at time of dry runs.

Figures 4-22 through 4-24 show the cooling system performance in terms of temperature of gasification product gas versus time. It is observed in all figures that all exit temperatures increase with time, however, their responses to the change in reactor temperatures are slow. Exit temperature 1 always read a much higher temperature than the rest of the exit points because the thermocouple is located before any of the cooling containers. The exit gas is cooled below 100^{o}C after passing through the first cooling container. By the time the gas passes through the last cooling container (at the location of exit temperature 4), the gas temperature is close to atmospheric so that the gas can be easily sampled at this location for a GC composition analysis.

General performance of the sensors and DAQ system were examined during the dry runs. It was found that some of the B-type thermocouples mounted on the reactor did not respond correctly probably due to a problem with wiring somewhere along the connection. Since all thermocouples were tested and found to perform properly prior to the assembly of the system, the problem had to develop during the assembly process. It was also discovered that the time delay in response of the thermocouple at the combustion chamber was an issue. Because an increase in temperature in the combustion chamber was used to confirm the proper ignition, slow response of the thermocouple at the beginning delays knowing whether or not ignition occurred. This meant that the chambers could be damaged with the ignition of an explosive mixture of hydrogen and oxygen, preventing another attempt at igniting the torch. In this case the system

had to be purged with carbon dioxide and the ignition procedure would be repeated. The pressure transducers located at both in the gasification reactor and at the reactor exit properly responded during the dry runs. Figure 4-25 shows the pressures versus time during the run on October 2. It is seen that the reactor pressure generally increased from around 0.2 psig to 0.4 psig, while the reactor exit pressure increased from at 0.15 psig to 0.3 psig. This indicates that the high temperature steam created in the combustion chamber properly exit the system without causing excessive pressure build up.

It is noticeable in Figure 4-27 (Oct 30 pressure) that there was a large fluctuation in the reactor pressure comparing to the reactor exit pressure. It was considered that this fluctuation was due to the sensor failure rather than a physical phenomenon occurring in the reactor. First, what was happening in the reactor is hydrogen combustion to generate steam. If the steam generation exceeded the steam exhaust to build a pressure in the reactor, the pressure increase should be close to a linear because the input flow rates of hydrogen and oxygen were almost steady through the test. Second, again because hydrogen combustion was the only activity occurring in the reactor through the test, there was no impact in the reactor to cause the pressure variation. Therefore, it was determined that the pressure fluctuation was attributed to the sensor itself. It was observed later that both pressure transducers stopped functioning properly.

Through the torch tests, it was determined that the optimum flow ratio of input hydrogen and oxygen gases, in terms of temperature increase in the combustion chamber, was 10:10 LPM. Based on this target ratio, several other input gas ratios were tested during the dry runs. As a results, it was found that a hydrogen to oxygen ratio of 10:16 LPM provided a gradual temperature increase in the combustion chamber up to 1600^{o}C with one exception in dry run 1 where a temperature increase up to 1430^{o}C was recorded. The ratio of 10:16 LPM results in a

mole ratio of 2:3.2 or 220% excess oxygen. There was a concern that this excess oxygen was extremely high even considering the general requirement of excess oxygen for a complete combustion of a fuel (10 to 20% excess oxygen). Because the rotameters used in this experiment were air-standard, any volume flow of gases with it density being different from air need to be corrected accordingly. Temperatures and pressure of gases also need to be corrected as well if they differ from standard STP. The volume flow corrections were made according to the equation below:

$$\dot{Q}_{reading} = \dot{Q}_{truegasflowrate}\sqrt{\frac{(SG)(T)(14.7)}{(530)(P)}} \qquad 4\text{-}1$$

where SG is specific gravity of metered gas (air = 1.0) at STP, T is temperature at operating conditions in Rankine, P is pressure at operating conditions in psia. The inlet gas flow rates used in the following gsification tests were corrected according to this equation.

4.2.3 Gasification of Woody Biomass

Gasification tests were conducted to demonstrate the high-temperature steam biomass gasification process with the bench-scale system as well as to analyze and to evaluate the system performance. In a gasification test, the full configuration presented in Figure 3-15 was used. There are four objectives to fulfill the general purpose of this phase of the work. The first objective was to conduct operational tests with the complete gasification system. The second objective was to examine the system behavior in terms of temperature, pressure and gas flow rates. The third objective was to analyze the syngas production and composition; and the final objective was to evaluate the system performance using energy and exergy analyses.

Operational tests were successful in determining the optimum torch operation, the effectiveness of the gas cleaning equipment and the production of syngas from woody biomass.

Six sets of gasification tests and analyses were conducted. Among the six, four data sets, test 1, test 2, test 3 and test 6, are not presented here. Test 1 data were eliminated because syngas exit pressure and exit flow rates were not recorded properly during the test thus the computation of syngas composition was impossible. Test 2 data were eliminated because the test had to be terminated due to safety issues which occurred during the test. In test 2, a sudden increase in pressure and exit gas flow rate were observed following the introduction of biomass to the gasification reactor. This increase in pressure forced the combustion gases through the ignition wire channels resulting in an open flame outside the gasifier. This phenomenon was later determined to be caused by excess oxygen sent to the reactor. Since combustion of the woody biomass rather than gasification occurred under this condition, the test was terminated. After this experience, it was decided that the inlet hydrogen and oxygen ratio needed to be adjusted to provide a slight excess hydrogen condition instead of an excess oxygen condition. While it was not preferred to have excess hydrogen since it could affect the gasification reactions and syngas analysis, it was more desirable than to have excess oxygen which would trigger a combustion reaction instead of a gasification reaction. Test 3 data were not included because there was an issue with the computation of syngas composition. During the gasification tests, there were three conditions that could result in the system depending on the hydrogen and oxygen feed rates and the efficiency of the torch combustions; (1) excess hydrogen results, (2) excess oxygen results or (3) both excess hydrogen and oxygen results. For the syngas composition analysis, it was necessary to determine the hydrogen amount which was produced solely by the gasification process. The excess hydrogen flow to the torch was subtracted from the overall hydrogen produced from the system during the gasification period to correct for this excess hydrogen. In test 3, because of the possible reading and recording errors of exit gas flow, the computed

hydrogen production turned out to be negative. Thus, these data were not included. Finally, test 6 was not included because there was an issue with biomass feeding timing. Since the biomass did not enter the reactor promptly after the feeding attempt, there was a time delay in syngas production thus the gas production versus time was not properly demonstrated. The results and discussion of the other two data sets are presented here.

4.2.3.1 Inlet conditions

Tables 4-15 and 4-16 present the summary of inlet gas conditions at the gasification test 4 on March 13, 2011 and test 5 on March 17, 2011, respectively. In any experimental tests including torch tests, dry runs and gasification test, the pressures and temperatures of the inlet gases were not controlled directly by the operators. Thus, in order to have specific inlet gas flow rates and ratios, the volume flow rate of hydrogen and oxygen needed to be controlled at the rotameters according to the pressure readings as the gas flow starts. The molar ratio of 2:1 of hydrogen to oxygen represents the stoichiometric condition of hydrogen combustion. However, it is important in the gasification tests to have a slight hydrogen rich environment rather than the stoichiometric condition or an oxygen rich environment in order to prevent a combustion reaction following the introduction of biomass in the reactor. For this reason, the hydrogen to oxygen ratio of 2 to slightly less than 1 was targeted. Since oxygen is the first gas to be released to the system, in order to aim for a 2.1:1 ratio of hydrogen to oxygen with 16 LPM (STP) of oxygen, the oxygen flow at the rotameter was set to 12.5 LPM at the conditions shown in Table 4-15. Then, in order to have 32 LPM (STP) or slightly higher flow of hydrogen under the pressure condition shown in Table 4-15, the hydrogen flow rate was controlled to 7.5 LPM. The pressures of the inlet flow gases were assumed to be constant here. The influence of change in pressure on the flow rate correction was calculated according to the correction formula presented in Equation 4-1. After the correction, the actual molar ratio of hydrogen to oxygen in test 4 was

determined as 2.6:1. Similarly, the volume flow rates of oxygen and hydrogen were controlled in test 5, which resulted in 2.6 to 1 molar ratio.

Figures 4-28 and 4-29 present the change in inlet gas temperatures to the torch versus time in test 4 and test 5, respectively. In test 4, the ignition occurred at t = 0 minute and the biomass introduction occurred at t = 37 minutes (Figure 4-28). This start up period was required to bring the system up to a proper operating temperature. Biomass gasification started as the biomass was introduced to the system. After 52 minutes from ignition of the torch, both hydrogen and oxygen inputs were terminated and carbon dioxide input started to purge and cool the system. The inlet hydrogen and oxygen gas temperatures to the torch were relatively stable and constant throughout the tests. In test 5, the ignition occurred at t = 0 minute, the first biomass introduction occurred at t = 36 minutes and the second biomass introduction occurred at t = 52.5 minutes (Figure 4-29). The temperatures of gases were approximately 1.5^{o}C higher in test 5 than test 4 due to the warmer ambient temperature. The trend of the inlet gases conditions was the same as that in test 4.

4.2.3.2 Gasification reactor conditions

Figures 4-30 and 4-31 present the gasification reactor temperature at the center core of the reactor versus time in test 4 and test 5, respectively. Again, in test 4, t = 0 corresponds to ignition of the torch, and the first 37 minutes represent the period of heating of the reactor (Figure 4-30). At 37 minutes, the combustion chamber temperature was 1500^{o}C and the bottom (10 cm from the flame) to top (40 cm from the flame) gasification module temperatures were at 1000, 720, 600 and 450^{o}C, respectively. It is shown that the temperatures of all measurement locations decreased following the biomass introduction to the reactor. After 57g (2 oz) of biomass was introduced, the temperatures of the reactor returned to pre-biomass introduction conditions within 2 minutes. Temperatures at all locations decreased rapidly after the hydrogen and the

oxygen introduction were terminated at 52 minutes and the carbon dioxide purge was initiated. In test 5, the torch ignition occurred at t = 0 minute, and the first and the second biomass introduction occurred at 36 and 52.5 minutes, respectively (Figure 4-31). The amount of biomass introduced each time was 28 g. A temperature decrease in the reactor was observed corresponding to the both biomass introductions, but the decrease at the second biomass introduction was larger than the first time. It is considered that the difference in temperature decrease was due to the amount of biomass which actually entered the reactor. This is further discussed in the following sections. Similar to test 4 case, there were several hundreds of degree Celsius decrease between each level of the temperature measurement.

In test 4, it is shown in Figure 4-30 that the temperature drops from the combustion chamber to the first module (10 cm from the flame) and between modules (10 cm each) were as large as 350^{o}C at the time of biomass introduction, and the difference between the combustion chamber and the top module (40 cm from the flame) was approximately 1000^{o}C. Likewise in test 5, the temperature decreases from the combustion chamber to 10 cm above were approximately 350^{o}C at the first biomass introduction and 300^{o}C at the second biomass introduction, and the decrease from the combustion chamber to 40 cm above was approximately 1000^{o}C at both first and second biomass introductions (Figure 4-31). Together with the dry run results, it can be said that there was always a large temperature gradient in the vertical direction in the reactor.

It was also found that there was a large temperature gradient in the radial direction in the reactor. Comparing the reactor center temperature (Figure 4-30) and the reactor wall temperatures (Figure 4-32) in test 4, the temperature drops from the center to the inner wall surface was approximately 300^{o}C at the height of 10 cm and 30 cm from the flame, and 450^{o}C at 40 cm above the flame. A large temperature decreases in radial direction could also be observed

in test 5 (Figures 4-31 and 4-33). It is shown in both test 4 and test 5 that it took approximately 10 minutes from the ignition for the reactor inner wall temperature at 10 cm above the flame to start increasing, and it took even longer for the wall temperatures at upper locations of the reactor to start increasing. It was not determined what triggered this delay in temperature increases at the wall, however, it is at least observed that the rate of temperature increase at the combustion chamber started slowing down when the wall temperatures started increasing. It is considered that the large temperature gradient in the reactor was created by the combined effects of convection and radiation. While the overall temperature increase in the reactor was caused by the convection heat transfer from the hydrogen combustion at the bottom of the reactor, naturally the center of the reactor was heated more than the reactor wall area because the reactor center provides the general gas flow path. Furthermore, it is likely that the center of the reactor also received radiation heat from the flame and the heated grate, which brought the center thermocouple temperatures much higher than the surrounding (reactor inner wall) area. Based on these observations, it is also indicated that the actual gas temperature in the reactor might have been lower than what was read by the thermocouple at the center of the reactor. In terms of the gasification temperature, however, regardless of the method of heat transfer, the high temperature that the biomass is exposed to is the important.

Based on this observation of temperature gradients in the reactor, the important thing to discuss is where in the reactor the biomass really was gasified because the gasification temperature varies depending on the location in the reactor. It is assumed that a portion of biomass introduced into the reactor was gasified immediately at the high level of the reactor (40 cm from the flame) where the temperature was at around 500^{o}C (Figures 4-30 and 4-31). The biomass gasified at this level of the reactor was likely to produce more hydrocarbon species such

as methane as well as some tars and particulates due to the low temperature reaction. Another portion of biomass reached the middle of the reactor (30 to 20 cm from the flame) where the temperature ranged from 700 to 1000^{o}C. The biomass gasification at this range of temperature produces a mixture of hydrogen, carbon monoxide, carbon dioxide and some hydrocarbons. It is noticed in both test 4 and test 5 that reactor wall temperatures at module 3 level (30 cm from the flame) responded when biomass was introduced, but the wall temperatures at module 1 level (10 cm from the flame) did not show a significant response. This implies that the majority of biomass introduced from the top of the reactor might have reached the module 3 level, but not the module 1 level. The rest of the biomass, thought the quantity may be small, reached the grate area (5 to 10 cm from the flame) and was gasified at 1000 to 1400^{o}C. The biomass gasification with this temperature range produces much more hydrogen and carbon monoxide but very little hydrocarbon fuels and very little or no tar and particulates. As a result, it is considered that the biomass could be gasified at a wide range of temperatures and the syngas collected may be a mixture of the gasification reactions at a range of thermal conditions.

The change in gasification reactor pressure as a function of time in test 5 is presented in Figure 4-34 (Note: the reactor pressure data in test 4 is not available due to a sensor issue). It is observed that the reactor pressure during the heating process was 0 psig or atmospheric pressure. The pressure increases of 1.5 psig and 6.5 psig were observed when the first and the second biomass materials were introduced to the reactor. These increases in pressure were due to the gas volume expansion in the reactor as the biomass was gasified. It is assumed that the difference in the amount of pressure increase between the first and the second biomass introduction can be attributes to the difference in amount of biomass which really gasified.

4.2.3.3 Gas cooling process

The hot syngas exiting the gasification reactor was cooled by going through the three cooling/cleaning containers. Figures 4-35 and 4-36 present the temperatures of the exit gas at four locations in test 4 and test 5: the first is the reactor exit which is between the gasification reactor and the first cooling container, the second point is between the first and the second cooling container, the third is between the second and the third cooling container and the last one is after the third cooling container where the gas exits the system. It is shown in both test 4 and test 5 that the reactor exit temperature started increasing immediately after the hydrogen ignition. In test 4, the highest gas temperature at the reactor exit was approximately 125^{o}C at 52 minutes from the ignition. This reading time corresponds to the reading of the highest temperatures in the reactor. Considering the top module temperature in the reactor at this time (550^{o}C at the center and 100^{o}C at the wall), and some heat loss between the reactor to this measurement point, 125^{o}C is an understandable level at this location. It is assumed that the sudden increase of the temperature after the biomass introduction to the reactor was due to the increase in hot product gas volume. It is observed in test 4 that the temperature after the first cooling container started increasing almost immediately after the hydrogen ignition while the temperature after the second container stayed almost the same until the biomass introduction and the temperature after the third container stayed the same until the gasification process was completed. In test 5, a similar trend in temperature variation was observed except the temperature after the first container started increasing at the first biomass introduction and the temperature after the second container started increasing at the second biomass introduction. It can be explained that the first cooling container, an empty container emerged in an ice bath, was not as efficient as the second container which had glass marbles to enhance the heat transfer. Since the temperature of the system exit (after the third container) stayed almost constant from the ignition moment to the end of the

gasification process, it can be said that the cooling/cleaning system overall served its purpose of cooling the syngas to an ambient temperature for sampling. It is further noted that the efficiency of the containers in cooling and subsequently in cleaning, increased as steam condensed in the containers, providing liquid to enhance heat transfer and scrub the gases.

4.2.3.4 Exit gas conditions

Figure 4-30 presents the change in exit gas pressure as a function of time where the gasification started at 37 minutes in test 4. It is observed that the pressure in the system had been essentially atmospheric pressure through the heating process. This indicates that the steam produced in the combustion chamber and the reactor flowed easily to and through the cooling/cleaning system and to the ambient. The pressure increase at the biomass introduction to the reactor was due to the volume expansion from the gas production during the gasificaion reaction. Similarly, the exit gas pressure had been atmospheric pressure in test 5 except at the second biomass introduction where the pressure increased to 6 psig. Again, this is because the gas volume in the system expanded as the biomass was gasified. There was no pressure increase observed at the first biomass introduction most likely because the amount of biomass which really entered the system was much less than intended (28 g) and not a significant quantity of gasification had occurred at this time.

The changes in volume flow rate of the exit gas in test 4 and test 5 are presented in Figures 4-39 and 4-40, respectively. In test 4, the volume flow rate at the ignition was 18 LPM and kept decreasing until 24 minutes due to steam condensing until it reached steady state when the flow finally stabilized at approximately 2.5 LPM (Figure 4-39). Similarly to test 4 case, the exit volume flow rate started high at the ignition moment and decreased with time in test 5 (Figure 4-40). The exit volume flow rate could increase if one or more of the following cases occurred: (1) There was excess hydrogen (either excess input or unburned), (2) There was excess oxygen

(either excess input or unburned) and (3) the steam did not condense before exiting the system. Case (1) is true since the excess hydrogen was intentionally introduced to the system to avoid an excess oxygen condition. Theoretically case (2) should not occur if there was excess hydrogen. In reality, however, it is possible that some oxygen may have been left unburned if the combustion was not perfect. It is not likely that case (3) could occur for two reasons. First, the temperature after the cooling/cleaning containers would be much higher than what is presented in Figures 4-35 and 4-36. Second, the steam produced by the hydrogen combustion and biomass gasification did not fully condense in the cooling/cleaning containers. The second case, however, is unlikely because almost all of the steam must have condensed in the cooling/cleaning containers. This is further discussed in the next section.

In both test 4 and test 5, it is observed that there was a large increase in the exit gas volume flow rate following the biomass introduction to the reactor. This confirms the gas production due to the gasification reaction. Since the biomass was introduced to the reactor as a batch, the exit volume flow rate, thus the syngas production from the gasification, decreased with time after the biomass gasification processes slowed down.

4.2.3.5 Water condensation

Table 4-17 presents the amount of condensed water collected in the cooling/cleaning containers from the gasification tests and the possible amount of water condensed in each test when the steam input to the system from hydrogen combustion during the specified time periods would all be condensed to water. To estimate the amount of steam input, a number of moles twice as many as the number of moles of oxygen was used assuming all oxygen was consumed in the combustion reaction. In the condensed water estimation, any steam consumption and production relating to the gasification process was neglected. It is shown in Table 4-17 that the total condensed water collected from the test 1 was 1090 ml, while the possible condensed water

when the all steam introduced to the system during the entire test run (from the ignition to the gases turn off) was only 997.96 ml. This indicates that some excess steam must have been produced during the gasification process to add up to 1090 ml. In the test 2, condensed water was collected from the 1st and 2nd cooling/cleaning containers but the reduction in the amount of water was observed in the 3rd container; there was originally 600 ml of water in the 3rd container to enhance the effect of cooling and cleaning, but only 540 ml was found after the completion of the test. It is assumed that some water in the 3rd container was collected by the gas flow and exited the system as moisture of the gas. The total amount of condensed water collected from the test 2 was 1070 ml. The possible water condensation if all steam introduced to the system up to the 1st biomass introduction would be 690.89 ml, up to the 2nd biomass introduction would be 1007.55 ml and the entire test period would be 1228.25 ml. Based on these comparisons, it can be concluded that almost all of the steam introduced to the system through the hydrogen combustion condenses through the cooling process in the tests.

4.2.4 Syngas Composition Analysis

The syngas composition in each sampling bag was computed as follows:

1. With the calibration gas prepared for the GC analysis, the volume% of hydrogen, carbon monoxide, methane and carbon dioxide in a sampling bag were detected.
2. The volume% of each gas component was converted to volume flow rate by multiplying by the volume flow rate (LPM) of the syngas mixture exiting the system corresponding to the sampling time.
3. The volume flow rate of each syngas component was corrected according to Equation 4-1. The system exit temperature and the pressure corresponding to the sampling time were used for the correction to STP conditions. The specific gravity, SG, was computed as the composition density divide by the air density at STP.
4. It was assumed that the sample taken prior to the introduction of the biomass to the system represented the excess hydrogen flow in the system. This excess hydrogen converted to the volume flow rate (LPM) was subtracted from the product hydrogen flow rate (LPM) sampled during the gasification process.

The summary of the syngas composition analysis result (volume flow rates of the syngas composition) and the system condition corresponding to the syngas sampling time in test 4 and test 5 are presented in Tables 4-18 and 4-19.

The volume flow rate of syngas (LPM, STP) as a function of gas sampling time in test 4 is presented in Figure 4-31. The syngas represents dry gas since the steam had condensed in cooling/cleaning containers prior to the gas sampling. Since the biomass was introduced to the reactor as a batch, the overall gas production decreased with time. In test 4, at 1 minute from the biomass introduction, there was 25 LPM (STP) of hydrogen production, 7.5 LPM (STP) of carbon monoxide production and approximately 2 LPM (STP) of methane and carbon dioxide production (Figure 4-41). The mole ratio of hydrogen to carbon monoxide was 3 to 1, which is a much larger hydrogen portion than the 2 to 1 ratio which is required for the FTS. The ratio of hydrogen to oxygen was 3 to 1 to 2 to 1 through the gasification period, though the absolute amount of the gas production decreased. Figure 4-42 presents the syngas composition production as a function of time corresponding to the first biomass introduction in test 5. It is observed that the trend in syngas composition production is very similar to that in test 4, but the quantity of gas production is much lower in this case. Again, it has been observed that the true amount of biomass that entered the reactor at the first biomass introduction in test 5 was much less than intended (28 g), which explains the small quantity of syngas composition production results. Figure 4-43 presents the syngas composition production as a function of time corresponding to the second biomass introduction in test 5. Unlike the first biomass introduction case, the quantity of volume flow rate of each composition is very high. This indicates that the majority of 28 g or even more than 28 g including the left over biomass from the first biomass introduction might have actually entered the reactor and gasified. It is observed that there was continuous 7 to 8

LPM of hydrogen production at 3 minutes after the biomass introduction and later. It is assumed that this flow rate relates to a reading error either at the rotameter or at the GC and/or the treatment of composition analysis. It is impossible that only hydrogen production continued while the production of the other composition approached to zero.

The batch mode syngas compositions from the experiments were compared with the analytical syngas composition (Table 4-20). For this comparison, the steam introduced to the system during the entire gasification period was compared with the total amount of biomass introduced to the system to obtain the corresponding steam to biomass ratio. Taking this steam to biomass ratio, the syngas compositions were simulated using the analytical model. Because the true temperature of the gasification could not be determined in the experiment, the simulation was run at 600, 1000 and 1500^{o}C. The gasification pressure of 1 bar was used in the simulation of all temperature cases. In test 5, it was observed that the actual amount of biomass introduced at the first biomass input was much less than that in the second biomass introduction, though the actual amount at each time is not known. For the following analysis, the results of the first and the second biomass introductions in test 5 were averaged. The molar steam to biomass ratios in the test 4 and the test 5 were computed as 6.07 and 12.57, respectively.

The results summarized in Table 4-20 were also plotted in Figures 4-44 and 4-45. It is shown in Figure 4-44 that the hydrogen production for the experiment was lower than the simulation cases for all temperatures selected for simulation. The production of carbon monoxide is comparable to the simulation result from the 1000^{o}C case. The molar ratio of hydrogen to carbon monoxide production in the experiment was approximately 3:1, which is higher than the typical FTS requirement of 2:1.

Since hydrogen and carbon monoxide are the main species required for FTS, this result is positive if the data can be verified. It is noticeable that the carbon dioxide production from the experiment is significantly lower than any of the simulation results. In simulations, the high production of carbon dioxide is considered to be the product of the water-gas shift reaction, since the high production of carbon dioxide corresponds to the high production of hydrogen. There was methane production observed in the experimental syngas while the methane productions in simulation cases were almost negligible. Because only hydrogen and carbon monoxide are the required species in FTS, methane needs to be removed if the syngas is used as a feedstock for FTS. However, since methane has a high heating value (50010 kJ/kg), it would be useful if successful separation of methane can be achieved. Based on the syngas production presented in Figure 4-44, it is still very difficult to determine the actual temperature the gasification occurred in the experiment.

The syngas production in test 5 was compared with the simulation results (Figure 4-45). Unlike test 4, the hydrogen production in test 5 is comparable to that in the simulation cases. Since the carbon monoxide production in test 5 is very similar to that of 1500^{o}C case, it seems that the gasification temperature was very close to 1500^{o}C by looking only at the hydrogen and carbon monoxide production. However, again the carbon dioxide production is much lower than any of the simulation cases, and methane production is much larger than any simulation cases.

A few reasons were considered in explaining the large difference in syngas production between experimental result and analytical simulations. First, as an experimental result treatment, it could be misleading to simply subtract the excess amount of hydrogen from the product hydrogen to estimate the true amount of hydrogen production from the system. The excess amount of hydrogen shifts the equilibrium conditions to decrease the hydrogen production.

Therefore the estimated hydrogen production may not represent the true amount of hydrogen from the biomass gasification with pure steam. Second, the syngas composition estimated from the analytical model is based on a fixed temperature of either 600, 1000 or 1500^{o}C. In the experiment, however, there was a wide variation in temperature in the gasification reactor, thus it is unable to truly determine the gasification temperature in the experiment. Because the gasification temperature is one of the most important factor influencing the syngas composition, not knowing the true gasification temperature made it very difficult to simulate the composition using the analytical model. Apart from the comparison between the experimental syngas production and analytical simulation, it was noticed that the amount of hydrogen production in was higher than the amount theoretically possible. This discrepancy is believed to be due to the large uncertainty involved with sensor readings. In the experiment, some of the important variables required to compute the syngas composition, such as gas flow rate and pressure were read and recorded manually due to the limited accessibility to automated sensors. The uncertainty of reading the rotameters as the gas flow fluctuated during the run created the largest error.

The overall system inputs including inlet hydrogen and oxygen to produce steam and biomass and syngas as the output are summarized in Table 4-21.

4.2.5 Energy and Exergy Analysis

4.2.5.1 Energy and exergy of syngas

The time rate of enthalpy change for syngas as a function of gas sampling time in test 4, the first biomass introduction case in test 5 and the second biomass introduction case in test 5 are presented in Figures 4-46 to 4-48. In test 4, the highest enthalpy rate corresponds to the highest syngas production time (1minute after the biomass introduction), and is 1.1 kJ/sec. The enthalpy value of the syngas decreases with time as the syngas production rate decreases. In test 5 with the

first biomass introduction case (Figure 4-47), the highest enthalpy production occurred 30 seconds after the biomass introduction. The enthalpy value, however, is only approximately 0.22 kJ/sec, while the amount of biomass introduced here is 28 g comparing with 56 g in test 4. As it has been observed, it is assumed that the true biomass amount gasified at the first biomass introduction in test 5 was much less than 28 g. Therefore, a significantly smaller amount of syngas was produced from this gasification process, which resulted in a small enthalpy value of the gas. In the second biomass introduction case of test 4, the highest enthalpy production occurred at 30 seconds after the biomass introduction and is 1.7 kJ/sec. Like the other two cases, the enthalpy value decreases with time as the syngas production rate decreases.

The time rate of exergy for syngas as a function of gas sampling time in test 4, the first biomass introduction case in test 5 and the second biomass introduction case in test 5 are presented in Figures 4-49 to 4-51. Similarly to enthalpy values, the highest exegy value of the syngas corresponds to the highest syngas volume production time. It is noticed in all three cases that the exergy values of the syngas (Figures 4-49 to 4-51) were much higher than the enthalpy values (Figures 4-46 to 4-48). It is also noticed that these high exergy values come from the chemical exergy of the syngas instead of physical exergy.

4.2.5.2 Energy and exergy of input and output

In this experimental study, one aspect that complicates the energy and exergy analyses was that the biomass input was conducted in a batch mode. Even in this mode, the biomass material did not enter the reactor uniformly. To compare the inputs and the output of the gasification test under this condition, the following treatment was applied. The basic strategy was to convert the time rate of the steam input and the syngas output to a total steam input and the total syngas output by multiplying by the gasification time so that these quantities were comparable to each

other. The total input of hydrogen and oxygen (steam) as well as the total energy and exergy of these inputs for two gasification test cases are summarized in Table 4-22.

The mass of biomass introduced in the two gasification tests as well as the energy and the exergy of the input biomass are presented in Table 4-23. Since the amount of biomass used in test 5 (conducted on March 17, 2011) was half as much as that in test 4 (conducted on March 13, 2011), the total energy and exergy in test 5 were halved from that in test 4.

Table 4-24 presents the summary of the gas production and the total energy (enthalpy) and the exergy of the product gas from the two gasification tests and corresponding analytical simulation cases. Again, analytical energy and exergy were computed based on the syngas composition simulated using the experimental inlet conditions. It is observed that the enthalpy of experimental syngas in both test 4 and test 5 are much lower (25 to 33%) of analytical syngas enthalpy. On the other hand, the exergy of experimental sygas is almost identical in level as the analytical syngas. In order to determine these differences, the enthalpy and exergy of test 5 was compared with the 1500^{o}C case. These two cases had very similar production of hydrogen and carbon monoxide, yet there exists a significant difference between their energy and exergy. Therefore, it is considered that the difference in enthalpy and the similarity in exergy mainly comes from the carbon dioxide and methane portion. Since the syngas composition was computed based on the gas exit temperature which was approximately 20^{o}C, enthalpy of formation of carbon dioxide and methane are compared. The enthalpy of formation of carbon dioxide is -93,522 kJ/kmol and enthalpy of formation of methane is -74,873 kJ/kmol. This explains the reason why the overall enthalpy of the syngas from the experiment, which contains lower quantities of carbon dioxide and significantly higher quantities of methane than analytical syngases, is much smaller than the enthalpy of analytical syngas. On the other hand, the

experimental syngas had almost an identical exergy value as analytical syngas. *The total exergy* can be divided to two components: physical exergy and chemical exergy. Since the majority of exergy contribution was from chemical exergy rather than physical exergy (Figures 4-41 to 4-43), the chemical exergy of carbon dioxide and methane were compared. At 298.15 K and 1 atm, the chemical exergy of carbon dioxide is 14,176 kJ/kmol and of methane is 824,348 kJ/kmol [66]. This large chemical exergy of methane contributed to bringing the overall exergy of the experimental syngas to a comparable level of the exergy of analytical syngas.

4.2.5.3 Energy and exergy efficiencies

The thermal and exergetic efficiencies for the gasification system were computed for both experimental and analytical cases using the following equation and the results are summarized in Table 4-25.

$$\eta_{th} = \frac{H_{gas}}{H_{biomass} + H_{steam}} \quad 4\text{-}2$$

$$\eta_{Ex} = \frac{Ex_{gas}}{Ex_{biomass} + Ex_{steam}} \quad 4\text{-}3$$

It is observed that the thermal efficiencies are lower in the experimental cases than analytical cases and the exergetic efficiencies are almost identical in the experimental cases and the analytical cases. These results are directly related to the energy and exergy values presented in Table 4-24 since the inlet conditions are identical between the experimental and analytical cases. There are a few factors to consider regarding the computation of efficiencies. One factor is that in the experimental case, because of the intentional excess hydrogen introduction to the system, the heat generated from the combustion needs to be distributed to heat the excess hydrogen in addition to providing heat required for the gasification reaction. It should also be noted that the steady state in terms of heating has not been reached in the experiments. Since the

analytical model assumes a steady state gasification reaction, the comparison of experimental results and analytical results would be difficult. Another factor is the misleading effect with the "batch mode" assumption. To treat the entire gasification period as one batch possibly overestimates the amount of steam utilized in the gasification reaction. In the batch mode treatment, the entire amount of steam introduced to the system through the gasification period was compared with the amount of biomass introduced to the system. However, in reality, it was only the biomass which was introduced in batch while there was a constant flow of steam introduction. Thus, what really happened in the experiment is that the majority of biomass was gasified in the first 30 seconds to a few minutes, and the gas production rate kept decreasing with time as the remaining biomass became less and less. It is expected that the excess steam introduced to the system during the middle to last part of the gasification period simply exited the system without participating in the gasification reaction. The last thing to note is that the product gas always had significantly lower energy than the input steam and the biomass. These results can be explained by the thermodynamic state selected to represent the product gas. The product gas state was selected at the location after the cooling system because this is where the gas was sampled and all the temperature, pressure and the flow rate data were available (There was a failure in a sensor at the reactor exit). At this location, the sygnas had already lost a significant amount of heat through the cooling system, which would otherwise contribute to the higher enthalpy value of the gas. However, in a syngas application process such as FTS, the syngas would only be available at this location since the gas prior to this point included tars and particulates which would work against the syngas processing.

4.2.5.3 Hydrogen conversion ratio

The amount of hydrogen consumed from the steam input was compared with the amount of hydrogen produced from the gasification process. For this comparison, the total hydrogen

input to the system during the gasification period and the hydrogen in the biomass were taken as the overall hydrogen input and the total hydrogen in the syngas mixture during the gasification period was taken as the output. Table 4-26 presents the summary of hydrogen consumption and production as well as the conversion ratio (hydrogen output/input) in two gasification tests. It was found that the hydrogen conversion was 19% in test 4 and was 16% in test 5. It is believed that these low hydrogen conversion rates are due to the large amount of hydrogen input to the system to create high-temperature steam. The high-temperature steam needs to meet both the mass and heat balance required in the gasification process. However, the amount of steam required for the heat balance in the reactor is much larger than the amount of steam required to meet the mass balance. There would always be excess steam in terms of mass balance when high-temperature steam is the sole source of heat supply and resulting in the low hydrogen conversion rates.

Summary of discussions

The following are the findings from the results and discussions above:

(1) It was found that the determination of the effect of steam biomass gasification at 1500^{o}C was very difficult because

   a. The reactor temperature did not achieve uniform temperature with the particular structure designed for the experiment.
   b. It was not possible to determine how much biomass was really gasified at what temperature due to the large gradient of temperature in the reactor.

(2) The syngas produced in this study had fairly comparable hydrogen and carbon monoxide content as the analytical syngas, while containing only 10% of the carbon dioxide than the analytical syngas. If this result can be reproduced as a

steady process, this quality syngas could serve as a FTS feedstock with very little additional treatment.

(3) This high temperature steam gasification cannot produce more hydrogen than what is consumed if the excess steam is used to supply the entire heat required in the reactor.

(4) The thermal efficiency of the system (when taking the steam and biomass as the input and cooled syngas as the output) was very low (8% and 4% in test 4 and test 5, respectively) in the experimental syngas production case for the following reasons:

   a. A steady state process was not achieved in the gasification reactor.
   b. The batch treatment of biomass makes it difficult to determine the amount of input steam, output syngas as well as the actual steam to biomass ratio during the gasification reactions.
   c. The amount of steam required to maintain reactor temperature is much larger than the amount of steam required for the optimum syngas production in terms of mass balance.
   d. The syngas considered for the analysis was taken at the state where the gas had already cooled by the cooling system, thus the gases had lost the thermal values which would otherwise contribute to the higher enthalpy value of the gas.
   e. Due to the nature of high-temperature gasification to produce more hydrogen than methane and other hydrocarbons, it is unavoidable that the syngas from high-temperature gasification tends to have low heating value.

(5) The exergy efficiencies of the system in experimental syngas were 43% and 32% in test 4 and test 5, respectively. These values are comparable to the exergy efficiencies of the analytical syngas cases: 51% and 30% in test 4 case and test 5 case, respectively.

Table 4-1. Summary of the simulation results of equilibrium composition for biomass gasification products (kmol/kmol of biomass input) (P = 2 bars, steam to biomass ratio = 0.5).

Gasification T (^oC)	C	CO	H_2	H_2O	CO_2	CH_4
700	0.2258	0.4547	0.8134	0.2515	0.2269	0.0926
800	0	0.8569	1.0482	0.1094	0.0969	0.0462
900	0	0.9273	1.1337	0.1018	0.0655	0.0073
1100	0	0.9534	1.1358	0.1138	0.0464	2.22E-04
1300	0	0.9634	1.1265	0.1235	0.0366	1.60E-05
1500	0	0.9697	1.1203	0.1297	0.0303	2.13E-06

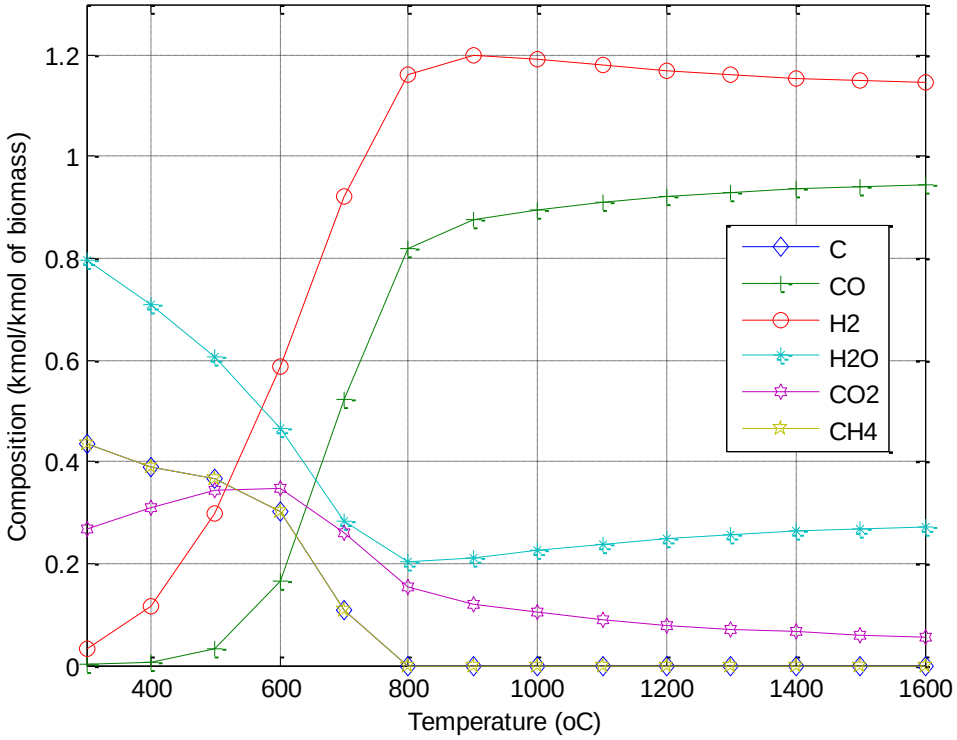

Figure 4-1. A simulation result of gasification product composition as a function of process temperature (P = 2 bar, steam to biomass ratio = 0.5).

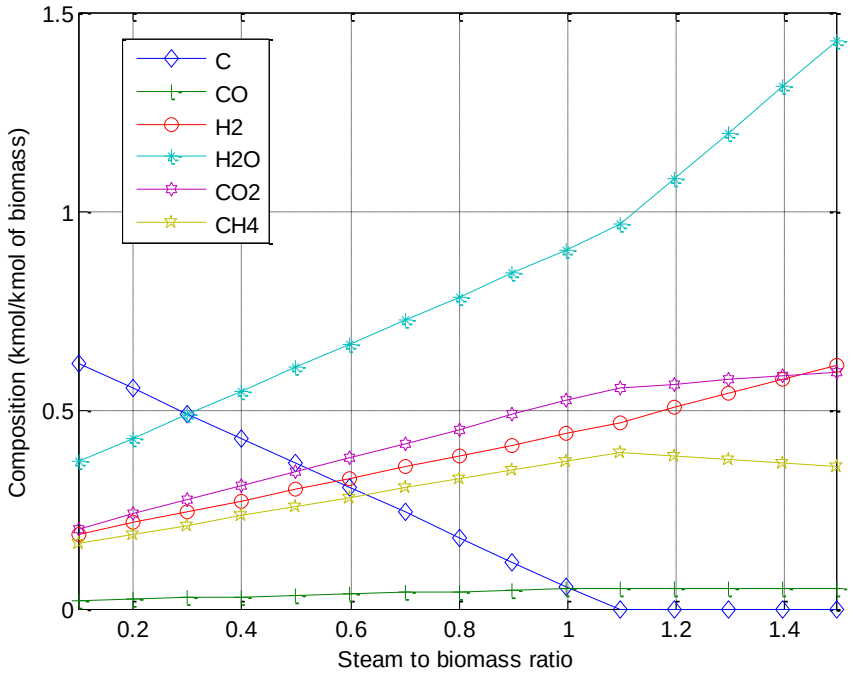

Figure 4-2. A simulation result of gasification product composition as a function of steam to biomass ratio (T = 500^{o}C, P = 2 bar).

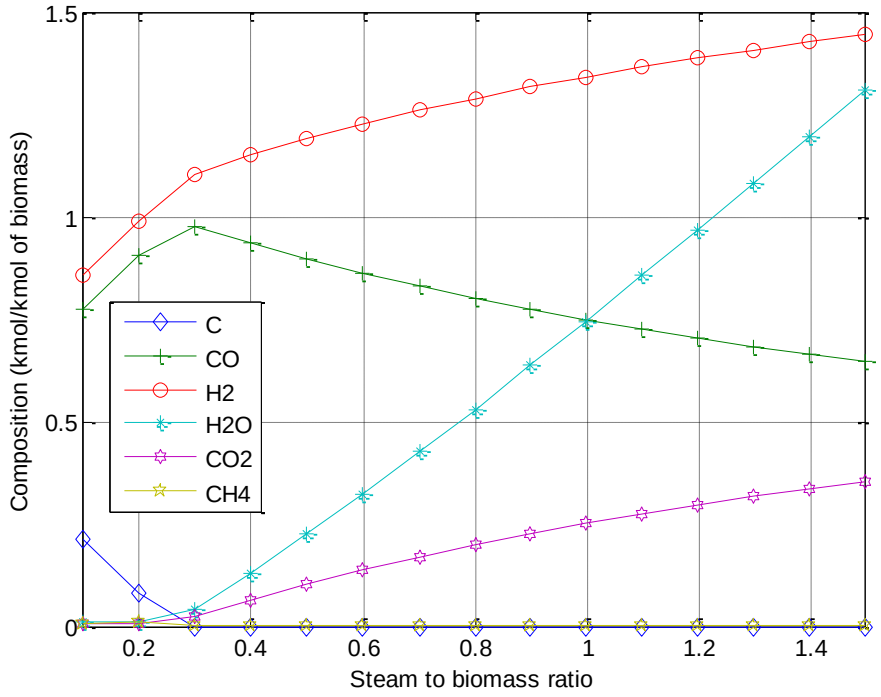

Figure 4-3. A simulation result of gasification product composition as a function of steam to biomass ratio (T = 1000^{o}C, P = 2 bar).

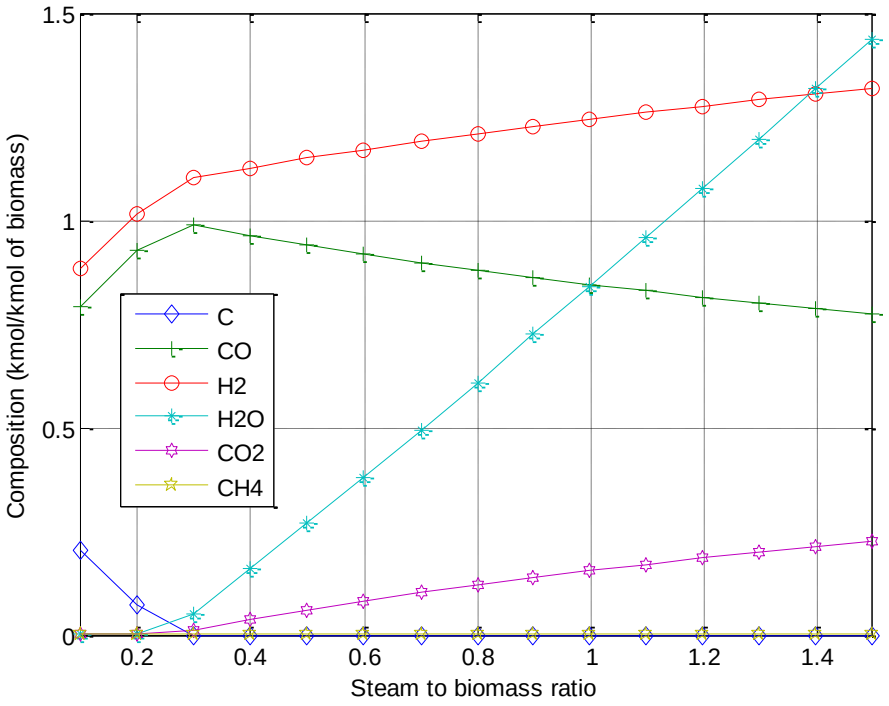

Figure 4-4. A simulation result of gasification product composition as a function of steam to biomass ratio (T = 1500^{o}C, P = 2 bar).

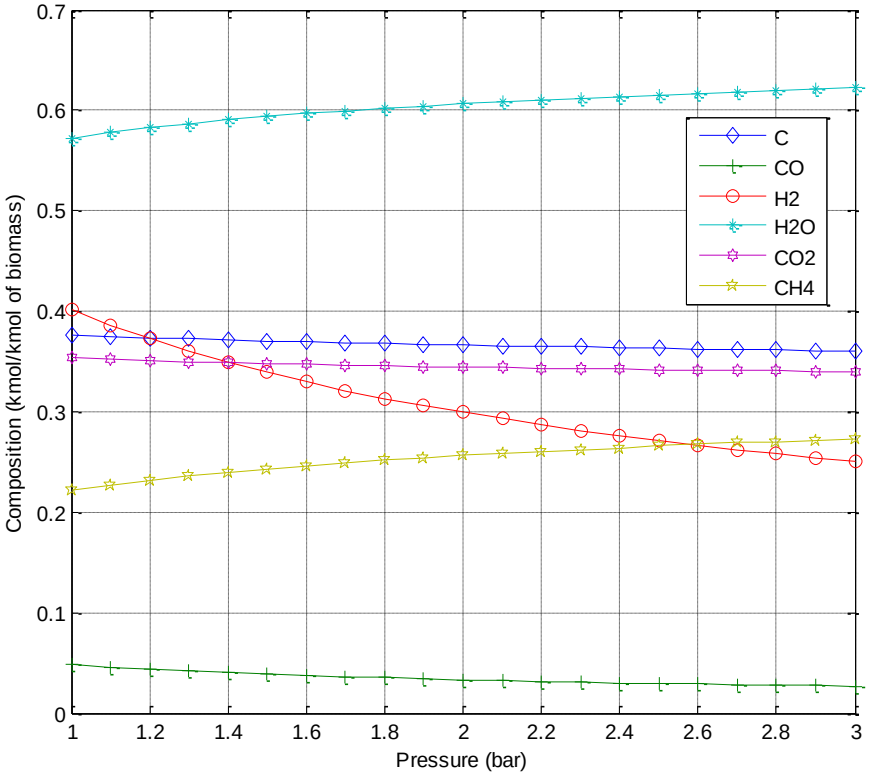

Figure 4-5. A simulation result of gasification product composition as a function of process pressure (T = 500^{o}C, steam to biomass ratio = 0.5).

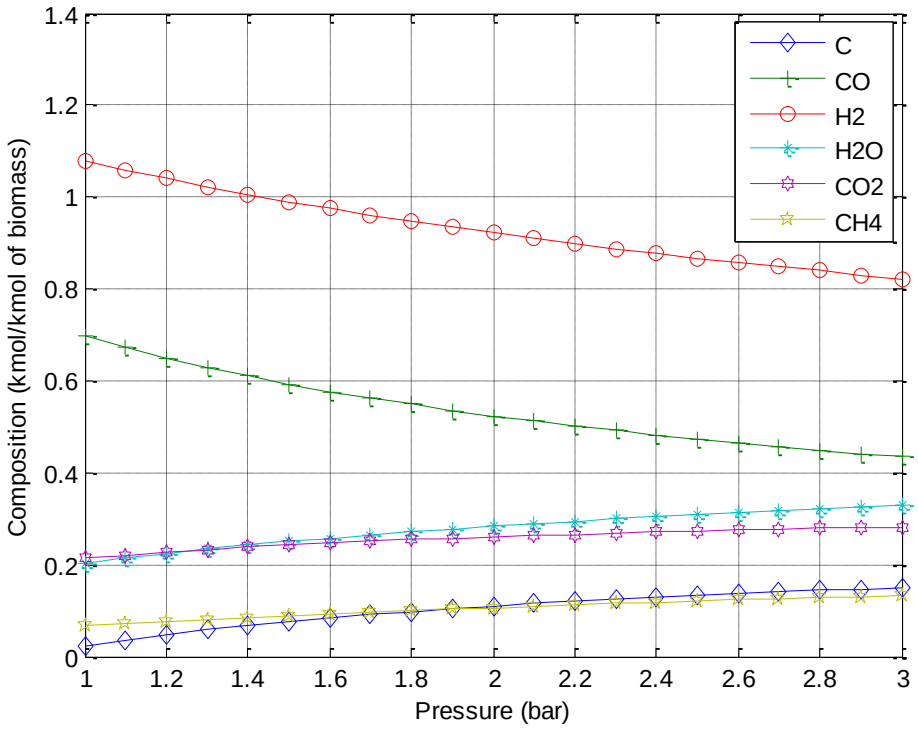

Figure 4-6. A simulation result of gasification product composition as a function of process pressure (T = 700^{o}C, steam to biomass ratio = 0.5).

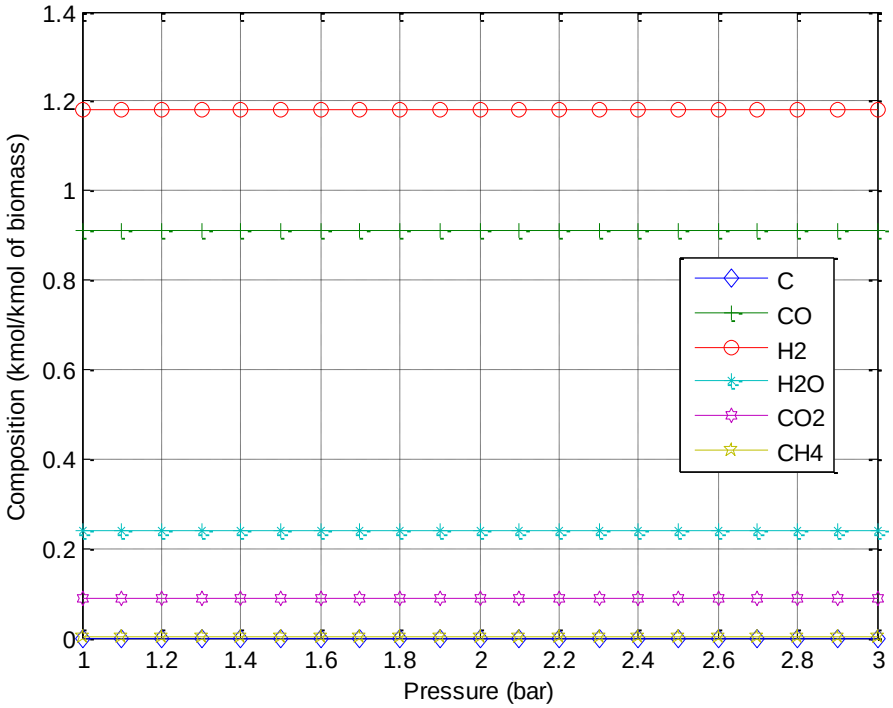

Figure 4-7. A simulation result of gasification product composition as a function of process pressure (T = 1100^{o}C, steam to biomass ratio = 0.5).

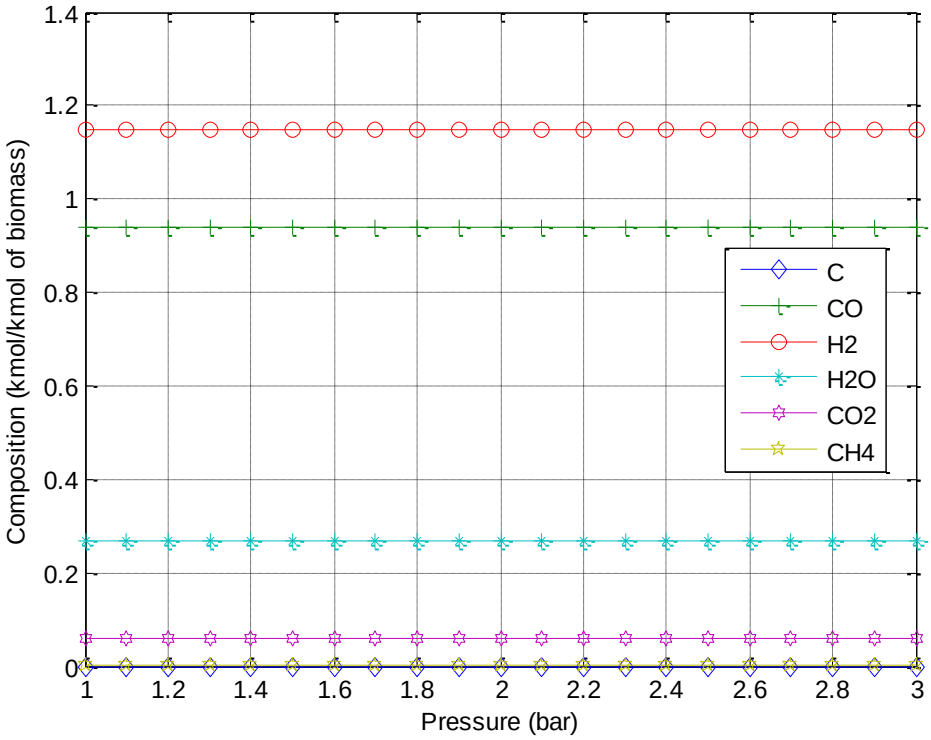

Figure 4-8. A simulation result of gasification product composition as a function of process pressure (T = 1500^{o}C, steam to biomass ratio = 0.5).

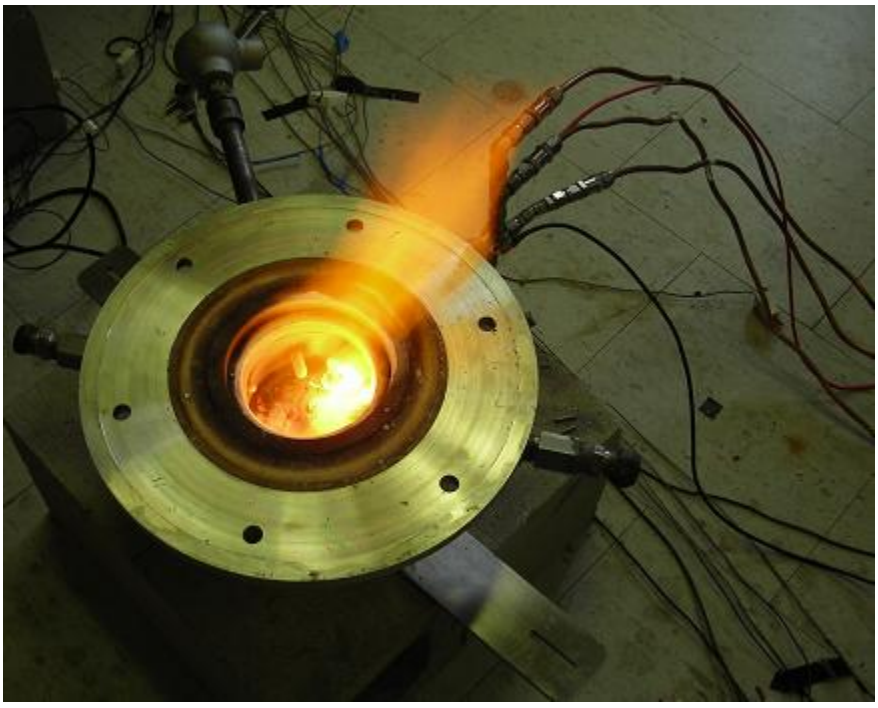

Figure 4-9. A view of the flame ignited torch (no grate) in the torch test on August 23, 2010.

Figure 4-10. A view of the flame through the grate in the torch test on August 24, 2010.

Table 4-2. Summary of the inlet gas conditions and the chamber temperature for the torch test 1 (Aug. 24, 2010).

Time (min)		Flow $Rate_{H2}$ (LPM)	Flow $Rate_{O2}$ (LPM)	T_{H2} (^oC)	T_{O2} (^oC)	P_{H2} at the regulator (psig)	P_{O2} at the regulator (psig)	Chamber T (^oC)
2.25	1st ignition	12	22	21.62	19.76	40	40	13.11
5.67	Gases turned off	0	0	22.35	20.34	40	40	1027
14.27	2nd ignition	12	22	23.46	21.81	40	40	336
20.33	Gases turned off	0	0	22.38	21.78	40	40	1680

H_2 pressure range: 2 to 7.5 psig

O_2 pressure range: 2 to 4 psig

Units reflect readings in actual instruments.

Table 4-3. The flow rates of inlet hydrogen and oxygen at STP (298.15 K and 1atm) after correcting the air-standard reading at rotameters (Torch test 1, Aug. 24, 2011).

Time (min)		Flow $Rate_{H2}$ (LPM)	Flow $Rate_{O2}$ (LPM)	Molar Ratio H_2:O_2
2.25	1st ignition	51.30	23.66	2.2:1
5.67	Gases turned off	0	0	
14.27	2nd ignition	51.14	23.58	2.2:1
20.33	Gases turned off	0	0	

Pressure of 4 psig was assumed for the flow rate correction for both hydrogen and oxygen flows.

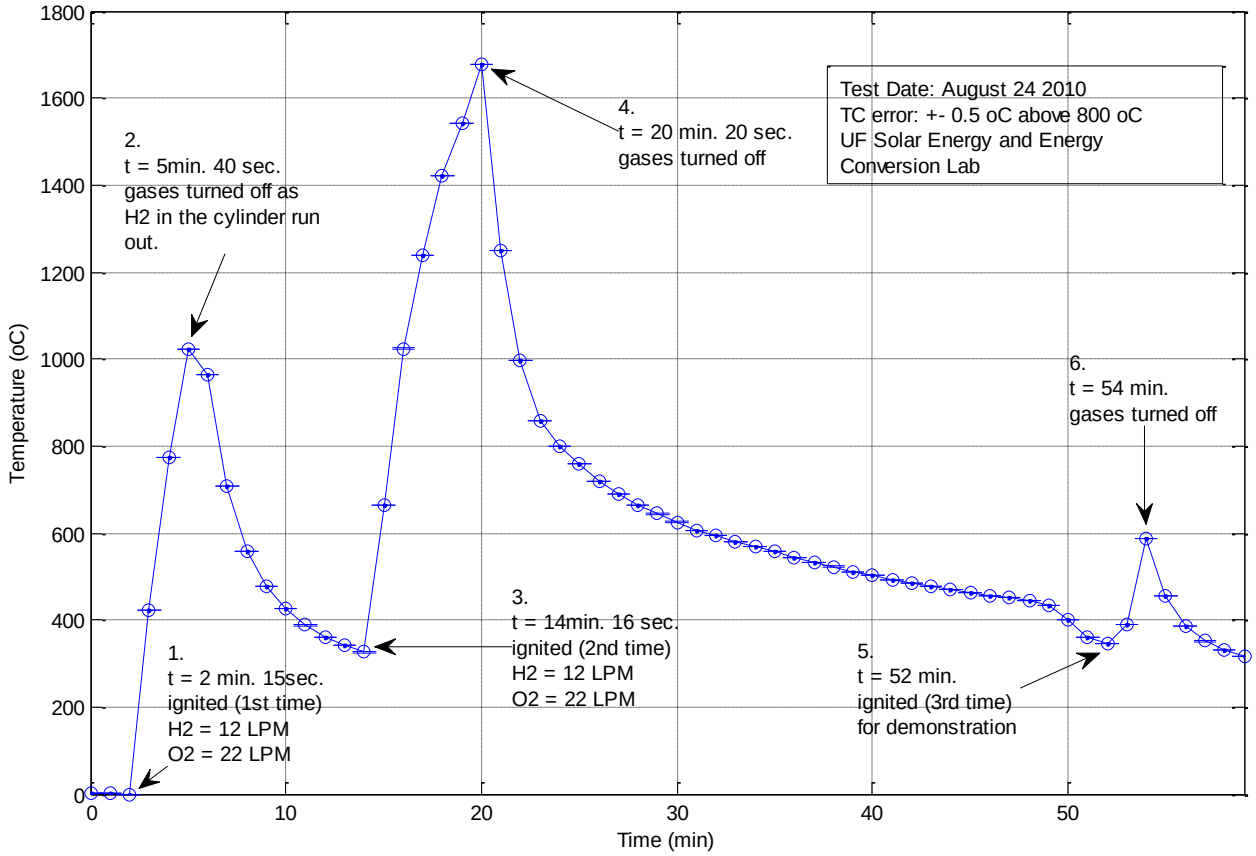

Figure 4-11. Combustion chamber temperature as a function of time with various inlet gas flow rates for the torch test 1 (Aug. 24, 2010).

Table 4-4. Summary of the inlet gas conditions and the chamber temperature for the torch test 2 (Aug. 26, 2010).

Time (min)		Flow $Rate_{H2}$ (LPM)	Flow $Rate_{O2}$ (LPM)	T_{H2} (^oC)	T_{O2} (^oC)	P_{H2} at the regulator (psig)	P_{O2} at the regulator (psig)	Chamber T (^oC)
0.43	ignited	2	10	25.73	24.73	40	40	18.11
17.00	changed flow rate	10	10	25.93	24.75	40	40	1005
22.83	changed flow rate	5	13	26.17	24.72	40	40	1620
28.75	changed flow rate	5	9	25.98	24.87	40	40	1480
30.50	changed flow rate	5	5	25.99	24.86	40	40	1340
35.00	changed flow rate	5	12	26.08	25.11	40	40	1220
39.67	gases turned off	0	0	25.97	24.90	40	40	1440

H_2 pressure range: 2 to 6 psig

O_2 pressure range: 3 to 4 psig

Units reflect readings in actual instruments.

Table 4-5. The flow rates of inlet hydrogen and oxygen at STP (298.15 K and 1atm) after correcting from the air-standard reading at rotameters (Torch test 2, Aug. 26, 2011).

Time (min)		Flow Rate$_{H2}$ (LPM)	Flow Rate$_{O2}$ (LPM)	Molar Ratio H_2:O_2
0.43	ignited	8.49	10.66	0.8:1
17	changed flow rate	42.44	10.66	4:01
22.83	changed flow rate	21.21	13.86	1.5:1
28.75	changed flow rate	21.22	9.60	2.2:1
30.5	changed flow rate	21.22	5.33	4:01
35	changed flow rate	21.21	12.79	1.7:1
39.67	gases turned off	0	0	

Pressure of 4 psig was assumed for the flow rate correction for both hydrogen and oxygen flows.

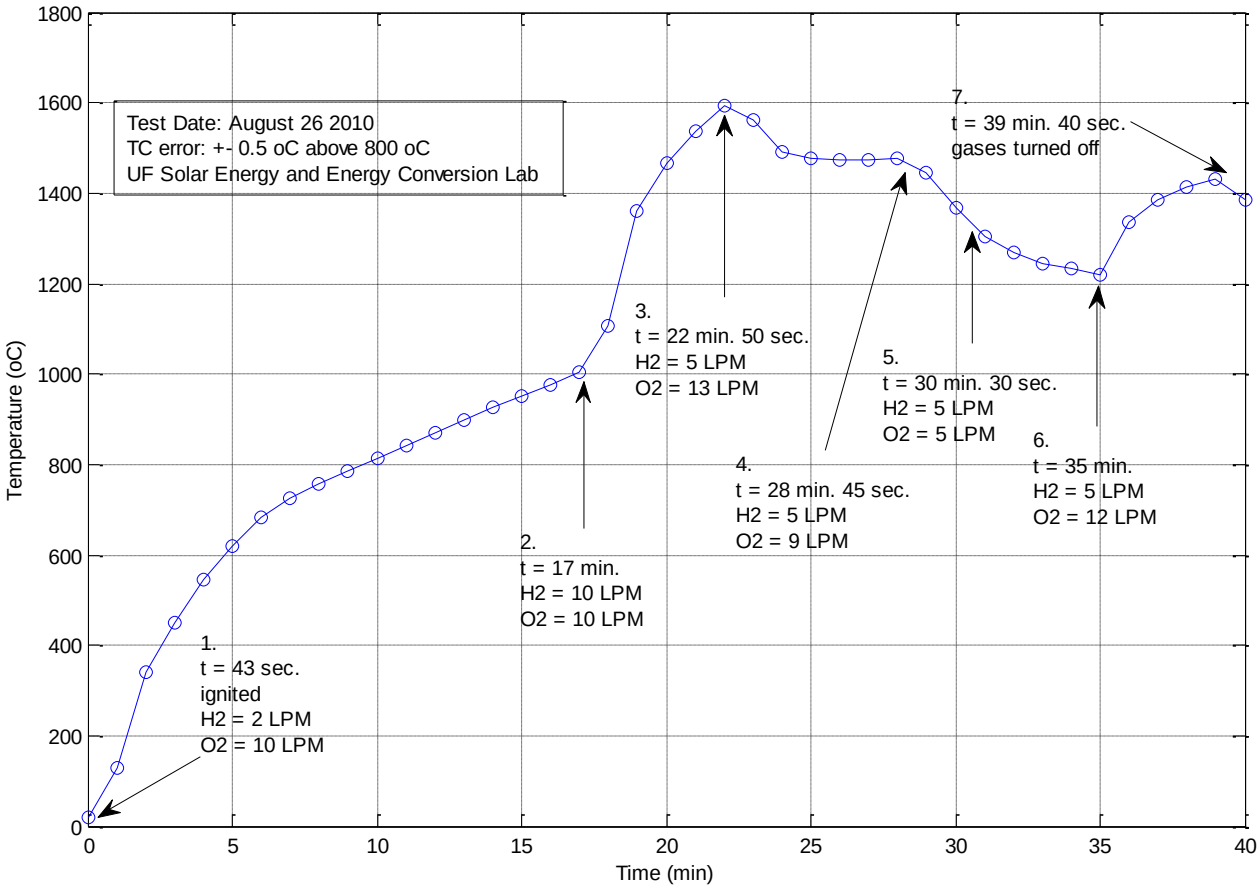

Figure 4-12. Combustion chamber temperature as a function of time with various inlet gas flow rates for the torch test 2 (Aug. 26, 2010).

Table 4-6. Summary of the inlet gas conditions and the chamber temperature for the torch test 3 (Sept. 7, 2010).

Time (min)		Flow $Rate_{H2}$ (LPM)	Flow $Rate_{O2}$ (LPM)	Flow $Rate_{CO2}$ (LPM)	T_{H2} (^oC)	T_{O2} (^oC)	T_{CO2} (^oC)	P_{H2} at the regulator (psig)	P_{O2} at the regulator (psig)	P_{CO2} at the regulator (psig)	Chamber T (^oC)
2.00	ignited	8	8	0	25.85	25.19		40	40	40	13
27.00		8	12	0	27.43	26.50		40	40	40	1020
37.33		8	16	0	27.12	26.47		40	40	40	1390
40.58		8	10	0	27.21	26.40		40	40	40	1655
48.00		8	12	0	27.84	27.00		40	40	40	1390
55.67		8	8	0	28.56	27.61		40	40	40	1475
65.00		10	8	0	28.32	27.56		40	40	40	1285
71.77		8	5	0	28.92	28.31		40	40	40	1385
75.50		5	4	0	28.78	28.11		40	40	40	1085
81.00		5	4	10	28.66	28.12	29.12	40	40	40	1065
82.50		4	3.5	20	28.41	27.86	28.70	40	40	40	1070
87.75		4	3.5	30	28.08	27.61	24.35	40	40	40	960
92.50	turned off	0	0	0	28.07	27.47	8.88	40	40	40	840

H_2 pressure range: 2 to 6 psig

O_2 pressure range: 3 to 4 psig

Units reflect readings in actual instruments.

Table 4-7. The flow rates of inlet hydrogen and oxygen at STP (298.15 K and 1atm) after correcting the air-standard reading at rotameters (Torch test 3, Sep. 7, 2011).

Time (min)		Flow $Rate_{H2}$ (LPM)	Flow $Rate_{O2}$ (LPM)	Flow $Rate_{CO2}$ (LPM)	Molar Ratio H_2:O_2
2	ignited	33.95	8.52		4:01
27		33.86	12.76		2.7:1
37.33		33.88	17.01		2:01
40.58		33.88	10.63		3.2:1
48		33.84	12.75		2.7:1
55.67		33.80	8.49		4:01
65		42.27	8.49		5:01
71.77		33.78	5.30		6.4:1
75.5		21.12	4.24		5:01
81		21.12	4.24	9.03	5:01
82.5		16.90	3.71	18.08	4.6:1
87.75		16.91	3.71	27.31	4.6:1
92.5	turned off	0	0	0	

Pressure of 4 psig was assumed for the flow rate correction for both hydrogen and oxygen flows.

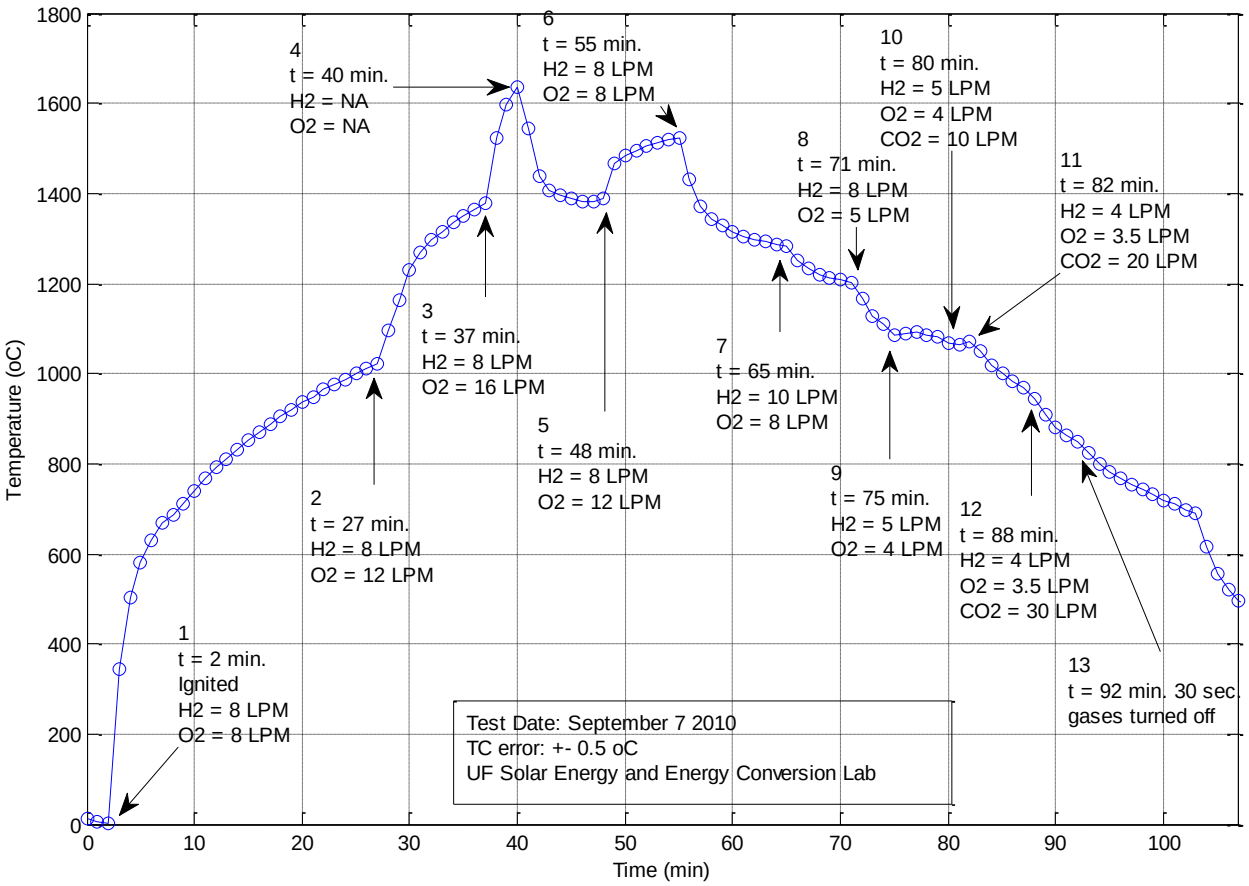

Figure 4-13. Combustion chamber temperature as a function of time with various inlet gas flow rates for the torch test 3 (Sept. 7, 2010).

Table 4-8. Overall summary of the relationship between inlet gas flow rates and combustion chamber temperatures for the torch test 1, 2 and 3 (Aug. 24 and 26, and Sept. 7, 2010).

H_2 (LPM)	O_2 (LPM)	CO_2 (LPM)	Heating rate (^oC/min)		Stabilization T (^oC) at the Chamber
2	10	0	120 (< 700^oC)	26 (> 700^oC)	> 1005
4	3.5	20			
4	3.5	10			< 695
5	4	10			< 1060
5	5	0			< 1220
5	9	0			< 1340
5	12	0			> 1440
5	13	0			at 1480
8	5	0			< 1100
8	8	0	200 (< 600^oC)	20 (> 600^oC)	< 1285
8	10	0			at 1390
8	12	0	56.60 (1000 < T < 1200^oC)	21 (> 1200^oC)	> 1390
8	16	0	126 (1380 < T < 1530^oC)	55.31 (> 1530^oC)	>> 1655
10	8	0			< 1206
10	10	0	330 (1000 < T < 1300^oC)	76.50 (> 1300^oC)	>> 1620
12	22	0	296 (<1000^oC)	151.27 (> 1000^oC)	>> 1680

H_2 pressure range: 2 to 7.5 psig

O_2 pressure range: 2 to 4 psig

Units reflect readings in actual instruments.

NOTE: Inlet gas flow rates are NOT corrected to STP. Corrected flow rates are provided in Tables 4-3, 4-5 and 4-7).

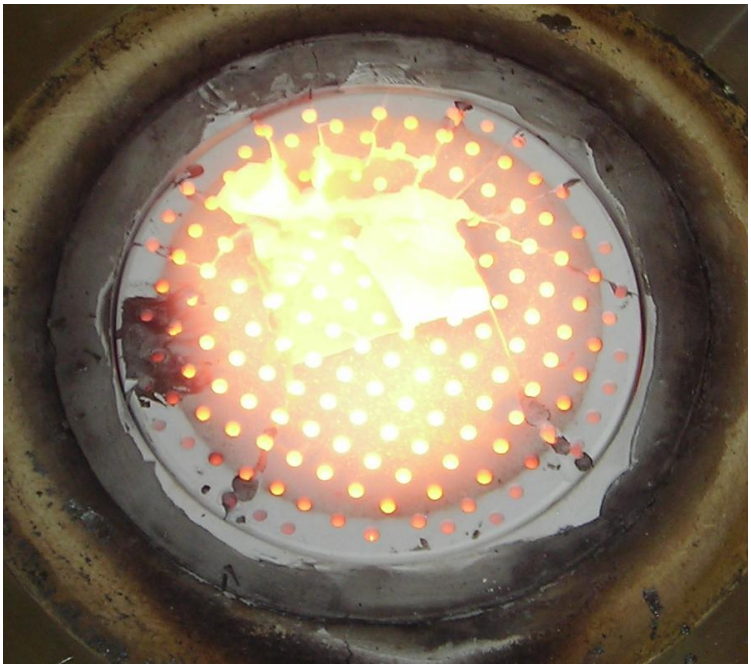

Figure 4-14. The view of the broken grate during the cooling period in torch test 1 (Aug. 24, 2010).

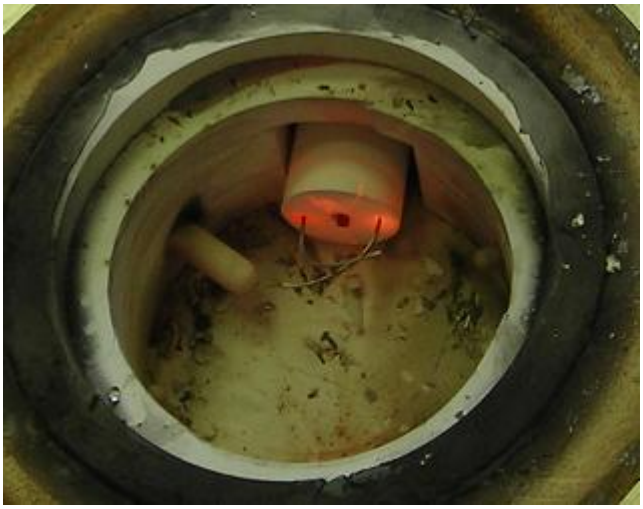

Figure 4-15. The view of the red hot torch after the combustion was terminated in a torch test.

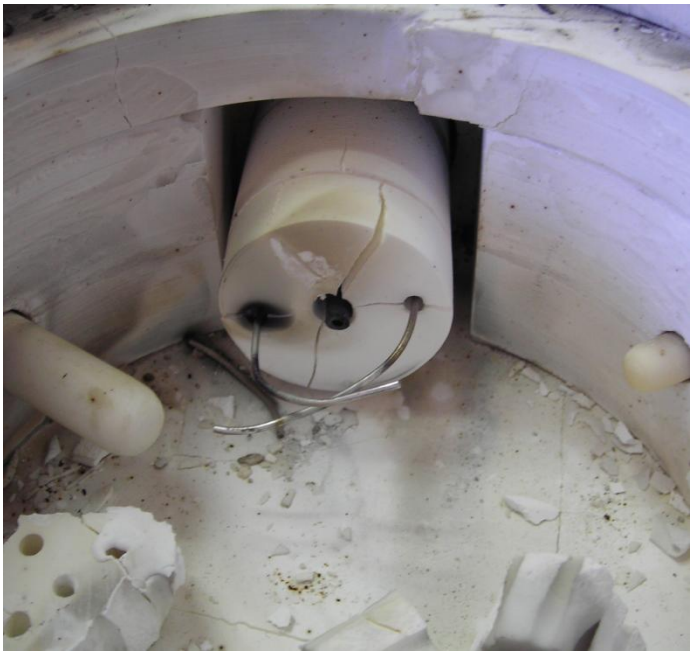

Figure 4-16. A torch view after the torch test1 showing cracking and debris on the combustion chamber floor (Aug. 24, 2010).

Figure 4-17. A view of the combustion chamber and a part of the torch showing pieces of broken and melted grate from the torch test 1 (Aug. 24, 2010).

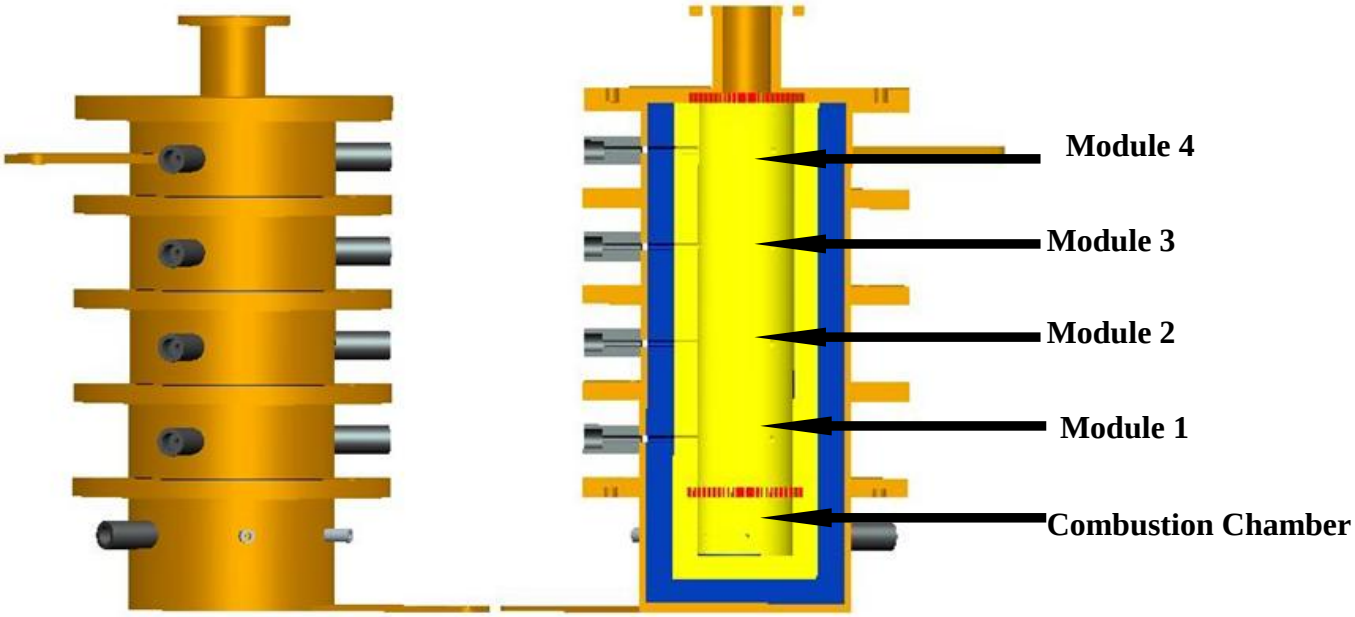

Figure 4-18. The image of the gasification reactor and numbering sequence for the modules.

Table 4-9. Summary of inlet gas conditions in dry run 1 (Oct. 2, 2010).

Time (min)		Flow $Rate_{H2}$ (LPM)	Flow $Rate_{O2}$ (LPM)	T_{H2} (^oC)	T_{O2} (^oC)	P_{H2} at the regulator (psig)	P_{O2} at the regulator (psig)	Chamber T (^oC)
0.00	ignited	10	22	22.81	21.88	40	40	13.73
5.75	flow rates changed to	10	15	23.28	22.06	40	40	1387
7.58		8	12	23.40	22.09	40	40	970
18.00		10	20	23.70	22.64	40	40	1150
22.30		10	16	23.64	22.94	40	40	1620
32.65	gases turned off	0	0	23.56	22.92	40	40	1430

H_2 pressure range: 2 to 6 psig

O_2 pressure range: 3 to 4 psig

Units reflect readings in actual instruments.

Table 4-10. The flow rates of inlet hydrogen and oxygen at STP (298.15 K and 1atm) after correcting the air-standard reading at rotameters (Dry run 1, Oct. 2, 2011).

Time (min)		Flow $Rate_{H2}$ (LPM)	Flow $Rate_{O2}$ (LPM)	Molar Ratio H_2:O_2
0	ignited	42.66	23.57	1.8:1
5.75	flow rates changed to	42.63	16.07	2.7:1
7.58		34.09	12.85	2.7:1
18		42.60	21.40	2:01
22.3		42.60	17.11	2.5:1
32.65	gases turned off	0	0	

Pressure of 4 psig was assumed for the flow rate correction for both hydrogen and oxygen flows.

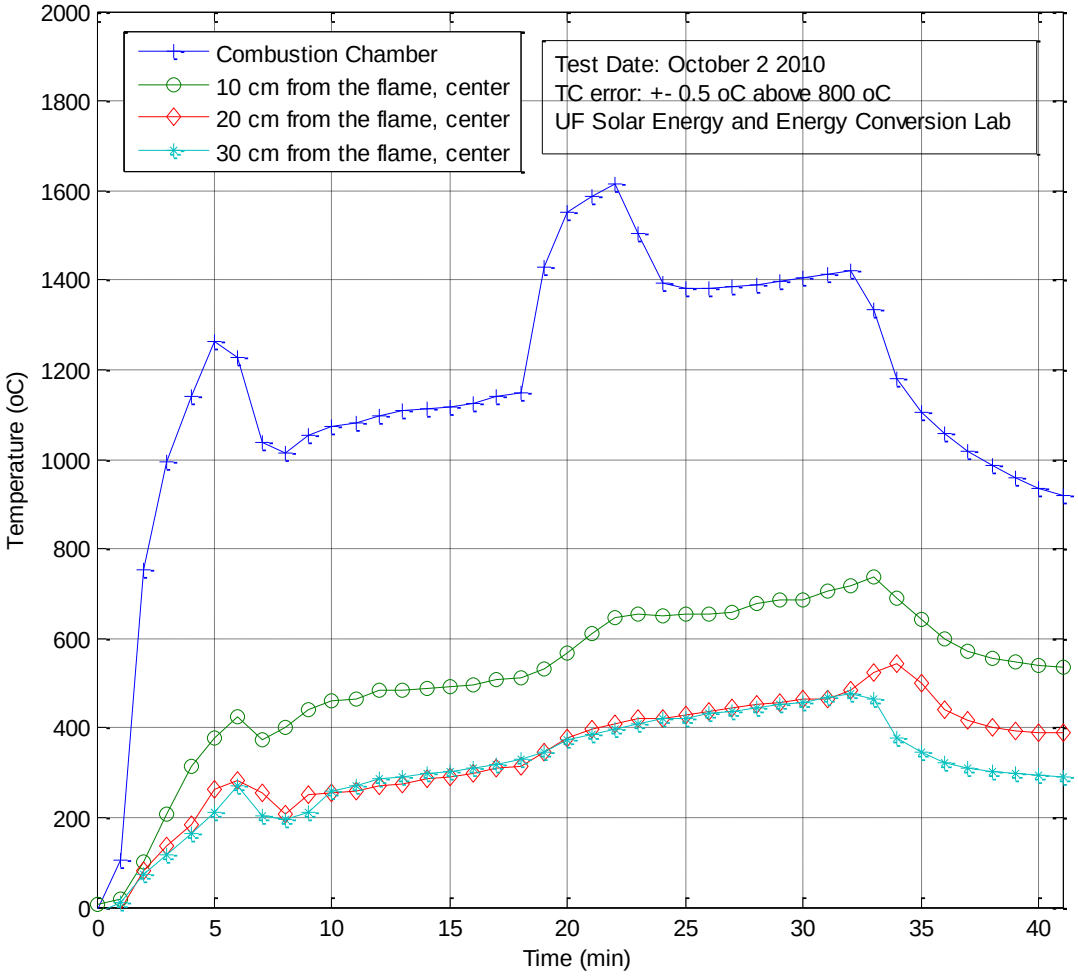

Figure 4-19. Gasification reactor temperatures at the center of the reactor as a function of time in dry run 1 (Oct. 2, 2010). Ignition occurred at time = 0 minute and the system was shut off at t = 32.65 minutes. The corresponding changes in inlet gas flow rates during the run are provided in Tables 4-9 and 4-10.

Table 4-11. Summary of inlet gas conditions in dry run 2 (Oct. 28, 2010).

Time (min)		Flow $Rate_{H2}$ (LPM)	Flow $Rate_{O2}$ (LPM)	T_{H2} (^oC)	T_{O2} (^oC)	P_{O2} (psig)	Chamber T (^oC)
0.00	ignited	10	16	24.94	23.88	4	11.7
21.58	flow rates changed to	9	10	26.20	25.24	3	1677
29.33	gases turned off	12	10	26.25	25.22	3	1154

H_2 pressure range: 2 to 6 psig

Units reflect readings in actual instruments.

Table 4-12. The flow rates of inlet hydrogen and oxygen at STP (298.15 K and 1atm) after correcting the air-standard reading at rotameters (Dry run 2, Oct. 28, 2011).

Time (min)		Flow Rate$_{H2}$ (LPM)	Flow Rate$_{O2}$ (LPM)	Molar Ratio H_2:O_2
0	ignited	10.660448	68.13296	0.2:1
21.58	flow rates changed to	37.141306	42.486006	0.9:1
29.33	gases turned off	49.517609	42.487429	1.2:1

Pressure of 4 psig was assumed for the flow rate correction for both hydrogen and oxygen flows.

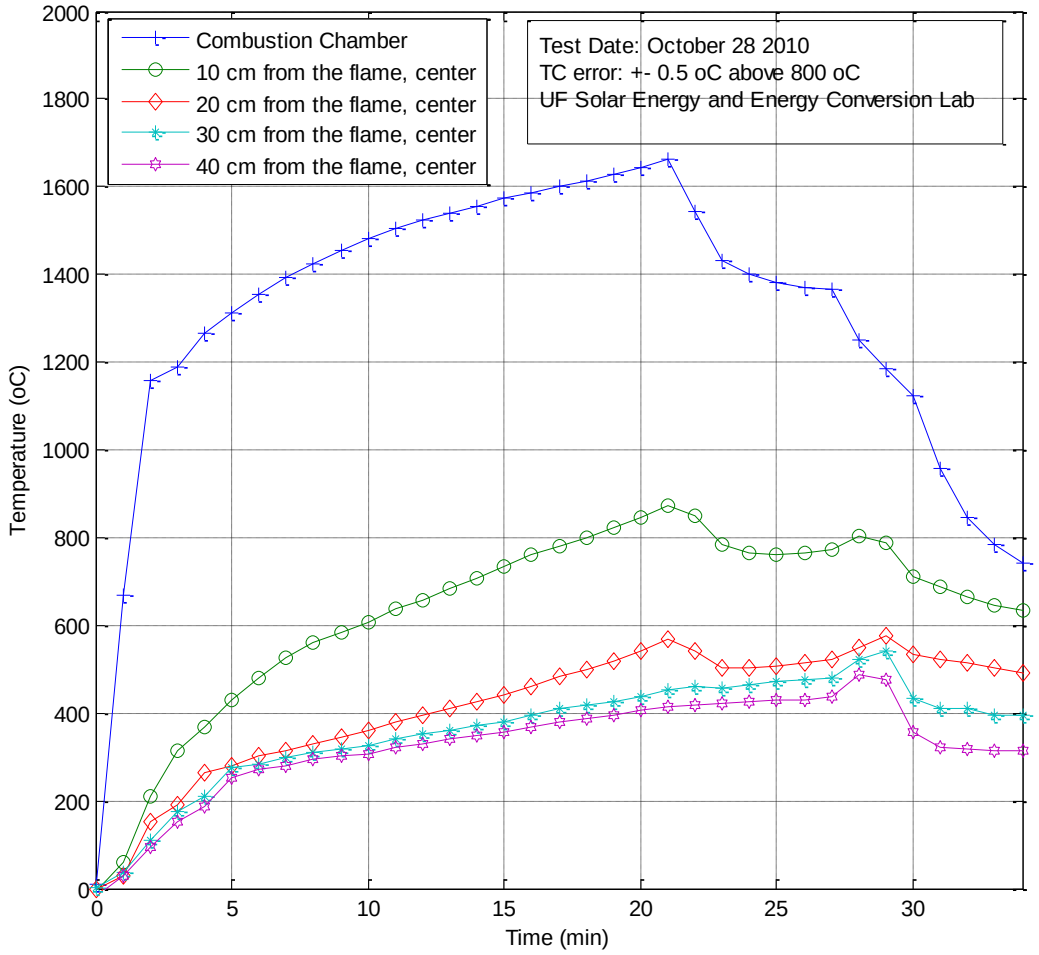

Figure 4-20. Gasification reactor temperatures at the center of the reactor as a function of time in dry run 2 (Oct. 28, 2010). Ignition occurred at time = 0 minute and the system was shut off at t = 29.33 minutes. The corresponding changes in inlet gas flow rates during the run are provided in Tables 4-11 and 4-12.

Table 4-13. Summary of inlet gas conditions in dry run 3 (Oct. 30, 2010).

Time (min)		Flow $Rate_{H2}$ (LPM)	Flow $Rate_{O2}$ (LPM)	T_{H2} (^oC)	T_{O2} (^oC)	H_2 P (psig)	P_{O2} (psig)	Chamber T (^oC)
0.00	ignited	10	16	19.85	18.99	4	4	12.16
15.13	flow rates changed to	10.5	16	20.73	19.56	4	4	1515
42.60		11	16	21.39	20.95	4	4	1577
57.75		11	17.5	21.66	21.60	4	5	1653
62.92		11	16	21.46	21.84	4	4	1652
68.13	gases trned off	0	0	21.33	22.03	0	0	1640

Units reflect readings in actual instruments.

Table 4-14. The flow rates of inlet hydrogen and oxygen at STP (298.15 K and 1atm) after correcting the air-standard reading at rotameters (Dry run 3, Oct. 30, 2011).

Time (min)		Flow $Rate_{H2}$ (LPM)	Flow $Rate_{O2}$ (LPM)	Molar Ratio H_2:O_2
0	ignited	42.87	17.23	2.5:1
15.13	flow rates changed to	44.95	17.21	2.6:1
42.6		47.04	17.17	2.7:1
57.75		47.02	19.26	2.4:1
62.92		47.03	17.15	2.7:1
68.13	gases trned off	0	0	

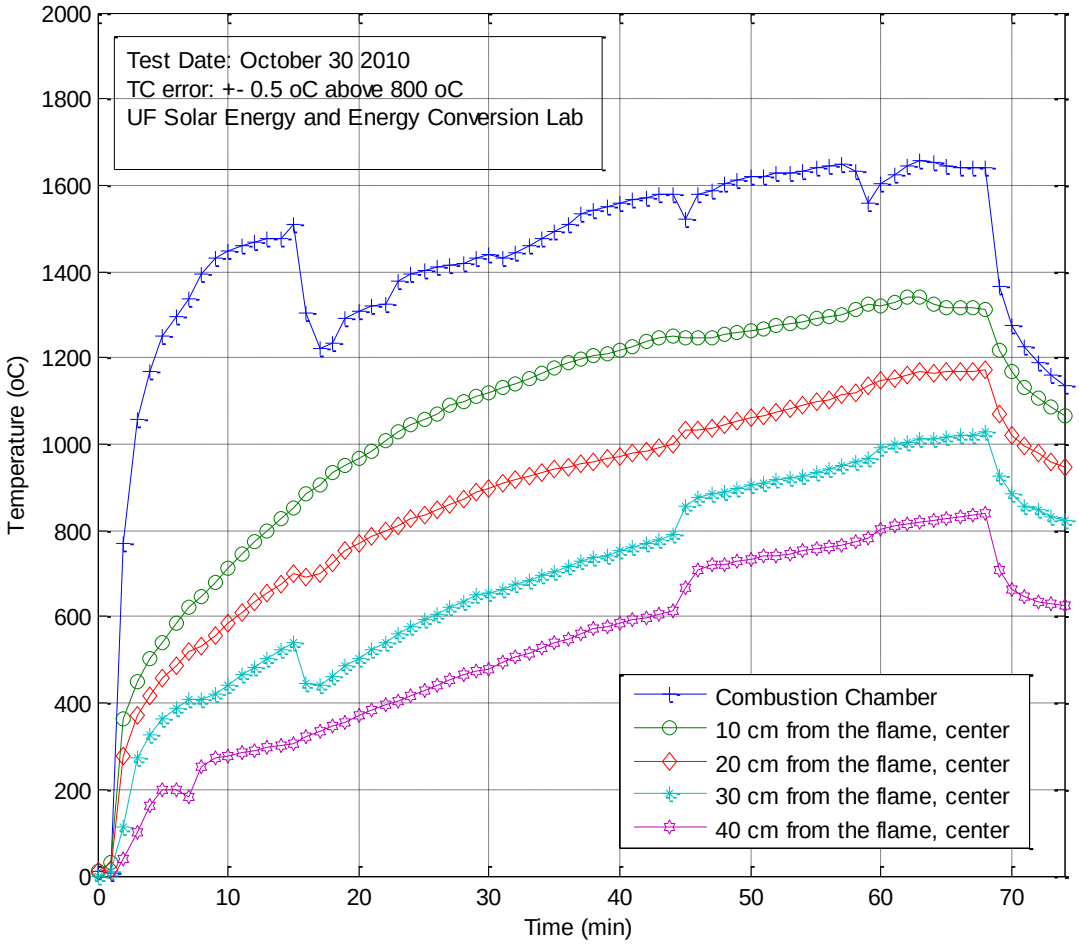

Figure 4-21. Gasification reactor temperatures at the center of the reactor as a function of time in dry run 3 (Oct. 30, 2010). Ignition occurred at time = 0 minute and the system was shut off at t = 68.13 minutes. The corresponding changes in inlet gas flow rates during the run are provided in Tables 4-13 and 4-14.

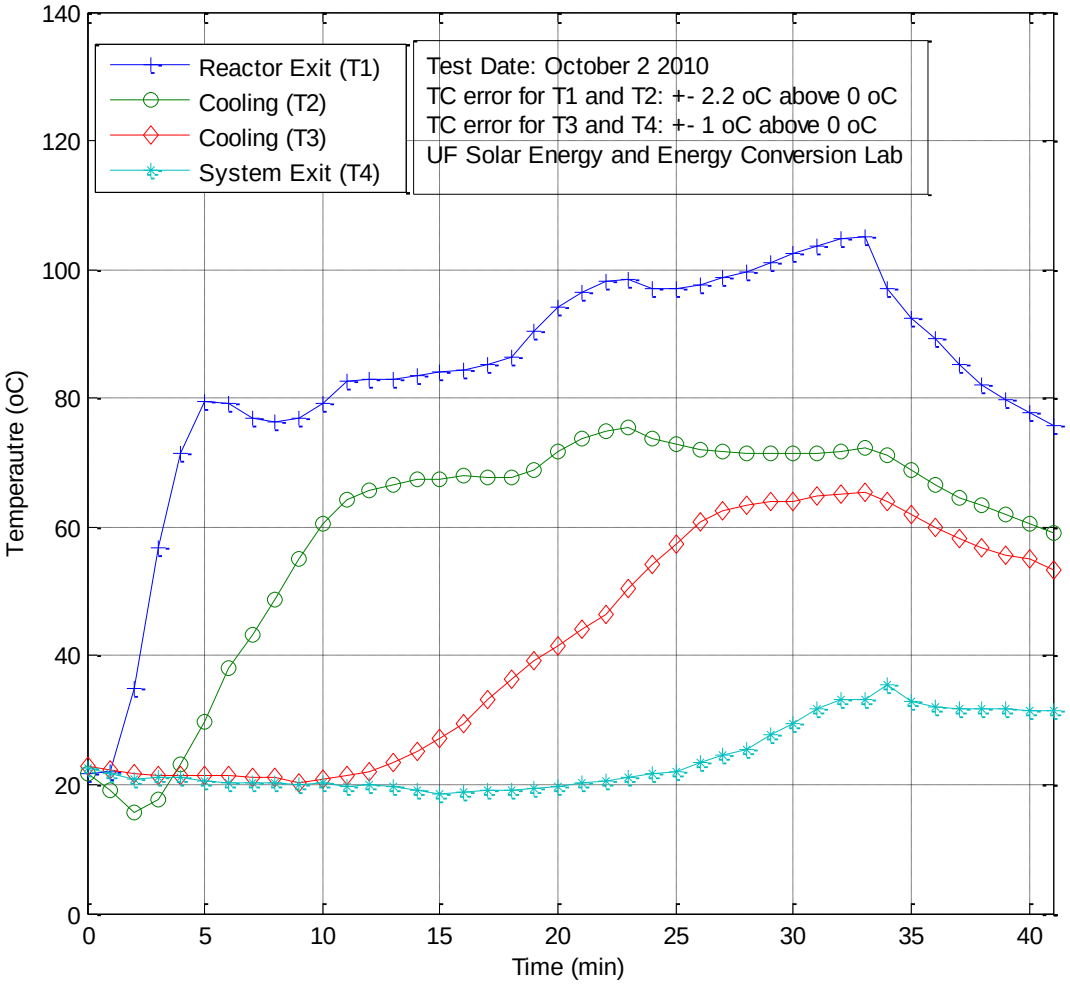

Figure 4-22. Exit gas temperatures as a function of time in dry run 1 (Oct. 2, 2010). Ignition occurred at time = 0 minute and the system was shut off at t = 32.65 minutes.

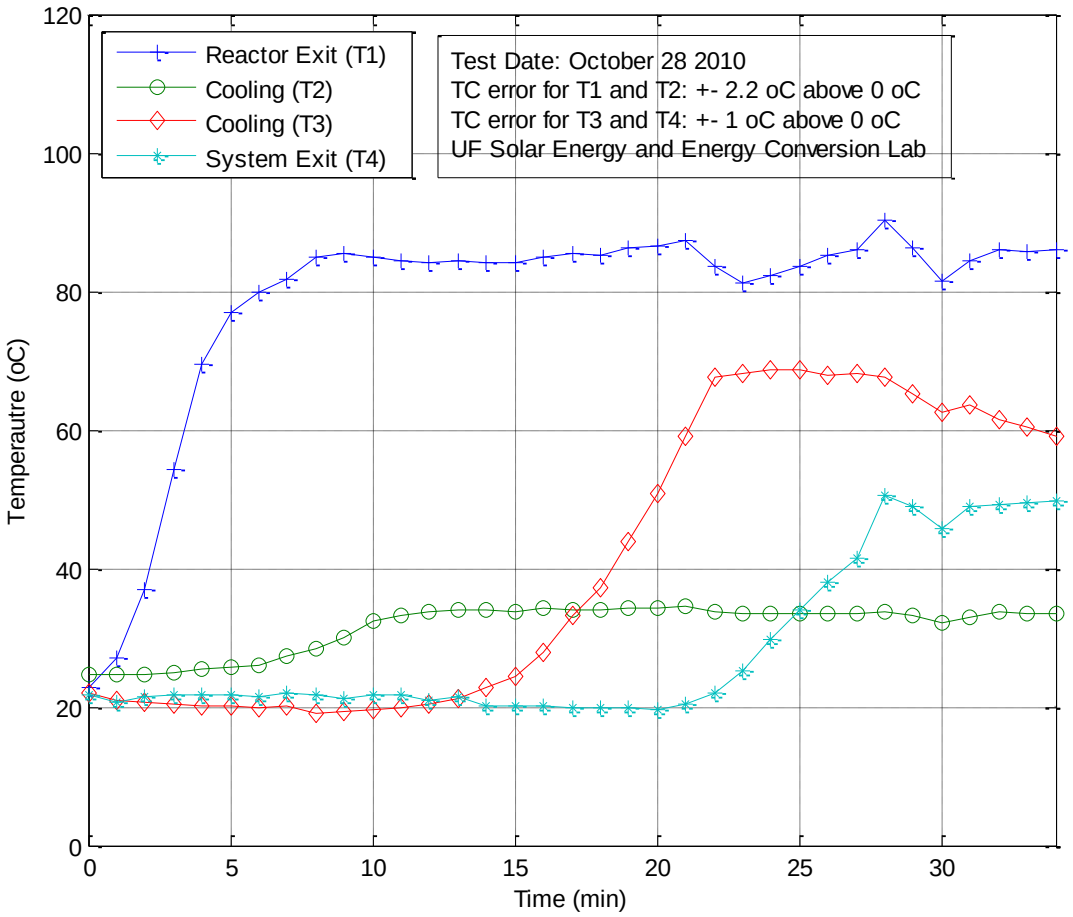

Figure 4-23. Exit gas temperatures as a function of time in dry run 2 (Oct. 28, 2010). Ignition occurred at time = 0 minute and the system was shut off at t = 29.33 minutes.

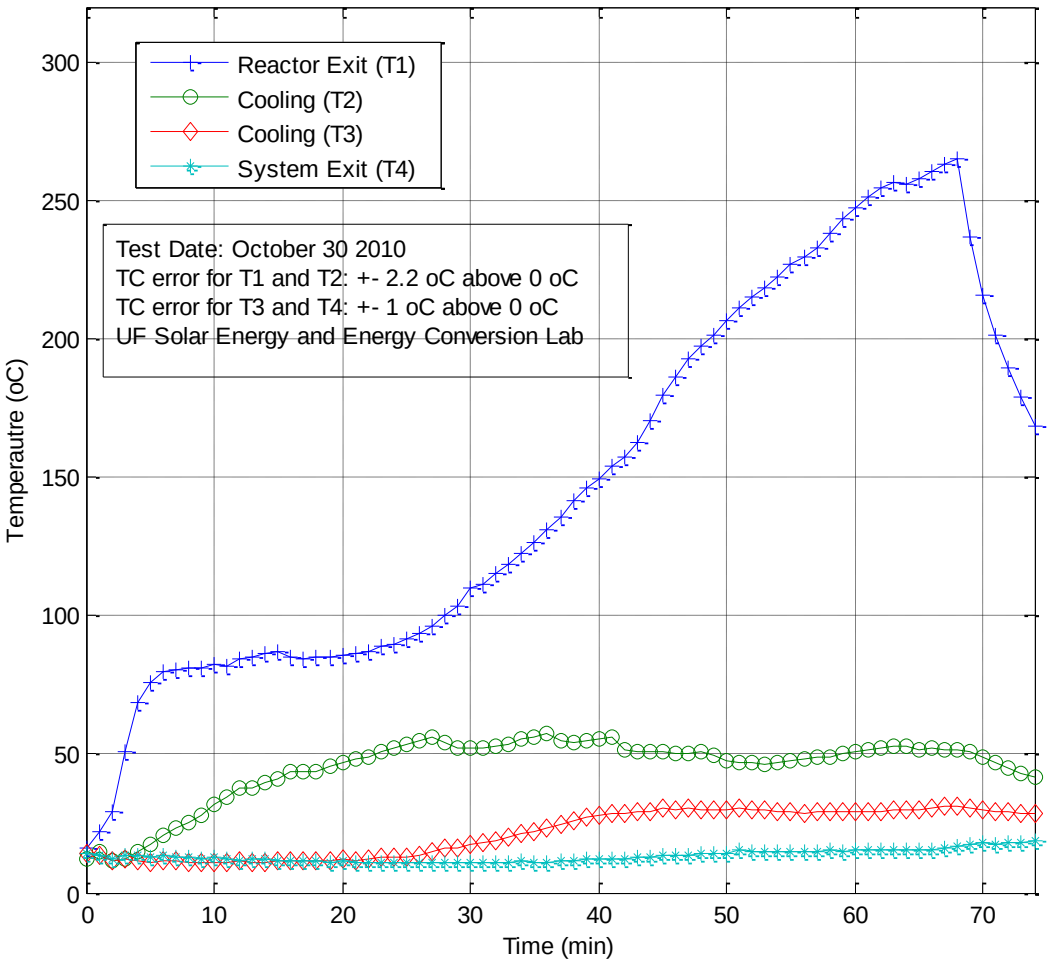

Figure 4-24. Exit gas temperatures as a function of time in dry run 3 (Oct. 30, 2010). Ignition occurred at time = 0 minute and the system was shut off at t = 68.13 minutes.

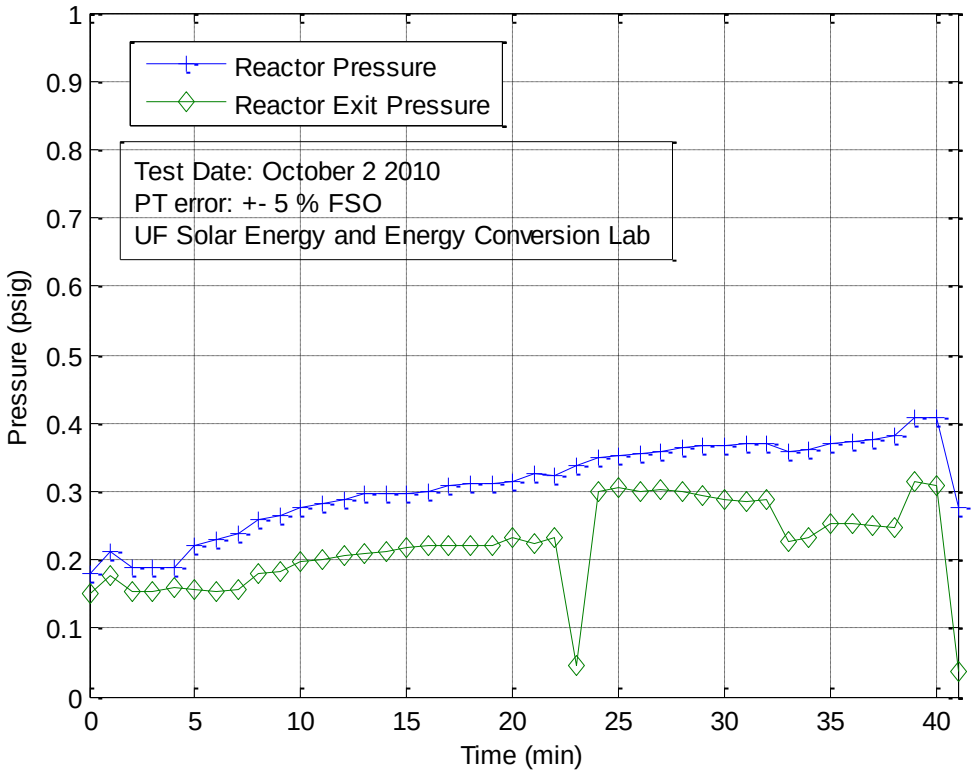

Figure 4-25. The gasification reactor pressure and the reactor exit pressure as a function of time in dry run 1 (Oct. 2, 2010). Ignition occurred at time = 0 minute and the system was shut off at t = 32.65 minutes.

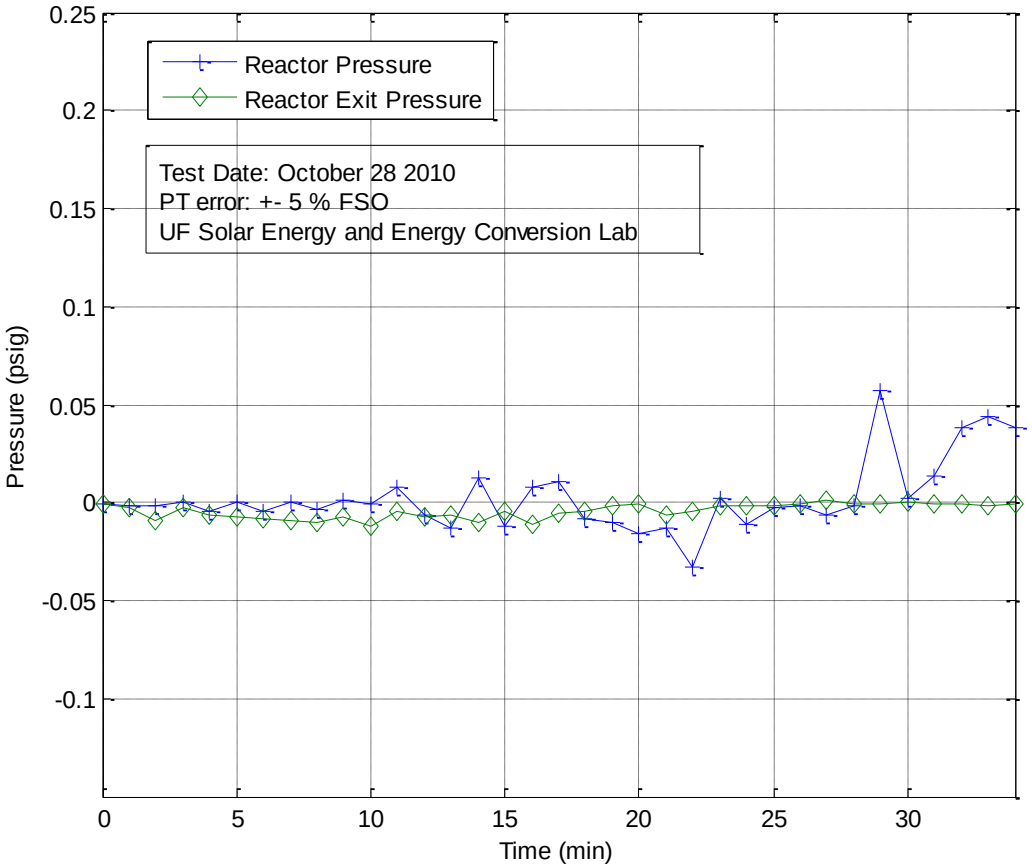

Figure 4-26. The gasification reactor pressure and the reactor exit pressure as a function of time in dry run 2 (Oct. 28, 2010). Ignition occurred at time = 0 minute and the system was shut off at t = 29.33 minutes.

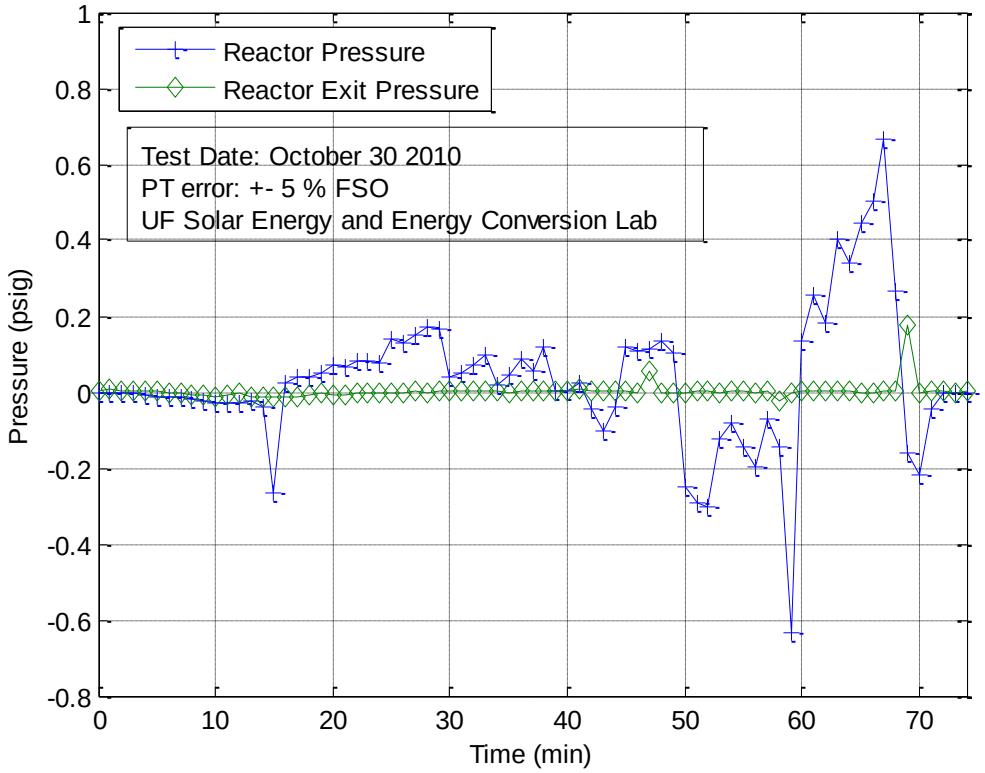

Figure 4-27. The gasification reactor pressure and the reactor exit pressure as a function of time in dry run 3 (Oct. 30, 2010). Ignition occurred at time = 0 minute and the system was shut off at t = 68.13 minutes.

Table 4-15. Summary of inlet gas conditions in Test 4 (March 13, 2011).

(i)	H_2	O_2
Flow rate on rotameters (LPM)	7.5	12.5
Pressure (psig)	4	3
Average Temperature (^oC)	18	17
SG(ρi/ρair)	0.0695	1.105
Flow Rate (LPM, STP)	32	13
number of mole (kmol/s)	2.86E-05	1.11E-05
n_{H2}:n_{O2} ratio	2.6	1

Table 4-16. Summary of inlet gas conditions in Test 5 (March 17, 2011).

(i)	H_2	O_2
Flow rate on rotameters (LPM)	7.5	12.5
Pressure (psig)	4	3
Average Temperature (^oC)	20.5	19.5
SG(ρi/ρair)	0.0695	1.105
Actual Flow Rate (LPM)	32.12	13.08
number of mole (kmol/s)	2.83E-05	1.09E-05
n_{H2}:n_{O2} ratio	2	0.77

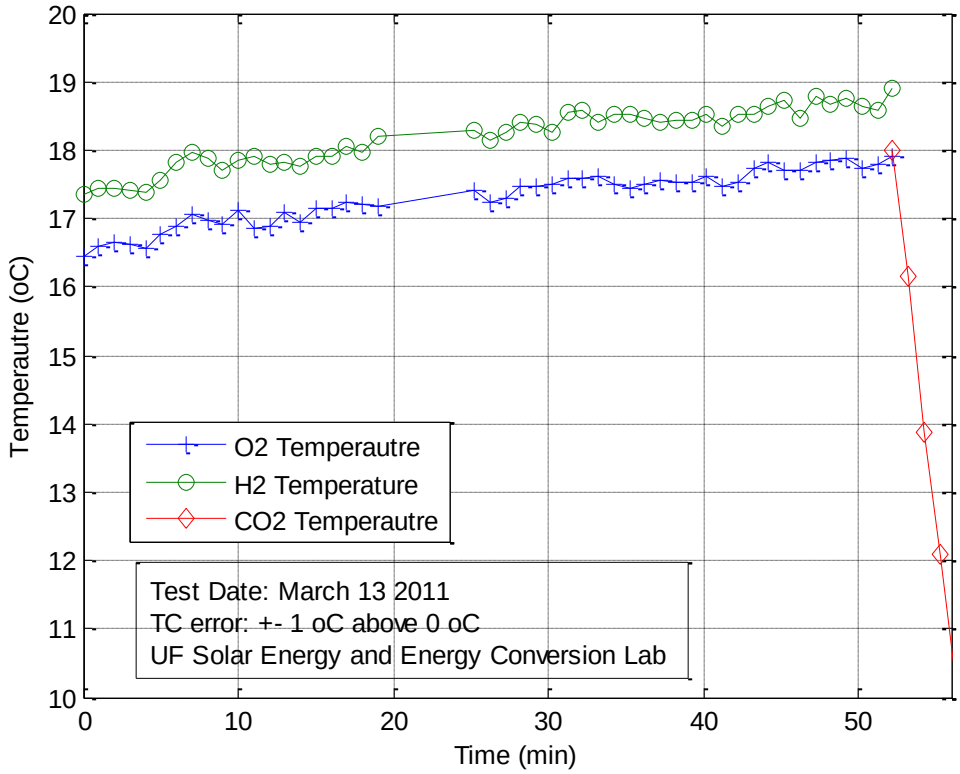

Figure 4-28. Inlet gas temperature versus time for the Test 4 with H_2:O_2 = 32:13 LPM (2.6:1). Ignition occurred at time = 0 minute. Biomass input of 57 g (2 oz) at t = 37 minutes. Hydrogen and oxygen input were stopped and carbon dioxide input was started at t=52 minutes.

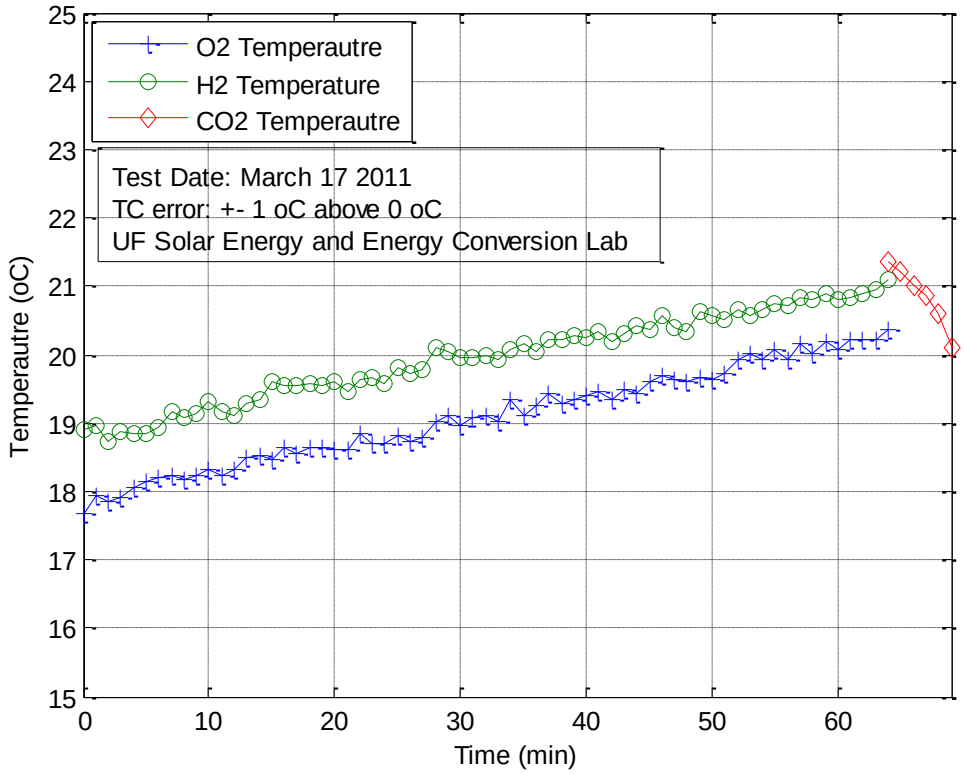

Figure 4-29. Inlet gas temperature versus time for the Test 5 with H_2:O_2 = 32:13 LPM (2.6:1). Ignition occurred at time = 0 minute, 1st biomass input of 28 g (1 oz) at t = 36 minutes, 2nd biomass input of 28 g (1oz) at t=52.5 minutes, hydrogen and oxygen input were stopped and carbon dioxide input was started at t=64 minutes.

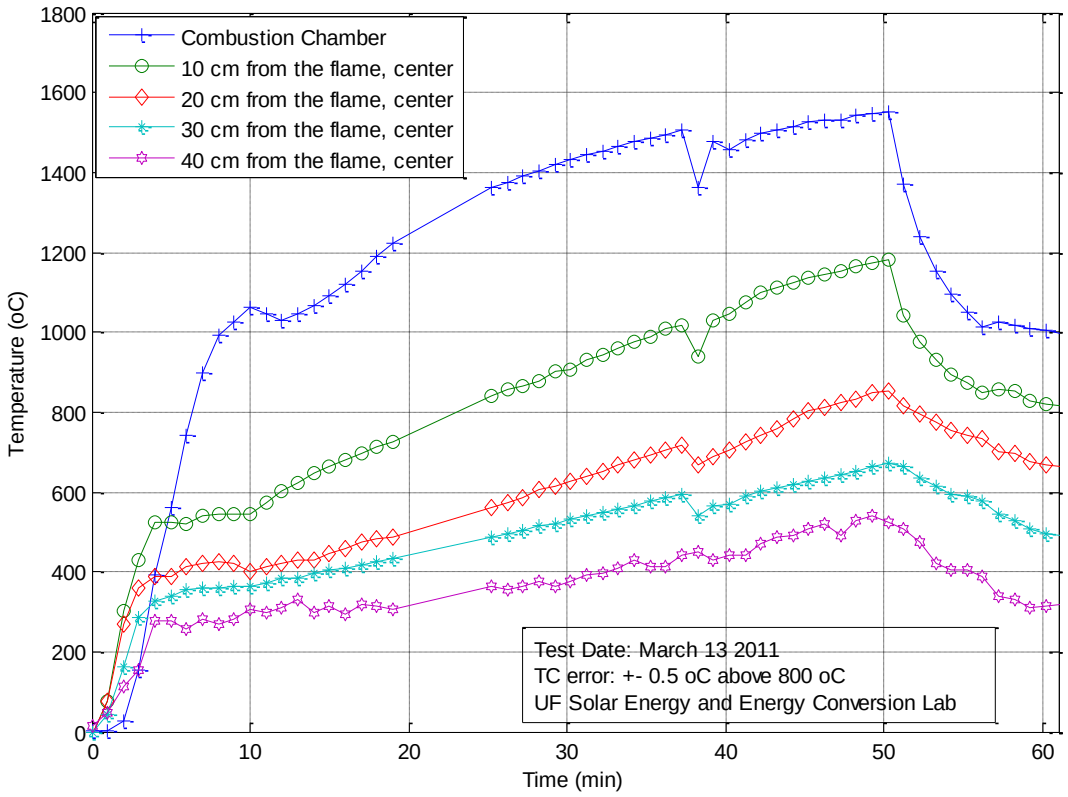

Figure 4-30. Gasification reactor temperatures at the center of the reactor versus time for Test 4 with H_2:O_2 = 32:13 LPM (2.6:1). Ignition occurred at time = 0 minute, biomass input of 57 g (2 oz) at t = 37 minutes, and the system was shut off at t = 52 minutes.

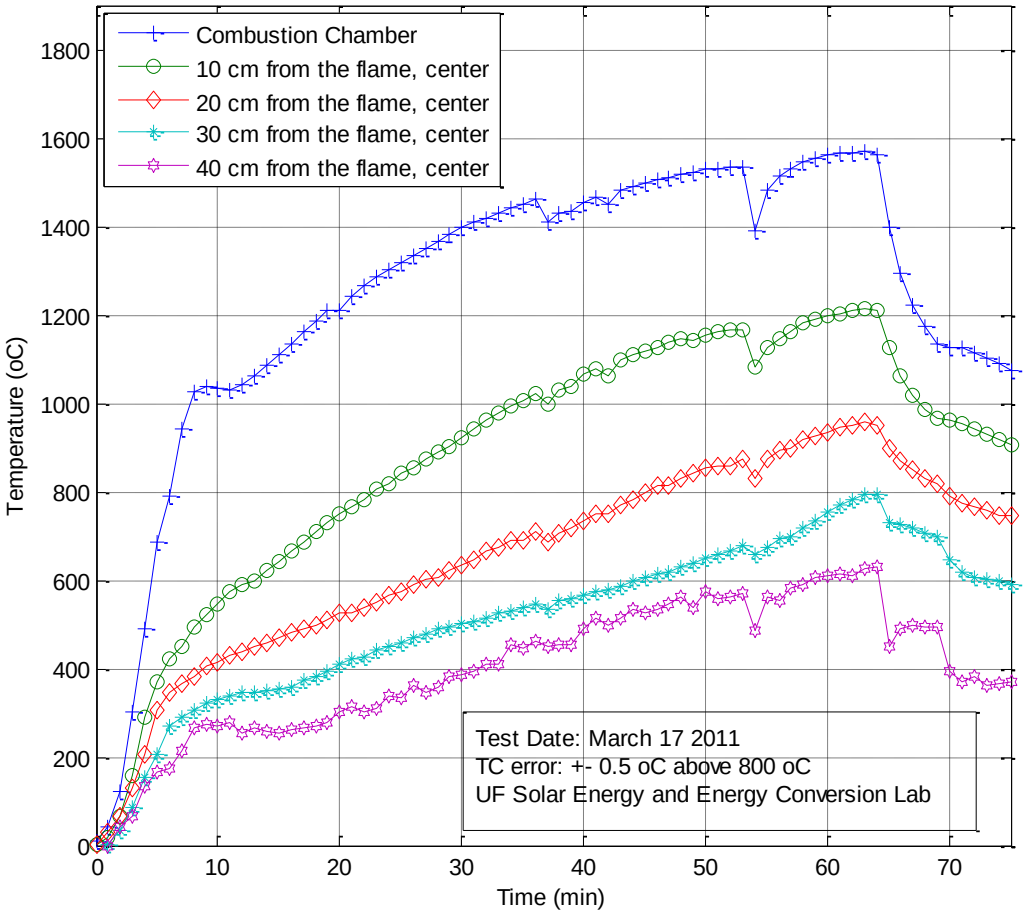

Figure 4-31. Gasification reactor temperature versus time for the Test 5 with H_2:O_2 = 32:13 LPM (2.6:1). Ignition occurred at time = 0 minute, 1st biomass input of 28 g (1 oz) at t = 36 minutes, 2nd biomass input of 28 g (1 oz) at t=52.5 minutes, hydrogen and oxygen input were stopped and carbon dioxide input was started at t=64 minutes.

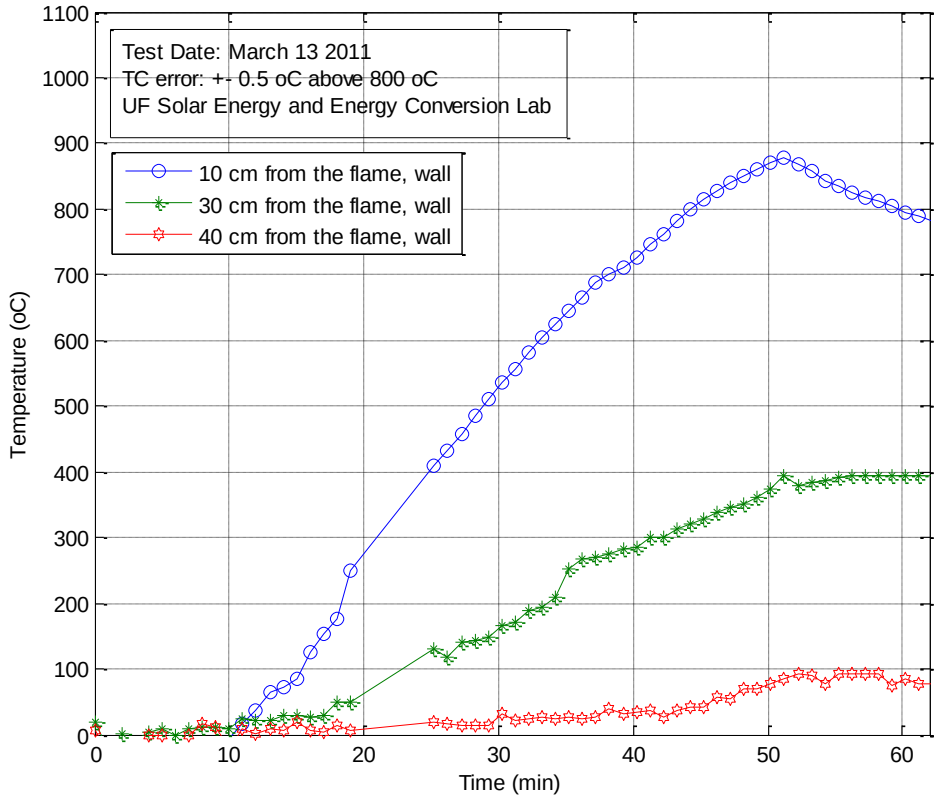

Figure 4-32. Gasification reactor inner wall temperatures versus time for the Test 4 with H_2:O_2 = 32:13 LPM (2.6:1). Ignition occurred at time = 0 minute, biomass input of 57 g (2 oz) at t = 37 minutes, and the system was shut off at t = 52 minutes.

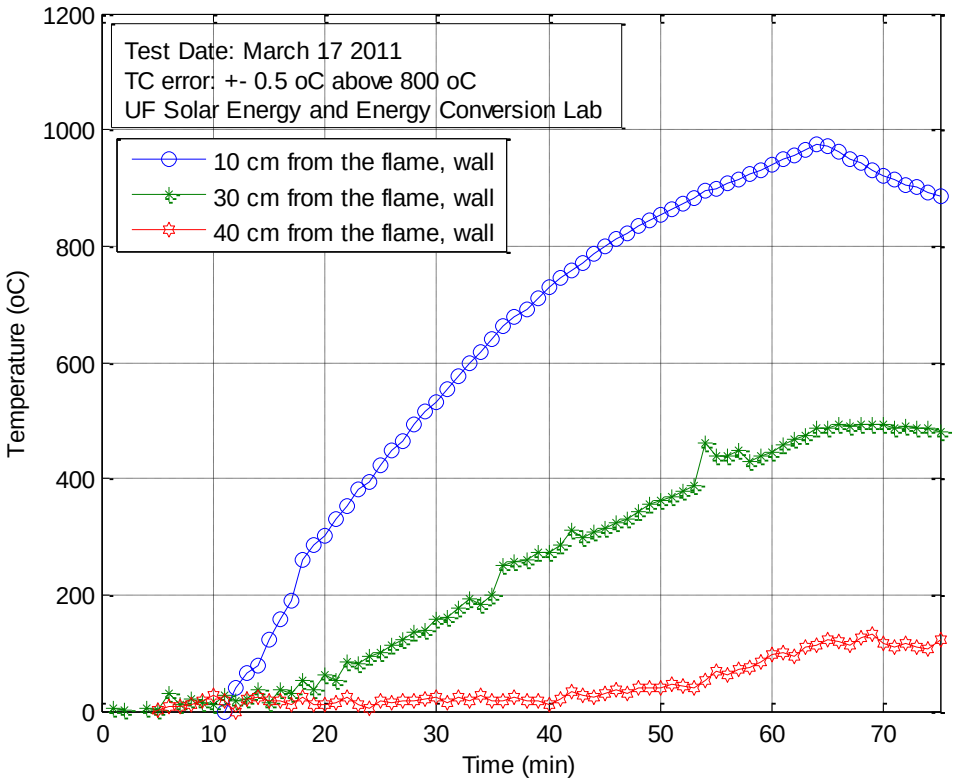

Figure 4-33. Gasification reactor inner wall temperature versus time for the Test 5 with H_2:O_2 = 32:13 LPM (2.6:1). Ignition occurred at time = 0 minute, 1st biomass input of 28 g (1 oz) at t = 36 minutes, 2nd biomass input of 28 g (1 oz) at t=52.5 minutes, hydrogen and oxygen input were stopped and carbon dioxide input was started at t=64 minutes.

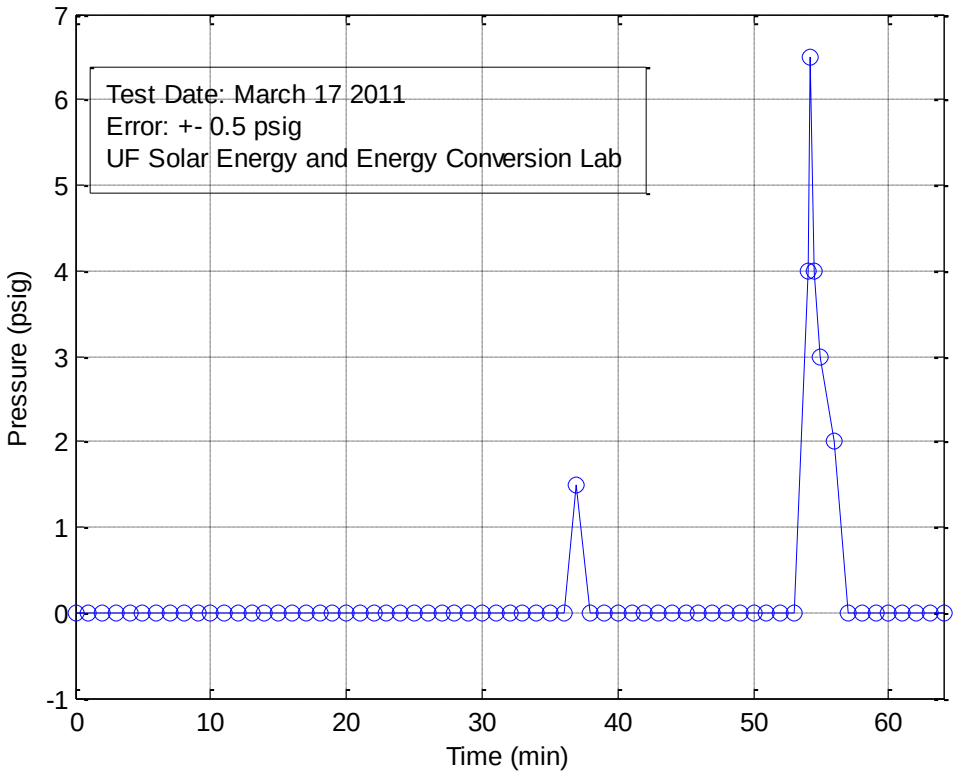

Figure 4-34. Gasification reactor pressure versus time for the Test 5 with H_2:O_2 = 32:13 LPM (2.6:1). Ignition occurred at time = 0 minute, 1st biomass input of 28 g (1 oz) at t = 36 minutes, 2nd biomass input of 28 g (1 oz) at t=52.5 minutes, hydrogen and oxygen input were stopped and carbon dioxide input was started at t=64 minutes.

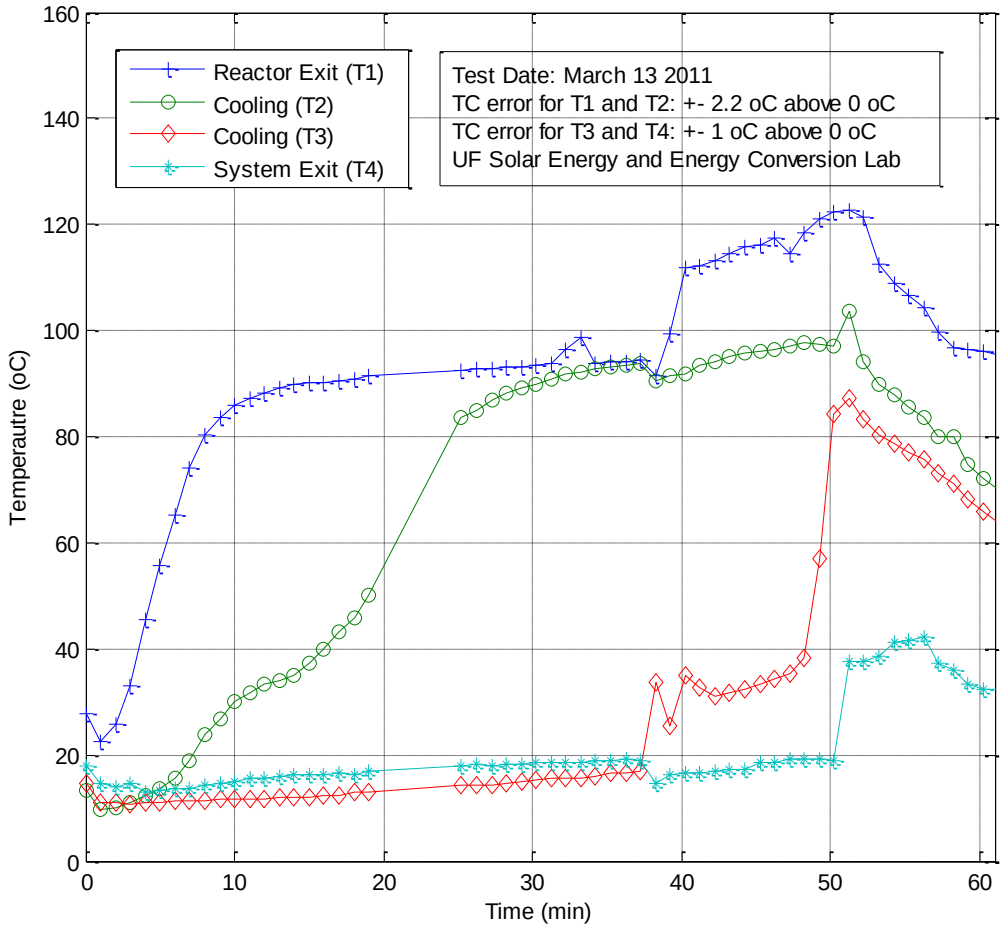

Figure 4-35. Exit gas temperatures versus time for the Test 4 with H_2:O_2 = 32:13 LPM (2.6:1). Ignition occurred at time = 0 minute, biomass input of 57 g (2 oz) at t = 37 minutes, and the system was shut off at t = 52 minutes.

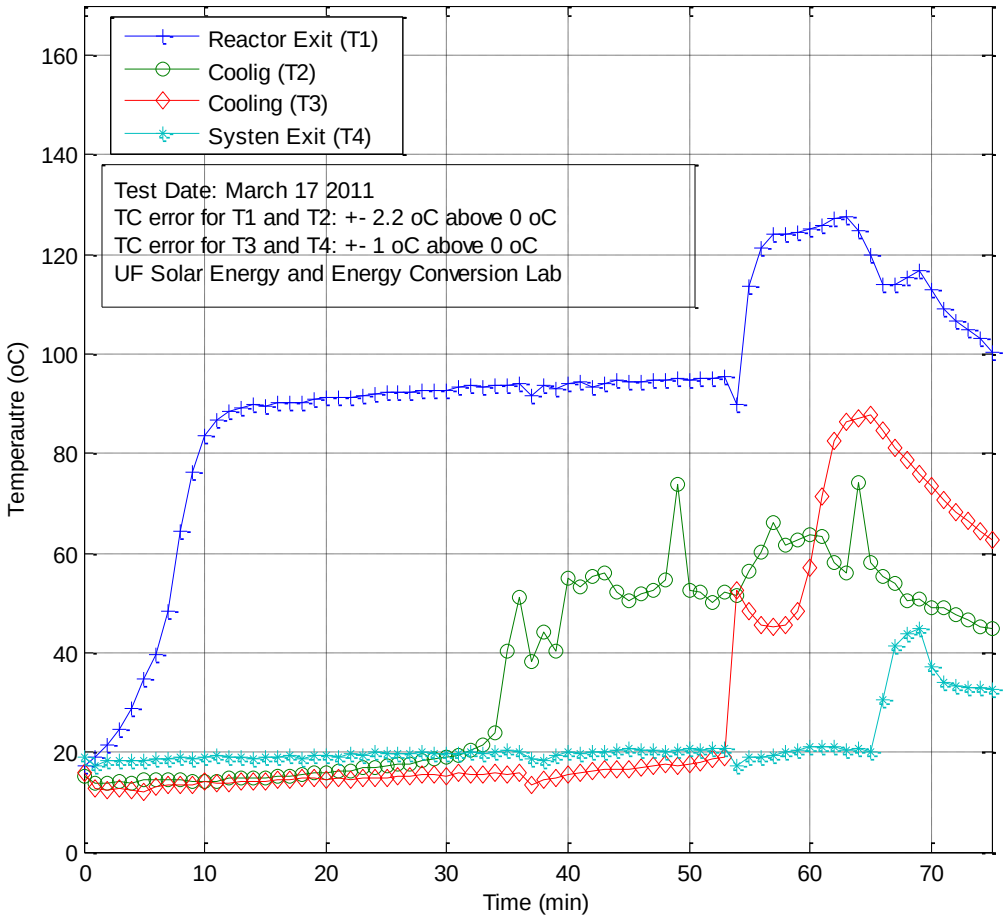

Figure 4-36. Exit gas temperature versus time for the Test 5 with H_2:O_2 = 32:13 LPM (2.6:1). Ignition occurred at time = 0 minute, 1st biomass input of 28 g (1 oz) at t = 36 minutes, 2nd biomass input of 28 g (1 oz) at t=52.5 minutes, hydrogen and oxygen input were stopped and carbon dioxide input was started at t=64 minutes.

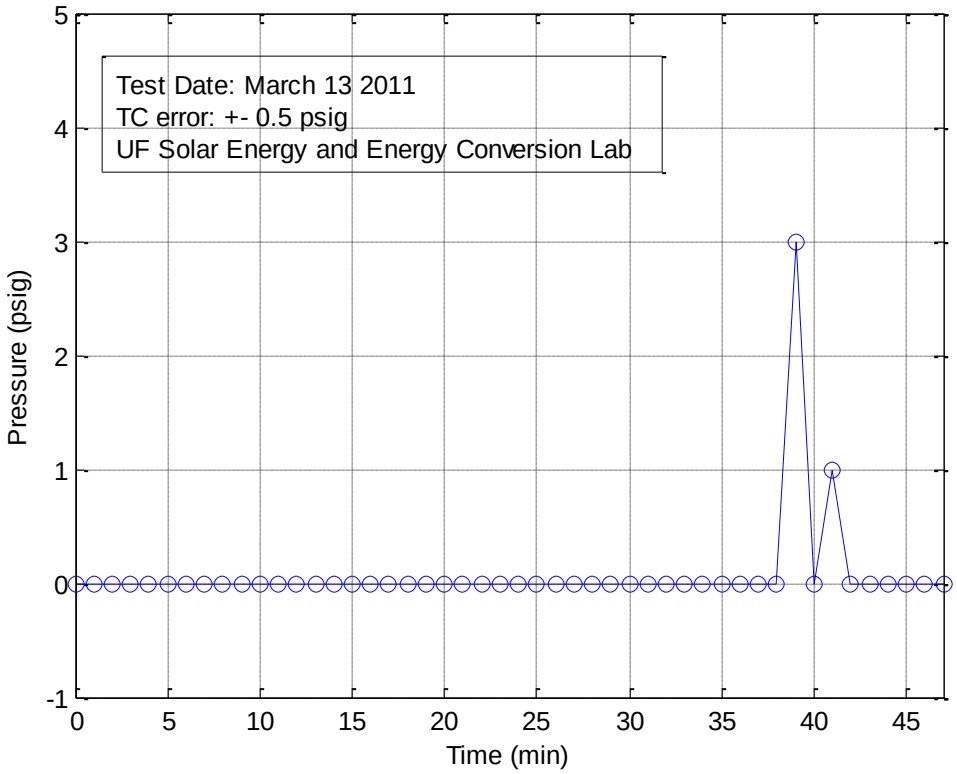

Figure 4-37. Exit pressure versus time for the Test 4 with H_2:O_2 = 32:13 LPM (2.6:1). Ignition occurred at time = 0 minute, biomass input of 57 g (2 oz) at t = 37 minutes, and the system was shut off at t = 52 minutes.

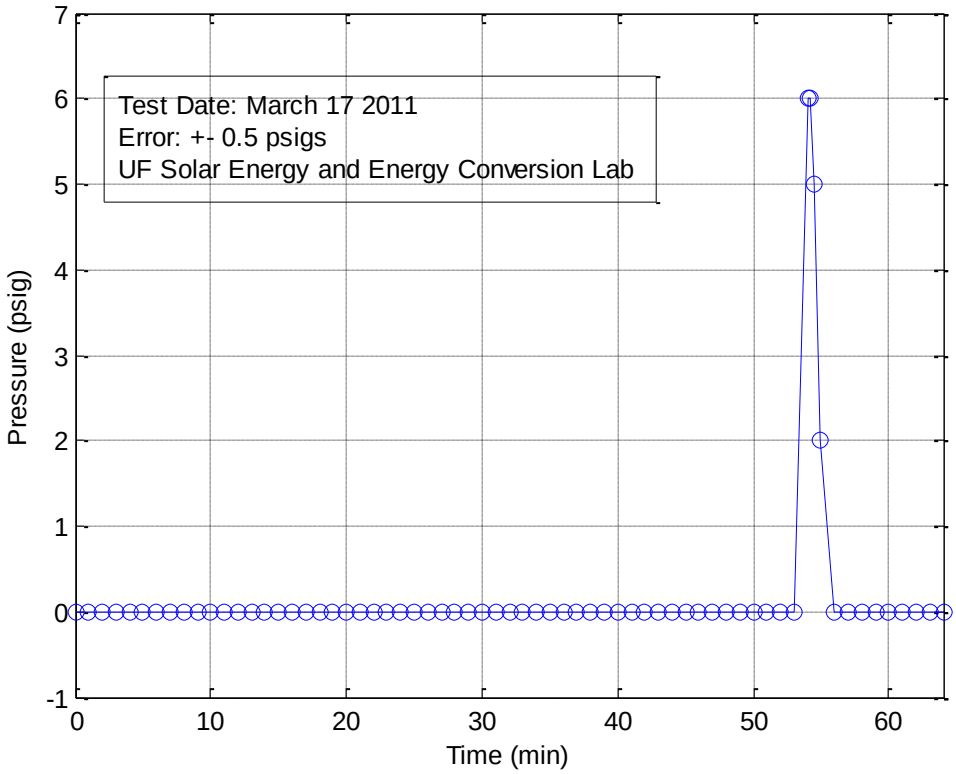

Figure 4-38. Exit gas pressure versus time for the Test 5 with H_2:O_2 = 32:13 LPM (2.6:1). Ignition occurred at time = 0 minute, 1st biomass input of 28 g (1 oz) at t = 36 minutes, 2nd biomass input of 28 g (1 oz) at t=52.5 minutes, hydrogen and oxygen input were stopped and carbon dioxide input was started at t=64 minutes.

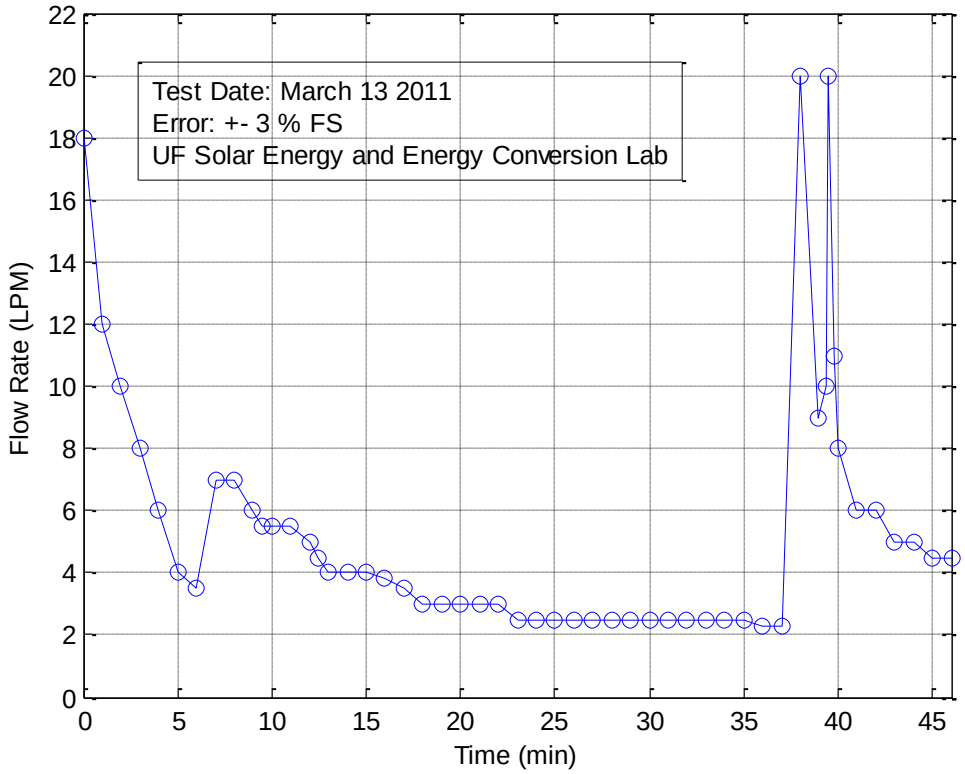

Figure 4-39. Volume flow rate of exit gas versus time for the Test 4 with H_2:O_2 = 32:13 LPM (2.6:1). Ignition occurred at time = 0 minute, biomass input of 57 g (2 oz) at t = 37 minutes, and the system was shut off at t = 52 minutes.

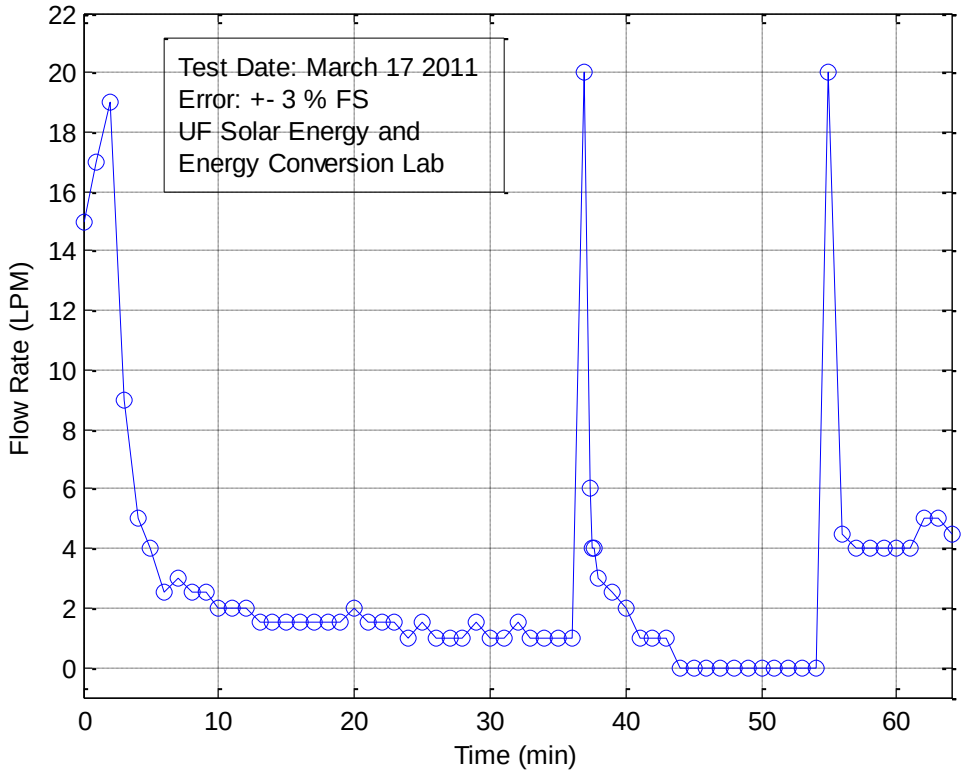

Figure 4-40. Volume flow rate of exit gas versus time for the Test 5 with H_2:O_2 = 32:13 LPM (2.6:1). Ignition occurred at time = 0 minute, 1st biomass input of 28 g (1 oz) at t = 36 minutes, 2nd biomass input of 28 g (1 oz) at t=52.5 minutes, hydrogen and oxygen input were stopped and carbon dioxide input was started at t=64 minutes.

Table 4-17. Summary of condensed water collected from test 4 and test 5, and the estimated water condensation if the introduced steam (from hydrogen and oxygen combustion) during the specified time was all condensed.

	Container	V_{H2O} (ml) collected from the container		Time (min)	V_{H2O} (ml) collected when the entire steam introduced to the system up to the specified time is condensed
13-Mar (test 1)	1st	600	Biomass introduction	37	710
	2nd	400	Gases turned off	52	997
	3rd	90			
	total	*1090*			
17-Mar (test 2)	1st	720	1st Biomass introduction	36	690
	2nd	350	2nd Biomass introduction	52.5	1007
	3rd	(-60)*	Gases turned off	64	1228
	total	*1070*			

*There was 600 ml of water in the 3rd container prior to the experiment, and 540 ml was found after the completion of the test.

Table 4-18. Summary of syngas compositions and corresponding system conditions in test 4 (March 13, 2011). The volume flow rates of syngas compositions are given in STP (273.15 K and 1 atm).

	H_2 (LPM)	CO (LPM)	CH_4 (LPM)	CO_2 (LPM)	Chamber T (^oC)	1st Module T (^oC)	Exit T (^oC)	Exit P (psig)	Exit Flow (LPM)
1st BM input (57 g)					1503	1014	19	0	2.3
1min	24.3	7.4	1.2	1.6	1396	955	15	0	20
2min	9.7	3.5	0.44	0.96	1461	1018	16	3	9
3min	7.4	2.9	0.41	0.69	1447	1031	16	0	8
4min	6.0	1.7	0.19	0.52	1477	1073	16	1	6
5min	6.4	1.4	0.13	0.51	1495	1090	17	0	6
6min	2.8	0.9	0.067	0.34	1506	1112	17	0	5
10min	4.6	0.6	0.026	0.28	1536	1155	19	0	4.5

Table 4-19. Summary of syngas compositions and corresponding system conditions in test 5 (March 17, 2011). The volume flow rates of syngas compositions are given in STP (273.15 K and 1 atm).

	H_2 (LPM)	CO (LPM)	CH_4 (LPM)	CO_2 (LPM)	Chamber T (^oC)	1st Module T (^oC)	Reactor P (psig)	Exit T (^oC)	Exit P (psig)	Exit Flow (LPM)
1st BM input (28g)					1467	1032	0	20	0	20
30sec after 1st BM input	4.3	1.5	0.24	0.31	1412	1005	2	20	0	4
1min	2.0	0.82	0.11	0.20	1421	1014	0	19	0	3
2min	1.6	0.48	0.049	0.14	1440	1043	0	18	0	2
3min	-0.021	0.15	0.010	0.058	1454	1059	0	20	0	1
5min	0.051	0.092	0.004	0.052	1455	1062	0	20	0	1
12min	-2.0	0.0	0.0	0.0	1522	1150	0	20	0	0
2nd BM input (28g)					1407	1082	4	21	6	20
30sec after 2nd BM input	27.4	9.7	2.1	1.4	1537	1171	4	21	5	20
1min	32.6	6.5	0.81	1.7	1424	1096	3	21	2	20
2min	6.3	1.1	0.083	0.36	1502	1142	0	18	0	5
3min	8.0	0.75	0.044	0.33	1525	1161	0	19	0	4
10min	7.1	0.38	0.012	0.22	1571	1216	0	21	0	4

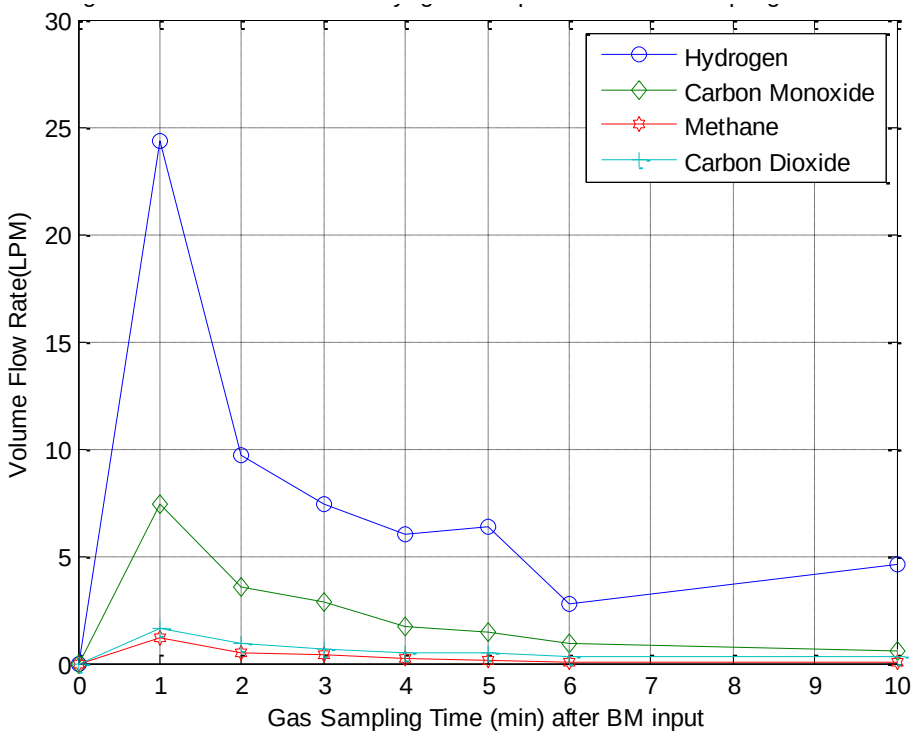

Figure 4-41. Volume flow rate of production in syngas composition (LPM, STP) versus time for the Test 4 (March 13, 2011) with H_2:O_2 = 32:13 LPM (2.6:1).

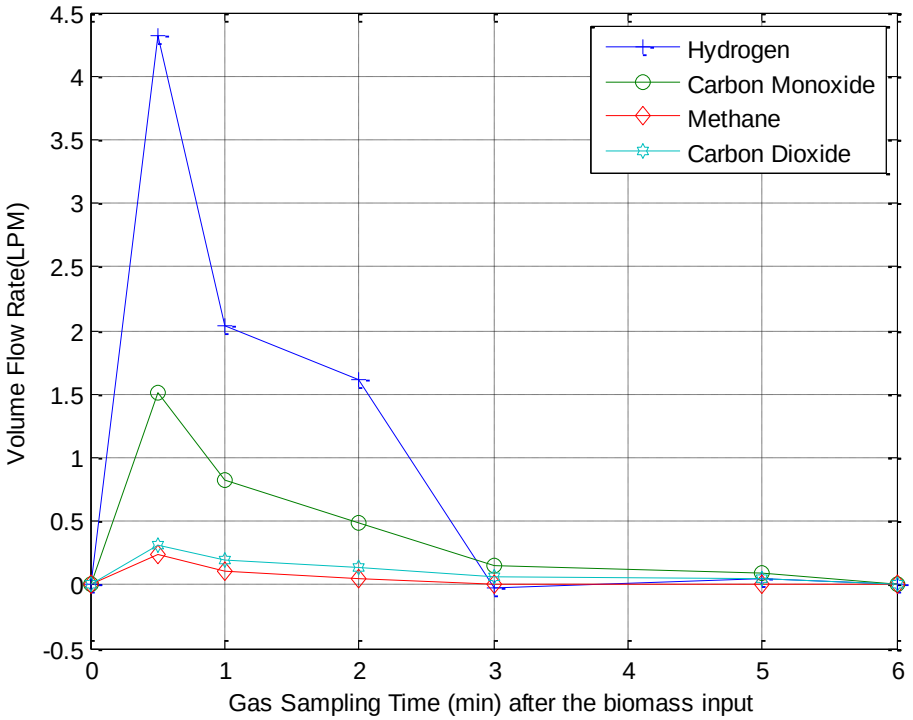

Figure 4-42. Volume flow rate of production in syngas composition (LPM, STP) versus time for the Test 5, first biomass introduction case (March 17, 2011) with H_2:O_2 = 32:13 LPM (2.6:1). 1st biomass input of 28 g (1 oz).

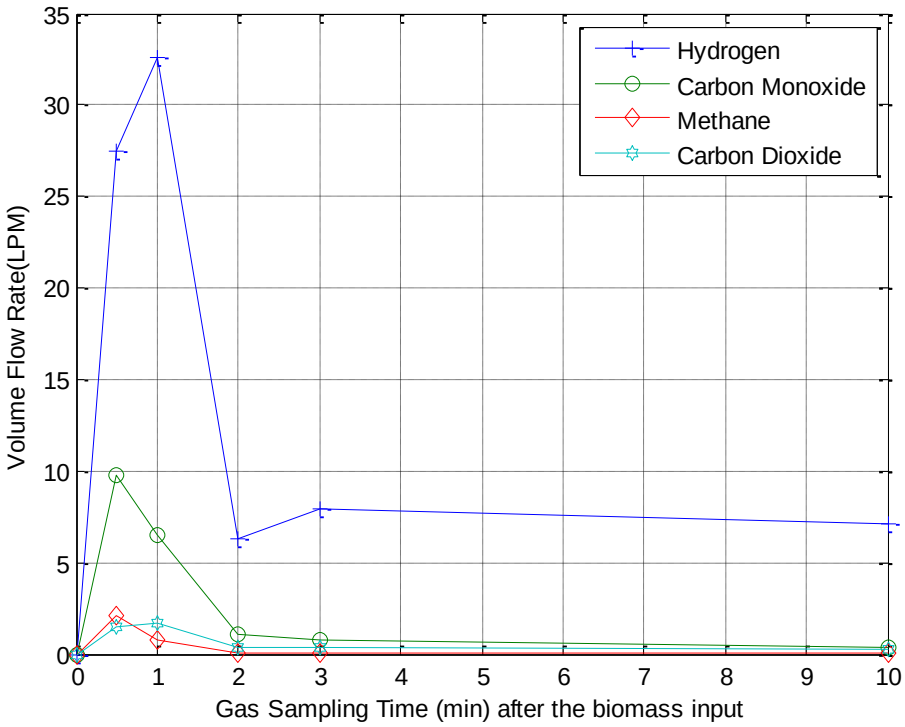

Figure 4-43. Volume flow rate of production in syngas composition (LPM, STP) versus time for the Test 5, second biomass introduction case (March 17, 2011) with H_2:O_2 = 32:13 LPM (2.6:1). 2nd biomass input of 28 g (1 oz).

Table 4-20. Summary of syngas component production from test 4, test 5 and analytical simulations based on gasification temperature of 600, 1000 and 1500°C.

			H_2 (kmol)	CO (kmol)	CO_2 (kmol)	CH_4 (kmol)	Biomass	STB
Test 4 (March 13)	Experimental		2.74E-03	7.30E-04	8.65E-05	2.18E-04	56g (2.33E-03 kmol)	6.07
	Analytical	600°C	4.62E-03	2.26E-04	2.10E-03	5.13E-06		
		1000°C	4.18E-03	6.89E-04	1.64E-03	6.35E-10		
		1500°C	3.81E-03	1.06E-03	1.27E-03	1.69E-12		
Test 5 (March 17)	Experimental (average of 1st + 2nd biomass introductions)		2.20E-03	3.46E-04	4.78E-05	9.73E-05	28g (1.16E-03 kmol)	12.57
	Analytical	600°C	2.37E-03	5.44E-05	1.11E-03	1.69E-07		
		1000°C	2.23E-03	1.96E-04	9.64E-04	2.84E-11		
		1500°C	2.08E-03	3.44E-04	8.16E-04	9.37E-14		

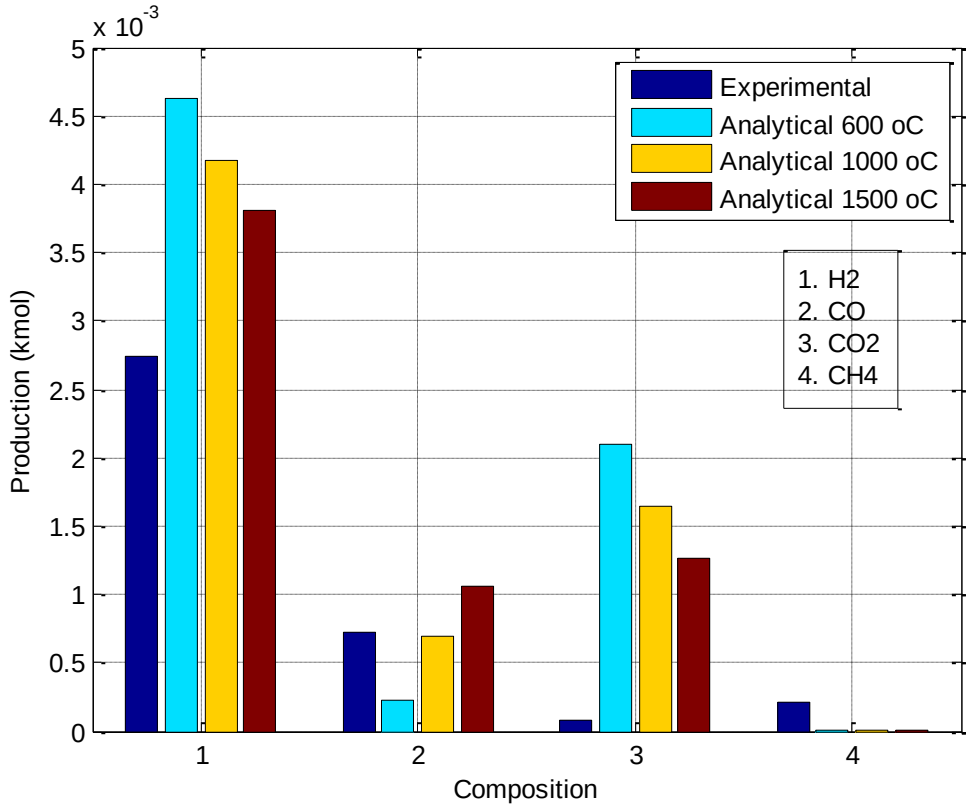

Figure 4-44. Syngas component production in test 4 (March 13, 2011) and analytical simulations based on the gasification temperature of 600, 1000 and 1500^{o}C.

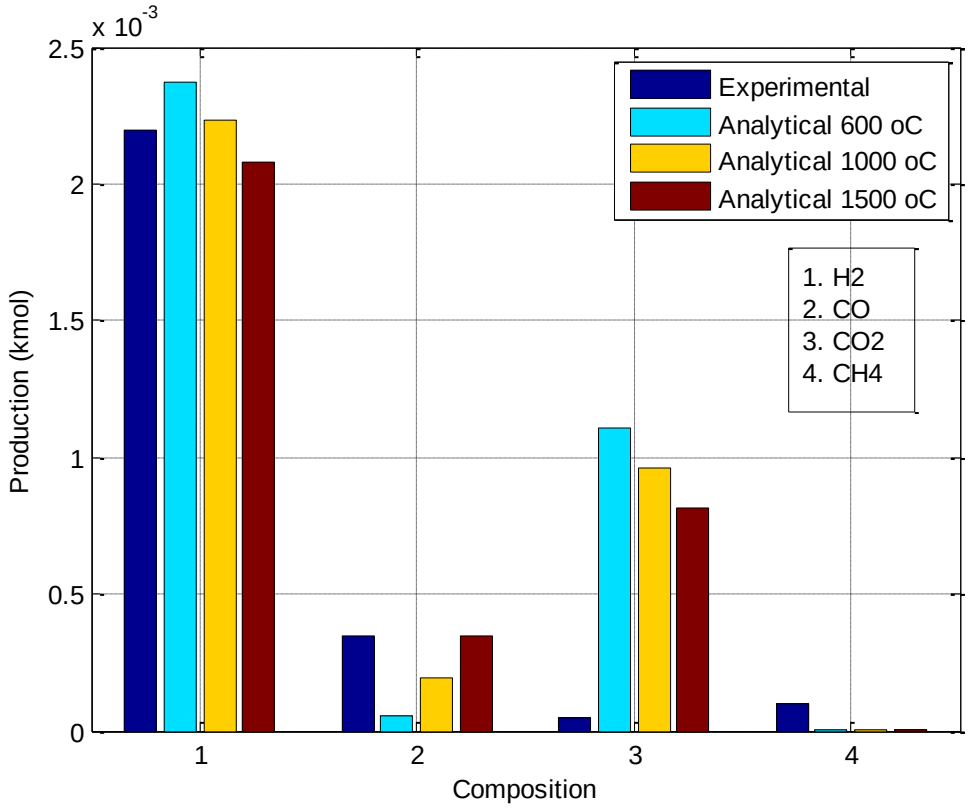

Figure 4-45. Syngas component production in test 5 (average between the 1st and the 2nd biomass introductions) (March 17, 2011) and analytical simulations based on the gasification temperature of 600, 1000 and 1500°C.

Table 4-21. Summary of overall system inputs (hydrogen, oxygen and biomass) and ouput (syngas) during the gasification period in test 4 and test 5.

	Gasification Time (min.)	H_2 consumed (kg)	O_2 consumed (kg)	Biomass (g)	Syngas (m^3)
Test 4	10	0.026	0.26	57	0.089
Test 5 ave.	11	0.029	0.32	28	0.060

Note: All units are given at STP

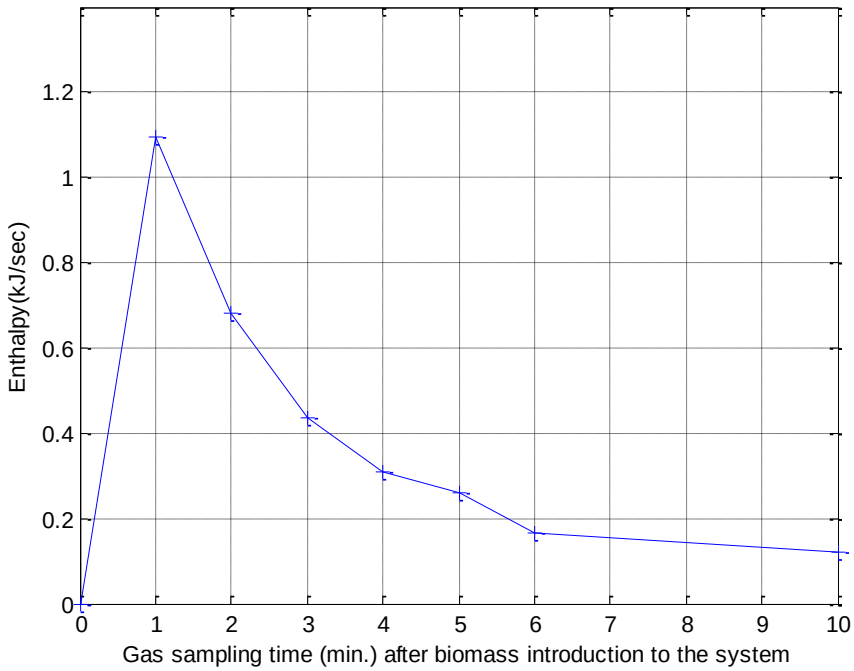

Figure 4-46. Time rate of enthalpy of exit gas versus time for the Test 4 (March 13, 2011) with H_2:O_2 = 32:13 LPM (2.6:1). Ignition occurred at time = 0 minute, biomass input of 57 g (2 oz) at t = 37 minutes, and the system was shut off at t = 52 minutes.

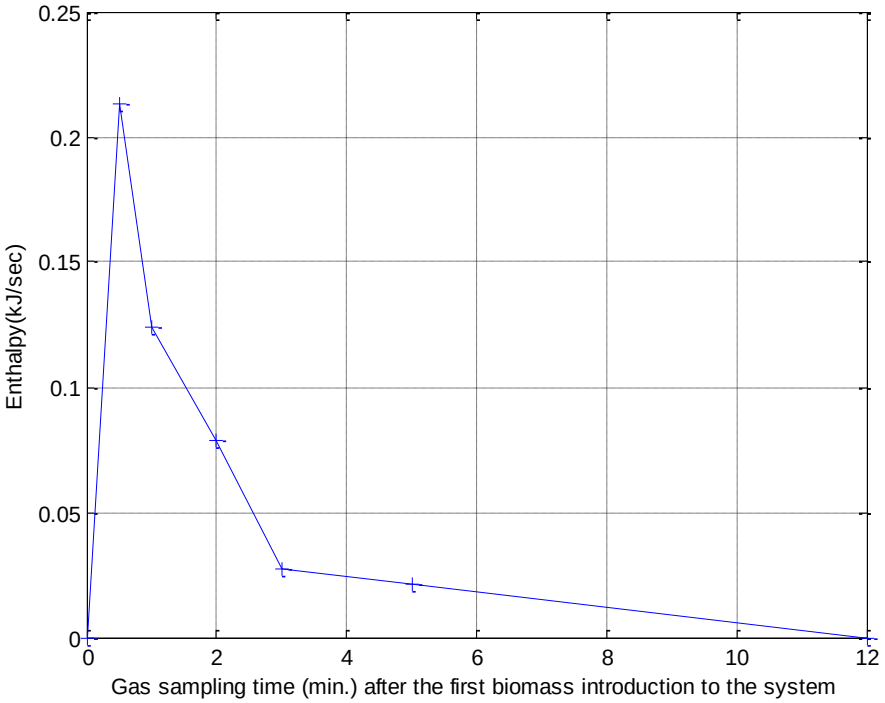

Figure 4-47. Time rate of enthalpy of syngas composition (LPM, STP) versus time for the Test 5, first biomass introduction (March 17, 2011) with H_2:O_2 = 32:13 LPM (2.6:1). First biomass input of 28 g (1 oz).

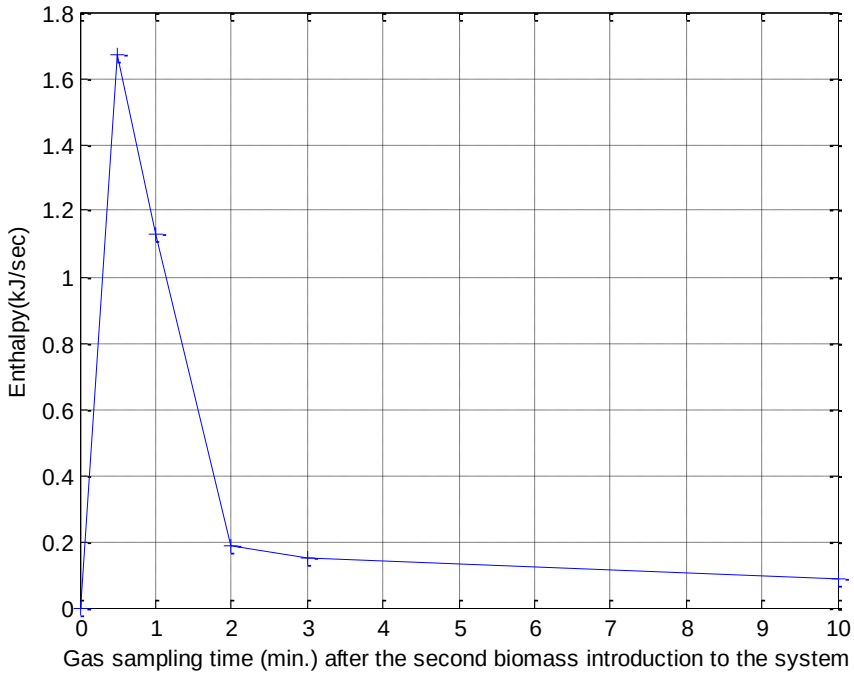

Figure 4-48. Time rate of enthalpy of syngas composition (LPM, STP) versus time for the Test 5, second biomass introduction (March 17, 2011) with H_2:O_2 = 32:13 LPM (2.6:1). Second biomass input of 28 g (1 oz).

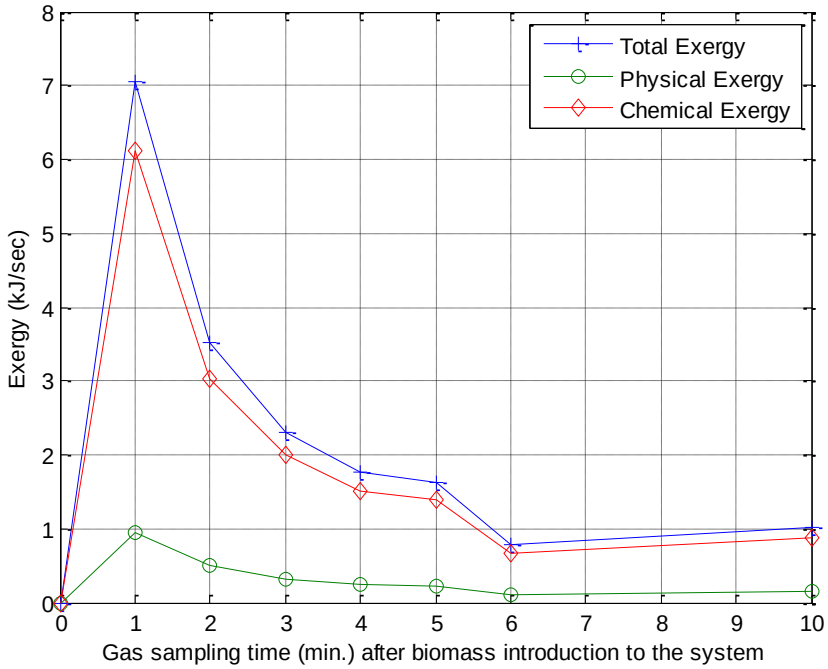

Figure 4-49. Time rate of exergy (total exergy, physical exergy and chemical exergy) of syngas versus time for the Test 4 (March 13, 2011) with H_2:O_2 = 32:13 LPM (2.6:1). Ignition occurred at time = 0 minute, biomass input of 57 g (2 oz) at t = 37 minutes, and the system was shut off at t = 52 minutes.

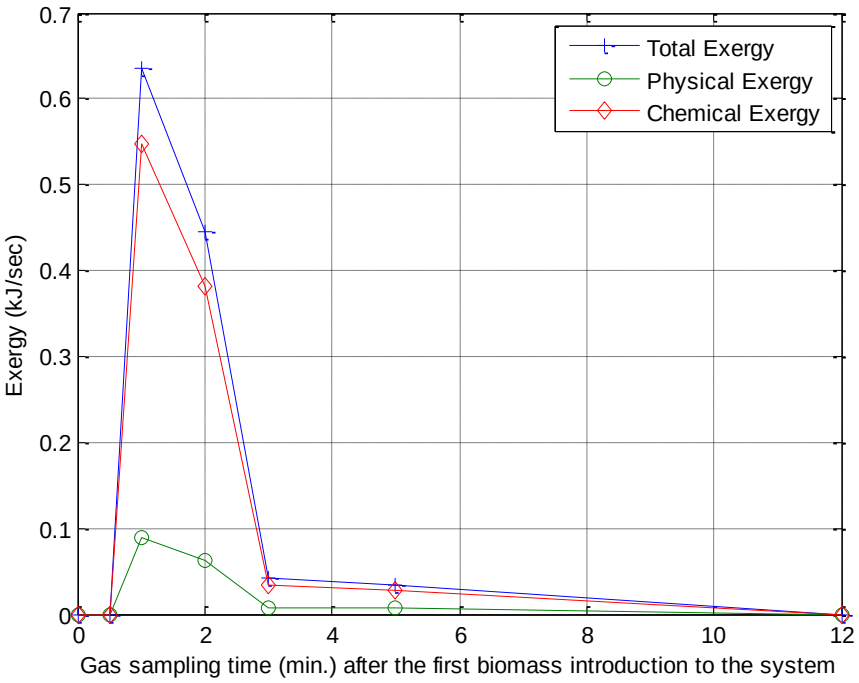

Figure 4-50. Time rate of exergy (total exergy, physical exergy and chemical exergy) of syngas versus time for the Test 5, first biomass introduction (March 17, 2011) with H_2:O_2 = 32:13 LPM (2.6:1). First biomass input of 28 g (1 oz).

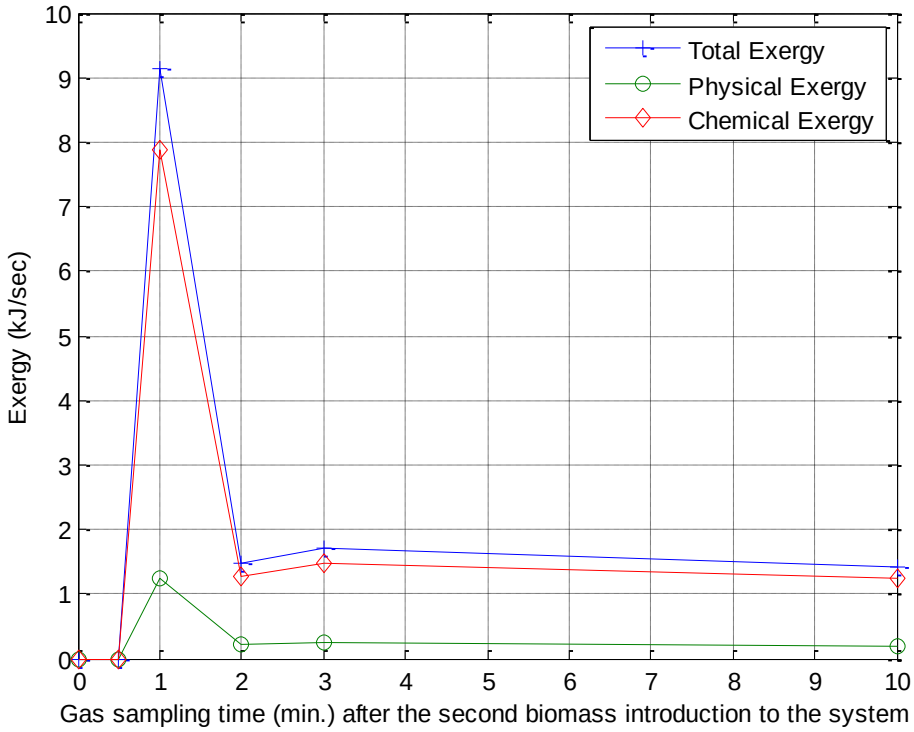

Figure 4-51. Time rate of exergy (total exergy, physical exergy and chemical exergy) of syngas versus time for the Test 5, second biomass introduction (March 17, 2011) with H_2:O_2 = 32:13 LPM (2.6:1). Second biomass input of 28 g (1 oz).

Table 4-22. Summary of inlet hydrogen and oxygen flow rates in test 4 and test 5 (March 13 and 17, 2011) and corresponding inlet energy and exergy values.

	H_2 input (LPM)*	O_2 input (LPM)*	Gasification Time (min.)	H_2 consumed (kg)**	O_2 consumed (kg)**	$\dot{H}$ (kJ/sec)[a]	$\dot{E}x$ (kJ/sec)[a]	H (kJ)[a]	Ex (kJ)[a]
Test 4	32	13	10	0.026	0.26	3.69	2.75	2212.92	1652.34
Test 5 ave.	32	13	11	0.029	0.32	3.65	2.73	2409.00	1801.80

* Volume flow rates given at STP

** Mass given at STP

[a] Calculated from the reference state:

Table 4-23. Summary of biomass energy and exergy input in test 4 and test 5 (March 13 and 17, 2011).

	Biomass (g)	H (kJ)[a]	Ex (kJ)[a]
Test 4	57	318.12	1197.34
Test 5 ave.	28	159.06	598.67

[a] Calculated from the reference state:

Table 4-24. Summary of energy and exergy values for the experimental (test 4 and test 5) and analytical syngas produced during the entire gasification period.

	Experimental		Analytical					
			600°C**		1000°C**		1500°C**	
	H (kJ)	Ex (kJ)	H (kJ)	Ex (kJ)	H (kJ)	Ex (kJ)	H (kJ)	Ex (kJ)
Test 4	214.78	1226.52	852.88	1464.00	723.63	1459.70	618.03	1452.30
Test 5, ave.	114.39	760.94	441.61	733.00	401.65	729.86	359.77	726.69

*The first and second biomass intorduction cases were added to simulate the overall results in test 5.

**Enthalpy and exergy were computed based on the analytical syngas production based on the gasification temperature listed.

Table 4-25. Summary of energy and exergy efficiencies for experimental and analytical biomass gasification process.

	Experimental		Analytical					
			600°C**		1000°C**		1500°C**	
	η_{Th}	η_{Ex}	η_{Th}	η_{Ex}	η_{Th}	η_{Ex}	η_{Th}	η_{Ex}
Test 4	0.08	0.43	0.34	0.51	0.29	0.51	0.24	0.51
Test 5, overall*	0.04	0.32	0.17	0.31	0.16	0.30	0.14	0.30

*The first and second biomass intorduction cases were added to simulate the overall results in test 5.

**Enthalpy and exergy were computed based on the analytical syngas production based on the gasification temperature listed.

Table 4-26. The ratio of hydrogen production to the hydrogen consumption in the experimental gasification system (test 4 and test 5, March 13 and 17, 2011).

		Steam	*Biomass*	*Syngas*	
	Gasification Time (min.)	H_2 consumed (g)**	H_2 consumed (g)**	H_2 produced (g)**	H2 out/in
Test 4	10	26.02	3.55	5.5	0.19
Test 5 ave.	10	26.02	1.77	4.4	0.16

** Mass given at STP

CHAPTER 5
CONCLUSIONS AND RECOMMENDATIONS

The first goal of this research was to design and build a high-temperature biomass gasification system to demonstrate high-temperature steam gasification. Next, the production of synthesis gas was attempted using this gasification system, where this syngas could serve as a feedstock for FTS for biodiesel production. The last objective was to investigate the biomass gasification process at the system level thermal efficiency. The conclusions from each of these goals are presented. Finally, future improvements of the experimental facility are suggested.

5.1 Conclusions

The following conclusions were made from this study:

1. In this study, a bench-scale high-temperature steam biomass gasification system was designed and constructed. High-temperature steam gasification was demonstrated. Although temperatures as high as 1650^{o}C were obtained in the gasifier there was not precise method to determine the actual temperature of gasification. As indicated earlier there was a significant temperature profile in the gasification reactor.
2. Using the bench-scale gasification system, synthesis gas was produced using woody biomass as a feedstock. It was determined that the syngas produced during the experiments contained approximately 3 to 6 times more moles of hydrogen than carbon dioxide. Since the molar ratio of hydrogen to carbon monoxide generally required for FTS is approximately 2:1, this syngas could meet the hydrogen/carbon monoxide ratio requirement of the FTS. However with the existing feeding and gas cleaning systems, the stable production of a high quality gas could not be achieved. An analytical model of the gasification reaction was also constructed for this study. This model was used first to predict the behavior of the gasification reactions and second to compare the

model's results with the experimental results. Based on the syngas production comparison between the experimental and analytical cases, it was found that the experimental syngas had almost comparative hydrogen and carbon monoxide production as analytical syngas. The carbon dioxide content of experimental syngas was only 1/10 of analytical syngas, and the methane content of experiental syngas was significantly larger than the analytical syngas.

3. The energy and exergy analysis were conducted to evaluate the system level thermal efficiency. It was found the thermal efficiencies of the system were very low for the experimental cases, while the exergetic efficiencies in experimental cases are comparable to those in analytical cases. The reasons of low thermal efficiency in experimental syngas include not achieving steady state in the experiment, a batch treatment analysis, heat and mass balance requirements for the input steam, the state of syngas considered for the analysis (at the lowest temperature in the system) and the nature of syngas components and their heating value in high-temperature gasification.

5.2 Recommendations

With regards to the experimental facility, there are several improvements that could be made. Recommendations and discussions to address these issues are presented here.

1. Overall DAQ system – Before proceeding with any more experiments using the system, it is strongly recommended to investigate the cause of sensor failure and to replace them with properly working sensors once the cause is determined.
2. Pressure Transducers – The pressure transducers at the gasification reactor and the reactor exit need to be repaired or replaced since these sensors also failed to operate properly. The cause of failure needs to be determined before they are replaced and modifications made as necessary to prevent future failure. The Bourdon pressure

gauges at the system exit should be replaced with a pressure transducer. The transducer makes it possible to read a very small pressure such as less than 1 psig and to record the corresponding data with the DAQ system. The exit pressure data are necessary information to compute the gas flow rates and syngas composition, thus the risk of missing these data due to human error should be minimized.

3. Flow reading and control – There are a total of four rotameters used in this system. Three at the inlet to measure and control the amount of hydrogen, oxygen and carbon dioxide input to the system, and the other is at the system exit to measure the syngas volume flow rate. It is recommended that these rotameters to be replaced by calibrated flow controllers. One obvious advantage of flow controllers is to make the flow control automatic. The second advantage of flow controllers is that the data recording will be automatic and will maintain readings throughout the experiment. It was repeatedly experienced in this study that to accurately determine the syngas production analysis (thus the rest of the thermal analysis) became impossible due to the failure and/or improper reading of the exit gas flow. By using automatic flow reading and recording, this issue will be resolved.
4. Labview GUI – Together with the replacement of pressure transducers and flow meters, the development of a Labview graphical user interface (GUI) is also recommended to unify the control of all sensors in the system. With this GUI, it will be possible for one person to monitor and control the system. The other advantage of GUI is the ease of data processing. By concentrating and managing all data at once, it will be easier to organize and process the data after the experiment is completed. However it is

recommended that some manual recording be continued to provide a back-up to the data acquisition.

5. Ignition Confirmation – It is suggested to develop a better way to confirm ignition, such as an optical system or more responsive thermocouple in the combustion chamber.
6. Torch – It is recommended that the material used to construct the torch be reconsidered. The main body of the torch was made with high-density alumina. It was observed that the torch cracked many times during experimental runs and several repairs were required. Since there was no replacement torch, damage to the torch often delayed the experiment. Tungsten is recommended as an alternative material choice for the torch since this metal has very high melting point (3695 K) and small thermal expansion (173 W/m-K at 300 K). However, tungsten is also a very hard metal and machining to the shape of the torch may be extremely difficult. A material investigation needs to be conducted before selecting an alternative material for the torch.
7. Grate – First of all, it is strongly recommended that the ignition timing be controlled and monitored carefully before considering a change in the grate material because a detonation due to a failure of ignition could damage the grate no matter what material was used to construct it. Once the ignition issue is addressed, there is a need to investigate the effect of the grate on the temperature distribution in the reactor. If the current grate design inhibits heat transfer from the flame to the upper portion of the reactor, an alternate material selection or design of the grate should be considered. A possible replacement material is tungsten because of the thermophysical properties of the metal mentioned in the previous recommendation.

8. Alternative oxidizers – It is recommended to investigate alternative oxidizers such as ozone in lieu of oxygen to reduce the future cost of operation.
9. Biomass Feeding System – It was observed that the wood sawdust was not fed smoothly to the reactor even with external vibration. The issues associated with this are the uncertainties in the rate of feedstock introduction to the gasifier. Incorrect feeding times and amounts created errors in calculating production.
10. Continuous biomass feeding –In this study, there was a constant steam flow into the system while the biomass was only fed in a batch mode. Because of this condition, the system did not have an opportunity to reach steady state, which made the gas composition analysis complicated. Therefore, the development of a continuous biomass feeding system is recommended to better analyze the behavior of steady state gas production. A new feeding system would include a gas-tight bin to store the feedstock and an auger system to introduce the feedstock into the gasifier. The auger would be driven by a magnetic coupling system with a DC motor or directly driven with the auger shaft penetrating the feed system through a gas-tight bearing or seal.
11. Reactor Heating – It is suggested to determine a more efficient method of bringing the reactor up to operating temperature rather than relying on hydrogen combustion to provide the entire heat. It is more rational to look for a method of heating the system without consuming hydrogen; possibly using electric heat strips.
12. Gas Cleaning – The gas cleaning system needs to be redesigned now that we have seen the present system in operation. During the experimental runs with woody biomass as the feedstock, there was some tar production and at times this tar would exit the gas cleaning apparatus and contaminate the rotameter. The present system uses filtering

materials and wet scrubbing technique to clean the gas. A more efficient dry filter before rotameter would improve the tar removal if tar is produced. Better control of the gasification temperature by decreasing the volume of the gasifier would result in higher gasification temperatures, thereby greatly decreasing the production of tar.

13. Condensed Water Analysis – The condensed water collected from the cooling and cleaning containers contained not only dissolved contaminants but also suspended solids. The solid and liquid components should be separated and both the solid and the liquid compositions should be analyzed.
14. Flame orientation – It is recommended to investigate the effect of the flame orientation on the heating rate and the temperature distribution in the gasification reactor. There is a concern that with the current flame orientation, the flame hits the combustion chamber wall then moves upward instead of directly moving upward. This could create a non-uniform temperature distribution in the reactor, which may affect the gasification temperature and product composition. It is also subjects the wall opposite the torch to extremely high temperatures which result in physical damage to the combustion chamber.
15. Sustainable Biomass – It is recommended to investigate the quantity of (woody) biomass in Florida which can be sustainably consumed for the energy production. There is speculation that an eight year rotation of pine tree production could be sustained without adverse affect on the environment.
16. Transient Model – A development of a transient analytical model is recommended to better compare the current experimental system.

17. Future Studies – It is recommended to conduct more gasification tests with woody biomass as well as other fuel sources including MSW, MSW/rubber tires and other wastes such as horse bedding and so on.

APPENDIX A
OVERVIEW OF FISCHER TROPSCH SYNTHESIS

Fischer Tropsch Synthesis

Fischer-Tropsch synthesis (FTS) is a conversion method of syngas to various long-chain hydrocarbon liquid fuels such as gasoline, diesel, wax and alcohols like ethanol [11], [4], [83]. The FTS is generally carried out at temperatures from 180 to 250^{o}C [11], [4], [5] and pressure from 0.1 to 4 MPa [4]. Since the number of mole decreased during the FT reaction, conversions increase rapidly with pressure increases with temperature being fixed [4]. FTS is an exothermic reaction and is catalyzed on metal catalysts, which split the carbon-oxygen bond of carbon monoxide to help the initiation and growth reactions of carbon chains [11], [4]. The basic conversion structure is the stepwise chain growth in polymerization of -CH_2- groups on the catalyst surface [4]. The basic polymerization reactions of the FTS are the followings [84]:

1. Reactant adsorption
2. Chain initiation
3. Chain growth
4. Chain termination
5. Product desorption
6. Readsorption and further reaction

There are a large number of reactions occur in the FTS and some of the major reactions are given in the followings [4]:

Paraffins $(2n + 1)H_2 + nCO \rightarrow C_nH_{2n+2} + nH_2O$

Olefins $2nH_2 + nCO \rightarrow C_nH_{2n} + nH_2O$

Alcohols $2nH_2 + nCO \rightarrow C_nH_{2n+1}OH + (n - 1)H_2O$

Water gas shift $CO + H_2O \rightarrow CO_2 + H_2$

Boudouard reaction $2CO \rightarrow C + CO_2$

Coke deposition $H_2 + CO \rightarrow C + H_2O$

With alkalized iron as a catalyst, the reactions of paraffins, olefins and alcohols productions are promoted. Consequently, the ratio of H_2/CO is adjusted. The selectivity control of the desired carbon number is one of the most important concerns. The FT off-gas can either be recycled back to dry the biomass, feed the gasifier and/or feed the reformer, or combusted to run turbine to produce electricity [43].

Fischer-Tropsch reactor types

There are three main kinds of FT reactors used in commercial applications today: the fluidized bed reactor, the fixed bed reactor and the slurry phase reactor [5]. All three reactors have been built with capacities of 2500 bbl/day or higher today [85]. A number of factors need to be taken into account for reactor selections such as optimum operation temperature and pressure, catalyst particle size, loading and unloading of catalyst, need of gas-solid or liquid-solid separation, distribution of reactants over the reactor, catalyst settling or agglomeration issue, and scaling-up aspects [85]. There are two types of FT operation modes depending on the process temperature. One is high-temperature (300-350^{o}C) process using iron-based catalysts. This mode is used for the production of gasoline and linear low molecular mass olefins [86]. The other mode is low-temperature (200-240^{o}C) process using either iron or cobalt catalysts. The aimed product with low-temperature process are high molecular mass linear waxes [86].

The gas-solid fixed fluidized bed (FFB) reactor is used in Sasol, a coal based FT plant in Sasolburg, South Africa [86]. This reactor was operated at about 2MPa and 340^{o}C, and used for light olefin C_2, C_7 productions [4], [85], [86]. Sasol originally used circulating fluidized bed

reactor, but later on various advantages were discovered on fixed fluidized bed reactor, and thus FFB reactors named Sasol Advanced Synthol (SAS) are used today [86]. One advantage of the gas-solid fluidized bed reactor is its excellent heat transfer characteristics, which can sustain the fairly uniform temperature through the reactor. This characteristic is suitable in dealing with highly exothermic FT reaction. The other advantage is the fluidized bed reactor is free from diffusion limitation. There are some limitations in fixed bed reactors that place some restrictions of the particle size of catalyst to be used [85]. A major issue in the fluidized bed reactor is the product deposition and agglomeration on the catalyst, which interrupt fluidization activity [85]. In FTS, the Anderson-Schulz-Flory (ASF) distribution describes the relation between the hydrocarbon yield and the chain growth probability [5], [85]. According to ASF, the molar yield in carbon number is expressed as $C_n = alpha^{n-1}(1-alpha)$, where alpha is chain growth probability, n is the length of the hydrocarbon, and 1-alpha indicates the probability of chain growth terminations [5]. The condition requirement of alpha less than 0.71 in the gas-solid fluidized bed reactor means that this reactor cannot be used for production of liquid fuels heavier than gasoline [85] such as diesel.

The multi-tubular fixed bed reactor is used in Shell at Bintuli, Sarawak, Malaysia. This FT reactor is built in 1989 for commercial Shell Middle Distillate Synthesis (SMDS) with the main objective of conversion of natural gas/methan to liquid transportation fuel [4]. This type of reactor is constructed with a chamber with divided sections by vertical metal sheets and horizontal cooling tubes crossing the sheets [4]. Catalysts are located between sheets and tubes. The fixed bed reactor is generally operated at low temperature of 200 to 240^{o}C and produces paraffins and high molecular weight products [4], thus suitable for heavy liquids production such as diesel. Some of the important design parameters in the fixed bed reactor are particle size and

shape, pressure drop and heat transfer effect. Because of pressure drop in the reactor, catalysts used in fixed bed process need to have a diameter size of 1mm or larger. For particles of this size, intraparticle diffusion can be a limiting factor for the overall reaction rate [85]. Intraparticle diffusion becomes important once particle diameter exceed about 0.5mm [85], thus this effect needs to be considered when catalyst particle size is selected. One of the disadvantages that fixed bed reactor holds is poor and uneven heat transfer characteristics in tube radial direction [85]. Because of high exothermicity in FTS, it is important to rapidly remove the heat of reaction from the catalyst particles in order to avoid decrease in catalyst activity and undesired reduction of selectivity [4], [85].

The slurry phase reactor or bubble column reactor is another type of FT reactor commercially used in both Exxon and Sasol. The slurry phase reactor also has a low operation temperature like a fixed bed reactor and is suited for the production of heavier products such as middle distillates, lube oils and waxes [85], [86]. There are several advantages of slurry bed reactor over multitubular fixed bed reactor such as lower reactor train cost (25% of fixed bed), lower pressure differential over the reactor (four times lower), four-fold lower catalyst consumption, isothermal characteristics in the reactor which results in higher conversion efficiency, and longer reactor runs [86]. One major disadvantage of the slurry phase reactor is that once any contaminants mingle in the reactor all of the catalysts are deactivated, while in a fixed bed reactor the top layer catalyst adsorb the poison [86].

Catalysts

There are four types of metals used as FT catalyst: Fe, Ni, Co and Ru. Among all metals, these four metals can convert CO/H2 mixture to aliphatic (long chain) hydrocarbons without intermediates being desorbed from the catalyst surface [87], [86]. However, because of

economic, physical and chemical constraints, only Fe and Co base catalysts are used in large scale commercial applications. Dry states that if the price of scrap iron is 1.0, the approximate cost of Ni is 250, of Co is 1000 and of Ru is 50,000 [86]. While being 2nd most economical, Ni catalyst posses some disadvantages such that it tends to form nickel carbonyl at elevated pressure and shifts the selectivity to mainly methane at increased reaction temperature [87]. Ru catalyst, on top of the large cost, is very limited in existing amount [87], [86], thus this is not a suitable candidate for the use in large commercial application. Away from the large-scale use, Ni and Ru catalysts can be used to produce high molecular weight hydrocarbons [87]. Another important factor of catalyst selection and design is the end product target of either being gasoline, diesel, waxes or chemicals (olefins, alcohols) [87].

There are two types of iron catalysts which are significance in commercial application. One is fused iron catalyst and the other is precipitated iron catalyst [86]. The fused iron catalyst is the least expensive FT catalyst available for large commercial application use. Fe is very flexible catalyst as it can be used in both high and low temperature FT reactions, and does not increase methane selectivity at even increased temperature (~340^{o}C) unlike Ni, Co and Ru catalysts [87]. With Fe catalyst, water gas shift reaction is promoted to adjust the H_2/CO ratio, which is particularly a favorable feature when the syngas is rich in CO [87] [48]. Generally, there are some alkali promotion of Fe catalyst in order to achieve high activity and selectivity; Cu for reduction promotion, SiO_2 and Al_2O_3 for structural promotion to enhance the surface area of the final catalyst [88] and Mn for selectivity promotion [87]. As a preparation of promoters, they are first added to a molen bath of magnetite. Next, the magnetite is cooled to form a solid, then the cooled magnetite is converted into a fine powder. Finally, these powder forms of promoters are

used in fluidized bed reactor [88]. The fused iron catalysts are the most desirable catalyst for the production of olefins in petrochemical industry [88].

The precipitated iron catalyst is the other type of iron catalyst. This catalyst is used when methane selectivity needs to be lower further that what is achieved using fused iron catalyst. To decrease the methane selectivity, both a lower temperature higher catalyst surface areas are required. For preparation of catalysts, iron metal is dissolved into an aqueous acidic solution and promoters such as alkali and copper are added. Then the catalyst is precipitated from the acidic solution by the addition of a basic solution. After that the precipitate is filtered, washed, dried and formed into the shape ready to be used in FT reactor [88].

The supported cobalt catalyst is the other common type of catalyst used in industrial application of FTS. Unlike Fe catalysts, Co catalyst is used only in low temperature FT reaction [86]. There is strong proportionality between catalytic activity and catalyst surface area, thus even considering of its high cost, it is particularly important in Co catalyst use to maximize the active surface area [86]. Co catalyst is typically supported by silica, alumina, titania or zinc oxide or combinations of these oxides [88]. For preparation of supports, spray drier is used to provide the desired particles sizes for used in a slurry phase reactor. Co catalyst is usually promoted with a small amount of noble metals such as Pt, Ru and Re to increase the reduction process [86]. Co is a preferred catalyst when diesel fuel is the target product. The diesel fuel selectivity of Co catalyst could reach 80% when FTS and hydrocracking process is combined.

Contaminants/Clean up

These metal catalysts are extremely sensitive to existence of sulfur in syngas [4]. Poisoning by sulfur compounds occurs mainly by adsorption of sulfur atoms on active metal sites, which destroy the catalytic activity [4].

FT selectivity

The product selectivity is influenced by the process conditions and the catalyst selection [48]. Some of the process conditions being important are temperature, partial pressures of hydrogen and carbon monoxide, catalyst promoters and time-on-stream.

When temperature increases, the selectivity shifts toward lower carbon number products and to more hydrogenated products. Increased temperature also results in increasing degree of branching and secondary products formation such as ketons and aromatics. These structural influences are logical in terms of thermodynamics that relative structural stability is seek at high temperature [86], [48].

In general, with increased total pressure, selectivity shift to heavier and more oxygenates product [48]. This is equivalent to say that increased H_2/CO ratio results in lighter hydrocarbons and lower carbon olefin products [86], [48].

Between Fe and Co based catalysts, Fe catalyst activity is largely influenced by existence of promoters, while Co catalyst is much less so [86]. For Fe catalyst, the probability of chain growth increase with increasing alkali promotion in order Li, Na, K and Rb [86]. Some oxides such as SiO_2 and Al_2O_3 also increase the basicity of the Fe catalyst [86].

Product selectivity is also influenced by FT operational time-on-stream. It is known that selectivity change with respect to time is caused by the formation of carbonaceous depoits on site with K promoters [48].

During FTS, stepwise polymerization of CH_2 occurs and when to stop this growth reaction decides the final product. This polymerization reaction consists of chain initiation reaction, chain growth reaction and chain termination reaction. During initiation reaction, hydrogenation of CO

occurs. Hydrogenation is a conversion of carbon double bonds of organic compounds to carbon single bond by addition of hydrogen according to the following reaction:

$$CO + 2H_2 \rightarrow CH_2 + H_2O$$

The product CH_2 serves as a monomer for the following chain growth reaction. Chain growth reaction is an oligomerization reaction of CH_2. At each stage of growth, olefins have the option of either to continue the growth reaction by adding another CH_2 or to terminate the reaction. The chain termination reaction occurs when olefins are either desorbed or hydrogenated to form the primary FT products [86].

In FTS, the Anderson-Schulz-Flory (ASF) distribution describes the relation between the hydrocarbon yield and the chain growth probability [5], [85], [48]. According to ASF, the molar yield in carbon number is expressed as

$$m_n = \text{alpha}^{n-1}(1\text{-alpha})$$

where m_n is the mole fraction of a hydrocarbon, n is the length of the hydrocarbon, alpha is chain growth probability, and 1-alpha indicates the probability of chain growth terminations [5], [48]. Alpha is defined by [48]

$$\text{alpha} = R_p/(R_p + R_t)$$

where Rp and Rt are the rates of propagation and termination, respectively. The growth probability alpha decreases with an increase of the reactor temperature, and alpha also depends on the H_2/CO ratio in the reactor [48].

FT products

Gasoline

Gasoline is one of the desired FT products. Dry [86] states that for maximum gasoline production the best FT operation condition is to use the high capacity FFB reactors at about

340^{o}C with iron catalyst. Product contains about 40% straight run gasoline, 20% propene and butene, which can later be oligomerised to produce highly branched gasoline [86]. The straight run gasoline with high linearity and low aromatic content has lower octane value than branched ones [86].

Diesel

Diesel is another major liquid fuel produced from FTS. Unlike gasoline, high linearity and low aromatic content are required factors for high quality diesel. The optimum process for diesel fuel production through FTS requires two steps. Fist process is the FTS using the high capacity slurry bed reactors with Co catalysts aiming to maximize wax production. Then hydrocracking process comes the second to convert was to diesel. This process employs high pressure, high temperature, catalysts and H_2. After the FTS, the products heavier than diesel consist about 45 to 50% of the total. During hydrocracking process, these products are broken down into smaller molecules by breaking carbon bonds. With this two stage process, the overall yields of diesel is about 80%, naphtha is 15% and $C_1 – C_4$ gas is 5% [86].

Because of its high quality, FT based diesel can be used as additive to petroleum based diesel. In general, petroleum based diesel contains high levels of aromatic compounds and nitrogen and sulfur containing compounds, thus, when this diesel is used in motor vehicles, an elevated amount of NOx and particulate matter emissions occur. However, since the Clean Air Act (CAA) amendments were signed on November 15, 1990, the EPA set standards for air quality, and the criteria pollutants include SO_2, PM, NO_X, CO, ozone and lead [89]. Therefore, it is required for diesel fuel and diesel engine to meet the pollutant emission criteria. There are two methods to improve the diesel fuel quality; one is to modify the composition of diesel itself to control the combustion characteristics, the other is to blend with additives, which will enhance

the overall diesel quality. In most times, use of additives is favorable because it is not only extremely cost effective but also able to maintain the fuel performance quality, while changing the composition itself could sometimes decrease the fuel performance [89]. The FT diesel fuel has a cetane number of 70 [86], where cetane number is the indicator of diesel quality and is related to the time required for a liquid fuel to ignite after injection into a compression ignition engine [61]. A high cetane number means a short ignition delay, and thus a higher quality of fuel. There are two standards to indicate cetane number: cetane (n-hexadecane) and heptamethylnonane (2, 2, 4, 4, 6, 8, 8-heptamethylnonane) with cetane number value of 100 and 15, respectively [61] Using these two standards, the cetane number can be obtained as follows [61]:

CN = vol% of cetane + 0.15 (vol% of heptamethylnonane)

Since the typical market requirement of cetane number for diesel is 45 [86], 70 means that this diesel is very high in quality. Thus FT diesel can serve as additive to enhance the lower quality diesel fuel [86], [89], or can also be used in areas possessing tight constraints on fuel quality [86].

The fuel formulations could also have significant effects on the pollutant emissions of NO_X, HC and CO [61]. For example, decreased sulfur content leads to reduction in PM and NO_X [61] as well as HC and CO. Also lower level of aromatics, particularly the polyaromatics, decrease the PM, CO and HCs emissions [61].

Chemicals

FTS can also produce linear alpha-olefins. For a large amount of alpha-olefins, the high-temperature fluidized bed FT reactors with Fe catalyst are recommended [86].

Hydrocracking

Hydrocracking of FT wax to diesel-range hydrocarbons ($C_{11} – C_{20}$) is an important process to increase the production of diesel [90]. Hydrocracking is a refinery process of heavy, high boiling hydrocarbons being broken down into smaller, lower boiling molecules by breaking carbon to carbon bond [91]. This process employs pressure of 85-200 bar, temperature of 300-450^{o}C, catalysts and presence of H_2, and the reaction rate depends on temperature and presence of catalysts. Hydrocracking produces saturated hydrocarbons and the major products are diesel, jet fuel, high octane gasoline and LPG. Hydrocracking products are generally very high in quality and contain very low level of sulfur and contaminants.

Hydrocracking has two functions, one is cracking function and the other is hydrogenation – dehydrogenation function. In order to support these two functions, hydrocracking catalyst need to have both metallic sits and acidic sites on its surface. The acidic site, consisting of amorphous oxide, a crystalline zeolite plus binder or a mixture of crystalline zeolite and amorphouse oxides, serves as a support surface for cracking and isomerization reactions [91]. The metallic sites provide the hydrogenation-dehydrogenation function, and type of metals include palladium, platinum, molybdenum, tungsten, cobalt and nickel [91]. Hydrogenation catalyzed by these metals make feedstock more reactive for cracking and dehydrogenation initiate the cracking by forming a reactive olefin intermediate [91]. Therefore, the control of the balance between cracking and hydrogentation rate is important for the product selectivity. The rate can be controlled by selection of metals and acids of different catalytic strength [91].

Typical hydrocracking process employs one or more reactors with multiple fixed catalyst beds. Hydrocracking reactions are exothermic and thus the catalyst beds are cooled with hydrogen recycle gas [91]. Two major categories of hydrocracking processes are single-stage process and two-stage process. The single-stage process consists of one type of catalyst in one or

two reactors in series. There are various design configuration of this type of reactor to maximize diesel products [91]. After the hydrocracking feedstock goes through the reactor, a high- and low-pressure separators recovers the hydrogen out of the product and the liquid product is sent to fractionation. The recovered hydrogen is recycled back to the reactor and the products in fractionation are separated from unconverted oil and separated to the final products [91]. In a two-stage process, after the hydrocracking takes place at the first stage just like the single-stage process, the effluent and unconverted oil go through the second reactor to be further hydrocrcked. There would be a large throughput from two-stage than single-stage process.

APPENDIX B
COMPUTATION OF A CHEMICAL EQUILIBRIUM COMPOSITION

First assuming i species of gasification product, C(s), H_2, CO, CO_2, H_2O and CH_4, a set of k chemical reactions (k = 3) was selected as follows:

$$C(s) + CO_2 \leftrightarrow 2CO$$

$$CO + 3H_2 \leftrightarrow CH_4 + H_2O$$

$$CO + H_2O \leftrightarrow H_2 + CO_2$$

The coefficient of the species i in the reaction k is set to $\nu_{k,i}$, and the degree of reaction for the reaction k is set to ξ_k,the change in the number of mole for species i can be expressed as follows:

$$dn_i = \sum_k \nu_{k,i} d\xi_k$$

$$dn_{C(s)} = -\xi_1$$

$$dn_{H_2} = -3\xi_2 + \xi_3$$

$$dn_{CO} = 2\xi_1 - \xi_2 - \xi_3$$

$$dn_{CO_2} = -\xi_1 + \xi_3$$

$$dn_{H_2O} = \xi_2 - \xi_3$$

$$dn_{CH_4} = \xi_2$$

or

$$n_C = n_{C,i} - \xi_1$$

$$n_{H_2} = n_{H_2,i} - 3\xi_2 + \xi_3$$

$$n_{CO} = n_{CO,i} + 2\xi_1 - \xi_2 - \xi_3$$

$$n_{CO_2} = n_{CO_2,i} - \xi_1 + \xi_3$$

$$n_{H_2O} = n_{H_2O,i} + \xi_2 - \xi_3$$

$$n_{CH_4} = n_{CH_4,i} + \xi_2$$

where n_i is the final number of mole of species i, while $n_{i,i}$ is the initial number of mole of species i. The mole fraction of species i is expressed as follows:

$$y_i = \frac{n_i}{n_{gas}}$$

where n_{gas} is the total number of mole of the gaseous species:

$$n_{gas} = n_{H_2} + n_{CO} + n_{CO_2} + n_{H_2O} + n_{CH_4}$$

$$y_{H_2} = \frac{n_{H_2}}{n_{gas}} = \frac{n_{H_2,i} - 3\xi_2 + \xi_3}{n_{H_2} + n_{CO} + n_{CO_2} + n_{H_2O} + n_{CH_4}}$$

$$y_{CO} = \frac{n_{CO}}{n_{gas}} = \frac{n_{CO,i} + 2\xi_1 - \xi_2 - \xi_3}{n_{H_2} + n_{CO} + n_{CO_2} + n_{H_2O} + n_{CH_4}}$$

$$y_{CO_2} = \frac{n_{CO_2}}{n_{gas}} = \frac{n_{CO_2,i} - \xi_1 + \xi_3}{n_{H_2} + n_{CO} + n_{CO_2} + n_{H_2O} + n_{CH_4}}$$

$$y_{H_2O} = \frac{n_{H_2O}}{n_{gas}} = \frac{n_{H_2O,i} + \xi_2 - \xi_3}{n_{H_2} + n_{CO} + n_{CO_2} + n_{H_2O} + n_{CH_4}}$$

$$y_{CH_4} = \frac{n_{CH_4}}{n_{gas}} = \frac{n_{CH_4,i} + \xi_2}{n_{H_2} + n_{CO} + n_{CO_2} + n_{H_2O} + n_{CH_4}}$$

The equilibrium constant K for reaction k can be expressed as:

$$\ln K_k = -\frac{\Delta G_k^0}{\bar{R}T}$$

where $\bar{R}$ is the Gas constant (8.31451 kJ/kmol-K) and T is the process temperature in Kelvin.

The change in the Gibbs function for reaction k is written as:

$$\Delta \bar{G}_k^0 = \sum_k \nu_{k,i} \bar{g}_i^0$$

$$\Delta\bar{G}_1^0 = 2\bar{g}_{CO}^0 - \bar{g}_{C(s)}^0 - \bar{g}_{CO_2}^0$$

$$\Delta\bar{G}_2^0 = \bar{g}_{CH_4}^0 + \bar{g}_{H_2O}^0 - \bar{g}_{CO}^0 - 3\bar{g}_{H_2}^0$$

$$\Delta\bar{G}_3^0 = \bar{g}_{H_2}^0 + \bar{g}_{CO_2}^0 - \bar{g}_{CO}^0 - \bar{g}_{H_2O}^0$$

where

$$\bar{g}_{C(s)}^0 = \bar{h}_{C(S)} - T\bar{s}_{T,C(s)}^0$$

$$\bar{g}_{H_2}^0 = \bar{h}_{H_2} - T\bar{s}_{T,H_2}^0 = \left[\bar{h}_f^0 + \left(\bar{h}_T - \bar{h}_{298.15}\right)\right]_{H_2} - T\bar{s}_{T,H_2}^0$$

$$\bar{g}_{CO}^0 = \bar{h}_{CO} - T\bar{s}_{T,CO}^0 = \left[\bar{h}_f^0 + \left(\bar{h}_T - \bar{h}_{298.15}\right)\right]_{CO} - T\bar{s}_{T,CO}^0$$

$$\bar{g}_{CO_2}^0 = \bar{h}_{CO_2} - T\bar{s}_{T,CO_2}^0 = \left[\bar{h}_f^0 + \left(\bar{h}_T - \bar{h}_{298.15}\right)\right]_{CO_2} - T\bar{s}_{T,CO_2}^0$$

$$\bar{g}_{H_2O}^0 = \bar{h}_{H_2O} - T\bar{s}_{T,H_2O}^0 = \left[\bar{h}_f^0 + \left(\bar{h}_T - \bar{h}_{298.15}\right)\right]_{H_2O} - T\bar{s}_{T,H_2O}^0$$

$$\bar{g}_{CH_4}^0 = \bar{h}_{CH_4} - T\bar{s}_{T,CH_4}^0 = \left[\bar{h}_f^0 + \left(\bar{h}_T - \bar{h}_{298.15}\right)\right]_{CH_4} - T\bar{s}_{T,CH_4}^0$$

Enthalpy of formation and absolute entropy of species i at 25^{o}C and 1 bar are listed as follows:

Table B-1. Enthalpy of formation and absolute entroy of syngas components.

	C(s)	H_2	CO	CO_2	H_2O(g)	CH_4
$\bar{s}^0(kJ/kmol-K)$	5.6	130.68	197.66	213.79	188.84	186.25
$\bar{h}_f^0(kJ/mol)$	0	0	-110.53	-395.52	-241.83	-74.87
MW (molecular weight)	12.0107	2.01588	28.0101	44.0095	18.0153	16.0425

Solid carbon (graphite)

The enthalpy and the entropy for the solid carbon (graphite) were computed using the specific heat, C_P:

$$\bar{h}_{C(s)} = \bar{h}_{f,C(s)}^0 + \int_{298.15}^{T} C_{P,C(S)}\,dT$$

$$\bar{s}^0_{T,C(s)} = \bar{s}^0_{C(s)} + \int_{298.15}^{T} \frac{C_{P,C(s)}}{T}\, dT$$

where

$$C_{P,C(s)} = A + B \cdot T + \frac{C}{T} + \frac{D}{T^2} + \frac{E}{T^3} + \frac{F}{T^4} \qquad [250\, to\, 3000\, K]$$

Table B-2. Coefficients of solid carbon (C).

	[kJ/kmol-K]
A	27.0690
B	0.00045787
C	-4536.443
D	-2.1834 x 10^6
E	8.0057 x 10^8
F	-7.2207 x 10^{10}

The other gaseous species, H_2, CO, CO_2, H_2O, and CH_4, enthalpy and entropy were computed using the Shomate Equation:

$$\bar{h}_T - \bar{h}_{298.15} = At + \frac{B}{2}t^2 + \frac{C}{3}t^3 + \frac{D}{4}t^4 - \frac{E}{t} + F - H \qquad \left[\frac{kJ}{mol}\right]$$

$$\bar{s}_T = A\ln(t) + Bt + \frac{C}{2}t^2 + \frac{D}{3}t^3 - \frac{E}{2t^2} + G \qquad \left[\frac{kJ}{kmol - K}\right]$$

$$t = \frac{T(K)}{1000}$$

Table B-3. Coefficients of hydrogen (H_2).

Temperature (K)	298 - 1000	1000 - 2500	2500 – 6000
A	33.066178	18.563083	43.41356
B	-11.363412	12.257357	-4.293079
C	11.432816	-2.869786	1.272428
D	-2.772874	0.268238	-0.096876
E	-0.158558	1.97799	-20.533862
F	-9.980797	-1.147438	-38.515158
G	172.707974	156.288133	162.081354
H	0	0	0

Table B-4. Coefficients of carbon monoxide (CO).

Temperature (K)	298 - 1300	1300 - 6000
A	25.26759	35.1507
B	6.09613	1.300095
C	4.054656	-0.205921
D	-2.671301	0.01355
E	0.131021	-3.28278
F	-118.0089	-127.8375
G	227.3665	231.712
H	-110.5271	-110.5271

Table B-5. Coefficients of carbon dioxide (CO_2).

Temperature (K)	298 - 1200	1200 - 6000
A	24.99735	58.16639
B	55.18696	2.720074
C	-33.69137	-0.492289
D	7.948387	0.038844
E	-0.136638	-6.447293
F	-403.6075	-425.9186
G	228.2431	263.3125
H	-393.5224	-393.5224

Table B-6. Coefficients of water (H_2O).

Temperature (K)	500 - 1700	1700 - 6000
A	30.092	41.96426
B	6.832514	8.622053
C	6.793435	-1.49978
D	-2.53448	0.098119
E	0.082139	-11.15764
F	-250.881	-272.1797
G	223.3967	219.7809
H	-241.8264	-241.8264

Table B-7. Coefficients of methane (CH_4).

Temperature (K)	298 - 1300	1300 - 6000
A	-0.703029	85.81217
B	108.4773	11.26467
C	-42.52157	-2.114146
D	5.862788	0.13819
E	0.678565	-26.42221
F	-76.84376	-153.5327
G	158.7163	224.4143
H	-74.8731	-74.8731

Finally, using the expressions discussed above, a set of k chemical equilibrium equations can be written as the followings:

$$K_k = \prod_i \left(y_i\right)^{\nu_{k,i}} \left(\frac{P}{P^0}\right)^{-\nu_{k,i}}$$

where P is the operation pressure and P^0 is the standard pressure (1 atm).

$$K_1 = \frac{y_{CO}^2}{y_{CO_2}} \left(\frac{P}{P^0}\right)^{2-1} = \frac{\left(n_{CO,i} + 2\xi_1 - \xi_2 - \xi_3\right)^2}{\left(n_{CO_2,i} - \xi_1 + \xi_3\right)\left(n_{H_2} + n_{CO} + n_{CO_2} + n_{H_2O} + n_{CH_4}\right)} \left(\frac{P}{P^0}\right)$$

$$K_2 = \frac{y_{CO} y_{H_2}^3}{y_{CH_4} y_{H_2O}} \left(\frac{P}{P^0}\right)^{1+3-1-1} = \frac{\left(n_{CO,i} + 2\xi_1 - \xi_2 - \xi_3\right)\left(n_{H_2,i} - 3\xi_2 + \xi_3\right)^3}{\left(n_{CH_4,i} + \xi_2\right)\left(n_{H_2O,i} + \xi_2 - \xi_3\right)\left(n_{H_2} + n_{CO} + n_{CO_2} + n_{H_2O} + n_{CH_4}\right)^2} \left(\frac{P}{P^0}\right)^2$$

$$K_3 = \frac{y_{CO_2} y_{H_2}}{y_{CO} y_{H_2O}} \left(\frac{P}{P^0} \right)^{1+1-1-1} = \frac{\left(n_{CO_2,i} - \xi_1 + \xi_3 \right) \left(n_{H_2,i} - 3\xi_2 + \xi_3 \right)}{\left(n_{CO,i} + 2\xi_1 - \xi_2 - \xi_3 \right) \left(n_{H_2O,i} + \xi_2 - \xi_3 \right)}$$

By solving a set of three chemical equilibrium equations, three unknowns, ξ_1, ξ_2 and ξ_3, can be obtained. Then the numbers of mole and the mole fractions of all species can be computed accordingly using ξ_1, ξ_2 and ξ_3.

APPENDIX C
OPERATIONAL PROCEDURE AND ASSEMBLY INSTRUCTIONS

Operational Procedure

Startup

1. Before starting, ensure that basic safety supplies such as first aid kit, eye wash station and fire extinguishers are available. Also secure the access to exits.
2. Make sure that gas pressures of carbon dioxides, hydrogen and oxygen are adequate for a run, and record these pressures as a reference for the next experiment. A run typically drops the hydrogen and oxygen pressure about 300 psig. Switch the regulator to a new cylinder if there is not enough gas for a run.
3. At least four people are required to operate this system. Each individual should have eye protection. Gloves should be used for some operations as needed.
4. Fill the ice bath with 70 to 80 lb or ice. Make sure that the first cooling container is fully covered by ice. Spread the rest of the ice evenly to the second and the third ice baths.
5. Make sure that valves at the inlet hydrogen, oxygen and carbon dioxide rotameters are closed. Later when withdrawing the gases, use these valves to control the gas flows.
6. Open the main valve for the carbon dioxide and set the regulator valve at the carbon dioxide tank at 40 psig.
7. Purge the biomass feeding system with carbon dioxide for 2 to 3 minutes, then place the biomass (wood sawdust) in the feeding system. Make sure both valves on the feeding systems are closed.
8. Purge the whole system for “4T” with carbon dioxide.

$$T = \frac{SystemVolume(l)}{CO_2\ flowrate(l/\min)} = \min.$$

$$4T \simeq 80l$$

9. Initiate iNet100 to ensure all K- and T-type thermocouples return ambient temperature and pressure transducers return ambient pressure. Ensure that the pressure gauges and rotameters respond properly. Note: While the thermocouple grade of B-type thermocouples are 0 to 1700^{o}C, the reading may not be very accurate until after 800^{o}C.
10. Open the main oxygen cylinder valve and set the regulator at the oxygen tank at 40 psig.
11. Set the regulator at the hydrogen tank at 40 psig by opening the main valve, then open the hydrogen regulator valve.
12. Connect the ejector to the exit hose and air compressor hose and turn on the air compressor.
13. Start releasing oxygen and adjust it to 16 LPM, STP based on the temperature and the pressure of the gas. Determine the required flow rate of hydrogen. (See Tables C-1 through C-4).
14. Turn on the hydrogen at the rotameter valve.
15. Click the piezoelectric igniter one second after the hydrogen release. Start recording data at iNET100 at the same time as ignition.
16. Monitor the temperature in the combustion chamber to validate hydrogen torch ignition. Due to the slow sensor response in the low temperature range, it may take up to 1 minute for the chamber thermocouple to pick up the temperature increase.
17. If a temperature increase in the combustion chamber is not confirmed, stop the hydrogen and oxygen and purge system with carbon dioxide for "4T" minutes. Stop recording at iNET100.
    → Repeat from step 13.
18. If a temperature increase in the combustion chamber is confirmed, continue the run.
19. Record the pressure of the reactor gas every 1 minute or whenever a large change is observed.

20. Record the pressure and the volume flow rate of the exit gas every 1 minute or whenever a large change is observed.
21. Once the thermocouple M1-1 reads 1000^{o}C, take an exit gas sample. At this point, no biomass has been introduced. This provides a blank sample for reference. To take a sample:
    1) Connect an evacuated gas sampling bag to the gas sampling port
    2) Open the fitting on the bag
    3) Open the valve connected to the sampling bag
    4) Close the valve to the exit
    5) Gas flows to the sampling bag
    6) Close the valve to the bag
    7) Close the fitting of the bag
    8) Open the valve to the exit rotameter
    9) Remove the bag from the port
    10) Connect another bag to the port for the next sampling
22. If any thermocouples read1650^{o}C or above, reduce the hydrogen and oxygen input flow rates to lower the temperature of the reactor in order to protect the reactor materials.
23. Once the thermocouple M1-1 reads the desired temperature, release the biomass to the gasification chamber. Vibrate the feeding system to help the biomass fall into the reactor. Make sure to close the valve between the feeder and the reactor once the feeding is finished.
24. Sample the exit gas. Make sure to record the time, the exit pressure and the exit flow rate corresponding to every sample.
25. In order to introduce a second load of biomass, purge the biomass feeding system with carbon dioxide, load biomass. → Repeat from 24.

26. Once the gasification is finished, turn off hydrogen and oxygen and start purging the system with carbon dioxide.
27. Turn off carbon dioxide after 4T minutes.
28. Close the main valves of hydrogen, oxygen and carbon dioxide cylinders.
29. Record the pressures of the hydrogen, the oxygen and the carbon dioxide cylinders.
30. Stop recording at iNet100 and save the data.
31. NOTE: Do not attempt to disconnect the torch from the combustion chamber or to open the gasification reactor on the same day of the experiment. Do not purge the oxygen and hydrogen lines to the torch until the system has cooled off.

Gas Analysis

1. Make sure that Argon gas cylinder is connected to the carrier gas port of the GC. Open the main valve of the cylinder if it is closed. (Do not touch the regulator pressure as this should stay at 40 psig all the time).
2. Make sure that the hydrogen gas cylinder is connected to the Flame Ionization Detector (FID) port of the GC. Open the main valve of the cylinder if it is closed. (Do not touch the regulator pressure as this should stay at 50 psig all the time).
3. Turn on the GC main power.
4. Open the red cover of the GC and turn on Thermal Conductivity Detector (TCD) signal sensitivity to high.
5. Confirm that FID is working. To check this, place a piece of metal in front of the FID combustion outlet. If the FID is working, steam will condense on the surface of the metal.
6. Wait for 5 minutes for the systems for stabilize.
7. Meanwhile, start up the computer at the work station and open the file PeakSimple which is located under C:\peak 328-32bit.

8. In PeakSimple, click File → Open control file → and select “gasifier.2”.
9. On the main screen of the PeakSimple, enable the Channel Control button (the button with 1234).
10. “Channel 1” on the “Channel Control” page indicates the setting of the FID. Click “Postrun”. In the open space beside the save file on top of the page, type the file name. Make sure that Auto increment box is checked. Click OK.
11. “Channel 2” on the “Channel Control” page indicates the setting of the TCD. “Postrun”. In the open space beside the save file as on top of the page, type the file name. Make sure that Auto increment box is checked. Click OK.
12. Click OK to get out of the Channel Control page. On the main page of PeakSimple, both FID and TCD channels with the file names specified in the step 7 and 8 are shown.
13. Go back to GC.
14. Connect your gas sample to the Sample In port of the GC.
15. Open the sample bag fitting and squeeze the bag for a few seconds to send the gas to GC. Make sure that the gas is sent to GC by observing bubbles coming out from the Sample Out port of the GC.
16. Hit the GC start button and close the sample bag fitting.
17. Let GC run for 20 minutes. The first run of the day shows residues in the column from previous runs and does not properly reflect the sample composition. Thus, start counting the second run as the first analysis.
18. Repeat steps 14 to 17 as many times as necessary.
19. Once the GC runs are finished, turn off the TCD sensitivity signal, close the main valve of the carrier gas (Argon) cylinder and wait for 10 minutes.

20. Turn off the GC main power.

21. The files of the analysis results are saved in the folder, peak 328-32bit.

22. Compare the analysis results to the calibration data to determine the actual volume% of each species.

Table C-1. Oxygen volume flow rate (LPM) readings at the rotameter equivalent to 16 LPM, STP.

Volume Flow Rate of O_2 (LPM)		P (psig)														
		1	1.5	2	2.5	3	3.5	4	4.5	5	5.5	6	6.5	7	7.5	8
T_{O2} (^{o}C)	10	15.86	14.90	14.02	13.22	12.48	11.81	11.18	10.61	10.08	9.58	9.13	8.70	8.30	7.93	7.59
	11	15.98	15.01	14.12	13.31	12.57	11.89	11.26	10.68	10.15	9.65	9.19	8.76	8.36	7.99	7.64
	12	16.09	15.11	14.22	13.41	12.66	11.97	11.34	10.76	10.22	9.72	9.26	8.82	8.42	8.05	7.70
	13	16.20	15.22	14.32	13.50	12.75	12.06	11.42	10.83	10.29	9.79	9.32	8.89	8.48	8.10	7.75
	14	16.32	15.32	14.42	13.59	12.84	12.14	11.50	10.91	10.36	9.86	9.39	8.95	8.54	8.16	7.80
	15	16.43	15.43	14.52	13.69	12.93	12.23	11.58	10.99	10.44	9.93	9.45	9.01	8.60	8.22	7.86
	16	16.54	15.54	14.62	13.78	13.02	12.31	11.66	11.06	10.51	9.99	9.52	9.07	8.66	8.27	7.91
	17	16.66	15.65	14.72	13.88	13.11	12.40	11.74	11.14	10.58	10.06	9.58	9.14	8.72	8.33	7.97
	18	16.77	15.75	14.82	13.98	13.20	12.48	11.82	11.22	10.65	10.13	9.65	9.20	8.78	8.39	8.02
	19	16.89	15.86	14.93	14.07	13.29	12.57	11.90	11.29	10.73	10.20	9.72	9.26	8.84	8.45	8.08
	20	17.00	15.97	15.03	14.17	13.38	12.65	11.99	11.37	10.80	10.27	9.78	9.33	8.90	8.50	8.13
	21	17.12	16.08	15.13	14.26	13.47	12.74	12.07	11.45	10.87	10.34	9.85	9.39	8.96	8.56	8.19
	22	17.24	16.19	15.23	14.36	13.56	12.83	12.15	11.53	10.95	10.41	9.92	9.45	9.02	8.62	8.25
	23	17.35	16.30	15.34	14.46	13.65	12.91	12.23	11.60	11.02	10.48	9.98	9.52	9.08	8.68	8.30
	24	17.47	16.41	15.44	14.56	13.75	13.00	12.32	11.68	11.10	10.55	10.05	9.58	9.15	8.74	8.36
	25	17.59	16.52	15.55	14.66	13.84	13.09	12.40	11.76	11.17	10.63	10.12	9.65	9.21	8.80	8.41
	26	17.71	16.63	15.65	14.75	13.93	13.18	12.48	11.84	11.25	10.70	10.19	9.71	9.27	8.86	8.47
	27	17.83	16.74	15.75	14.85	14.03	13.27	12.57	11.92	11.32	10.77	10.25	9.78	9.33	8.92	8.53
	28	17.94	16.85	15.86	14.95	14.12	13.35	12.65	12.00	11.40	10.84	10.32	9.84	9.39	8.97	8.58
	29	18.06	16.97	15.97	15.05	14.21	13.44	12.73	12.08	11.47	10.91	10.39	9.91	9.46	9.03	8.64

Table C-2. Hydrogen volume flow rate (LPM) reading at the rotameter for H_2:O_2 = 2:1 with 16 LPM, STP of oxygen flow.

Volume Flow Rate of H_2 (LPM)		P (psig)														
		1	1.5	2	2.5	3	3.5	4	4.5	5	5.5	6	6.5	7	7.5	8
T_{H2} (^{o}C)	10	8.01	7.88	7.76	7.65	7.54	7.44	7.34	7.24	7.15	7.06	6.97	6.89	6.81	6.73	6.66
	11	8.02	7.90	7.78	7.66	7.55	7.45	7.35	7.25	7.16	7.07	6.99	6.90	6.82	6.75	6.67
	12	8.04	7.91	7.79	7.68	7.57	7.46	7.36	7.27	7.17	7.08	7.00	6.92	6.84	6.76	6.68
	13	8.05	7.92	7.81	7.69	7.58	7.48	7.38	7.28	7.19	7.10	7.01	6.93	6.85	6.77	6.69
	14	8.06	7.94	7.82	7.70	7.59	7.49	7.39	7.29	7.20	7.11	7.02	6.94	6.86	6.78	6.71
	15	8.08	7.95	7.83	7.72	7.61	7.50	7.40	7.30	7.21	7.12	7.03	6.95	6.87	6.79	6.72
	16	8.09	7.97	7.85	7.73	7.62	7.52	7.41	7.32	7.22	7.13	7.05	6.96	6.88	6.80	6.73
	17	8.11	7.98	7.86	7.74	7.63	7.53	7.43	7.33	7.24	7.15	7.06	6.98	6.89	6.82	6.74
	18	8.12	7.99	7.87	7.76	7.65	7.54	7.44	7.34	7.25	7.16	7.07	6.99	6.91	6.83	6.75
	19	8.13	8.01	7.89	7.77	7.66	7.55	7.45	7.36	7.26	7.17	7.08	7.00	6.92	6.84	6.76
	20	8.15	8.02	7.90	7.78	7.67	7.57	7.47	7.37	7.27	7.18	7.10	7.01	6.93	6.85	6.78
	21	8.16	8.03	7.91	7.80	7.69	7.58	7.48	7.38	7.29	7.20	7.11	7.02	6.94	6.86	6.79
	22	8.18	8.05	7.93	7.81	7.70	7.59	7.49	7.39	7.30	7.21	7.12	7.04	6.95	6.88	6.80
	23	8.19	8.06	7.94	7.82	7.71	7.61	7.50	7.41	7.31	7.22	7.13	7.05	6.97	6.89	6.81
	24	8.20	8.08	7.95	7.84	7.73	7.62	7.52	7.42	7.32	7.23	7.14	7.06	6.98	6.90	6.82
	25	8.22	8.09	7.97	7.85	7.74	7.63	7.53	7.43	7.34	7.24	7.16	7.07	6.99	6.91	6.83
	26	8.23	8.10	7.98	7.86	7.75	7.64	7.54	7.44	7.35	7.26	7.17	7.08	7.00	6.92	6.84
	27	8.24	8.12	7.99	7.88	7.76	7.66	7.55	7.46	7.36	7.27	7.18	7.09	7.01	6.93	6.86
	28	8.26	8.13	8.01	7.89	7.78	7.67	7.57	7.47	7.37	7.28	7.19	7.11	7.02	6.94	6.87
	29	8.27	8.14	8.02	7.90	7.79	7.68	7.58	7.48	7.38	7.29	7.20	7.12	7.04	6.96	6.88

Table C-3. Hydrogen volume flow rate (LPM) reading at the rotameter for H_2:O_2 = 2.1:1 with 16 LPM, STP of oxygen flow.

Volume Flow Rate of H_2 (LPM)		P (psig)														
		1	1.5	2	2.5	3	3.5	4	4.5	5	5.5	6	6.5	7	7.5	8
T_{H2} (^{o}C)	10	8.41	8.28	8.15	8.03	7.92	7.81	7.70	7.60	7.51	7.41	7.32	7.24	7.15	7.07	6.99
	11	8.42	8.29	8.17	8.05	7.93	7.82	7.72	7.62	7.52	7.43	7.34	7.25	7.16	7.08	7.00
	12	8.44	8.31	8.18	8.06	7.95	7.84	7.73	7.63	7.53	7.44	7.35	7.26	7.18	7.10	7.02
	13	8.45	8.32	8.20	8.08	7.96	7.85	7.74	7.64	7.55	7.45	7.36	7.27	7.19	7.11	7.03
	14	8.47	8.34	8.21	8.09	7.97	7.86	7.76	7.66	7.56	7.46	7.37	7.29	7.20	7.12	7.04
	15	8.48	8.35	8.22	8.10	7.99	7.88	7.77	7.67	7.57	7.48	7.39	7.30	7.21	7.13	7.05
	16	8.50	8.36	8.24	8.12	8.00	7.89	7.79	7.68	7.58	7.49	7.40	7.31	7.23	7.15	7.07
	17	8.51	8.38	8.25	8.13	8.02	7.90	7.80	7.70	7.60	7.50	7.41	7.32	7.24	7.16	7.08
	18	8.53	8.39	8.27	8.15	8.03	7.92	7.81	7.71	7.61	7.52	7.43	7.34	7.25	7.17	7.09
	19	8.54	8.41	8.28	8.16	8.04	7.93	7.83	7.72	7.62	7.53	7.44	7.35	7.26	7.18	7.10
	20	8.55	8.42	8.29	8.17	8.06	7.95	7.84	7.74	7.64	7.54	7.45	7.36	7.28	7.19	7.11
	21	8.57	8.44	8.31	8.19	8.07	7.96	7.85	7.75	7.65	7.55	7.46	7.37	7.29	7.21	7.13
	22	8.58	8.45	8.32	8.20	8.08	7.97	7.87	7.76	7.66	7.57	7.48	7.39	7.30	7.22	7.14
	23	8.60	8.46	8.34	8.22	8.10	7.99	7.88	7.78	7.68	7.58	7.49	7.40	7.31	7.23	7.15
	24	8.61	8.48	8.35	8.23	8.11	8.00	7.89	7.79	7.69	7.59	7.50	7.41	7.33	7.24	7.16
	25	8.63	8.49	8.37	8.24	8.13	8.01	7.91	7.80	7.70	7.61	7.51	7.42	7.34	7.26	7.18
	26	8.64	8.51	8.38	8.26	8.14	8.03	7.92	7.81	7.71	7.62	7.53	7.44	7.35	7.27	7.19
	27	8.66	8.52	8.39	8.27	8.15	8.04	7.93	7.83	7.73	7.63	7.54	7.45	7.36	7.28	7.20
	28	8.67	8.54	8.41	8.28	8.17	8.05	7.94	7.84	7.74	7.64	7.55	7.46	7.38	7.29	7.21
	29	8.69	8.55	8.42	8.30	8.18	8.07	7.96	7.85	7.75	7.66	7.56	7.47	7.39	7.30	7.22

Table C-4. Hydrogen volume flow rate (LPM) reading at the rotameter for H_2:O_2 = 2.2:1 with 16 LPM, STP of oxygen flow.

Volume Flow Rate of H_2 (LPM)		P (psig)														
		1	1.5	2	2.5	3	3.5	4	4.5	5	5.5	6	6.5	7	7.5	8
T_{H2} (^{o}C)	10	8.81	8.67	8.54	8.42	8.30	8.18	8.07	7.97	7.86	7.77	7.67	7.58	7.49	7.41	7.33
	11	8.82	8.69	8.56	8.43	8.31	8.20	8.09	7.98	7.88	7.78	7.68	7.59	7.51	7.42	7.34
	12	8.84	8.70	8.57	8.45	8.32	8.21	8.10	7.99	7.89	7.79	7.70	7.61	7.52	7.43	7.35
	13	8.85	8.72	8.59	8.46	8.34	8.22	8.11	8.01	7.90	7.81	7.71	7.62	7.53	7.45	7.36
	14	8.87	8.73	8.60	8.47	8.35	8.24	8.13	8.02	7.92	7.82	7.73	7.63	7.54	7.46	7.38
	15	8.89	8.75	8.62	8.49	8.37	8.25	8.14	8.04	7.93	7.83	7.74	7.65	7.56	7.47	7.39
	16	8.90	8.76	8.63	8.50	8.38	8.27	8.16	8.05	7.95	7.85	7.75	7.66	7.57	7.49	7.40
	17	8.92	8.78	8.65	8.52	8.40	8.28	8.17	8.06	7.96	7.86	7.77	7.67	7.58	7.50	7.42
	18	8.93	8.79	8.66	8.53	8.41	8.30	8.18	8.08	7.97	7.87	7.78	7.69	7.60	7.51	7.43
	19	8.95	8.81	8.68	8.55	8.43	8.31	8.20	8.09	7.99	7.89	7.79	7.70	7.61	7.52	7.44
	20	8.96	8.82	8.69	8.56	8.44	8.32	8.21	8.10	8.00	7.90	7.81	7.71	7.62	7.54	7.45
	21	8.98	8.84	8.70	8.58	8.46	8.34	8.23	8.12	8.01	7.91	7.82	7.73	7.64	7.55	7.47
	22	8.99	8.85	8.72	8.59	8.47	8.35	8.24	8.13	8.03	7.93	7.83	7.74	7.65	7.56	7.48
	23	9.01	8.87	8.73	8.61	8.48	8.37	8.25	8.15	8.04	7.94	7.85	7.75	7.66	7.58	7.49
	24	9.02	8.88	8.75	8.62	8.50	8.38	8.27	8.16	8.06	7.95	7.86	7.77	7.68	7.59	7.50
	25	9.04	8.90	8.76	8.64	8.51	8.39	8.28	8.17	8.07	7.97	7.87	7.78	7.69	7.60	7.52
	26	9.05	8.91	8.78	8.65	8.53	8.41	8.30	8.19	8.08	7.98	7.88	7.79	7.70	7.61	7.53
	27	9.07	8.93	8.79	8.66	8.54	8.42	8.31	8.20	8.10	7.99	7.90	7.80	7.71	7.63	7.54
	28	9.08	8.94	8.81	8.68	8.56	8.44	8.32	8.21	8.11	8.01	7.91	7.82	7.73	7.64	7.55
	29	9.10	8.96	8.82	8.69	8.57	8.45	8.34	8.23	8.12	8.02	7.92	7.83	7.74	7.65	7.57

LIST OF REFERENCES

[1] Energy Information Administration - EIA - Official Energy Statistics from the U.S. Government, http://www.eia.doe.gov/, 2008.

[2] HH Schobert, Coal, the energy source of the past and future, American Chemical Society, Washington, DC, 1987.

[3] BGMS Miller, Coal energy systems, Elsevier Academic Press, Amsterdam ; Boston, 2005.

[4] I Wender. Reactions of synthesis gas, Fuel Processing Technology. 48 (1996) 189-297.

[5] MJA Tijmensen, APC Faaij, CN Hamelinck, MRM van Hardeveld. Exploration of the possibilities for production of Fischer Tropsch liquids and power via biomass gasification, Biomass and Bioenergy. 23 (2002) 129-152.

[6] Research and Innovative Technology Administration (RITA) - United States Department of Transportation (USDOT), http://www.rita.dot.gov/, 2008.

[7] JJ Ewel, RL Myers, Ecosystems of Florida, University of Central Florida Press, Orlando, 1990.

[8] RM Burns, BH Honkala, United States Forest Service, Silvics of North America, U.S. Dept. of Agriculture, Forest Service; For sale by the Supt. of Docs., U.S. G.P.O., Washington, D.C., 1990.

[9] P McKendry. Energy production from biomass (part 1): overview of biomass, Bioresource Technology. 83 (2002) 37-46.

[10] J Rezaiyan, NP Cheremisinoff, Gasification technologies : a primer for engineers and scientists, Taylor & Francis, Boca Raton, 2005.

[11] Harold Boerrigter, Herman den Uil, Hans-Peter Calis, Green Diesel from Biomass via Fischer-Tropsch synthesis: New Insights in Gas Cleaning and Process Design, (2002).

[12] EPA's 2008 Report on the Environment - US EPA, http://www.epa.gov/roe/, 2008.

[13] NCDC: Greenhouse Gases, http://lwf.ncdc.noaa.gov/oa/climate/gases.html, 2008.

[14] DY Goswami, JF Kreider, F Kreith, Kreith,Frank Principles of solar engineering, Principles of solar engineering, 2nd ed., Taylor & Francis, Philadelphia, PA, 2000.

[15] P McKendry. Energy production from biomass (part 3): gasification technologies, Bioresource Technology. 83 (2002) 55-63.

[16] P McKendry. Energy production from biomass (part 2): conversion technologies, Bioresource Technology. 83 (2002) 47-54.

[17] A Williams, JM Jones, M Pourkashanian, Combustion and gasification of coal, Taylor & Francis, New York, 2000.

[18] BV Babu, AS Chaurasia. Modeling, simulation and estimation of optimum parameters in pyrolysis of biomass, Energy Conversion and Management. 44 (2003) 2135-2158.

[19] P Mathieu, R Dubuisson. Performance analysis of a biomass gasifier, Energy Conversion and Management. 43 (2002) 1291-1299.

[20] GP Van Der Laan, AACM Beenackers. Kinetics and Selectivity of the Fischer–Tropsch Synthesis: A Literature Review, Catalysis Reviews. 41 (1999) 255.

[21] C Franco, F Pinto, I Gulyurtlu, I Cabrita. The study of reactions influencing the biomass steam gasification process⋆, Fuel. 82 (2003) 835-842.

[22] R Kramreiter, M Url, J Kotik, H Hofbauer. Experimental investigation of a 125 kW twin-fire fixed bed gasification pilot plant and comparison to the results of a 2 MW combined heat and power plant (CHP), Fuel Processing Technology. 89 (2008) 90-102.

[23] C Hindsgaul, J Schramm, L Gratz, U Henriksen, J Dall Bentzen. Physical and chemical characterization of particles in producer gas from wood chips, Bioresource Technology. 73 (2000) 147-155.

[24] Y Matsumura, T Minowa. Fundamental design of a continuous biomass gasification process using a supercritical water fluidized bed, International Journal of Hydrogen Energy. 29 (2004) 701-707.

[25] Energy research Centre of the Netherlands: ECN, http://www.ecn.nl/nl/, 2008.

[26] M Hrabovsky, M Konrad, V Kopecky, M Hlina, T Kavka, G van Oost, et al. Gasification of biomass in water/gas-stabilized plasma for syngas production, Czechoslovak Journal of Physics. 56 (2006) B1199-B1206.

[27] Z Zhao, H Huang, C Wu, H Li, Y Chen. Biomass Pyrolysis in an Argon/Hydrogen Plasma Reactor, Engineering in Life Sciences. 1 (2001) 197-199.

[28] L Tang, H Huang. Biomass gasification using capacitively coupled RF plasma technology, Fuel. 84 (2005) 2055-2063.

[29] M HlÃna, M HrabovskÃ½, V KopeckÃ½, M KonrÃ¡d, T Kavka, S Skoblja. Plasma gasification of wood and production of gas with low content of tar, Czechoslovak Journal of Physics. 56 (2006) B1179-B1184.

[30] T Hanaoka, S Inoue, S Uno, T Ogi, T Minowa. Effect of woody biomass components on air-steam gasification, Biomass and Bioenergy. 28 (2005) 69-76.

[31] C Sheng, JLT Azevedo. Estimating the higher heating value of biomass fuels from basic analysis data, Biomass and Bioenergy. 28 (2005) 499-507.

[32] SA Channiwala, PP Parikh. A unified correlation for estimating HHV of solid, liquid and gaseous fuels, Fuel. 81 (2002) 1051-1063.

[33] J Parikh, SA Channiwala, GK Ghosal. A correlation for calculating HHV from proximate analysis of solid fuels, Fuel. 84 (2005) 487-494.

[34] LP White, LG Plaskett, Biomass as fuel, Academic Press, London ; New York, 1981.

[35] YG Pan, X Roca, E Velo, L Puigjaner. Removal of tar by secondary air in fluidised bed gasification of residual biomass and coal, Fuel. 78 (1999) 1703-1709.

[36] PM Lv, ZH Xiong, J Chang, CZ Wu, Y Chen, JX Zhu. An experimental study on biomass air–steam gasification in a fluidized bed, Bioresource Technology. 95 (2004) 95-101.

[37] A van der Drift, J van Doorn, JW Vermeulen. Ten residual biomass fuels for circulating fluidized-bed gasification, Biomass and Bioenergy. 20 (2001) 45-56.

[38] A Saravanakumar, TM Haridasan, TB Reed, RK Bai. Experimental investigations of long stick wood gasification in a bottom lit updraft fixed bed gasifier, Fuel Processing Technology. 88 (2007) 617-622.

[39] G Chen, J Andries, Z Luo, H Spliethoff. Biomass pyrolysis/gasification for product gas production: the overall investigation of parametric effects, Energy Conversion and Management. 44 (2003) 1875-1884.

[40] P Kaushal, T Pröll, H Hofbauer. Model for biomass char combustion in the riser of a dual fluidized bed gasification unit: Part 1 — Model development and sensitivity analysis, Fuel Processing Technology. 89 (2008) 651-659.

[41] C Lucas, D Szewczyk, W Blasiak, S Mochida. High-temperature air and steam gasification of densified biofuels, Biomass and Bioenergy. 27 (2004) 563-575.

[42] M J. Prins, K J. Ptasinski, F J. J. G. Janssen. Thermodynamics of gas-char reactions: first and second law analysis, Chemical Engineering Science. 58 (2003) 1003-1011.

[43] CN Hamelinck, APC Faaij, H den Uil, H Boerrigter. Production of FT transportation fuels from biomass; technical options, process analysis and optimisation, and development potential, Energy. 29 (2004) 1743-1771.

[44] JPA Neeft , HAM Knoef, Stichting Energieonderzoek Centrum Nederland., BTG Biomass Technology Group., Behaviour of tar in biomass gasification systems : tar related problems and their solutions, Novem ; MHP Management & Secretary Services [distr.], Utrecht; Maarn, 1999.

[45] W Yang, A Ponzio, C Lucas, W Blasiak. Performance analysis of a fixed-bed biomass gasifier using high-temperature air, Fuel Processing Technology. 87 (2006) 235-245.

[46] Y Cao, Y Wang, JT Riley, W Pan. A novel biomass air gasification process for producing tar-free higher heating value fuel gas, Fuel Processing Technology. 87 (2006) 343-353.

[47] L Devi, KJ Ptasinski, FJJG Janssen. A review of the primary measures for tar elimination in biomass gasification processes, Biomass and Bioenergy. 24 (2003) 125-140.

[48] Z AbuEl-Rub, EA Bramer, G Brem. Review of Catalysts for Tar Elimination in Biomass Gasification Processes, Ind. Eng. Chem. Res. 43 (2004) 6911-6919.

[49] R Zhang, RC Brown, A Suby, K Cummer. Catalytic destruction of tar in biomass derived producer gas, Energy Conversion and Management. 45 (2004) 995-1014.

[50] L Devi, KJ Ptasinski, FJJG Janssen, SVB van Paasen, PCA Bergman, JHA Kiel. Catalytic decomposition of biomass tars: use of dolomite and untreated olivine, Renewable Energy. 30 (2005) 565-587.

[51] D Sutton, B Kelleher, JRH Ross. Review of literature on catalysts for biomass gasification, Fuel Processing Technology. 73 (2001) 155-173.

[52] T Nordgreen, T Liliedahl, K Sjöström. Metallic iron as a tar breakdown catalyst related to atmospheric, fluidised bed gasification of biomass, Fuel. 85 (2006) 689-694.

[53] C Myrén, C Hörnell, E Björnbom, K Sjöström. Catalytic tar decomposition of biomass pyrolysis gas with a combination of dolomite and silica, Biomass and Bioenergy. 23 (2002) 217-227.

[54] H. Boerrigter, H.P. Calis, D.J. Slort, H. Bodenstaff, A. J. Kaandorp, H. den Uil, L.P.L.M. Rabou, Gas Cleaning for Integrated Biomass Gasification (BG) and Fischer-Tropsch (FT) Systems, (2004).

[55] S Fujimoto, T Yoshida, T Hanaoka, Y Matsumura, S Lin, T Minowa, et al. A kinetic study of in situ CO2 removal gasification of woody biomass for hydrogen production, Biomass and Bioenergy. 31 (2007) 556-562.

[56] RJ Gorte, S Zhao. Studies of the water-gas-shift reaction with ceria-supported precious metals, Catalysis Today. 104 (2005) 18-24.

[57] D Andreeva, V Idakiev, T Tabakova, L Ilieva, P Falaras, A Bourlinos, et al. Low-temperature water-gas shift reaction over Au/CeO2 catalysts, Catalysis Today. 72 (2002) 51-57.

[58] Q Fu, W Deng, H Saltsburg, M Flytzani-Stephanopoulos. Activity and stability of low-content gold–cerium oxide catalysts for the water–gas shift reaction, Applied Catalysis B: Environmental. 56 (2005) 57-68.

[59] P Lv, Z Yuan, C Wu, L Ma, Y Chen, N Tsubaki. Bio-syngas production from biomass catalytic gasification, Energy Conversion and Management. 48 (2007) 1132-1139.

[60] T Hanaoka, T Yoshida, S Fujimoto, K Kamei, M Harada, Y Suzuki, et al. Hydrogen production from woody biomass by steam gasification using a CO2 sorbent, Biomass and Bioenergy. 28 (2005) 63-68.

[61] CS Hsu, I Mochida, C Song, Chemistry of diesel fuels, Taylor & Francis, New York, 2000.

[62] P Norton, K Vertin, B Bailey, N Clark, D Lyons, S Goguen, J Eberhardt, Emissions from Trucks using Fischer-Tropsch Diesel Fuel, http://www.fischer-tropsch.org/DOE/DOE_reports/982526/SAE-TPS-982526.pdf, (1998).

[63] TL Alleman, Fuel property, emission test, and operability results from a fleet of class 6 vehicles operating on gas-to-liquid fuel and catalyzed diesel particle filters, 2004 SAE Powertrain & Fluid Systems Conference & Exhibition, http://www.nrel.gov/docs/fy06osti/36363.pdf, (2005).

[64] USGS - U.S. Geological Survey, http://www.usgs.gov/, 2011.

[65] J Szargut, DR Morris, FR Steward, Exergy analysis of thermal, chemical, and metallurgical processes, Hemisphere, New York, 1988.

[66] A Bejan, MJ Moran, G Tsatsaronis, Thermal design and optimization, John Wiley, New York, 1996.

[67] IUPAC - GOLD book, http://goldbook.iupac.org/, 2008.

[68] KJ Ptasinski, MJ Prins, A Pierik. Exergetic evaluation of biomass gasification, Energy. 32 (2007) 568-574.

[69] MS Rao, SP Singh, MS Sodha, AK Dubey, M Shyam. Stoichiometric, mass, energy and exergy balance analysis of countercurrent fixed-bed gasification of post-consumer residues, Biomass and Bioenergy. 27 (2004) 155-171.

[70] M Baratieri, P Baggio, L Fiori, M Grigiante. Biomass as an energy source: Thermodynamic constraints on the performance of the conversion process, Bioresource Technology. 99 (2008) 7063-7073.

[71] MJ Prins, KJ Ptasinski, FJJG Janssen. Exergetic optimisation of a production process of Fischer–Tropsch fuels from biomass, Fuel Processing Technology. 86 (2005) 375-389.

[72] MJ Prins, KJ Ptasinski. Energy and exergy analyses of the oxidation and gasification of carbon, Energy. 30 (2005) 982-1002.

[73] LF Pellegrini, J de Oliveira Silvio. Exergy analysis of sugarcane bagasse gasification, Energy. 32 (2007) 314-327.

[74] MR Mahishi, DY Goswami. Thermodynamic optimization of biomass gasifier for hydrogen production, International Journal of Hydrogen Energy. 32 (2007) 3831-3840.

[75] NIST Chemistry Web Book, http://webbook.nist.gov/chemistry/, 2008.

[76] MatWeb, http://www.matweb.com/, 2008.

[77] ZIRCAR Ceramics, http://www.zircarceramics.com/pages/rigidmaterials/specs/sali.htm, 2009.

[78] Cotronics Rescar 960 Alumina Properties, http://www.cotronics.com/vo/cotr/pdf/55960.pdf, 2009.

[79] ASM - Aerospace Specification Metals, http://www.aerospacemetals.com/, 2009.

[80] EnvironmentalChemistry.com, http://environmentalchemistry.com/, 2009.

[81] DR McIlveen-Wright, F Pinto, L Armesto, MA Caballero, MP Aznar, A Cabanillas, et al. A comparison of circulating fluidised bed combustion and gasification power plant technologies for processing mixtures of coal, biomass and plastic waste, Fuel Process Technol. 87 (2006) 793-801.

[82] PR Wander, CR Altafini, RM Barreto. Assessment of a small sawdust gasification unit, Biomass and Bioenergy. 27 (2004) 467-476.

[83] RB Anderson, H Kölbel, M Rálek, The Fischer-Tropsch synthesis, Academic Press, Orlando, 1984.

[84] AA Adesina. Hydrocarbon synthesis via Fischer-Tropsch reaction: travails and triumphs, Applied Catalysis A: General. 138 (1996) 345-367.

[85] ST Sie, R Krishna. Fundamentals and selection of advanced Fischer–Tropsch reactors, Applied Catalysis A: General. 186 (1999) 55-70.

[86] ME Dry. The Fischer–Tropsch process: 1950–2000, Catalysis Today. 71 (2002) 227-241.

[87] H Schulz. Short history and present trends of Fischer–Tropsch synthesis, Applied Catalysis A: General. 186 (1999) 3-12.

[88] M Dry, A Steynberg, Fischer-Tropsch technology, Elsevier, Amsterdam ; Boston, 2004.

[89] MR Khan, JG Reynolds, Designing transportation fuels for a cleaner environment, Taylor & Francis, Philadelphia, Pa., 1999.

[90] Y Liu, T Hanaoka, K Murata, K Okabe, M Inaba, I Takahara, et al. Hydrocracking of Fischer–Tropsch Wax to Diesel-range Hydrocarbons over Bifunctional Catalysts Containing Pt and Polyoxocation-pillared Montmorillonite, Chem.Lett. 36 (2007) 1470-1471.

[91] J Scherzer, AJ Gruia, Hydrocracking science and technology, Marcel Dekker, New York, 1996.

BIOGRAPHICAL SKETCH

Akiko Hiramatsu was born in Saitama, Japan. After graduating high school in Japan, she moved to the United States and studied two years in Northern State University South Dakota. In 1999, she transferred to the University of Florida where she earned her B.S. in environmental science. She continued her study at the University of Florida and earned her B.S. in mechanical engineering in 2004, M.S. in 2007 and Ph.D. in 2011.